ERDC/LAB TR-0X-X

Coastal and Hydraulics Laboratory

US Army Corps
of Engineers®
Engineer Research and
Development Center

DRAFT

Impacts of Savannah Harbor Expansion Project

Jane McKee Smith, Donald K. Stauble, Brian P. Williams, Raymond Chapman

October 2006

ERDC/CHL TR-0X-X
October 2006

Impacts of Savannah Harbor Expansion Project

Jane McKee Smith and Donald K. Stauble

Coastal and Hydraulics Laboratory
U.S. Army Engineer Research and Development Center
3909 Halls Ferry Road
Vicksburg, MS 39180-3999

Brian P. Williams

Charleston District

Raymond Chapman

Coastal and Hydraulics Laboratory

Draft report

Prepared for U.S. Army Corps of Engineers, Savannah District

1 Introduction

Savannah Harbor is a deep-draft harbor on the South Atlantic at Savannah, Georgia. The harbor and deep-draft navigation channel comprise the lower 21.3 miles of the Savannah River and 11.4 miles of channel across the bar to the Atlantic Ocean. This study evaluates the impact of deepening the Savannah navigation channel from the present -44 ft MLW to -50 ft MLW. This report documents the results of the numerical circulation, wave, and sediment transport modeling and the updated sediment budget analysis performed by Wilmington and Charleston District and the Engineer Research and Development Center.

This study was conducted under two tasks. The first task was analysis of shoreline and sediment volume. This task is documented in Chapter 2. The second task involved numerical modeling of circulation, waves, and potential sediment transport for the existing bathymetry and the deepened channel bathymetry. The models were run for four month-long simulations (November 1979, January 1992, July 1999, and December 1999) and for Hurricane Hugo (September 1989) re-tracked to directly hit Savannah. The circulation, wave, and sediment transport modeling is documented in Chapter 3, 4, and 5, respectively. A summary and conclusions is provided in Chapter 6.

2 Shoreline and Volume Change Analysis

Introduction

Congress authorized construction of the Federal navigation project at Savannah Harbor, and it was initially constructed in 1874. The Savannah River empties into the Atlantic Ocean on the border between Georgia and South Carolina. The shoreline is composed of several shore barrier islands known as the Sea Islands along the Georgia Bight, an embayment in the north-south orientation of the coast (Figure 2-1). The barrier islands to the north of the Savannah River entrance are Hilton Head, Daufuskie and Turtle. Calibogue Sound is a north/south oriented inlet separating Hilton Head Island from the embayed Daufuskie Island. The New River Entrance bisects Daufuskie and Turtle Islands. The Wright River Entrance separates Turtle Island from Oyster Bed Island. The main navigation channel of the Savannah River is south of Oyster Bed Island. Cockspur Island separates the main navigation channel from the South Channel of the Savannah River. Two jetties were constructed at the mouth of the Savannah River entrance, completed in 1896, and a submerged offshore breakwater, completed in 1897 to stabilize the inlet and provide a shelter for shipping entering Tybee Roads. Tybee Island is located on the south side of the entrance channel to the Savannah River. Tybee Creek separates Tybee Island from Little Tybee Island on the south.

The navigation channel of the Savannah River was deepened from 21.5 ft mlw to a depth of 26 ft mlw in 1912 to accommodate larger ships. Depth increases were later made in 1936 to 30 ft mlw and 1945 to 36 ft mlw. The channel was widened and deepened in 1972 to a depth of 40 ft mlw. In 1994, the authorized depth of the channel was increased to 44 ft mlw. At present, approximately 31 miles of navigation channel exist, extending from Savannah Harbor across Tybee Roads into the Atlantic Ocean. Construction and maintenance of the Federal navigation channel at Savannah Harbor has resulted in disruption of sediment transport pathways across Tybee Roads. Sediment shoaling in the navigation channel has necessitated annual dredging in order to maintain navigability (Figure 2-2). The magnitude and frequency of channel dredging confirms intersection of sediment pathways in this complex coastal setting of high tidal ranges and short barrier islands bisected by numerous tidal inlets.

Northern Tybee Island, located directly downdrift of the Savannah Harbor navigation channel has experienced shoreline recession, particularly along the north-south oriented oceanfront between 1st St and 6th St. To mitigate for this erosion, a beach nourishment project placed sand on the beach at four separate times from 1986 to 2000. An 800-ft-long north terminal groin was constructed in 1975 to trap sand from moving north along the shoreline. A 600-ft-long South Terminal Groin was constructed in 1986/87 to trap and hold fill sand on the southern end of Tybee Island. Erosion south of this groin required construction of two additional T-head Groins

and an L-head terminal groin further to the south in 1994 to retain sand at the very southern end of the island.

The purpose of this report is to evaluate the impact of deepening the Federal navigation project at Savannah Harbor. This chapter investigates the long-term trends at Savannah to place the deepening in perspective. The goals of this study are to assess the impact of the Savannah Harbor navigation project on the regional morphology and to quantify the influence of the navigation project on increased shoreline recession rates along Tybee Island. These will be evaluated through a combination of quantitative shoreline change analysis, volume change calculations, and hydro/sediment modeling. A review of aspects of the ATM (2001) report is included in this effort based on critical comments of the review of that document.

For the Savannah Harbor Channel, data available prior to the date of construction (1874) based on early National Oceanic and Atmospheric Administration (NOAA) National Ocean Survey (NOS) topographic (known as T sheets) and hydrographic surveys (known as H sheets) are likely to have a higher degree of error, inherent with early survey data. Therefore, the determination of regional shoreline change trends over the lifetime of the project was done to minimize errors in the volume change analyses. Regional trends will allow comparison of shoreline change over contemporary time periods during which coastal processes are similar.

Shoreline Change Analysis

Shorelines were acquired from various sources to evaluate the shoreline change history of both Tybee Island on the Georgia side of Savannah River Entrance and the three islands on the South Carolina side of the entrance. Table 2-1 summarizes the mean high water (MHW) shorelines that were used in this study and the sources of the data. All of the early data were digitized field surveys from NOAA T sheets. The USACE Savannah District (SAS) supplied some of the data from their digital files from the NOAA T sheets. Some of the shorelines were digitized by Coastal Carolina University from paper maps from a joint NOAA/CERC (Coastal Engineering Research Center) shoreline movement study covering Tybee Island Georgia to Cape Fear, North Carolina (Anders et al. 1990). These shorelines were compiled by NOAA from field survey T sheets and the 1982 shoreline was from aerial photography and is archived at the USACE Coastal and Hydraulics Laboratory (CHL). The US Geological Survey (USGS) has completed a study on long-term shoreline change along the Southeast Atlantic coast using four shoreline periods to calculate change rates (Miller, Morton and Sallinger 2005). This analysis used the NOAA/CERC shorelines from 1863, 1920 (South Carolina beaches only) and 1963 shorelines, and NOAA T-sheets from 1925 for Georgia beaches (Tybee Island). The 1999 Georgia and 2000 South Carolina shorelines were derived from LIDAR surveys conducted by the USGS. The Savannah District supplied a set of beach profiles surveyed in February 2005. The MHW shoreline was derived from the MHW elevation (3.07 ft above NAVD88) on each profile based on the NOAA tide station 8670870 at Ft Pulaski, located on Cockspur Island at the mouth of the Savannah River and contoured using ArcView GIS software. A digital aerial photograph flown in October 2005, with a resolution of 1 ft, was supplied by Wilber Wiggins of SAS. A visual shoreline was digitized off the high-resolution air photo in the GIS using the local high water mark visible on the air photo.

Table 2-1. Historic Shorelines used in report

Date	Georgia	Source	South Carolina	Source
1854	x	SAS	x	SAS
1863	x	USGS NOAA/CERC	x	USGS NOAA/CERC
1900	x	SAS		
1920	x	SAS	x	SAS/USGS
1925	x	USGS		
1964	x	NOAA/CERC	x	USGS NOAA/CERC
1970			x	NOAA/CERC
1971	x	USGS		
1982/84			x	NOAA
1992		NOAA		
1993	x	SAS	x	SAS
1997	x	SAS	x	SAS
1999	x	USGS LIDAR		
2000			x	USGS LIDAR
2005	Profiles-Feb Air Photo Oct	SAS		

The historical shoreline positions generated for this study for Tybee Island are shown in Figure 2-3. A distinct change in shoreline orientation can be seen between the 1863 shoreline and the 1900 shoreline. A bulge in the northern Tybee shoreline present in the 1854 and 1863 shoreline was removed by the 1900 shoreline. This bulge was also present on an 1867 NOAA nautical chart. The loss of this large volume of sand was most likely due to the jetty construction (1886-1896, Sargent 1988). The island grew southward at its southern tip and accreted seaward south of the budge at the same time as the ocean shoreline was reorienting itself. The northern end of the island also expanded to the north and west. A more detailed look at the shoreline change over time is illustrated in Figure 2-4 which shows the historical shoreline position change at the north end of the island. The general trend is for the north tip of Tybee Island to migrate northward into the southern channel of the Savannah River and also to progressively move westward over time.

The central portion of Tybee Island has shown erosion of the bulge between 1867 and 1900 with a movement of sand both north and south and accretion to the north and south of the area formerly occupying the bulge. A hot spot is located between 1st and 6th Streets where the shoreline has rotated around a nodal point in the vicinity of 2nd Street (Figure 2-5). South of the nodal point the shoreline has moved seaward over time. The southern part of the island has grown to the south and seaward over the historic period with the most change taking place between 1863 and 1900 (Figure 2-6).

Shore protection efforts that affected the shoreline position are summarized in Table 2-2. Numerous seawall and groin structures were constructed from 1912 to 1941 to protect the upland from erosion. Figure 4-5 in the ATM report identifies the locations of these historic seawall and groins along the Tybee Island shoreline. In 1976 the North Terminal Groin was constructed and a 2.2 mil cy beach fill was placed on the beachfront from the groin south to 18th Street (Figure 2-7). The South Terminal Groin was constructed in 1986-87 and the North Terminal Groin was rehabilitated. A second 1.2 mil cy fill was placed on the beach between the two terminal groins at that time as well as placement of 0.157 mil cy of fill to the south of the South Terminal Groin. Fill material was placed between the North Terminal Groin and 3rd Street in 1993 to mitigate for the hot spot erosion. Erosion persisted at the south end of the island so two T-Head Groins and a

L-Head groin were constructed in 1994 south of the South Terminal Groin to help retain sand. In 1995, 285,000 cy of fill was placed on the southern end of the island between 13th Street and the South Terminal Groin and 50,000 cy of fill was placed between that Groin and the L-Head groin. Another 1.5 mil cy of fill was placed between the two Terminal Groins in 2000, with an additional 0.2 mil cy of fill placed between the South Terminal Groin and the L-Head Groin on the south end.

Table 2-2. Navigation and Shoreline Erosion Control Efforts, Tybee Island Vicinity

Date	Construction
1874	Initial dredging of navigation channel to 21.5 ft mlw
1886-1896	Construction of North and South Jetties at entrance to Savannah R.
1897	Construction of submerged offshore Breakwater at Tybee Roads
1912	Construction of steel pile old seawall 1st St vicinity
1915	Navigation channel deepened to 26 ft mlw
1928	Construction of wood groins along beach
1930	Construction of 2 groins along Ft Screven beachfront
1931	Construction of 3 additional groins along Ft Screven beachfront
1936	Construction of wood groins by WPA along beachfront
	Navigation channel deepened to 30 ft mlw
1937	Construction of wood groins by WPA along beachfront
1938	Construction of wood groins by WPA along beachfront
1939	Construction of wood groins by WPA along beachfront
1940	Construction of wood groins by WPA along beachfront
	Construction of concrete bulkhead (seawall) along ocean front.
1941	Construction of wood groins by WPA along beachfront
1945	Navigation channel deepened to 36 ft mlw
1964	Placed riprap in front of seawall
1972	Navigation channel deepened to 40 ft mlw
1975-1976	Construction of 800 ft long North Terminal Groin
	2.2 mil cy beach fill placed between North Terminal Groin and 18th St.
1986-1987	600 ft South Terminal Groin constructed
	North Terminal Groin rehabilitated
	1.2 mil cy fill placed between groins
	0.157 mil cy fill placed south of South Terminal Groin
1993-1994	1.5 mil cy Fill placed North Terminal Groin to 3rd St.
	Navigation channel deepened to 44 ft mlw
	South Beach 2 T-Head Groins and 1 L-Head Groin constructed
1995	0.282 mil cy fill placed between 13th St. and South Terminal Groin
	0.05 mil cy fill placed between South Terminal Groin and L-Head Groin
2000	1.5 mil cy fill placed between Terminal groins
	0.2 mil cy fill placed between South Terminal Groin and L-Head Groin

Source: Oertel et al. 1985, Savannah District

The historical shoreline positions for the three islands in South Carolina are shown in Figure 2-8. The general trend is for erosion of Turtle Island marsh-like open coast shoreline with steady landward retreat of the shoreline. The shoreline has moved to the south into Wright River entrance. Turtle Island is composed of mostly fine grained material typical of a marsh shoreline with little sandy open beach material. Early charts show that this has been the case since the

1850's. Daufuskie Island has also exhibited landward retreat over time, but this island has a narrow sandy beachfront more typical of an open coast barrier island shore. A private beach nourishment project placed 1.4 mil cy of sand along the island in 1998 (ATM 2001). Across Calibogue Sound entrance, the southern end of Hilton Head Island has shown accretion of the shoreline over the study period. Erosion of the northern end of Hilton Head Island required beach fills in 1980 of 550,000 cy, 1982 of 800,000 cy of fill and 1990 of 2 mil cy (Valverde et al. 1999). Drift is to the south along this island as indicated by the growth of the south end of the island to the south.

Bathymetry Change Analysis

Historic bathymetry was collected from several sources. ATM supplied bathymetry used in their report which already contained corrections for sea level rise and a correction for each data set to the NGVD 29 vertical datum. Additional historic bathymetric data sets were collected from NOAA's GEODAS database of NOS hydrographic surveys of coastal waters in the study area and were referenced either to mlw or mllw depending on date of collection. The Savannah District supplied before and after dredging surveys, as well as examination surveys of the navigation channel and a February 2005 beach and nearshore survey. Table 2-3 summarizes the historic bathymetric data sets used in this study. All data was converted to a common datum of NAVD88 meters vertical datum and latitude/longitude NAD83 horizontal datum to allow comparisons and change analysis.

The first bathymetric data set available was collected in 1854. Figure 2-9 shows the orientation of the pre-project nearshore bathymetry and natural channel orientations of the Calibogue Sound, New River, Wright River and Savannah River entrances. The Calibogue Sound bisects into two channels with a small marginal flood channel next to Hilton Head Island. The New River channel is oriented to the south. The Wright River and the Savannah River and South Channel all converge on one main channel in the vicinity of Tybee Roads. Figure 2-10 shows the 1897 bathymetry just after completion of jetty construction in 1896 at the entrance to the Savannah River and the 1897 submerged breakwater. The breakwater was constructed at the landward edge of the southern limit of Barrett Shoals (Figure 2-1). Due to the short time frame after construction, these structures may not have had time to fully affect the bathymetry. The survey is limited in area but shows the South Channel and hints at the fact that the bulge still exists on the north end of Tybee Island and that the three channels of the Wright and Savannah Rivers still converge in Tybee Roads. The 1920 bathymetry is shown in Figure 2-11 and is also limited in area coverage. Calibogue Sound channel has migrated to the south and has its distal limits controlled by the submerged breakwater which deflects the channel to the east. The jetties at the Savannah River Entrance have caused the main navigation channel to be the main channel with the South Channel shoaling in as the north end of Tybee Island eroded back and to the north and south along the shoreline. The 1920 shoreline shows a spit growing into the area formally occupied by the South Channel. The 1920 bathymetry shows deflation of the north Tybee Shelf region along the south edge of the channel and accumulation in the North Tybee Shoal. These trends are consistent with the sediment modeling in Chapter 5. The 1930/31 data set was limited just to the mouth of the Savannah River and was not used in this report due to its small area of coverage. The 1970/83 bathymetry is shown in Figure 2-12 and is a combination of several early 1970's NOAA NOS surveys that has a wide area of coverage. A 1980/83 survey was used to increase the coverage area to the south. This survey best represents the post construction area bathymetry. The dredged channel is seen as well established at this time and extends from the jetty out to the nearshore shelf. The channel is maintained to 12 m (40 ft) mlw at this time. The New River entrance channel has migrated northward and the Calibogue Sound Channel has migrated back to the north, leaving behind a cut off channel just north of the submerged breakwater. The North Tybee Shoal continues to grow, with accumulation north of the South

Table 2-3. Historic Bathymetry Data Sets

Date	Source	Original Data	Vertical Conversion	Horizontal Conversion	Remarks
Hydrographic Survey					
1854	ATM	NOAA - H439	convert from NGVD29 to NAVD88	Ga State Plane East to Lat/Lon NAD83	ATM applied original conversions
1897	ATM	NOAA - H2296	convert from NAVD29 to NGVD88	Ga State Plane East to Lat/Lon NAD83	
1920	ATM	NOAA - H4154	convert from NAVD29 to NGVD88	Ga State Plane East to Lat/Lon NAD83	
1931-34	NOAA-GEODAS	H05134 – 03601015 1931	convert from mlw to NAVD88		Covers Savannah River Entrance area only not used
		H05549 - 03F11077 1934	convert from mlw to NAVD88		
		H05592 - 03F11085 1934	convert from mlw to NAVD88		
		H05599 - 03F11088 1934	convert from mlw to NAVD88		
		H05571 - 03F11218 1934	convert from mlw to NAVD88		
		H09197 - 03F12061 1971-73	convert from mlw to NAVD88		
1970-83	NOAA-GEODAS	H09314 - 03081138 1973	convert from mlw to NAVD88		
		H09144 - 03081139 1973	convert from mlw to NAVD88		
		H09459 - 03F12085 1974	convert from mlw to NAVD88		
		H09865 - 03141047 1980	convert from mllw to NAVD88		
		H10577 - 03081184	convert from mllw to NAVD88		
		H10582 - 03081186	convert from mllw to NAVD88		
1994-95	NOAA-GEODAS	H10591 - 03081187	convert from mllw to NAVD88		
		H10629 - 03081195	convert from mllw to NAVD88		
		H10631 - 03081197	convert from mllw to NAVD88		
Channel Surveys only					
17-18 Dec 1998	SAS	bd_99.xyz	convert from mlw to NAVD88	Ga State Plane East to Lat/Lon NAD83	Before Dredge
Jan, Feb, Apr 1999		ad-99.xyz	convert from mlw to NAVD88	Ga State Plane East to Lat/Lon NAD83	After Dredge
Jan, Feb 2000		bd_00.xyz	convert from mlw to NAVD88	Ga State Plane East to Lat/Lon NAD83	Before Dredge
Sep-05		exam-savhbar-sept2005.xyz	convert from mllw to NAVD88	Ga State Plane East to Lat/Lon NAD83	Exam survey
Profile Surveys					
Feb-05	SAS	tybee-feb2005land.xyz profiles	convert from mllw to NAVD88	Ga State Plane East to Lat/Lon NAD83	Land survey
		tybee-feb2005-1.xyz profiles	convert from mllw to NAVD88	Ga State Plane East to Lat/Lon NAD83	Boat survey

Channel. Figure 2-13 shows more recent bathymetric surveys from the 1993/94 time frame, but is limited in coverage to the southern portion of the study area. The material dredged from the channel and deposited in the Offshore Dredge Material Disposal Site (ODMDS) can be seen in shoals in that area. The channel is maintained at 13 m (44 ft) mlw at this time.

The only recent surveys available for this study consist of before and after dredge and examination surveys of the navigation channel itself. Figures 2-14 to 2-16 are a series of surveys of just the channel from 1989 (before dredge), 1999 (after dredge) and 2000 (before dredge) that show that the dredging requires removal of a small area on the south side of the channel just off Tybee island and to the east side of the channel on the southern end of the channel as it passes the lower end of Barrett Shoals. A survey consisting of beach and nearshore boat surveys along designated profiles was conducted in February 2005 along Tybee Island. That survey is limited to the nearshore area but shows the condition of the beach and nearshore at 5 years after the most recent beach nourishment placement (Figure 2-17). An exam survey was conducted in September of 2005 of the navigation channel again showing the tip of the North Tybee Shoal encroaching on the channel just off the jetties and the encroachment of the southern tip of Barrett Shoals on the southern area of the channel. These appear to be the dominant areas where sediment enters the channel.

Sediment Budget and Volume Changes

This analysis was limited to the 1854 pre-project bathymetry coverage, the 1920 survey, and a composite of 1970 to 1974 and 1980 to 1983 bathymetry. The early data were collected by NOAA NOS's predecessor the U.S. Coast and Geodetic Service (USC&GS) using lead line. The accuracy of the surveys is the best of that day. No standard datums were available at that time. The data were transformed by ATM (2001) to the standard vertical datum of NGVD 1929 and a horizontal datum of Georgia State Plane East Zone. This transformation also included sea level corrections. The data was further transformed to the present NAVD 1988 datum by CHL using ArcView software. The 1970 data was collected at a datum of mlw. NOAA switched to a vertical datum of mllw around 1980. The data were converted to a common datum of NAVD88 using the ArcView software. Table 2-4 shows the correction factors used based on the NOAA tidal gauge elevation information. The conversion from NGVD 29 to NAVD88 was 0.29 m (0.96 ft). Each of these conversions has the potential to add uncertainty to the analysis, but care was taken to bring all of the data into a common horizontal and vertical datum for analysis.

Table 2-4. Elevatioin Information for NOAA Tide Gauge Station 8670870
Referenced to 1983-2001 tidal Epoch

Tidal Datum	mllw	NGVD29	NAVD88
Mean Higher High Water - MHHW	2.29 m (7.50 ft)	1.34 m (4.4 ft)	1.05 m (3.44 ft)
Mean High Water - MHW	2.17 m (7.13 ft)	1.23 m (4.03 ft)	0.94 m (3.07 ft)
North American Vertical Datum - NAVD88	1.24 m (4.06 ft)	0.29 m (0.96 ft)	0
Mean tide Level - MTL	1.12 m (3.67 ft)	0.17 m (0.57 ft)	-0.12 m (-0.39 ft)
National Geodetic Vertical Datum - NGVD29	0.95 m (3.1 ft)	0	-0.29 m (-0.96 ft)
Mean Low Water - MLW	0.07 m (0.22 ft)	-0.88 m (-2.88 ft)	-1.17 m (-3.48 ft)
Mean Lower Low Water - MLLW	0	-0.95 m (-3.10 ft)	-1.24 m (-4.06 ft)

In order to understand the impact of the Federal navigation channel has had on the Savannah River Entrance, area a comparison was made between the conditions that existed before any channel improvements were done to conditions that exist after dredging to deepen and widen the channel and construction of navigation improvement structures. The project was initiated with

dredging of the channel in 1874 and had been deepened five times from 3.8 m (21.5 ft) to the present 13.4 m (44 ft) mlw (Table 2-5). Each time the channel was deepened or widened new dredging was initiated and required removal of larger quantities of sediment from the channel (Figure 2-2). Almost annual maintenance has been required to keep the channel at the design depth (Figure 2-2). Most of the sediment was placed on the ODMDS, except for a beach fill in 1993/94 where the dredged channel material was placed on the beach.

The study has been hampered by lack of good coverage both spatially and temporally of historic shoreline position, bathymetry, multiple dredging records and storm climatology. There is only one good bathymetric survey in 1854 before the project was initiated. This data set was surveyed before a standard national vertical datum was established. ATM (2001) has done the calculations to correct to the NGVD 1929 datum and this present study has adjusted to the new NAVD 1988 datum. They also have corrected for sea level rise.

Difference maps were constructed using the ArcView GIS software to assess the changes in bathymetry between surveys. Figure 2-18 shows the change between the pre-project 1854 and the immediate post construction of the two navigation jetties and the offshore submerged breakwater surveyed in 1897. The 1897 survey was limited in coverage so the difference map was limited to the smallest common area between the two surveys. Areas of loss of bed elevation are shown in red and gain in bottom elevations are shown in green. The channel centerlines show the change in orientation of the several channels over the time period. The main change was the reorientation of the channels at the entrance of Savannah River, Wright River, and New River from four channels that merged into one to two channels due to the construction of the two jetties at the mouth of the main channel of the Savannah River in 1896. The channel complex exiting Calibogue Sound has four distinct channel branches trending off the main channel to the east in 1854. The limited coverage of the 1897 data does not cover all of the channels but the general trend is for movement to the south. Loss of sediment was measured in Calibogue Sound entrance channel and in most of the channels in the vicinity of Tybee Roads. Gain of sediment was measured at the submerged breakwater at the southern end of Barrett Shoals and on the north tip of Tybee Island where the channel exiting the South Channel was moved further north. Further deflation is seen on the north portion of the Tybee Island Shelf and accumulation on the North Tybee Shoal. Both the digital 1854 and 1863 shorelines show the bulge on the north end of Tybee Island. No shorelines exist between a chart of 1873 and 1900 to pinpoint when the bulge began to erode away.

From 1897 to 1920 the four channels of the Calibogue Sound entrance remain but move further southward (Figure 2-19). Accretion of the bed is found in the lee of the submerged breakwater on the north end of Tybee Roads. The shoreline bulge of north Tybee Island has eroded and the shoreline spit has formed on the north end of the island. Accretion is also present in the north part of the North Tybee Shoal area. The growth of the shoal and spit along the shoreline has deflected the South Channel to the north to merge with the main navigation channel of the Savannah River. The north portion of the Tybee Island Shelf continues to deflate, and it appears the sediment is moving to the northwest, toward the North Tybee Shoal (which is consistent with the sediment transport modeling presented in Chapter 5). The New River Channel also meets with the main channel just seaward of the jetty tips. There is general loss of sediment on the bed on the rest of the shelf area. From 1920 to 1970/83 there is a general southward shift in the individual east-west channels coming off the Calibogue Sound entrance (Figure 2-20). The 1920 channel locations have filled in and a new channel has eroded sediment south of each for the four channels. The southernmost channel has moved south and is now deflected to the east by the submerged breakwater. The southern tip of Barrett Shoals is now accreting (consistent with sediment transport modeling results). The New River entrance channel has migrated to the north and is now detached from the main Savannah River navigation Channel.

Table 2-5. Bar Channel Dredging

Year	Channel Depth (ft-MLW)	New Dredging Vol. (cy)	Maint Dredging Vol (cy) Multiple Source
1910	21.50		1,640,000
1915	26.00		667,000
1921	26.00		565,000
1922	26.00		156,690
1923	26.00		270,200
1924	26.00		1,142,197
1925	26.00		322,794
1926	26.00		502,244
1927	26.00		217,000
1928	26.00		716,727
1930	26.00	2,470,490	
1931	26.00	NO	NO
1944	30.00	DATA	DATA
1945	36.00	BETWEEN 1931-1945	BETWEEN 1931-1945
1946	36.00		2,380,977
1947	36.00		695,709
1948	36.00	671,350	
1950	36.00	2,830,694	
1951	36.00		2,864,450
1953	36.00		916,454
1954	36.00		667,330
1956	36.00		450,636
1957	36.00		1,826,336
1958	36.00		202,234
1959	36.00		66,752
1961	36.00		1,368,231
1962	36.00		1,414,182
1963	36.00		1,339,289
1964	36.00		903,051
1965	36.00		655,518
1966	36.00		879,518
1968	36.00		458,430
1969	36.00		401,814
1970	36.00		677,949
1971	36.00		582,442
1972	40.00	3,469,633	489,687
1973	40.00	2,151,664	771,923
1974	40.00	1,146,262	1,415,731
1975	40.00	1,146,262	96,503
1976	40.00	979,235	1,066,024
1977	40.00	1,806,359	2,811,201
1978	40.00	988,500	2,763,715
1980	40.00		471,064
1981	40.00		865,736
1982	40.00		188,266
1983	40.00		644,940
1984	40.00		789,754

Table 2-5. (*continued*) Bar Channel Dredging

1985	40.00		1,212,478
1986	40.00		1,166,528
1989	40.00		442,414
1990	40.00		600,000
1991	40.00		1,104,991
1993	40.00		554,707
1994	44.00	2,454,441	
1995	44.00		1,993,061
1996	44.00		486,108
1997	44.00		544,508
1998	44.00		548,044
1999	44.00		508,885
2000	44.00		1,217,300
2001	44.00		1,117,856
2002	44.00		186,537
2003	44.00		635,163
2004	44.00		620,642
2005	44.00		888,101

Notes: Maintenance Dredging data sources are:
Annual Reports data in black, Dredging Records data in green, and Recent SAS Data in blue

There is a gain in sediment in the old 1920 New River channel and erosion of the bed in the new orientation, as well as a gain in sediment deposition at the mouth of that new channel. The spit on north Tybee Island has eroded and the South Channel is now next to the island. The main navigation channel has migrated northward out from between the jetties and the old channel has filled in due to the northwest movement of sediment and accumulation in the North Tybee Shoal. The pattern of deflation continues on the Tybee Island Shelf and the southern portion of the North Tybee Shoal. There is general loss of sediment on the Tybee Island shelf platform in front of the island.

The long-term change in the bathymetry from the 1854 pre-project bathymetry to the more modern 1970/83 bathymetry shows a trend of southward channel migration of the four channels of the Calibogue Sound entrance channel with erosion in the present location of the centerlines and a filling in of the older channel locations (Figure 2-21). All of the channels from Calibogue Sound are now north of the submerged breakwater. The New River entrance channel has migrated northward and filled in the old channel orientation. The south end of Barrett Shoals has gained sediment on its southern tip just north of the navigation channel. This is the area where dredging is the greatest. The dredging of the main navigation channel has removed sediment from that area. The green areas in Figure 2-21 adjacent to the channel are areas where the dredging requirement is greatest at present. The large change in the Tybee Island shoreline and removal of the bulge has resulted in gain of sediment on the North Tybee Shoal as the South Channel and main navigation channel of the Savannah River have moved slightly to the north. The remainder of the Tybee Island Shelf has lost sediment.

An update to the change in bathymetry was added to this report by adding the change in the bathymetry reflected by the 1994 NOAA bathymetry. Unfortunately the coverage is limited to the southern portion of the study area (Figure 2-22). The seaward end of the navigation channel shows the effects of dredging with a loss of sediment in the channel. The gain in sediment in the

ODMDS area can be seen where most of the dredge material was placed. The rest of the shelf platform area shows little change to slight loss of elevation.

The available newer bathymetry is limited to surveys of the navigation channel. A comparison of the before- to after-dredge surveys of 1998 and 1999 are shown in Figure 2-23, where there is a slight gain in sand on the northern end of the Tybee Knoll Bar Channel and at the western end of the Tybee Roads Bar Channel. A loss of sediment was found in the central part of the Tybee Roads Bar Channel, which is most likely due to the dredging. Between the after 1999 dredging and the before 2000 dredging the difference plot shows a gain of sediment in the Tybee Roads Bar Channel where the southern tip of Barrett Shoals abuts the channel (Figure 2-24). A gain in sediment along the southern side of Tybee Knoll Bar Channel indicated that sediment is moving into the channel from the south along the North Tybee Shoal platform. Erosion of the north side of the channel is evident, probably in response to North Tybee Shoal accumulation. A longer term change between 2000 and 2005 indicate that the channel has been dredged for the most part except for the lower end of the Tybee Roads Bar Channel which has shown accretion (Figure 2-25). This accretion indicates that the southern tip of Barrett Shoals is a source of sediment to fill in the channel as sand moves southward and westward across the shoal. Accretion in the channel is also evident due to encroachment of the North Tybee Shoal. A comparison of the beach and nearshore survey in February 2005 with the 1970/83 survey along the Tybee Island beachfront shows accretion of the nearshore reflecting the four beach nourishment placements since 1975. The nearshore on the north end of the island shows accretion indicating northward transport of fill from the hot spot around 2nd Street. That area shows a net loss of sediment in the nearshore. A slight gain in sand is found on the shelf along the central part of the island where the shoreline orientation changes from north/south to more northeast/southwest. Accretion is also shown at the southern end of the island where sediment is transported southward onto the ebb shoal of Tybee Creek Inlet.

Storms are an important force in transport of sediment and the formation/evolution of coastal morphology. Table 2-6 (see end of chapter) lists all tropical storms that have come within 200 miles of Tybee Island since 1851. This data was downloaded from the NOAA Coastal Services Center and contained a GIS database of all tropical storms from 1851 to 2002. Data for 2003 to 2005 was downloaded from the National Weather Service and transformed into GIS compatible data. Figure 2-26 shows the occurrence of these tropical storms by year. There were several active tropical storm seasons with more than three storms per season. This analysis does not include extratropical storms so there may be more storms than listed that could have affected the Tybee Island area. The period between 1872 and 1916 was active with several years having multiple occurrences of storms. There may be some correlation between the change in the bulge in the north Tybee Island shoreline and the number of storms that occurred during this time period.

The USGS has recently completed a study of the long-term change in shoreline position along the southeastern US East Coast from North Carolina to Florida (Miller et al. 2005). Long-term rates of shoreline change, in units of m/yr, were calculated at 50-m transect spacing using linear regression applied to shoreline positions from the earliest (1863) to the most recent (1999/2000). Linear regression was selected because it has been shown to be the most statistically robust quantitative method when a limited number of shorelines are available and it is the most commonly applied statistical technique for expressing shoreline movement and estimating rates of change. Uncertainties for the long-term rates are also reported in units of m/yr and represent a 90 percent confidence interval for the slope of the regression line. This means with 90 percent statistical confidence that the true rate of shoreline change falls within the range of ±0.01 to 5.5 m/yr depending on location (Miller et al. 2005). One of their calculations was to measure the rate of change in shoreline movement from their first shoreline data set to their most recent LIDAR

derived shoreline. In the case of the Tybee Island area, the shorelines were the 1863 to 1999 in Georgia and 2000 in South Carolina which include the effects of the beach fills. Figure 2-27 shows a graphic of the rate of change in m/yr for the barrier islands in the study area over this 162-163 year period. These long-term rates are similar to rates measured on a few points between the 1854 and 1971 shorelines in this study to provide consistent dates between the bathymetric data and shoreline data. The USGS rate of change data are representative of the study period and will be used even though the dates are different from the bathymetry change period of 1854 to 1970/83.

Data for Hilton Head Island shows that the center portion of the island is either stable (± 0.5 m/yr in yellow bands, Figure 2-27) or eroding at a rate of -0.5 to -2 m/yr (light red bands). The south end of the island is growing around +0.5 to +2 m/yr (light green) and +2 to +4 m/yr (dark green) as the island shoreline progresses southward. The maximum seaward movement was +4.2 m/yr at the tip of the island. In spite of the beach fill on Daufuskie Island in 1998, the long-term trend is for erosion along the entire length of the island. Rates range from either -0.5 to -2 m/yr (light red) or -2m to 4 m/yr (dark red) with a maximum landward retreat of -2.1 m/yr. Turtle Island is eroding up to -3 m/yr except for the southern end that has migrated into the Wright River inlet at a rate of up to +3.8 m/yr. The long-term shoreline change rate for Tybee Island reflects the erosion of the bulge on the north end with erosion of the shoreline from the North Terminal Groin southward in this area. The USGS analysis does not extend to the north of the North Terminal Groin due to the truncated position of the 1863 shoreline. The later shorelines visually show a gain as the spit and later shorelines extend to the north. The erosion rate in the area of the hot spot between 1st and 6th Streets is up to -3.6 m /yr. The nodal point around 2nd Street remains stable as the shoreline erodes to the north and accretes to the south of that area. The area south of the nodal point has shown accretion of up to +1.6 m/yr from 1863 to 1999, which included all but the last beach fill period. The USGS data stops at the South Terminal Groin since the 1863 shoreline terminates at that point. The later shorelines have migrated to the south and the southern part of the island has grown to the south. The South Terminal Groin and the two T-Head groins and terminal L-Head groin as well as the beach fills have stabilized this southern portion of the island. The construction of the jetties at the mouth of the Savannah River Entrance and initial dredging corresponds with the loss of the bulge on Tybee Island. Possible new flow patterns as a result of the jetties would confine the flow between the jetties and have higher velocities that would move the channel further seaward. The Tybee island shoreline responded by moving north and south of the nodal point. This may be an indication that the tidal flow patterns changed at the entrance and the shoreline responded to these flow pattern changes. A summary of the changes to the channels from the river entrances show that the channel centerlines have migrated south over the study period (except New River, which has migrated north). Figure 2-28 shows the positions of the channel centerlines mapped from the pre-project 1854 bathymetry. The location of the seaward end of all of the channels have migrated to the south in all cases by the 1920 time period after the initial dredging and construction of the jetties and breakwater. By the 1970's the Savannah River entrance navigation channel was dredged and fixed in its present location. All of the other channels have continued to migrate southward except for the New River entrance channel which has migrated northward. There are four identified channels trending to the east from the Calibogue Sound entrance through most of its history. These channels migrate to the south consistent with net movement of sediment to the south along Barrett Shoals. By the1970's an additional channel had formed. Beginning in the north, the marginal flood channel that is adjacent to the southern shoreline of Hilton Head Island has moved to the south as the island has migrated in that direction. The southern most channel of that group has been controlled by the location of the submerged breakwater, limiting the southern movement. The main navigation channel of the Savannah River entrance has moved north in the Tybee Knoll range as the jetties have controlled this part of the channel location. The channel

from the South Channel has also migrated northward as sand has accumulated in the Tybee Shoal and Tybee Island has migrated northward, consistent with northward movement of sand at north Tybee due to changing tidal flow patterns reshaping the nearshore in front of Tybee Island.

The general trends in morphologic change in the nearshore can be illustrated with the change in the -5 m (-16.4 ft) depth contour. The general trends in shoreline evolution can be illustrated by the change in the shoreline position of the 1854 and 1971 shorelines (represented by the brown arrows in Figure 2-29). The black arrows show the trends in bathymetric change from the pre-project 1854 bathymetry and present day configuration illustrated by the 1970/83. The shelf in front of Hilton Head Island shows a landward movement. The channels trending eastward from the main Calibogue Sound channel have also migrated south. The New River Channel has migrated northward on the Daufuskie/Turtle Island platform area but otherwise that platform has had little change. The -5 m contour on the shelf platform in front of Tybee Island has migrated toward the shore and southwest, while the North Tybee Shoal has grown to the north. Of interest is the fact that the -10 m (-32.8 ft) contour has remained relatively stable over this same time period. The shoreline of the southern end of Hilton Head has grown to the south. The shorelines of Daufuskie and Turtle Islands have retreated landward and in the case of Turtle Island have also moved to the south. The shoreline of Cockspur Island has also retreated landward. The ends of Tybee Island have migrated both north and south of the hot spot nodal point as the bulge has retreated landward somewhere between the 1870's and 1900.

Based on bathymetric change patterns and distinct morphologic characteristics, eight morphologic areas have been identified to calculate volume changes for the study area. Figure 2-30 shows the boundaries of each of these areas. The largest of these areas is Barrett Shoals, which is composed of several channels trending eastward with adjacent shoals that are related with the Calibogue Sound entrance channel. The main thalweg of the Sound is also identified as a separate area. The shallow platform in front of Daufuskie and Turtle Islands is also identified as an area of shoals and the thalweg of the New River entrance channel. The main navigation channel of the Savannah River is divided into the more east/west Tybee Knolls Bar Channel and the more northwest/southeast trending Tybee Roads Bar Channel. The area on the north side of these bar channels has been called the Breakwater Lee Shoal area in the lee of the submerged breakwater area of Tybee Roads and is composed of shoals outside of the dredged channel. The shallow shelf platform in front of Tybee Island has been divided into two sections: the North Tybee Shoal and the Tybee Island shelf based on the change in shoal configuration and depth contours over the study period.

An analysis of the difference in depths between the 1854 bathymetry and the 1970/83 bathymetry was done using ArcView Spatial Analysis. The differences at specific grid points spaced 7.6 m (25 ft) apart were summed for each area shown in Figure 2-30 and divided by the number of years between the surveys to produce an average rate of change for each morphologic area. Figure 2-31 shows the results of this analysis. The Barrett Shoals area has lost only 4,200 m^3/yr (essentially zero volume loss) as the southward shifting channels fill in the old channel locations. The Calibogue Sound channel has a net loss rate of 40,000 m^3/yr as the channel has deepened and elongated to the south. The Daufuskie/Turtle Islands shelf platform has gained +5,200 m^3/yr (essentially zero volume) as sediment is eroded off the beaches of the two islands and the shift in New River entrance channel orientation to the north has filled in the old channel as the newer channel is cut. The Breakwater Lee Shoal area has gained around 11,500 m^3/yr of sediment as sediment has possibly been added from all adjacent areas. Both the Tybee Knoll Bar Channel and the Tybee Roads Bar channel have been dredged on a near annual basis and from the period of 1854 to 1970/83 a net loss of sediment was measured in both areas (-119,800 m^3/yr for Tybee Knoll Bar Channel and -100,000 m^3/yr for Tybee Roads Bar Channel for a total of 219,800 m^3/yr). That material was for the most part disposed of in the ODMDS during the dates of this

analysis. The ODMDS was outside the limits of the 1854 bathymetry so no measurement of change could be made from the difference analysis. Dredging records indicate some 40 million m^3 was removed from both bar channels between 1910 and 1979 (note that dredging records in Table 2-5 is in cubic yards). The difference between the net volume changes in the channels and the dredging volume is an indication of the sediment input from the North Tybee Shoal and Barrett Shoals, but the dredging records are incomplete over the full time period. The North Tybee shoal area has gained 99,800 m^3/yr of sediment with the erosion of the bulge on Tybee Island and the reorientation of the South Channel. Tidal flows also indicate that material is carried into that area on flood tide. The shoal platform in front of Tybee Island has a net loss rate of 219,000 m^3/yr. This net loss corresponds to the -5 m depth contour migration inland and to the south. Table 2-7 provides a summary of the volume changes for 1854 to 1970/83 and rates calculated for 1920 to 1970/83. The 1920 to 1970/83 rates provide some idea of change in rates over time following initial construction of the navigation project. The deflation on the Tybee Island Shelf appears to be slowing, while Barrett Shoals is growing at an increased rate. The Breakwater Lee Shoal area remains relatively stable.

The accuracy of the early surveys was less that present day results and were taken with lead line, but the data represents the best available data. The more recent bathymetric surveys were taken by digital echosounder to a class three hydrographic survey standards. The shoreline change analysis done by the USGS (Miller et al. 2005) indicated that the 1863 shoreline was digitized from NOAA USC&GS T-Sheets and the shoreline was based on plain table survey techniques to identify the MHW shoreline. The recent 1999/2000LIDAR surveys were identified by MHW tidal elevations based on the Cockspur Island NOAA tidal gauge. Uncertainties were estimated to show the significance of the volume change rates. The uncertainties are very high due to accuracy of the early surveys, and they indicate that even moderate volume changes may not be meaningful. Uncertainties assigned to the survey depths were 1 m for 1854, 0.5 m for 1920, and 0.3 m for 1970/83. These values are probably optimistic (Gibbs and Gelfenbaum 1999, Byrnes et al. 2002, Mills 2006 personal communication). Survey errors can be systematic or random (random error will tend to average out over volume calculations). Potential contributors to errors include use of lead line in early surveys (particularly in areas with a soft bottom), vertical reference, tide correction, horizontal reference, sea conditions, sampling, and interpolation. The uncertainty in depth change is estimated as root-mean-square of the errors is depth (depth change uncertainty = $((error_1)^2 + (error_2)^2)^{1/2}$), or approximately 1 m for 1854 to 1970/83 and 0.6 m for 1920 to 1970/83. The uncertainty in volume change is estimated as the difference between the total volume change over a region and the volume change calculated exceeding the uncertainty in depth change (Byrnes et al. 2002). These volume change uncertainties have been converted to rates in Table 2-7.

Table 2-7. Volume Change Summary by Area (see Figures 2-30 to 2-32)

Area	Volume Change Rate (1854 -1970/83) m^3/yr	Volume Change Rate (1920-1970/83) m^3/yr
Tybee Island Shelf 25 million m^3	-220,000 ± 26,000	-76,000 ± 3,000
North Tybee Shoal 7 mill m^3	+100,000 ± 6,000	+78,000 ± 2,000
Daufuskie/Turtle Island Shelf 29 mill m^3	+5,200 ± 12,000	+90,000 ± 7,000
Calibogue Sound Channel 5 mill m^3	-40,000 ± 3,000	+24,000 ± 4,000
Barrett Shoals 40 mill m^3	-4,200 ± 9,000	+150,000 ± 3,000
Breakwater Lee Shoal 5 mill m^3	+12,000 ± 1,000	-260 ± 1,000
Tybee Knoll Bar Channel 4 mill m^3	-120,000 ± 1,000	-74,000 ± 1,000
Tybee Roads Bar Channel 4 mill m^3	-100,000 ± 2,000	-91,000 ± 1,000
Uncertainty estimated using 1 m depth error for 1854 to 1970/86 and 0.6 m error for 1920 to 1970/86 (time = 122 or 56 yrs)		

The ATM (2001) study estimated the volume change of the Tybee subaqueous platform at -120,000 m^3/yr for the period 1920-1970/80 (their Table 8-5), slightly higher than the value in Table 2-7, but well within the range of confidence. The values in Table 2-7 are close to the ATM Tybee North Shoal rate of +58,000 m^3/yr and Barrett Shoals rate of +140,000 m^3/yr for the period 1920-1970/80.

While extending over a longer time period (1863 to 1999/2000), the USGS shoreline change analysis supports the bathymetric change patterns. The USGS data are shoreline position change rates in m/yr while the bathymetric analysis is measuring volume change in m^3/yr. Growth of the south end of Hilton Head Island indicated net longshore drift along the shoreline is to the south in this area. The long-term retreat of the MHW shoreline along Daufuskie and Turtle Islands and the gain in sediment in the Daufuskie/Turtle Island shelf platform indicates that the sediment (mostly fine sands and silts) are being eroded off the shoreline and deposited on the shelf in that area. Longshore transport rates were reported by ATM (2001). The Tybee Island shoreline change rates indicate that the nearshore net sediment transport is to the north from the nodal point north, which adds material into the North Tybee Island shoal area. South of the nodal point sediment is transported south along the beach and ending up on the ebb shoal of Tybee Creek Inlet.

A complete sediment budget was not produced due to lack of broad coverage for bathymetry, lack of multiple surveys pre-project to establish the baseline, and uncertainty in rates of some key pathways. A conceptual sediment pathway map was produced to indicate the probable movement of sediment between the areas within the study area (Figure 2-33). Details on the shoreline volume changes along the barrier islands were not part of the scope of this work. Southerly growth in Hilton Head Island provides input of sediment into the Barrett Shoals area due to the north east/southwest orientation of the island. Some sediment may be input into the Calibogue Sound Channel from the Sound itself. Little change in volume within the Barrett Shoal area indicates that sediment input is equal to output. Sediment flows into the Tybee Roads Bar Channel from this Shoal area based on bathymetric changes from before and

after dredging. The sediment dredged from the channel has mostly been placed on the ODMDS during the period of analysis. The north-south shoreline orientation of Tybee Island and the shoreline change patterns indicate that the sediment is being transported to the north and south of the nodal point in the very nearshore zone. The change in nearshore bathymetry from 1970/83 and 2005 indicate that this is the case. The North Tybee Shoal area is gaining sediment from the shoreline and some from the Tybee Island Shelf platform. Some of this material is likely to be transported into the Tybee Knoll Bar Channel. The Tybee Island Shelf is losing sediment to the northwest and southwest and is generally being deflated as little sediment is transported to the south over the Tybee Roads Bar Channel to replace material generally transported to the northwest and southwest the shelf.

Sediment Transport

The sediment grain size distributions shown in Figure 2-34 are from several sediment sampling efforts from 1981 to 1998 show that the typical sediment in this area is a fine sand with a mean grain size of 0.125 to 0.25 mm (2.0 to 3.0 phi). Very Fine sands (mean grain size of 0.0625 to 0.125 mm or 3.0 to 4.0 phi) were also common on the nearshore shelf and in the dredged Tybee Roads Bar Channel. Some coarse sediment (medium to coarse sands with mean grain sizes between 0.25 and 2 mm or 2.0 to -1.0 phi) was found in the Tybee Knolls Bar Channel and from the bed between the jetties. There areas have the highest tidal flows and would winnow out the finer grain sizes.

Impact Assessment

The sediment volume change analysis and modeling results were integrated to assess the impact of the Federal navigation channel to Savannah Harbor on sediment transport pathways in the Savannah Bight. Chapter 5 presents results of the GTRAN modeling. Limited shoreline position data and bathymetry from the time period of initial project construction in the years between 1874 and 1900 have limited the assessment of the most dramatic impact of the project dredging and jetty construction. Changes to the morphology on Tybee Island were compared with regional changes during a similar period of time beginning prior to construction (1854 to 1863) and ending with the present (1970/83 and additional partial surveys of the shoreline, shelf and channel up to 2005). The major change, the removal of the bulge on the north end of Tybee Island between 1863 and 1900, occurred as the channel was dredged and the jetties were placed. The jetties were constructed between 1886 and 1896 and the offshore submerged breakwater in 1897. It is suspected that the large change in measured shoreline position resulted from the modification of the entrance, but measurements are lacking between 1863 and 1900. This time period is also particularly active in terms of tropical storms (Table 2-5). From both morphologic and modeling data, the sediment lost from the oceanfront of North Tybee Island was transported northward into a spit that formed on the north end and on to the North Tybee Island Shoal. The deflection of the South Channel to the north into the main navigation channel of the Savannah River also allowed sediment to be deposited on the north shoal. The nodal point in longshore transport appears to be around 2nd Street. The material in the bulge was mainly north of that area and the transport is to the north of that point. South of that point the transport is to the south. The growth of the south end of Tybee Island and the growth of the ebb shoal of Tybee Creek Inlet support a southerly transport pattern south of the nodal point. The history of shore protection efforts (seawall and groin construction and placement of the four beach fills) indicated that it is difficult to maintain sand on the beach at the nodal point/hot spot. With the construction of the seawall and groins and the newer terminal groins and T-Head and L-Head groins on the south end of the island, the shoreline change has slowed in recent times. The beach fill has supplied additional sand to the northern and southern beach and nearshore area. Sand transport modeling

indicates that on the flood tide sediment transport across the Tybee platform is to the northwest on the northern portion and to the southwest/west on the southern portion of the platform. The shoreward movement of the -5 m contour on the shelf platform in front of Tybee Island is consistent with this sand transport pattern. The ebb directed net movement of sediment is generally confined to the navigation channel.

With the lack of data in both the spatial and temporal scale it is difficult to make a definitive assessment of how the dredging and construction of the jetties and breakwater have effected the Tybee Island shoreline changes. A hypothesis for this case/effect relationship is presented later in light of modeling results. The storm climate indicates that the turn of the century was an active time for tropical systems and they have most likely had an impact on the shoreline and shelf changes. It is difficult to discern any strong link between storm activity and the cause of what has taken place in the evolution of the Tybee Island area. The general sediment transport in the region is from north to south, so impacts of the project would be expected to the south. The volume change analyses support this, with little volume change on Barrett Shoals and the Daufuskie/Turtle Island Shelf and deflation of the Tybee Island Shelf. The initial construction of the jetties and dredging very likely contributed to the erosion of the bulge on the north end of Tybee Island and the increase in volume on the North Tybee Shoal (possibly resulting from collapse of a portion of the ebb shoal feature. It appears that dredging of the channel has cut off any bypassing that occurred from Barrett Shoals to the Tybee Island Shelf (dredge volumes have remained relatively constant in recent times, in spite of continued deepening of the channel. The volume of the Tybee Island Shelf area is deflating at a rate of 220,000 m^3/yr over the historic period. This rate appears to be decreasing with time, but more broad coverage survey data is required. Sediment transport patterns in the very nearshore are adjacent to Tybee Island are dictated by flood tidal flow directing sediment to the north on the northern end and to the south on the southern end, creating a hot spot due to flow divergence. Data are lacking to fully quantify the impact of the project on Tybee Island (primarily multiple full coverage surveys prior to the project to establish historic rate and recent surveys to establish present rates). The major impact is the cut off of bypassing from Barrett Shoals to the Tybee Island Shelf through dredging and deepening and changes induced in the shelf east of Tybee Island. A reasonable upper bound of this impact is the estimated 360,000-370,000 m^3/yr (ATM 2001, based on 1999-2000 dredging records and 1996-2005 dredging records assuming 80 percent of dredging volume is from Tybee Roads and 77 percent of material is sand) of sand bypassed from Barrett Shoals to the Tybee Roads Bar Channel (arguments to reduce this number could include that some of this volume originated in the Tybee Knoll Bar Channel or the Savannah River and that some portion of the bypassing from Barrett Shoals would have been transported offshore in the channel even if the project had not been constructed).

Acknowledgements

Mr. Matt Goodrich of Applied Technology and Management Inc., Charleston, SC supplied some of the historic bathymetry. Mr. Wilber Wiggins, USACE Savannah District, supplied several data sets and air photographs and information on dredging records, surveys and erosion control efforts on Tybee Island. Ms Mary Clair Allison, CHL provided assistance with GIS analysis.

Table 2-6. Tropical Systems within 200 miles of Tybee Island

Year	Dates	Name	Category	Pressure mb	Winds mph
1850					
1851	8/24/1851	Not Named	H1	n/a	80
1852	8/27-8/28		TS		45
	10/10/1852		TS		70
1853	10/21/1853		H2		105
1854	9/8-9/1854		H3	950	115
1855					
1856	8/31-9/1		TS		70
1857	9/12/2006		H1		90
1858	9/15/2006		TS		70
1959	10/28/2006		H1		90
1860	8/13-14/1860		TS		60
1861	11/1/2006		TS		60
1862					
1863	9/17/2018		TS		70
1864					
1865	8/20/2006		TS		60
1866					
1867	6/21-23/1867		H1		80
	10/6-8/1867		TS		70
1868	10/5/1868		TS		45
1869					
1870					
1871	8/18-23/1871		H1		80
	8/27-28/1871		TD		35
	9/6-7/1871		TS		70
	10/5-6/1871		TS		60
1872	10/23-24/1872		H1		80
1873	6/2/2006		TS		45
	9/19-20/1873		TS		70
	9/23/2006		TS		45
1874	9/28/1874		H1	981	90
1875					
1876	9/21/2006		H1		90
1877	9/20-21/1877		TS		45
	9/28/1877		TS		60
	10/3-4/1877		TS		60
	10/27/1877		TS		45
1878	9/11-12/1878		H1	985	90
	10/11/1878		TS		45
1879	8/18/1879		H3		115
	10/28/1879		TS		60
1880	9/8-9/1880		TS		70
	10/9/1880		TS		70
1881	8/27-28/1881		H2	970	105
1882	9/11/1882		TS		45

	9/22/1882	TS		45
	10/11-12/1882	TS		70
1883	9/10/2011	H2		105
1884	9/10-13/1884	TS		60
1885	8/24-25/1885	H3		115
	8/31/1885	TS		45
	9/21/1885	TS		45
	9/30-10/1	TS		60
	10/12/1885	TS		60
1886	6/21-22/1886	H1		75
	7/1/1886	TS		60
	7/19/1886	TS		65
1887	8/19/1887	H3		115
	8/23-24/1887	H3		125
	10/20/1887	TD		35
	10/30/1887	TS		45
1888	9/9-10/1888	TS		50
	10/11/1888	H1		80
1889	6/17-18/1889	TS		45
	9/24/1889	TS		50
1890				
1891	10/8/1891	TS		45
	10/10/1891	TS		50
1892				
1893	6/16/1893	TS		60
	8/28/1893	H3	954	115
	10/3-4/1893	TS		50
	10/13/1893	H3		120
1894	9/26-27/1894	H1		90
	10/9/1894	H1		80
1895				
1896	7/8/1896	TS		40
	9/29/1896	H3	963	115
1897	9/21-22/1897	TS		60
1898	8/30-9/1/1898	H1		85
	10/2/1898	H4	938	135
1899	8/14-15/1899	H3		120
	10/5-6/1899	TS		45
	10/31/1899	H2		110
1900	10/12/1900	E		40
1901	7/3/1901	TS		40
	9/18/1901	TS		40
1902	6/15/1902	TS		40
1903	9/16/1903	TD		35
1904	9/14/1904	H1		80
	11/4/1904	TD		35
1905				
1906	9/17-18/1906	H1	977	80
	10/19-21/1906	H1		90
	10/17/1906	TS		40

1907	6/29/1907	TS		65
	9/29/1907	TS		40
1908	5/27-28/1908	H1		75
	7/30/1908	H1		80
	10/23/1908	E		45
1909	7/2-3/1909	TD		35
	8/31/1909	TS		40
1910	10/19/1910	TS		70
	8/27/1910	E		40
	10/20-21/1910	TS		70
1911	8/27-30/1911	H1	983	75
1912	6/14/1912	TS		40
	7/15/1912	TS		50
1913	10/8-10/1913	TS		50
1914	9/16-17/1914	TS		45
1915	8/1-3/1915	TS		50
1916	7/13-15/1916	H2	983	100
	9/5/1916	TS		40
	9/13/1916	TD		35
	10/4/1916	TS		45
1917				
1918				
1919				
1920	9/30/1920	TS		40
1921	10/26/1921	H1		90
1922				
1923				
1924	9/16/1924	TS		50
	9/30/1924	E		50
1925	12/1-2/1925	H2		100
1926	7/28-29/1926	TS	975	70
1927	10/3/1927	TS		60
1928	9/9-11/1928	TS		45
	9/17-18/1928	H2	974	105
1929	10/1-2/1929	TS		45
1930	9/10-11/1930	TS		60
1931				
1932	9/15/1932	TS		50
1933	9/5-7/1933	TS		50
1934	5/28-31/1934	TS		60
	7/21-22/1934	TS		45
1935	9/5/1935	TS		70
1936	8/21-22/1936	TS		50
1937	7/30/1937	TS		45
	8/30/1937	TS		60
	9/21/1937	TD		35
1938				
1939	10/24/1938	TS		45
1940	8/2-3/1940	TS		45
	8/11-12/1940	H1	975	80

1941	10/8/1941		TS		65
	10/20-21/1941		TS		45
1942					
1943					
1944	8/1/1944		H1	990	90
	10/19-20/1944		TS	978	70
1945	6/24-25/1945		H1		80
	9/16-17/1945		H1	982	75
1946	5/6/1946		TS		45
	10/8-9/1946		TS		40
	11/2-3/1946		TD		30
1947	9/24/1947		TS	989	60
	10/7-8/1947		TS		45
	10/14-16/1947		H1	973	85
1948					
1949	8/27-28/1949		TS	982	65
1950	9/7/1950	EASY	TS		50
	10/19/1950	KING	TS		40
	10/21/1950	LOVE	TS		40
1951					
1952	8/30-31/1952	ABLE	H2		105
1953	8/31-9/1/1953		TS		60
	9/20/1953		TS		45
	9/27/1953	FLORENCE	E		60
1954	8/29-30/1945	CAROL	H2		100
1955					
1956	9/25-26/1956	FLOSSY	E		40
1957	6/9/1957		TS		40
1958	9/27/1958	HELENE	H3	934	125
1959	6/2/1959	ARLENE	TD		30
	7/5-9/1959	CINDY	H1		75
	9/29-30/1959	GRACIE	H4	950	140
1960	7/29/1960	BRENDA	TS		50
	9/11/1960	DONNA	H2	966	105
1961	9/13-14/1961		TD		35
1962	8/27/1962	ALMA	TS		50
1963	10/24-25/1963	GINNY	H2	976	105
1964	6/7-8/1964		TD		35
	8/28-30/1964	CLEO	TS	995	65
	9/9-13/1964	DORA	H3	964	115
1965	6/15/1965		TS		45
1966	6/10/1966	ALMA	TS		65
1967					
1968	6/6-12/1968	ABBY	TS		60
	6/19-20/1968	BRENDA	TD	1012	30
	8/11/1968	DOLLY	TD	1011	30
	10/19/1968	GLADYS	H1	966	85
1969	9/8/1969	GREDA	TS	1002	50
	10/3-4/1969	JENNY	TD		35
1970	7/25-26/1970	ALMA	TD	1005	30

	8/16-17/1970		TD	1013	35
1971					
1972	5/27-28/1972	ALPHA	SS	991	65
	6/20-21/1972	AGNES	TD	992	35
	9/13-14/1972	DAWN	TD		35
1973					
1974	6/25/1974	Subtropical #1	SS	1000	65
	10/7/1974	Subtropical #4	SS		45
1975	6/27-28/1975	AMY	TD	1012	30
	10/25-26/1975	HALLIE	SD	1005	35
1976	5/24/1976	subtropical #1	SS	998	45
	8/20/1976	DOTTIE	TS	999	45
	9/13-15/1976	subtropical #3	SS	1011	45
1977	9/8/1977	BABE	TD		30
	9/5/1977	CLARA	TD	1014	25
1978	9/12/1978	HOPE	TD	1010	30
1979	9/4-5/1979	DAVID	H2	970	100
1980					
1981	8/19/1981	DENNIS	TS	1002	45
1982	6/18/1982	subtropical #1	SS	992	70
1983					
1984	9/9-13/1984	DIANA	H3	960	115
	9/29/1984	ISADORE	TS	1004	50
1985	7/24-25/1985	BOB	H1	1002	75
	8/9/1985	CLAUDETTE	SD	1013	30
	10/10-13/1985	ISABEL	TD	1011	35
	11/22/1985	KATE	H1	983	75
1986	6/6/1986	ANDREW	TS	1004	50
	8/13-16/1986	CHARLEY	TS	1002	45
1987					
1988	8/28/1988	CHRIS	TS	1005	50
1989	9/22/1989	HUGO	H4	935	140
1990					
1991					
1992	9/29-30/1992	EARL	TS	1002	45
1993					
1994	11/21/1994	GORDON	TD	1013	25
1995	6/5-6/1995	ALLISON	TS	993	50
	8/25-27/1965	JERRY	TD	1004	30
1996	6/18-19/1996	ARTHUR	TS	1004	40
	7/12/19916	BERTHA	H2	975	100
	9/5/1996	FRAN	H3	952	115
	10/8/1996	JOSEPHINE	E	990	50
1997					
1998	8/26/1998	BONNIE	H3	965	115
	9/3-4/1998	EARL	TS	990	50
1999	8/29-30/1999	DENNIS	H2	964	105
	9/15-16/1999	FLOYD	H3	943	115
	10/17/1999	IRENE	H1	984	75
2000	9/18/2000	GORDON	TD	1006	35

	9/23/2000	HELENE	TD	1011	30
	10/4-5/2000	LESLIE	SD	1010	35
2001	6/13/2001	ALLISON	SD	1004	30
	9/15/2001	GABRIELLE	TS	999	50
2002	9/2-5/2002	EDOUARD	TS	1002	65
	10/10-11/2002	KYLE	TS	1008	40
2003	9/6-7/2003	HENRI	TD	1006	35
2004	8/14/2004	CHARLIE	H1	994	75
	8/28-8/30	GASTON	TS	991	60
2005	9/13-9/14	OPHELIA	H1	980	75
	10/5-10/6	TAMMY	TS	1001	45

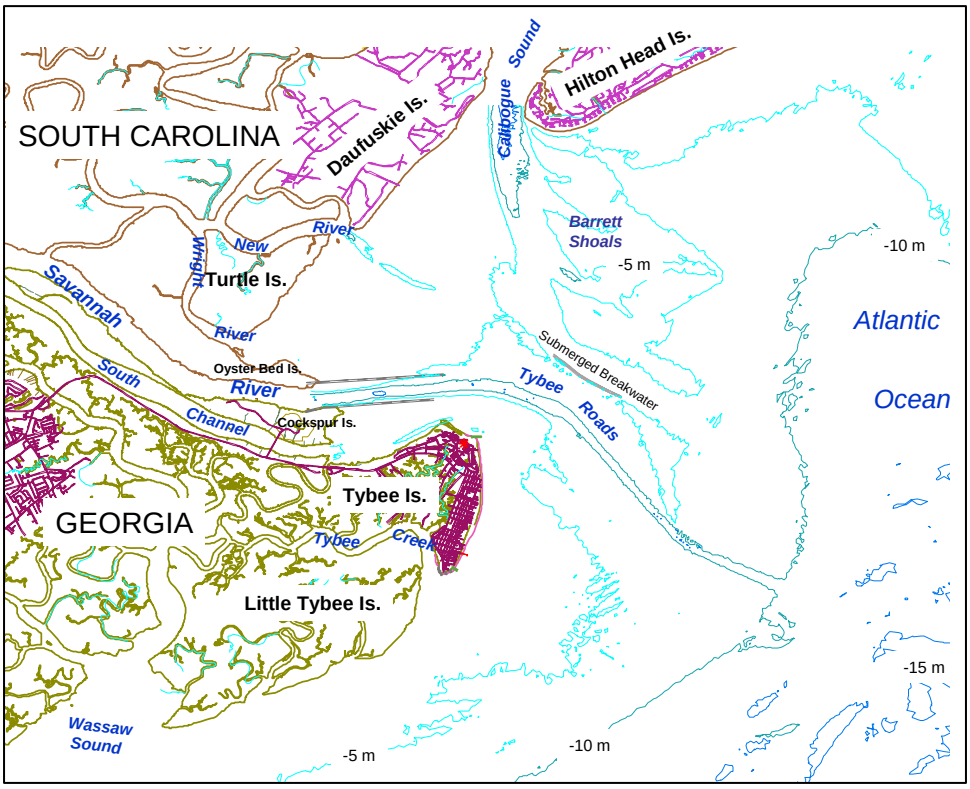

Figure 2-1. Location map of the Savannah River Entrance.

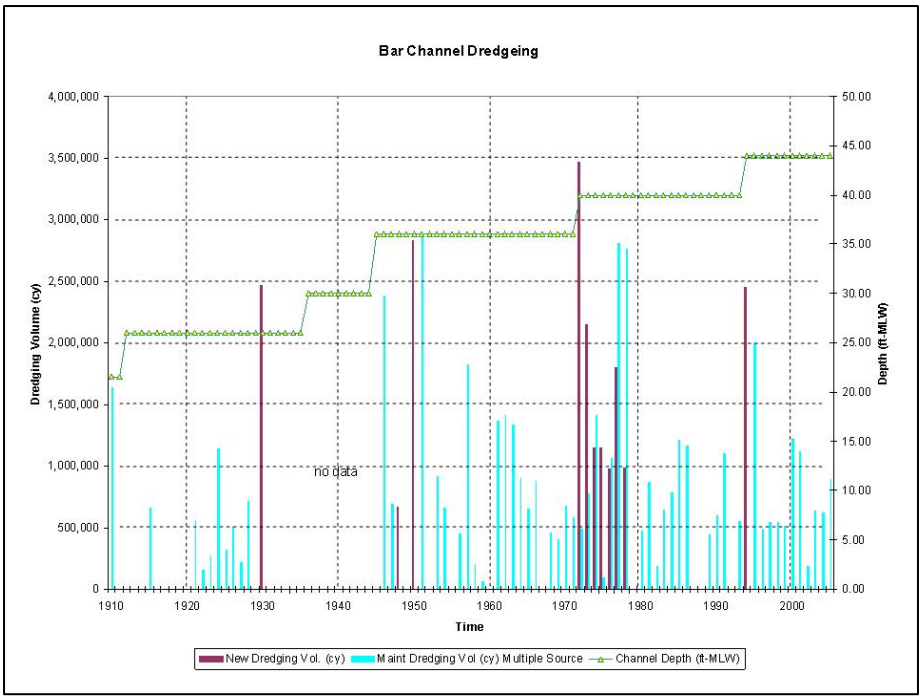

Figure 2-2. Plot of navigation channel depth and dredging volumes with time for the Savannah River Bar Channel.

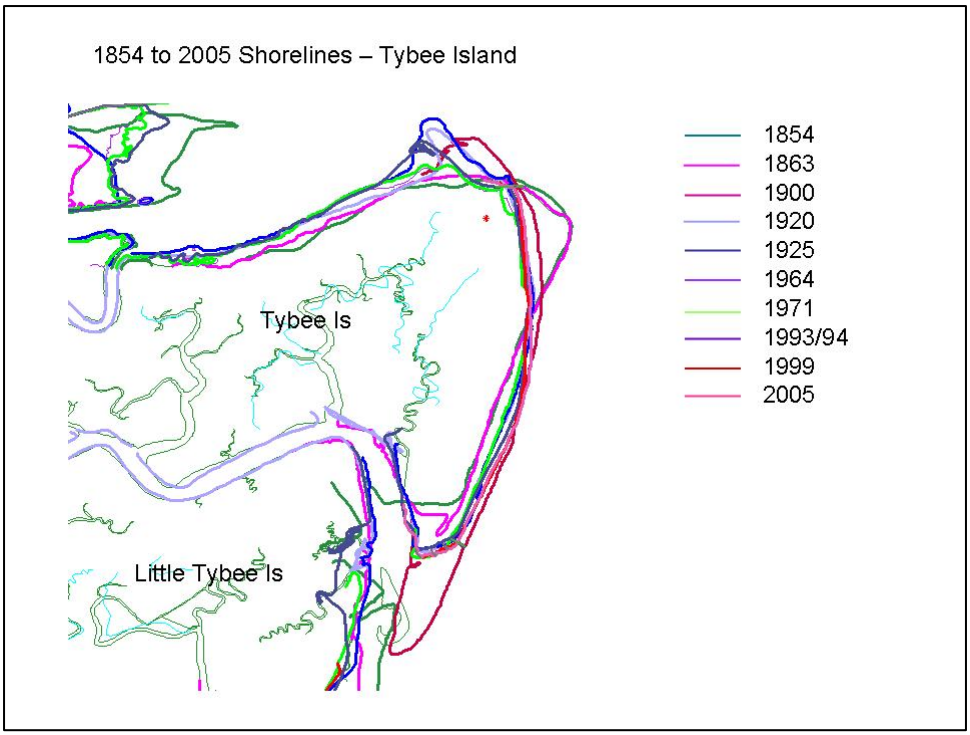

Figure 2-3. Historical shoreline positions of Tybee Island, GA from digital shoreline used in study.

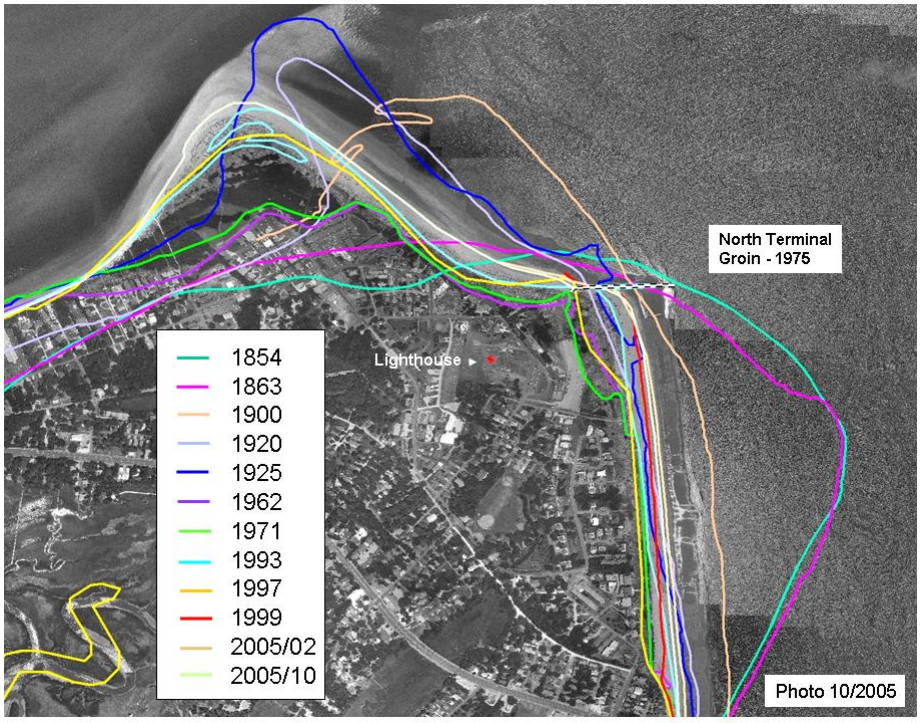

Figure 2-4. Historical shoreline positions along the North end of Tybee Island.

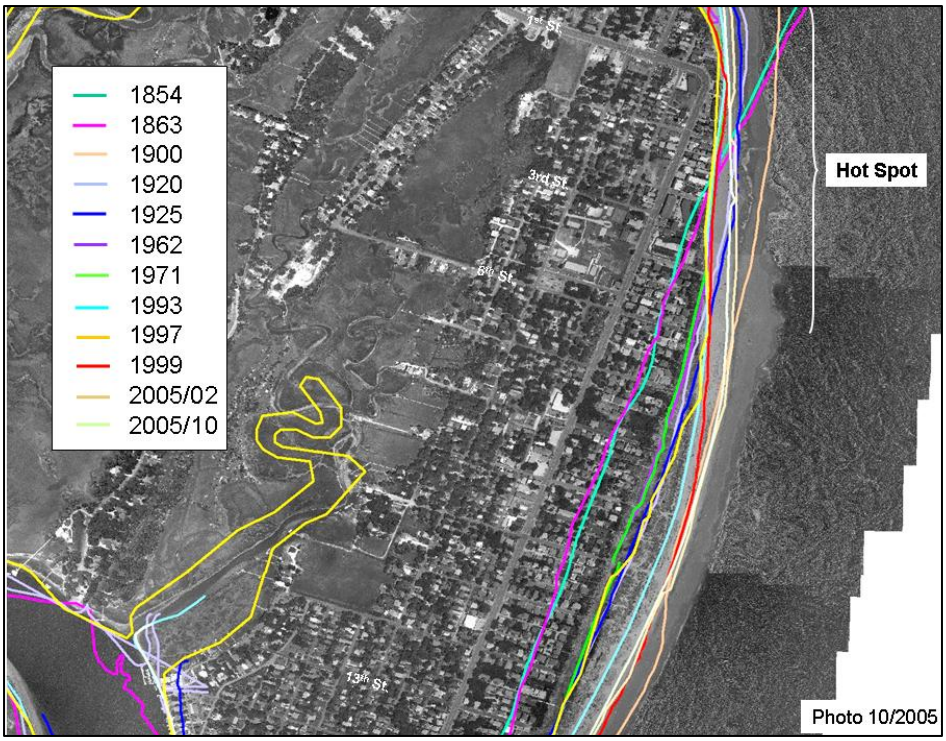

Figure 2-5. Historical shoreline positions along the central portion of Tybee Island in the vicinity of the hot spot.

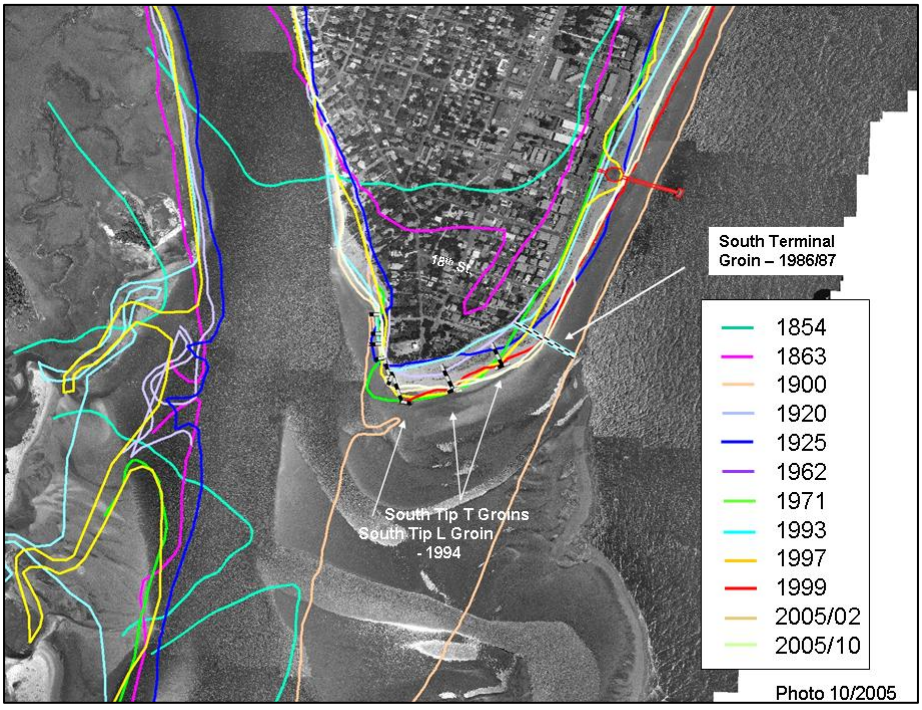

Figure 2-6. Historical shoreline positions along the South end of Tybee Island.

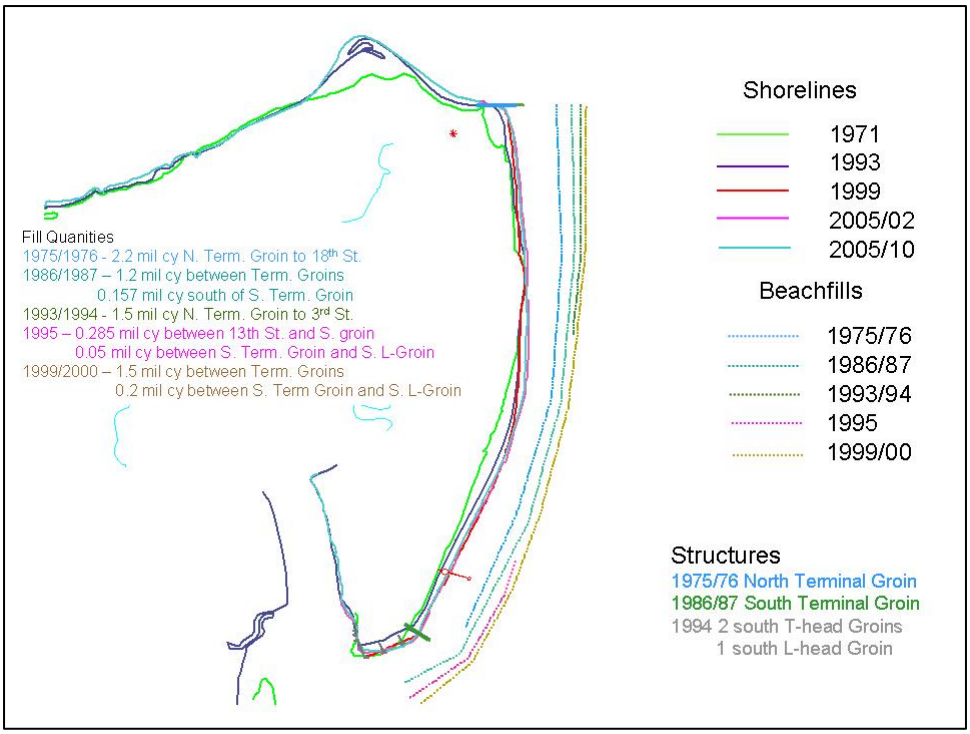

Figure 2-7. Shoreline change relative to recent beach fills and shore protection structure construction.

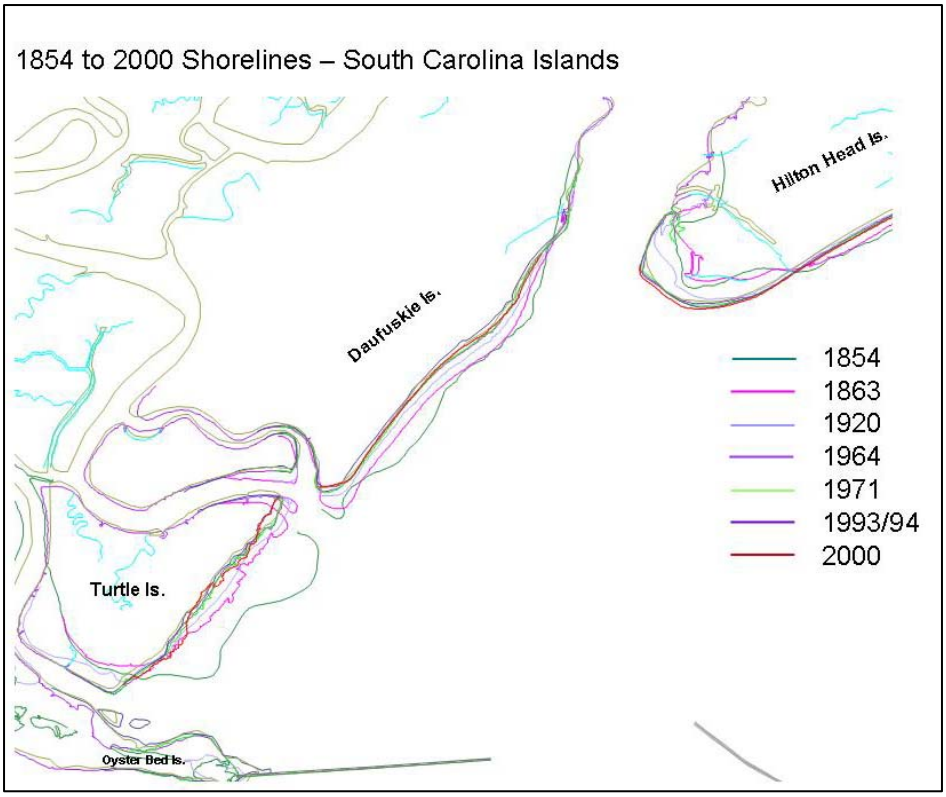

Figure 2-8. Historical shoreline positions of Turtle, Daufuskie and Hilton Head Islands, SC from digital shoreline used in study.

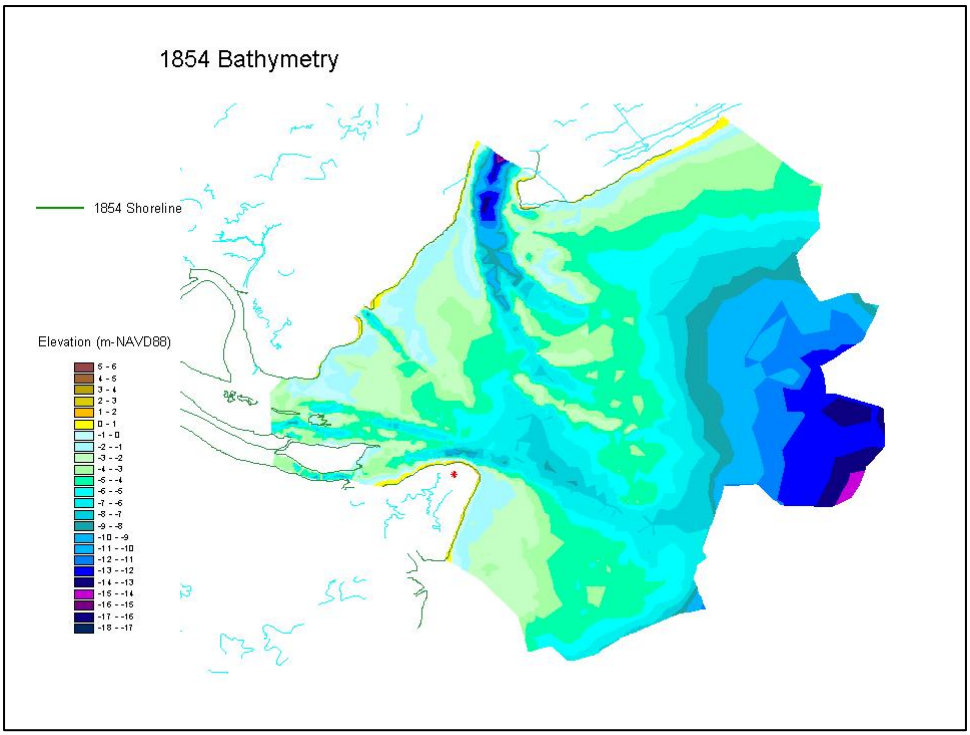

Figure 2-9. 1854 Bathymetry representing the pre 1871 project conditions.

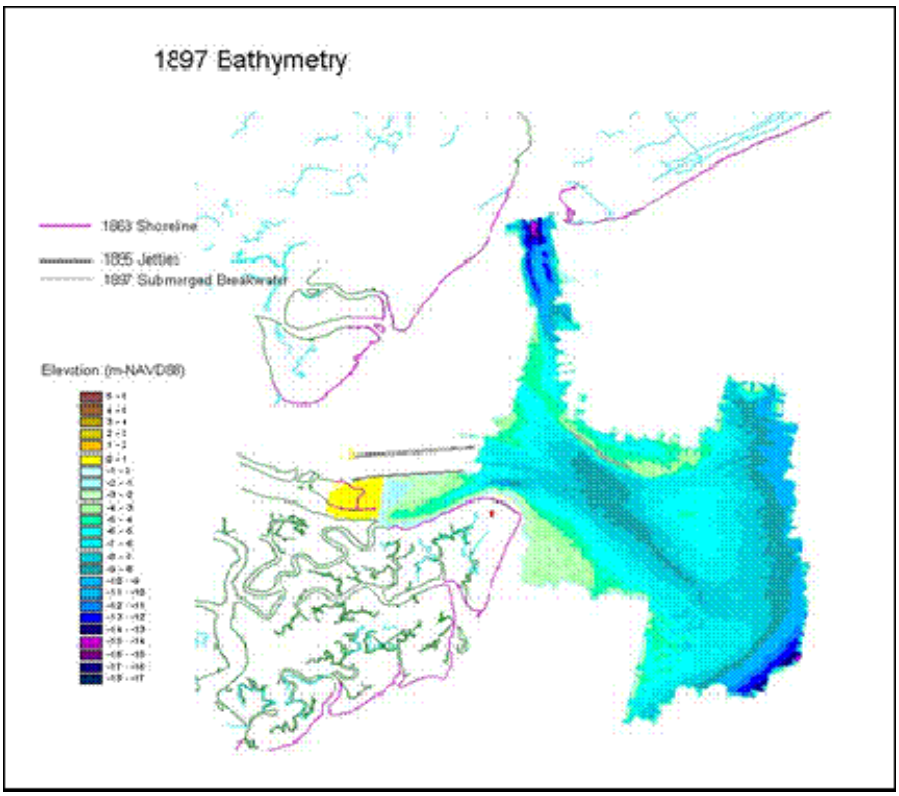

Figure 2-10. 1897 Bathymetry representing the immediate post-jetty and submerged breakwater construction conditions.

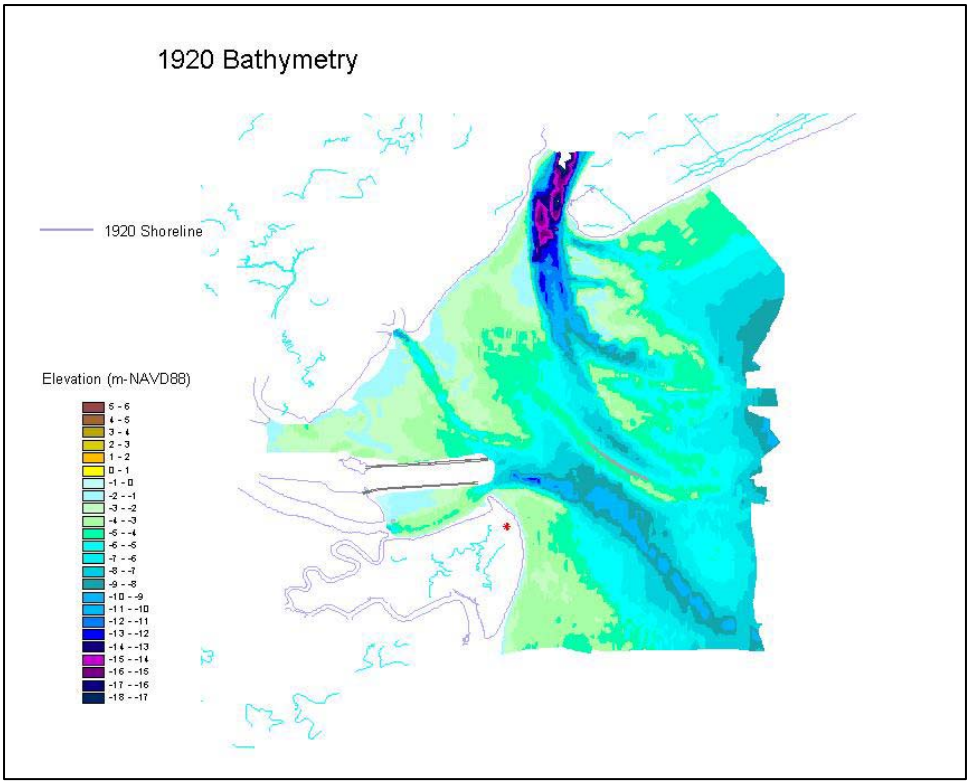

Figure 2-11. 1920 Bathymetry.

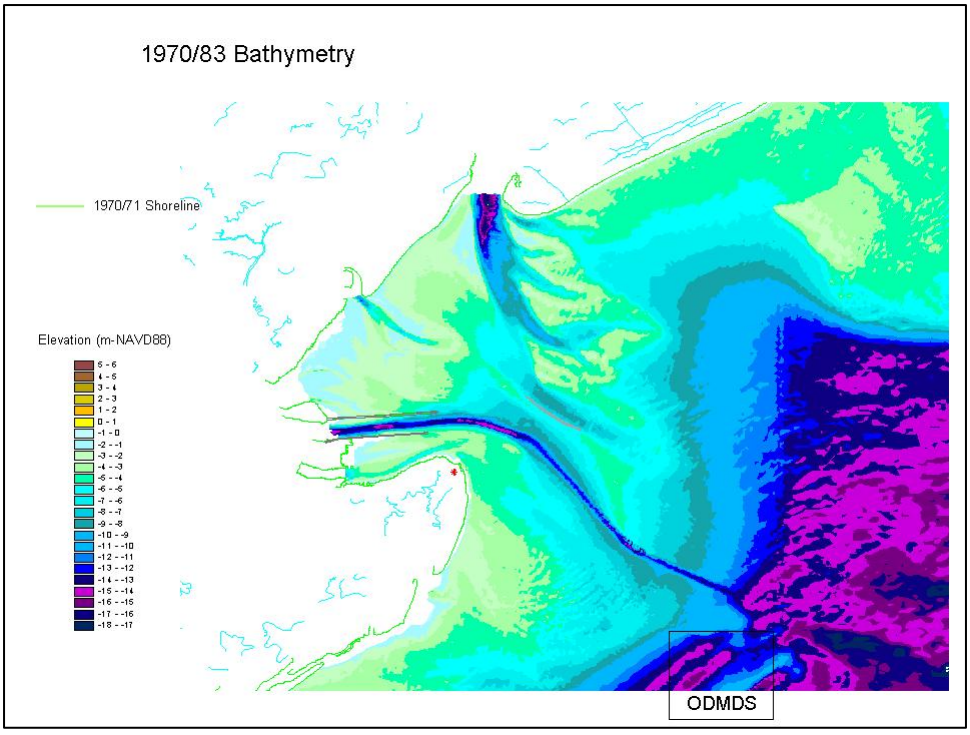

Figure 2-12. 1970/83 Bathymetry.

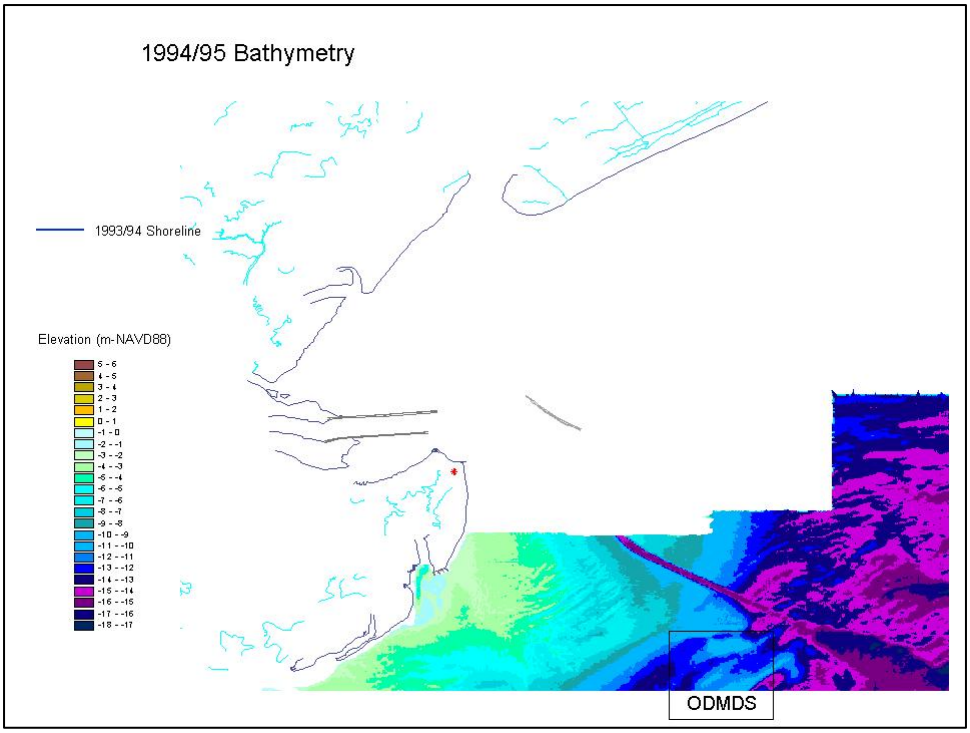

Figure 2-13. 1993/94 Bathymetry.

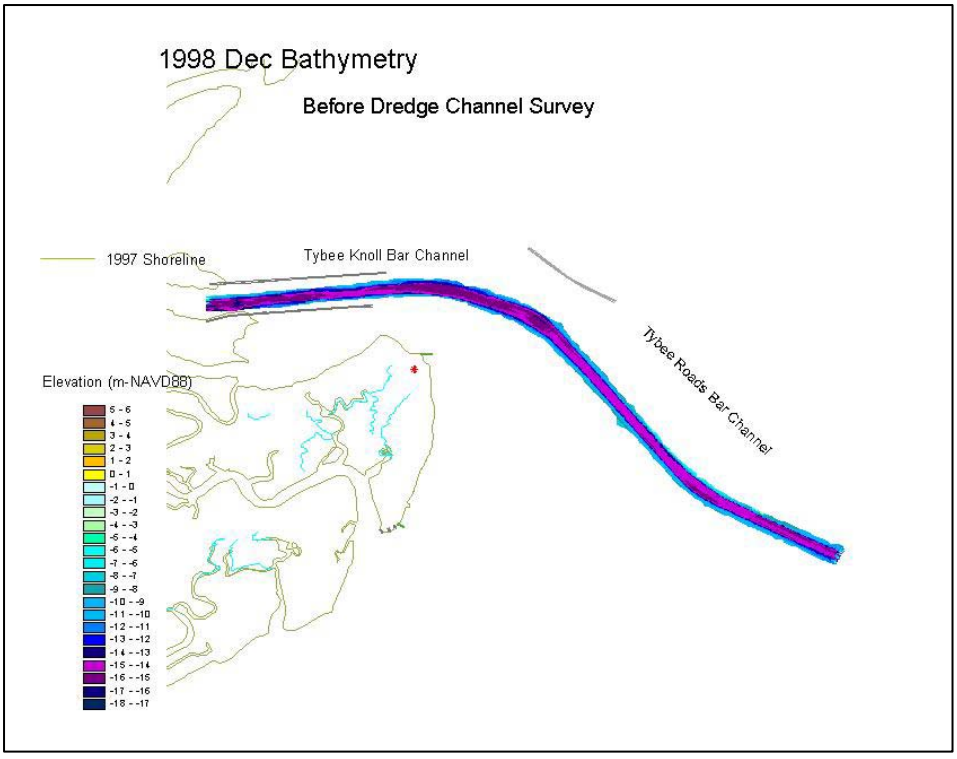

Figure 2-14. December 1998 Channel before dredge survey.

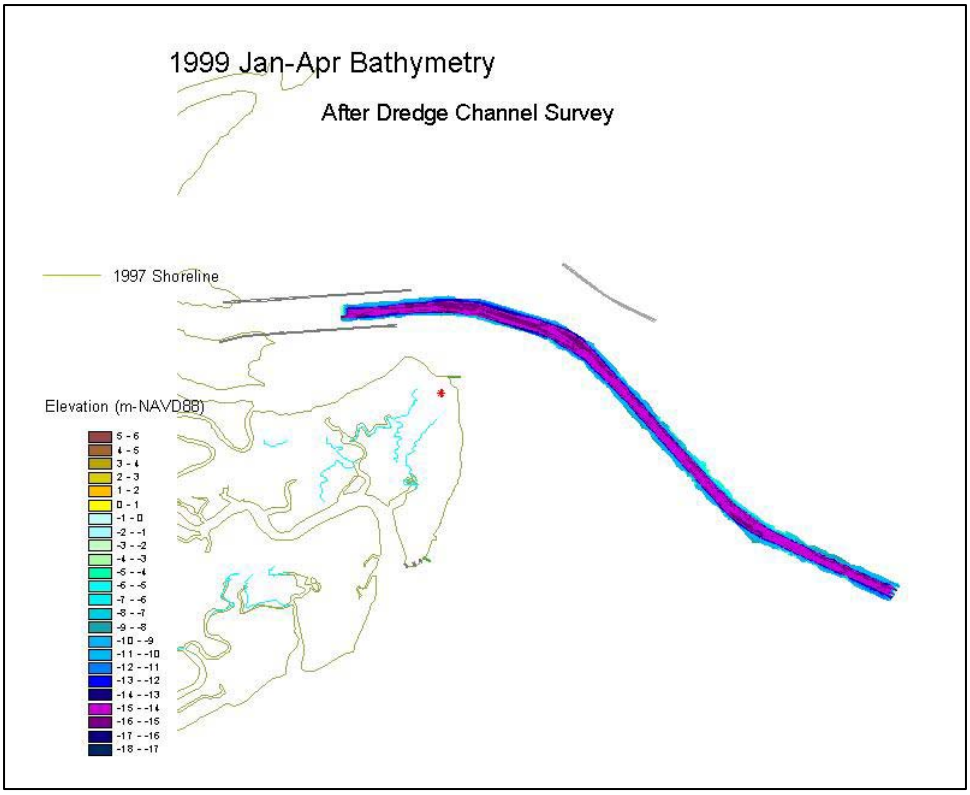

Figure 2-15. January/April 1999 Channel after dredge survey.

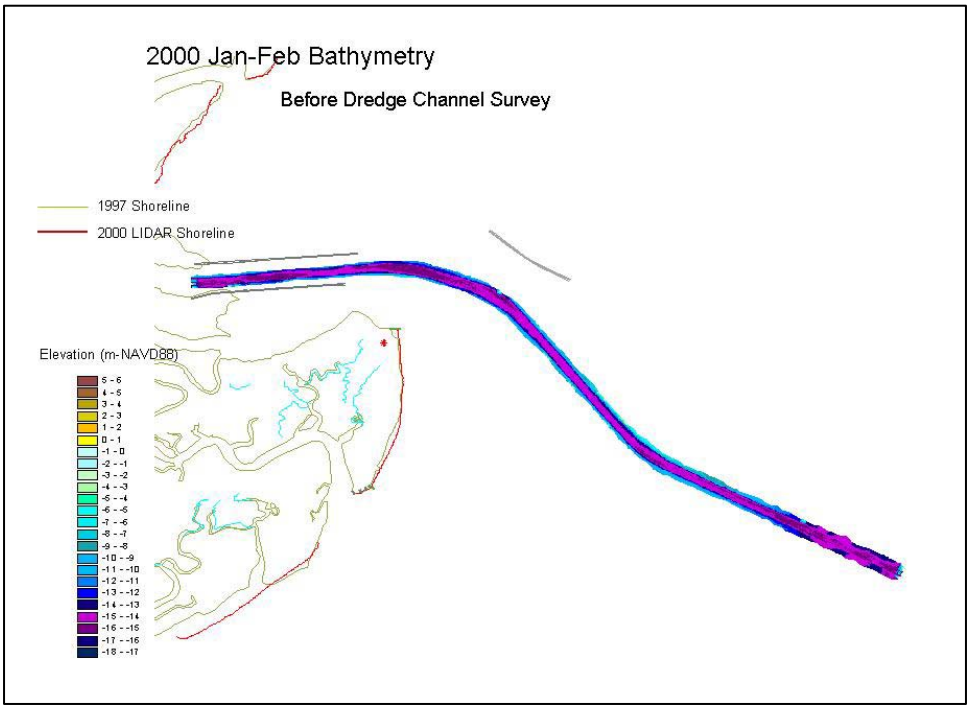

Figure 2-16. January – February 2000 Channel before dredge survey.

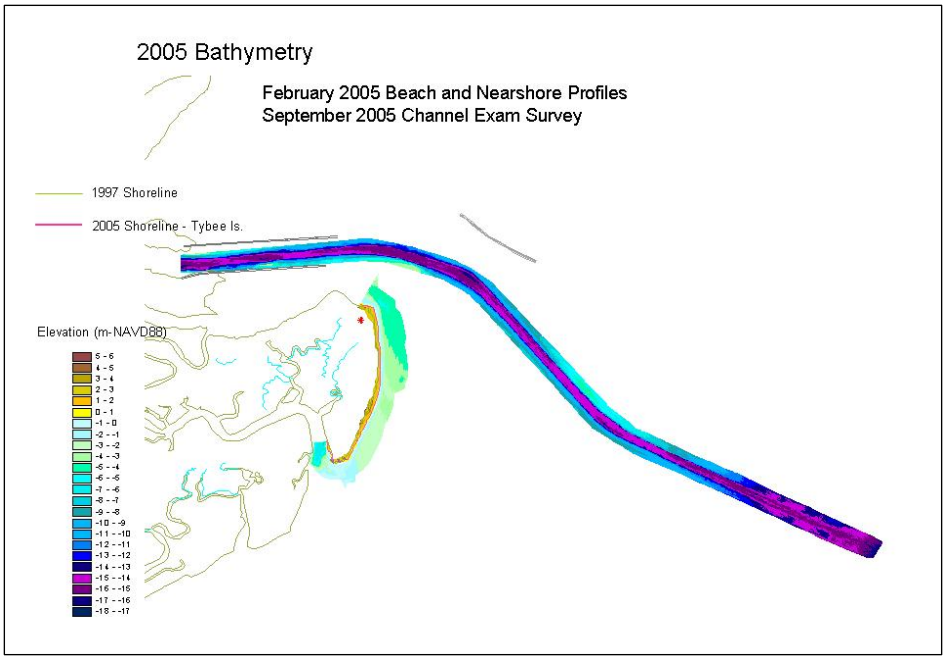

Figure 2-17. February 2005 Tybee Island profiles and September 2005 Channel exam survey.

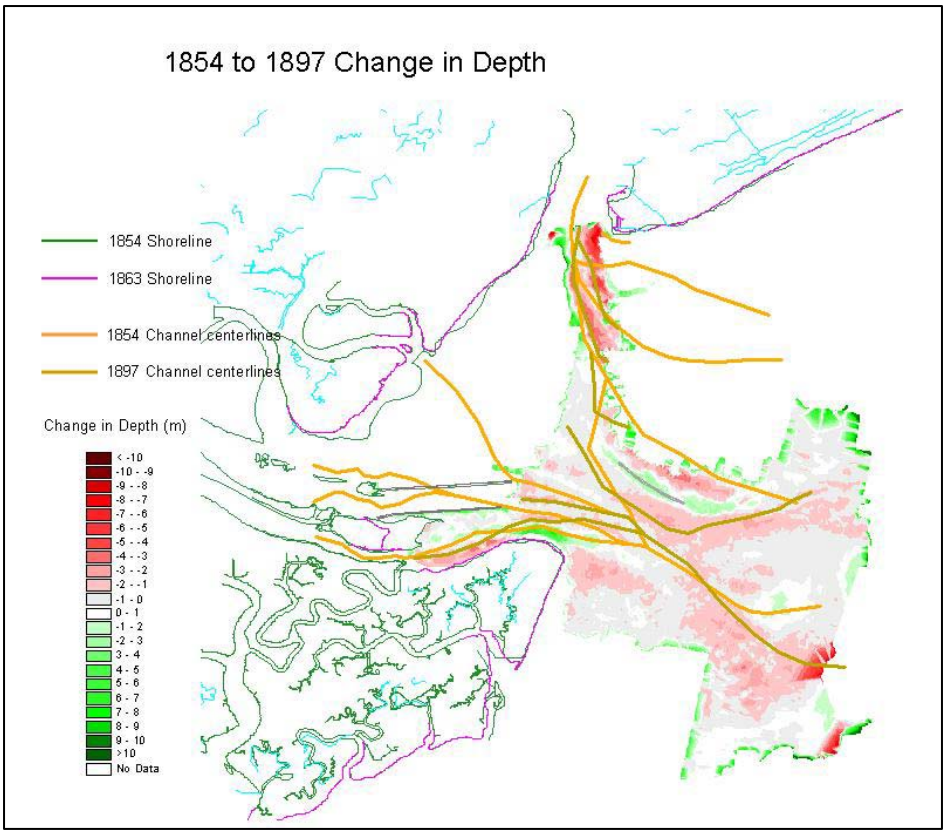

Figure 2-18. 1854 to 1897 change in bathymetry.

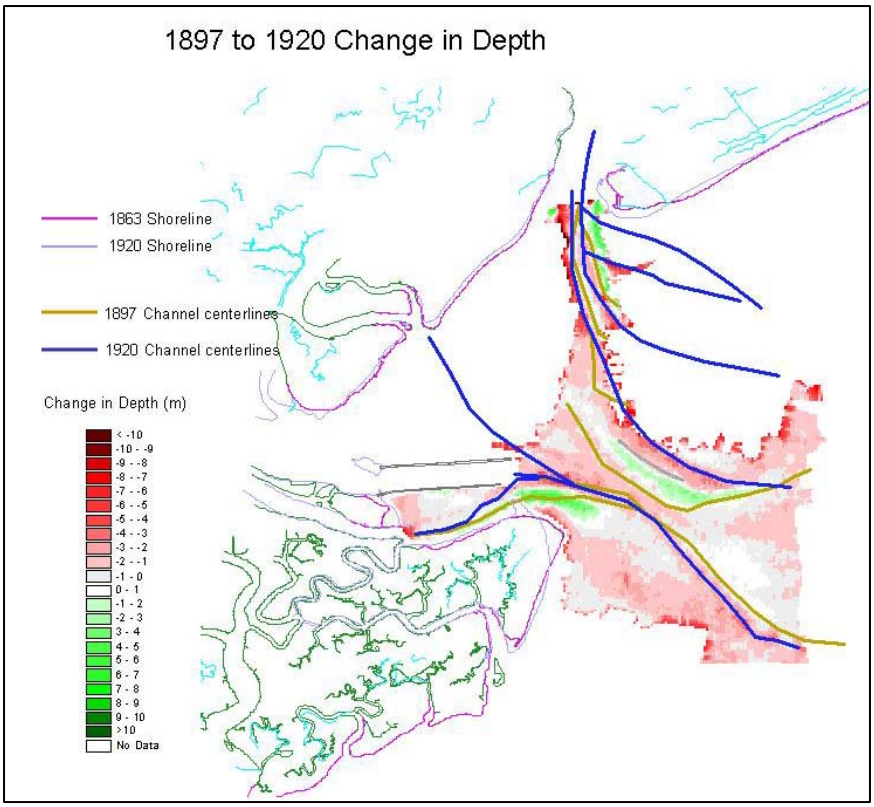

Figure 2-19. 1897 to 1920 change in bathymetry.

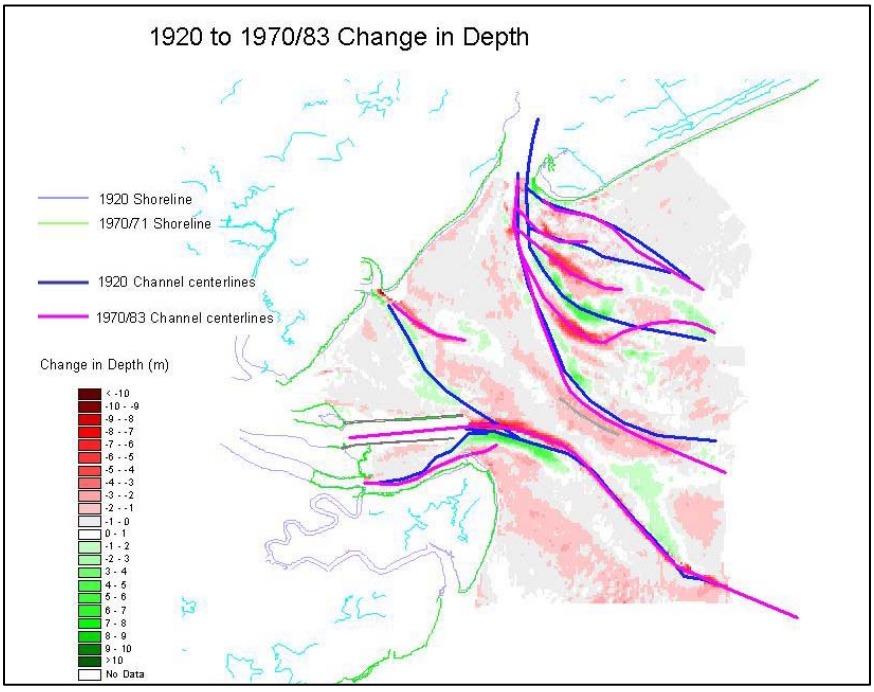

Figure 2-20. 1920 to 1970/83 change in bathymetry.

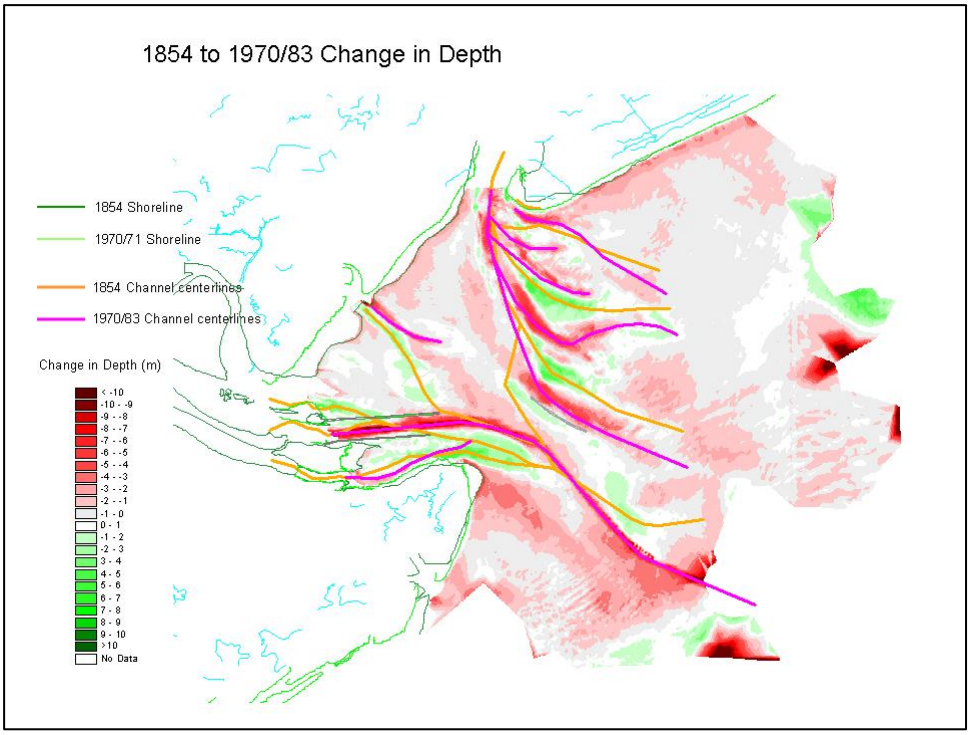

Figure 2-21. 1854 to 1970/83 change in bathymetry.

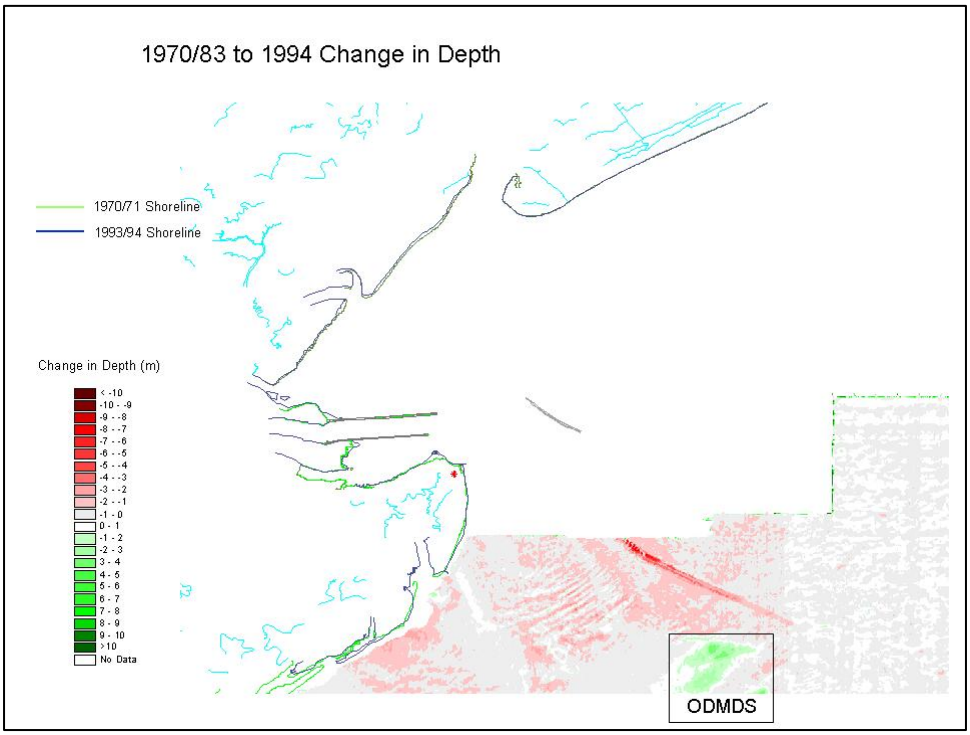

Figure 2-22. 1970/83 to 1993/94 change in bathymetry.

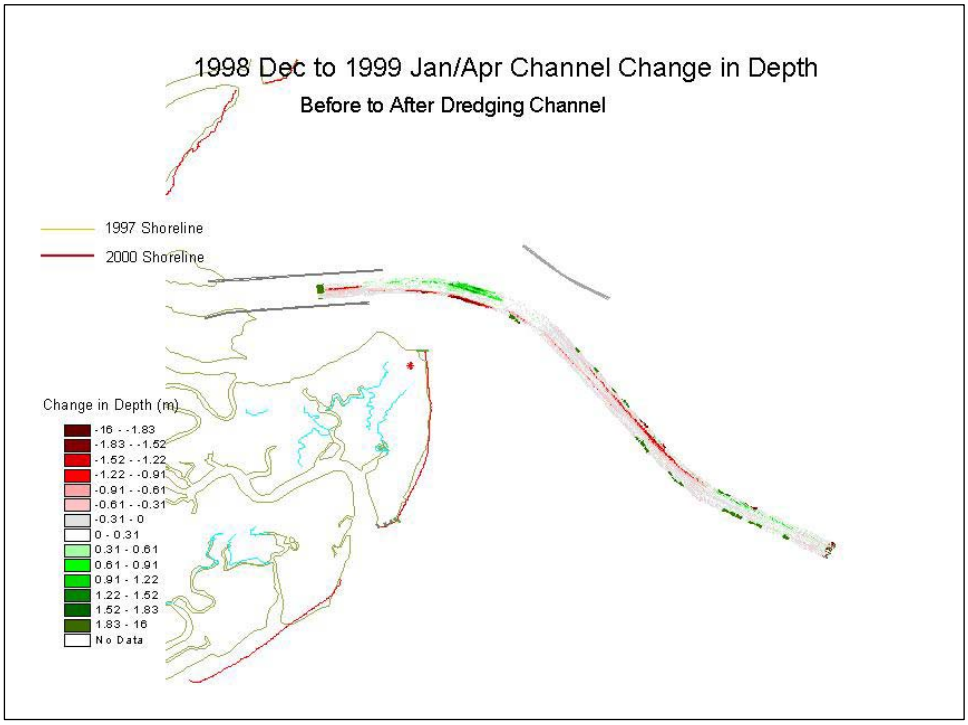

Figure 2-23. December 1998 before dredge to January/April 1999 after dredge survey change in channel bathymetry.

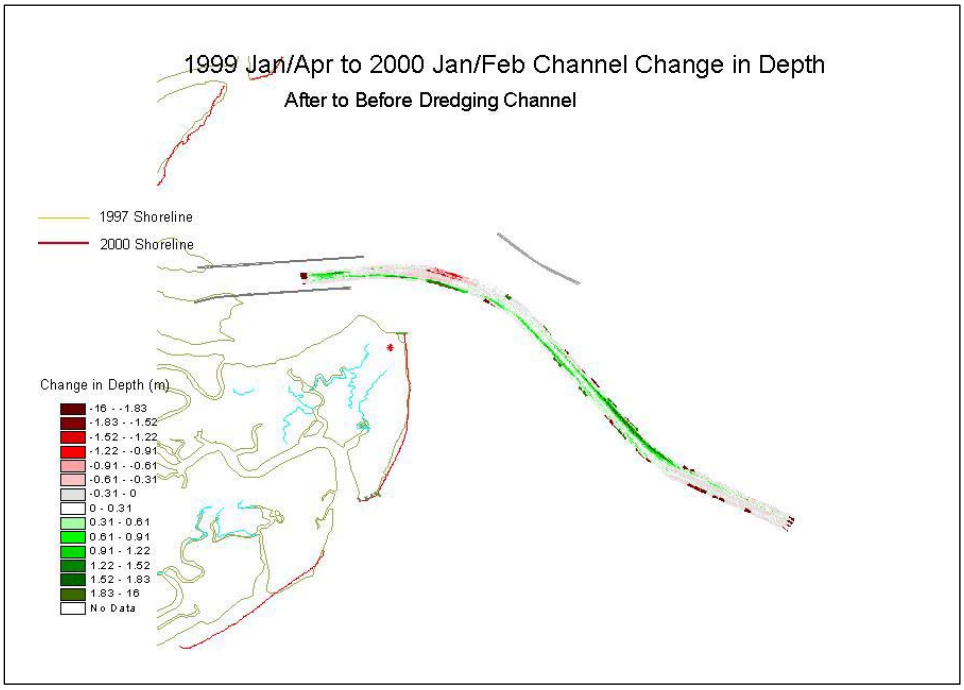

Figure 2-24. January/April 1999 after dredge survey to January/February 2000 before dredge survey change in channel bathymetry.

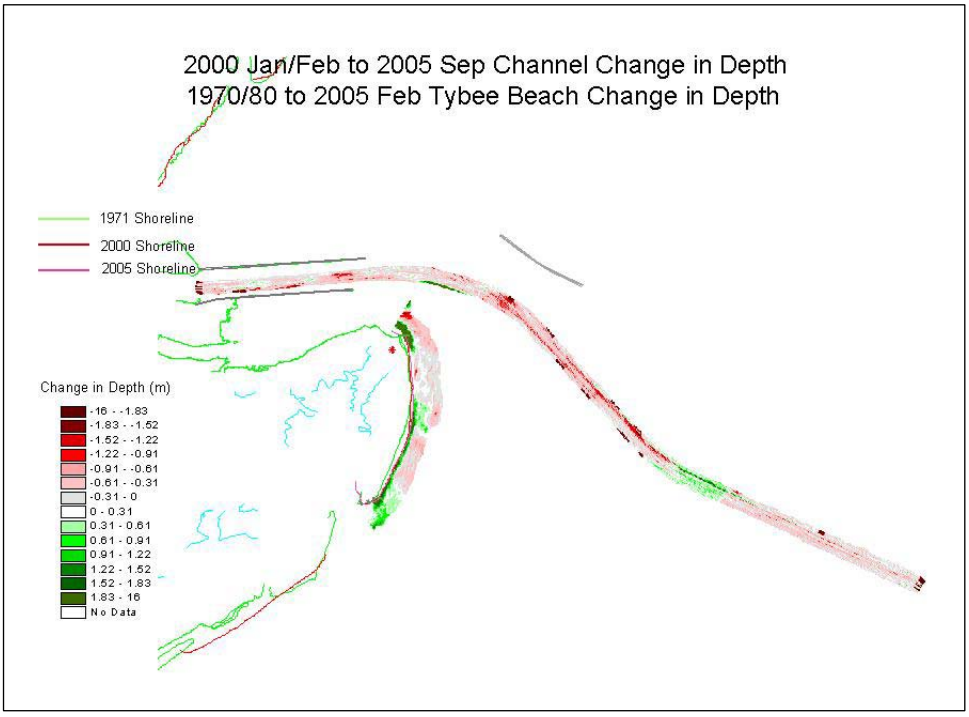

Figure 2-25. January/February 2000 to September 2005 change in channel bathymetry and 1970/83 to February 2005 change in nearshore bathymetry.

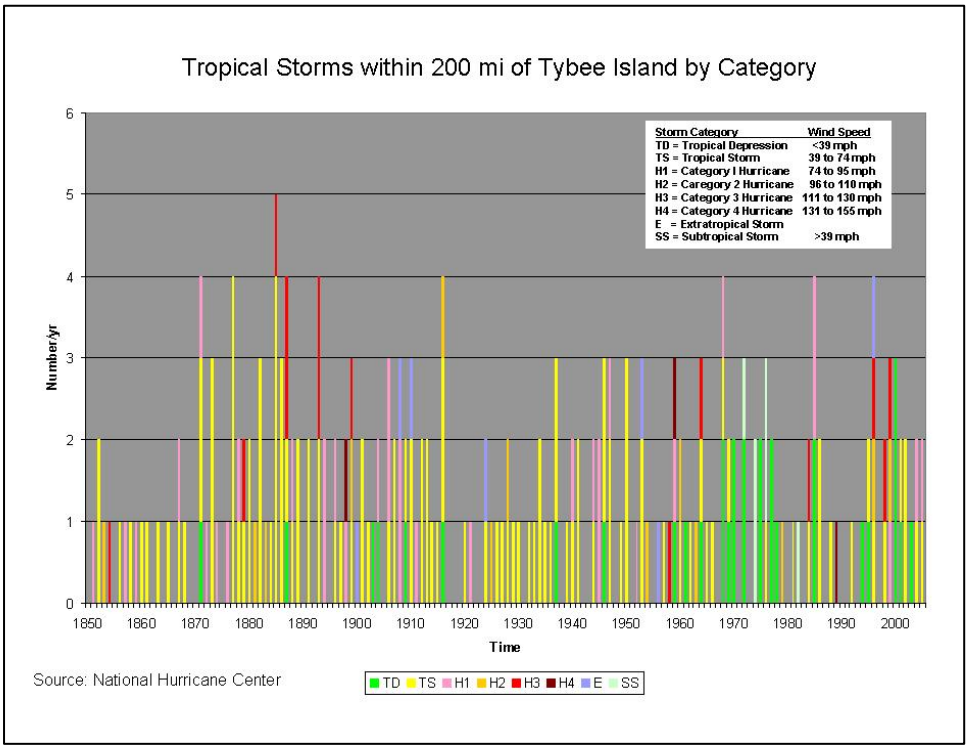

Figure 2-26. Tropical storm occurrence within 200 mi of Tybee Island 1850 to 2005.

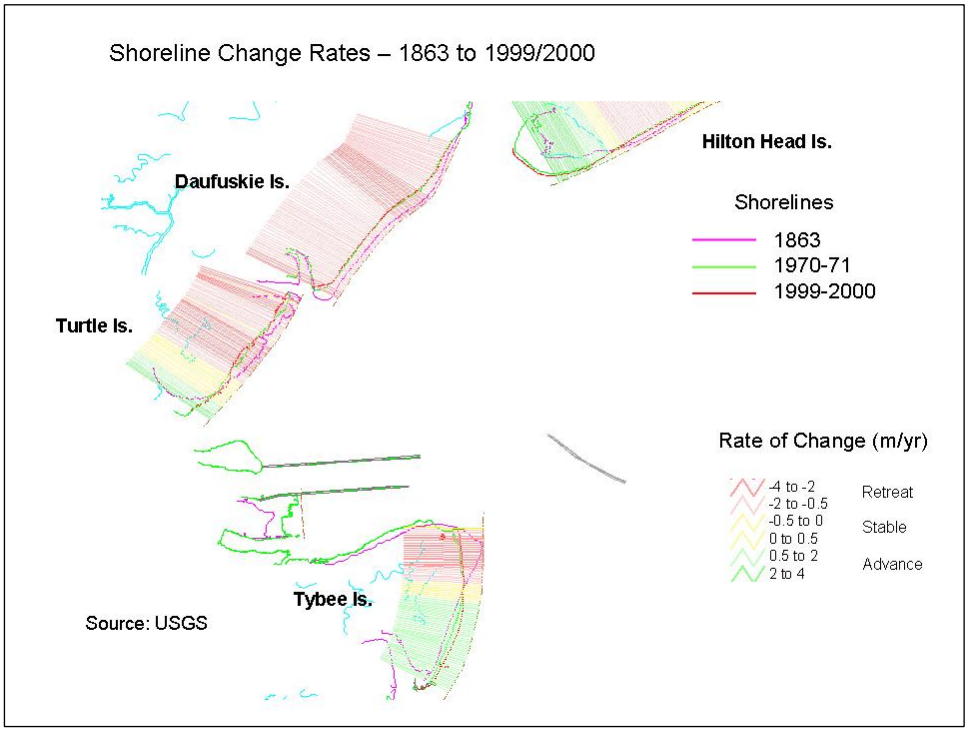

Figure 2-27. USGS shoreline change rate 1863-1999/2000 (after Miller et al 2005).

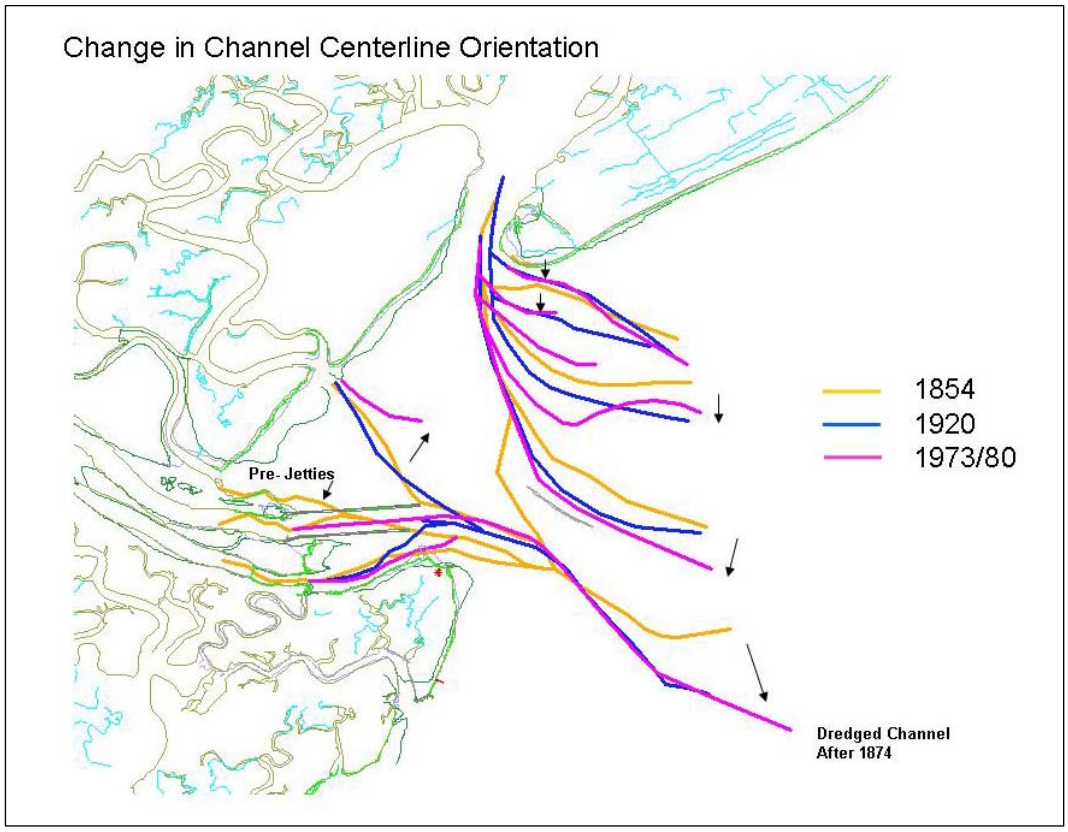

Figure 2-28. Change in channel centerline orientation.

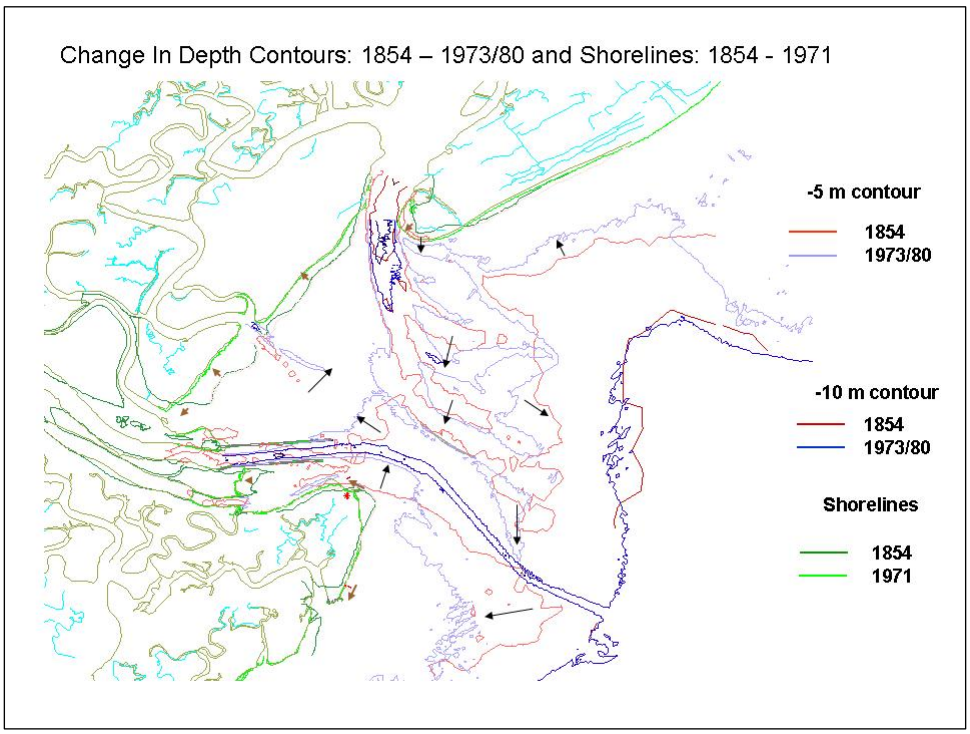

Figure 2-29. Change in 5m NAVD depth contour 1854 to 1970/83.

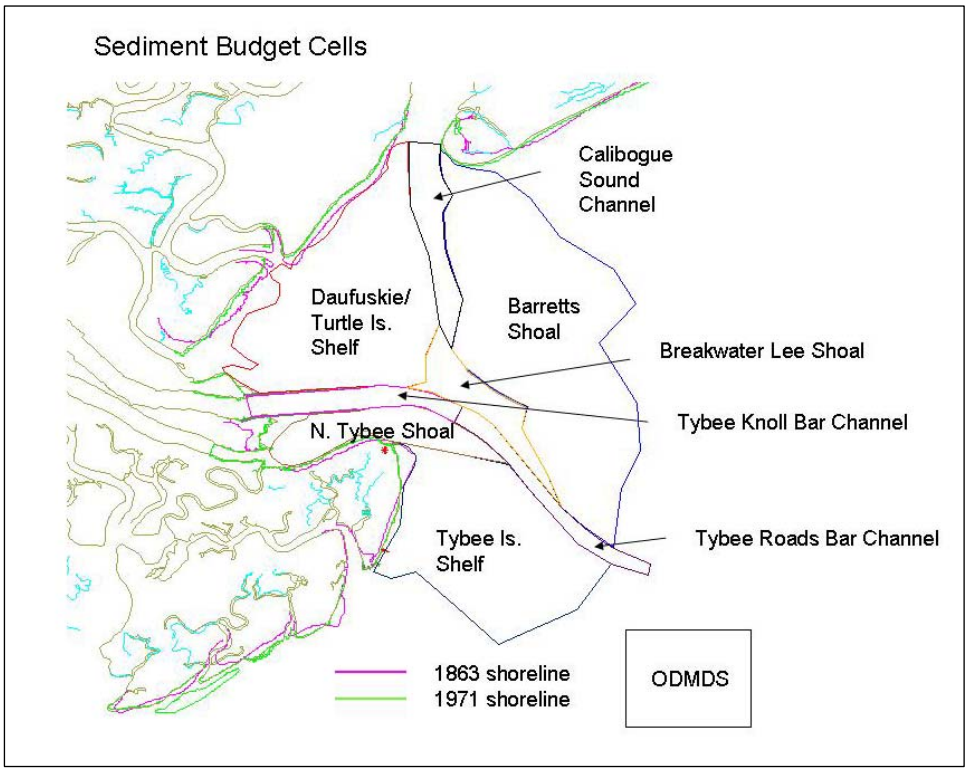

Figure 2-30. Volume Change Cells.

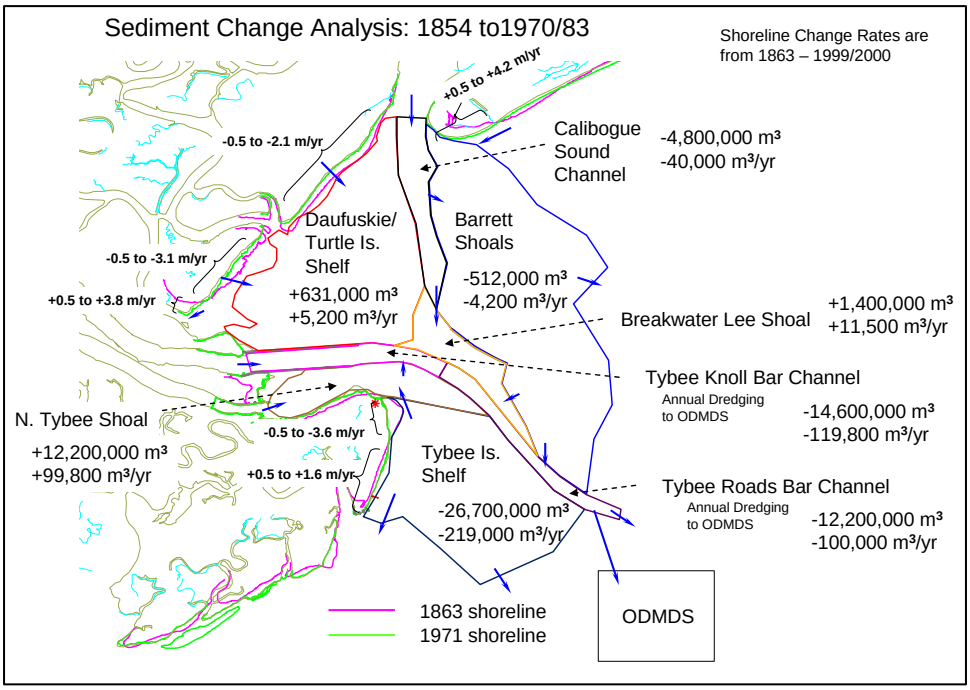

Figure 2-31. 1854 to 1970/83 Volume Change.

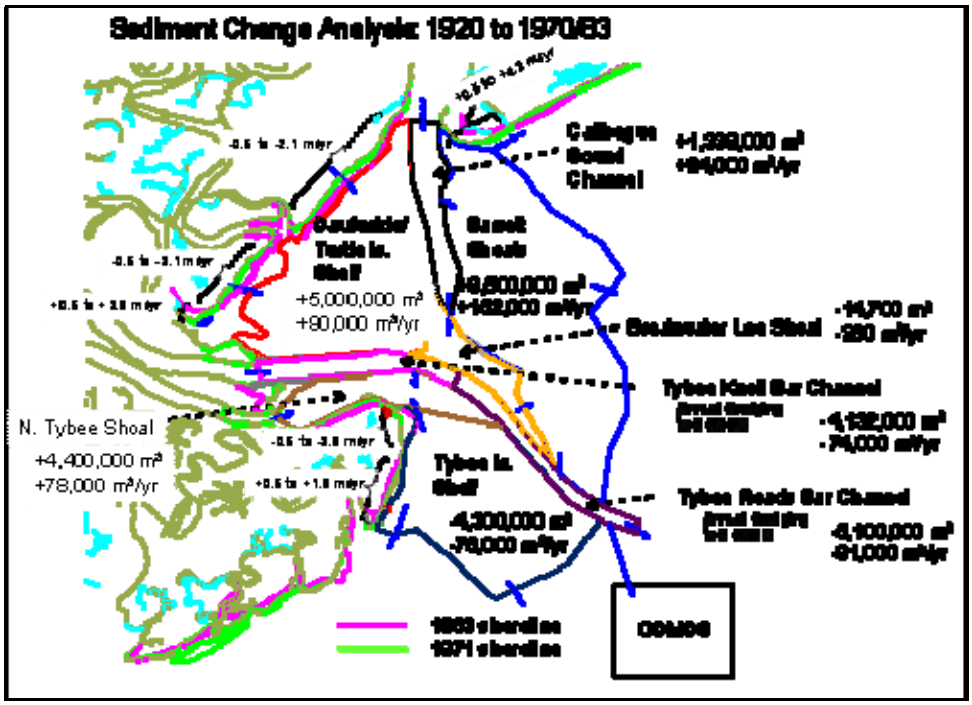

Figure 2-32. 1920 to 1970/83 Volume Changes

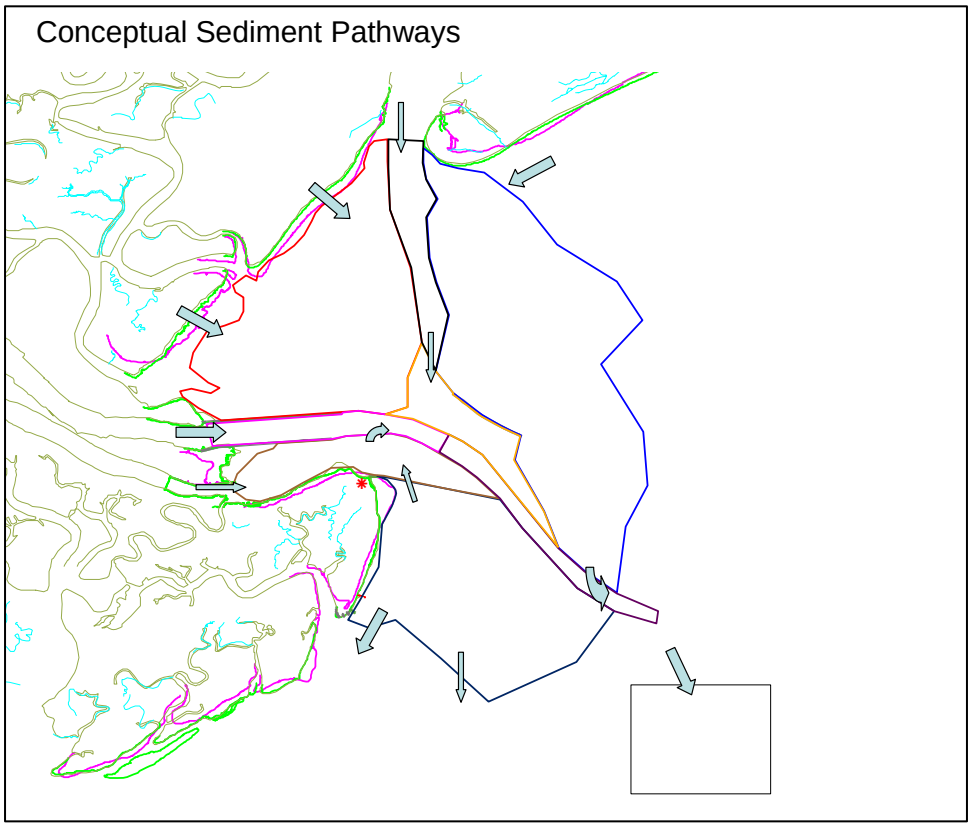

Figure 2-33. Conceptual Sediment Pathways.

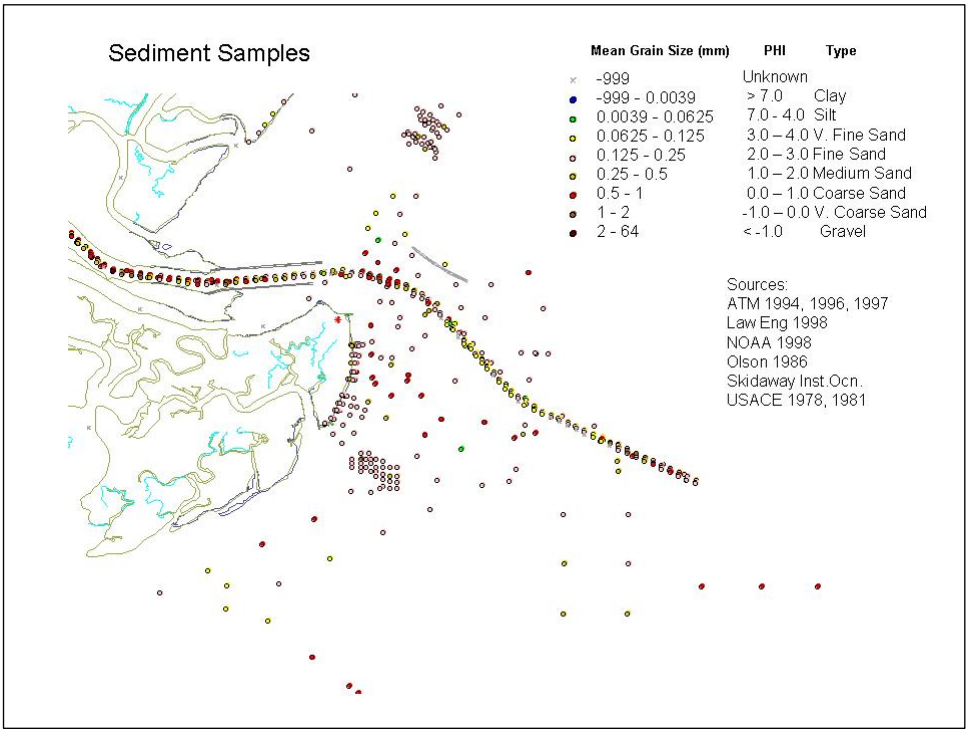

Figure 2-34. Sediment distribution.

3 Circulation Modeling

A major task completed during the Savannah Harbor Entrance Channel: Nearshore Placement of Dredged Material Study (Gailani et al. 2003) was the development, calibration, and application of a fine-grid hydrodynamic model of the Savannah River Entrance Channel and the surrounding ebb shoal and ocean-exposed coast. The ADvanced CIRCulation (ADCIRC) model (Luettich and Westerink 2004) was applied for generation of tidal currents, wind-driven currents and storm surges needed for the sediment transport and wave models. ADCIRC is a two-dimensional, depth-integrated, finite-element, ocean circulation model that has been proven to accurately simulate tidal and storm conditions in nearshore regions. ADCIRC-predicted velocities and water levels were used to develop storm and non-storm hydrodynamic conditions in the river and on the ebb shoal. The accuracy of the model was evaluated using available tidal data at Fort Pulaski, in Tybee Creek, and offshore. In addition, Acoustic Doppler Current Profiler (ADCP) current data provided by Applied Technology and Management, Inc. (2001), were used to evaluate the model.

During that study, the ADCIRC hydrodynamic model was applied for the following simulations: a) December 1999 was simulated as the model calibration period. The hydrodynamic simulations included tidal, river flow, and atmospheric forcing; b) Hurricane Hugo (hypothetically re-tracked to strike Savannah), which occurred during 14-22 September 1989, was simulated to represent an extreme storm event. An atmospheric model was applied to develop the wind and pressure fields; c) November 1979, which included a number of storms, was simulated to represent an active month. The hydrodynamic simulations included tidal, river flow, and atmospheric forcing; d) January 1992 was simulated to represent a typical dredging window operational month. The hydrodynamic simulations included tidal, river flow, and atmospheric forcing; and e) July 1999 was simulated to represent a low wind condition summer month, in which forcing with tidal constituents were included.

The purpose of the present circulation modeling effort is to evaluate the changes in the water surface elevation and depth-averaged velocity patterns in the vicinity of the channel entrance between the existing and channel deepening conditions. The results of the Savannah Harbor Entrance Channel: Nearshore Placement of Dredged Material Study were utilized in the present effort to represent the exiting conditions. The development of the ADCIRC model grid, boundary forcing functions, and the model verifications are presented in detail within the Savannah Harbor Entrance Channel: Nearshore Placement of Dredged Material Study Report.

The tasks to examine and compare pre- and post-channel deepening hydrodynamics include reconstituting the ADCIRC model grid, input, and output files; repeating the December 1999 calibration exercise; modifying the ADCIRC grid to represent channel deepening; and the comparison of the pre- and post-channel deepening hydrodynamic model results for the five simulation periods described above. Table 3-1 summarizes the ADCIRC simulation parameters (see Luettich and Westerink 2005). The final ADCIRC model simulations included the application of wave radiation stress gradients provided by the STWAVE model (Chapter 4).

Table 3-1. ADCIRC Simulation Parameters	
Coordinate system	Spherical
Model run type	Two dimensional, depth integrated
Nonlinear Terms	Nonlinear quadratic bottom friction, finite amplitude terms included, advective terms included (including time derivative portion)
Forcing	Tidal potential, wind, pressure (for re-tracked Hugo), river inflow, and wave stresses
Ramp	One day, hyperbolic tangent ramp
τ_0 (generalized wave continuity equation weight)	0.01
Time Step	1 sec for all runs except July 1999 (deepened), which is 0.5 sec
Flood and dry parameters	Nominal water depth for dry node = 0.1 m, minimum number of time steps cell must remain dry before rewetting = 150, minimum number of time steps node must remain wet before drying = 0, minimum velocity for wetting 0.05 m/sec
Bottom friction coefficient	0.0025
Lateral eddy viscosity	3.0 m^2/sec
Tidal Constituents	K1, O1, Q1, M2, S2, N2, K2

Calibration

The results of the December 1999 model calibration simulation are shown in Figure 3-1, in which water surface elevation field measurements at Fort Pulaski (blue line) are compared to model predictions (red line). Comparison of the present model calibration with Figure 8 of the Savannah Harbor Entrance Channel: Nearshore Placement of Dredged Material Study Report demonstrates that the reconstitution of the original calibrated ADCIRC grid and input files was successful.

Additional model verification comparisons are presented for the re-tracked Hurricane Hugo and November 1979. Figure 3-2 presents measured and predicted water surface elevations at Fort Pulaski during the re-tracked Hurricane Hugo simulation period. The figure shows that the measured and predicted water surface elevation compare well up to the time when the storm track was altered to directly impact the area (0000 to 1200 UTC 22 September 1989). Finally, a validation comparison of measured and predicted water surface elevations for the November 1979 simulations is presented in Figure 3-3, in which it is seen that model predictions compare well to the gauge data.

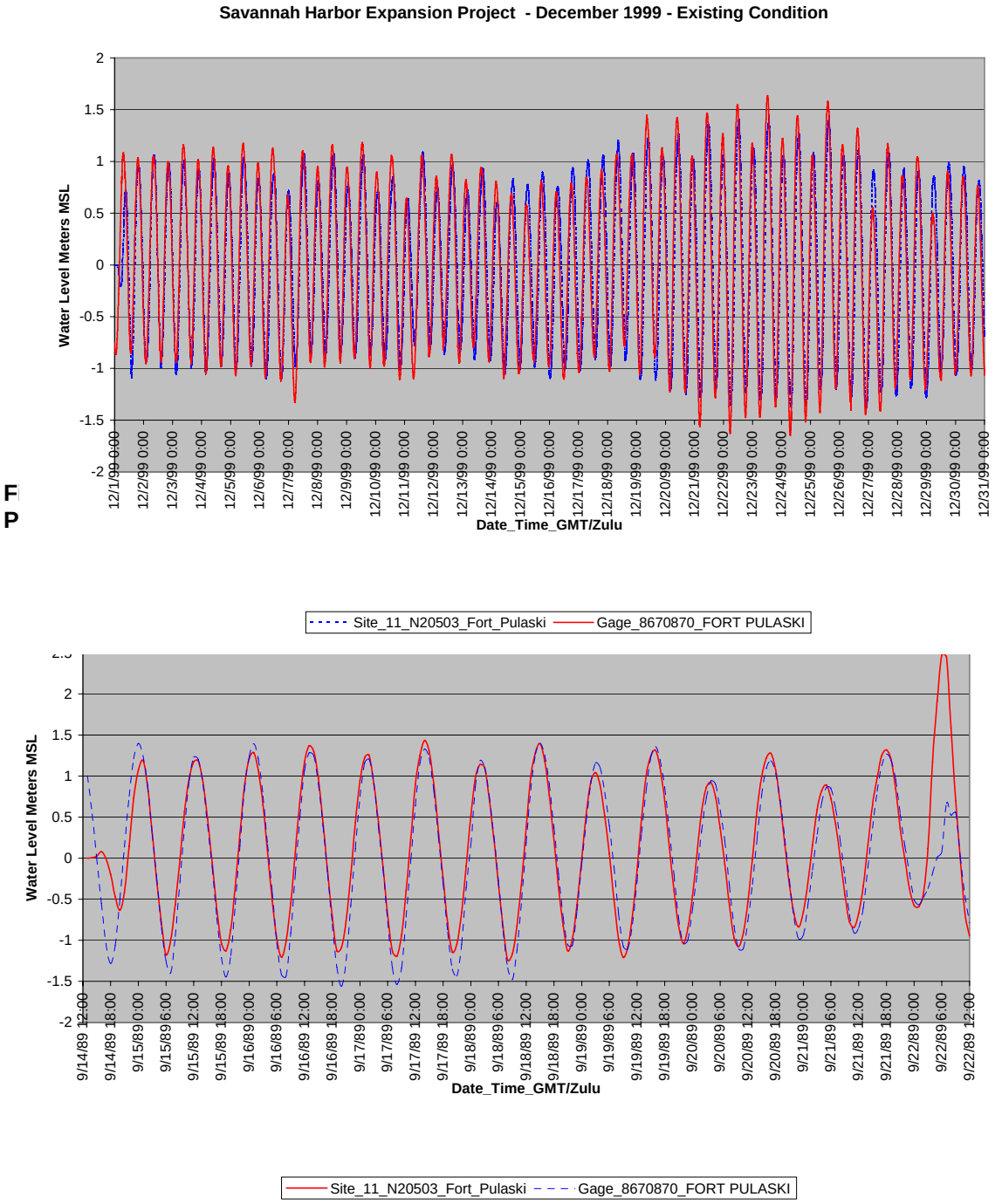

Figure 3-2. Comparison of measured and predicted water surface elevations for the retracked Hurricane Hugo. Note the divergence from measurements on 22 September when the storm track was altered to strike Savannah.

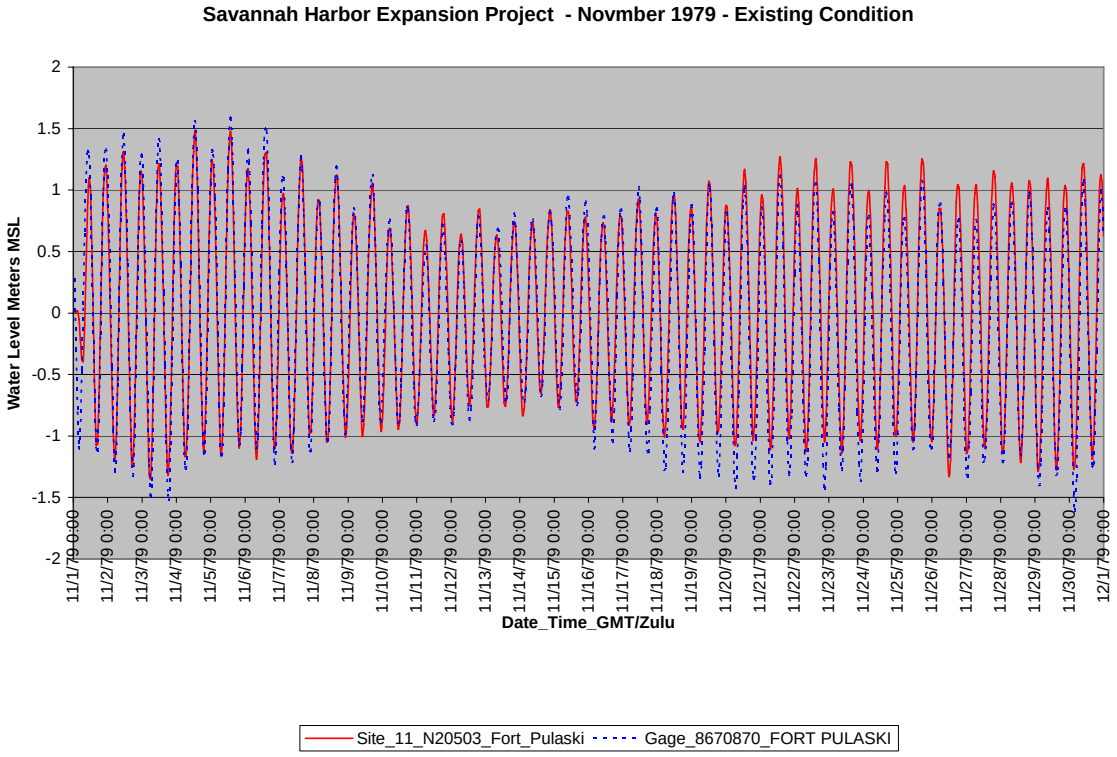

Figure 3-3. Comparison of measured and predicted water surface elevations for the November 1979 simulation period.

Circulation Model Results

Figure 3-4 shows the water levels and current vectors for the existing bathymetry at the peak of the re-tracked Hurricane Hugo. The maximum current velocities are 2 m/sec and the maximum water surface elevations (WSE) range from 2.8 m at Tybee Island to 3.3 m at the southern end of Hilton Head Island. Figure 3-5 shows an expanded view of the surge and longshore currents at Tybee Island at the peak of the storm. Figure 3-6 shows the maximum water surface elevation over the entire simulation for each node in the domain. Differences in the water surface elevations and depth-averaged velocity patterns were obtained by subtracting the global maximum value fields of the existing simulation results from the channel deepening simulation results. The differences, thus, are difference in maximum values over an entire simulation. Figure 3-7 shows the difference in maximum water surface elevation for the deepened channel simulation minus the existing condition simulation. The nearshore peak water level is approximately 0.20 m lower for the deepened channel. The deepened channel provides slightly less resistance to flow (more conveyance) to the nearshore, so the surge peaks earlier and at a slightly lower level. The difference in maximum depth-averaged current magnitude is shown in Figure 3-8. The maximum current magnitudes are 0.15 to 0.20 m/sec stronger in the channel for the deepened channel. The maximum currents along Tybee Island are generally slightly weaker with the deepened channel. In other very shallow areas (e.g., at the shoreline and on ebb shoal), there are localized maximum current differences on the order of 0.5 m/sec. These are most likely a remnant of the nonlinearity of flooding and drying or accelerations in very shallow water and are not representative of mean processes.

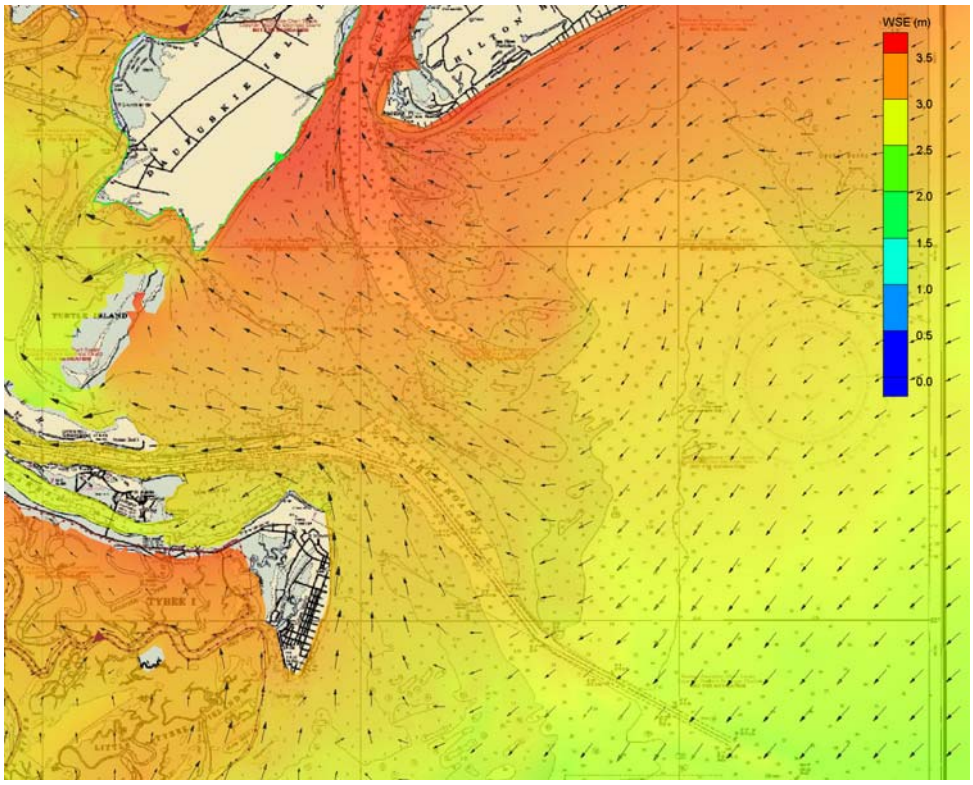

Figure 3-4. Water surface elevations and current vectors at the peak of the re-tracked Hurricane Hugo.

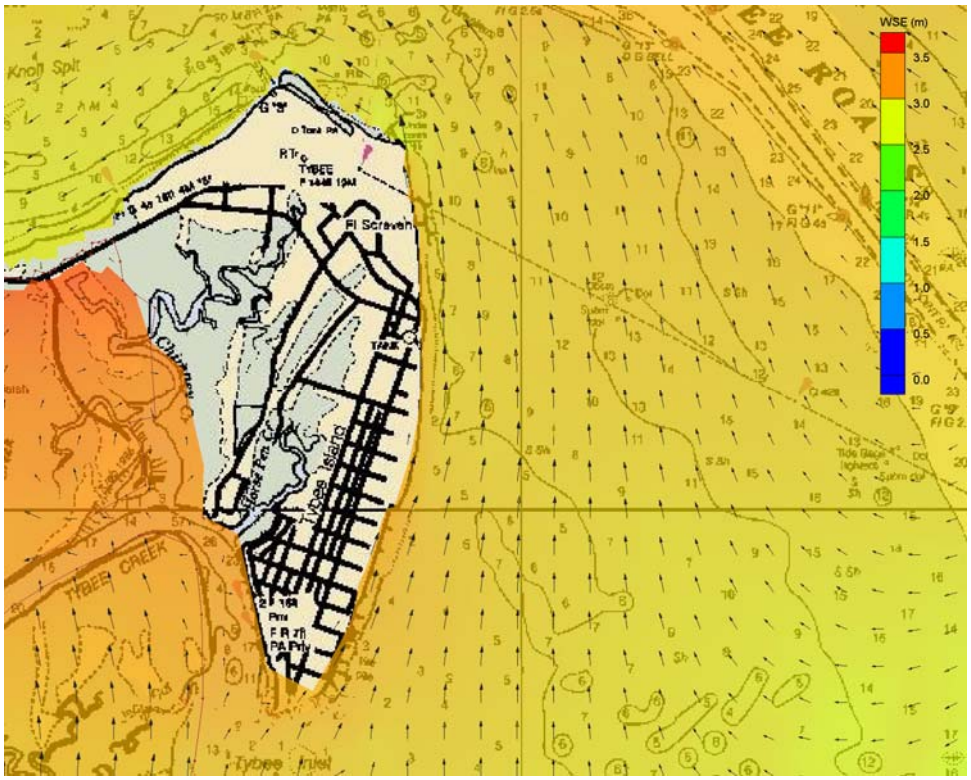

Figure 3-5. Water surface elevations and current vectors at Tybee Island at the peak of the re-tracked Hurricane Hugo.

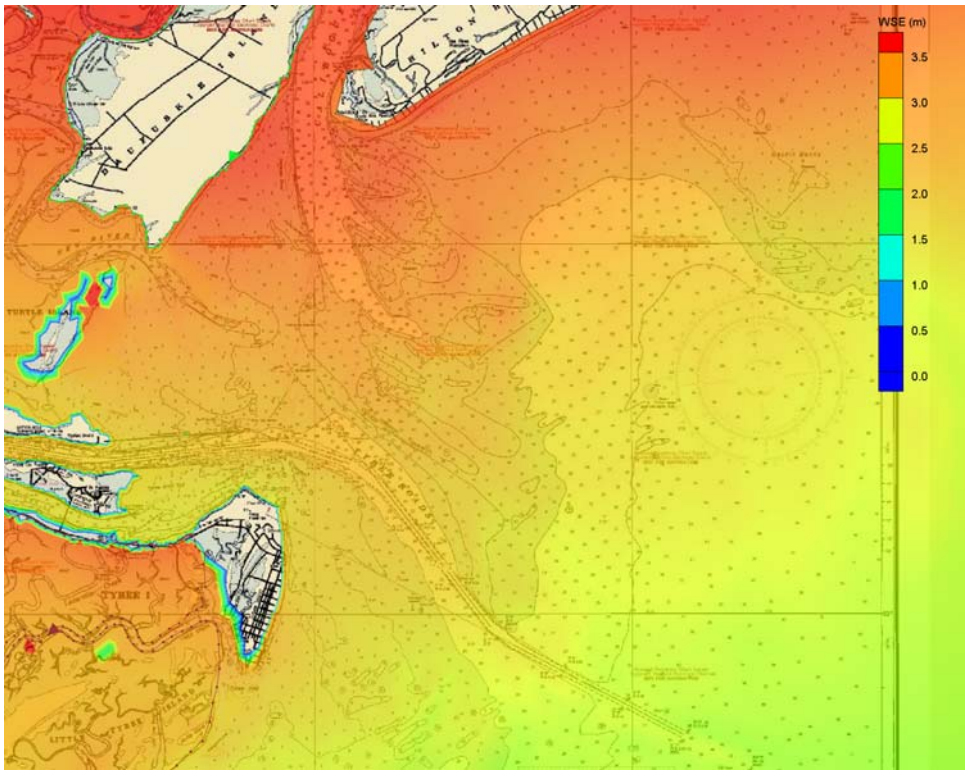

Figure 3-6. Maximum water surface elevations for the re-tracked Hurricane Hugo (existing).

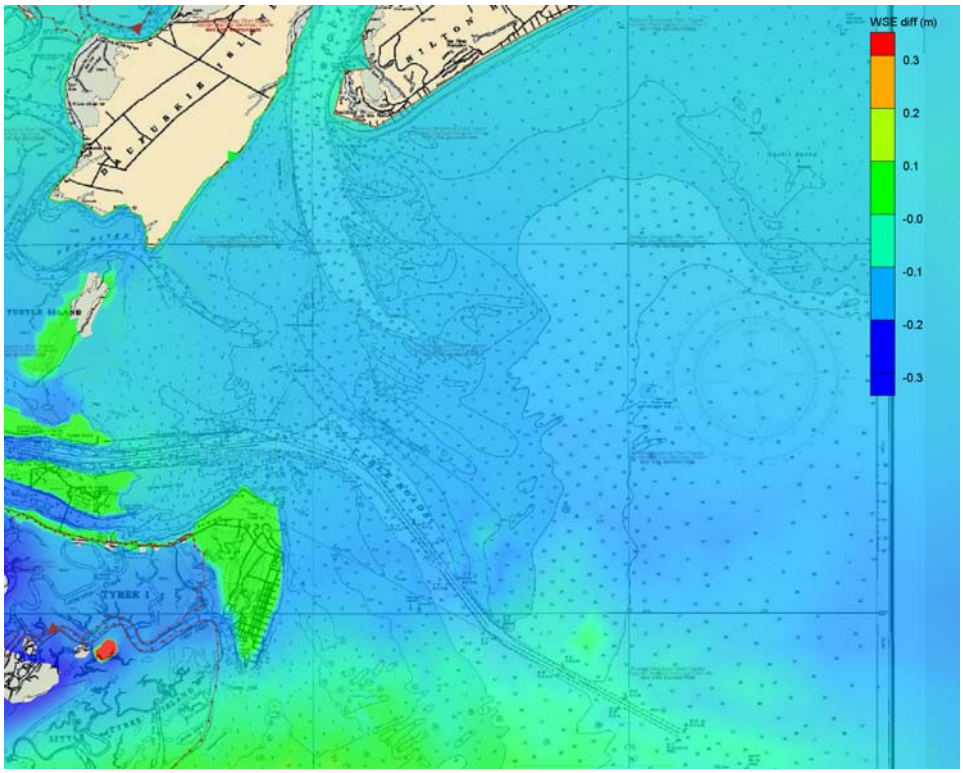

Figure 3-7. Difference in maximum water surface elevations for the re-tracked Hurricane Hugo (deepened channel minus existing bathymetry).

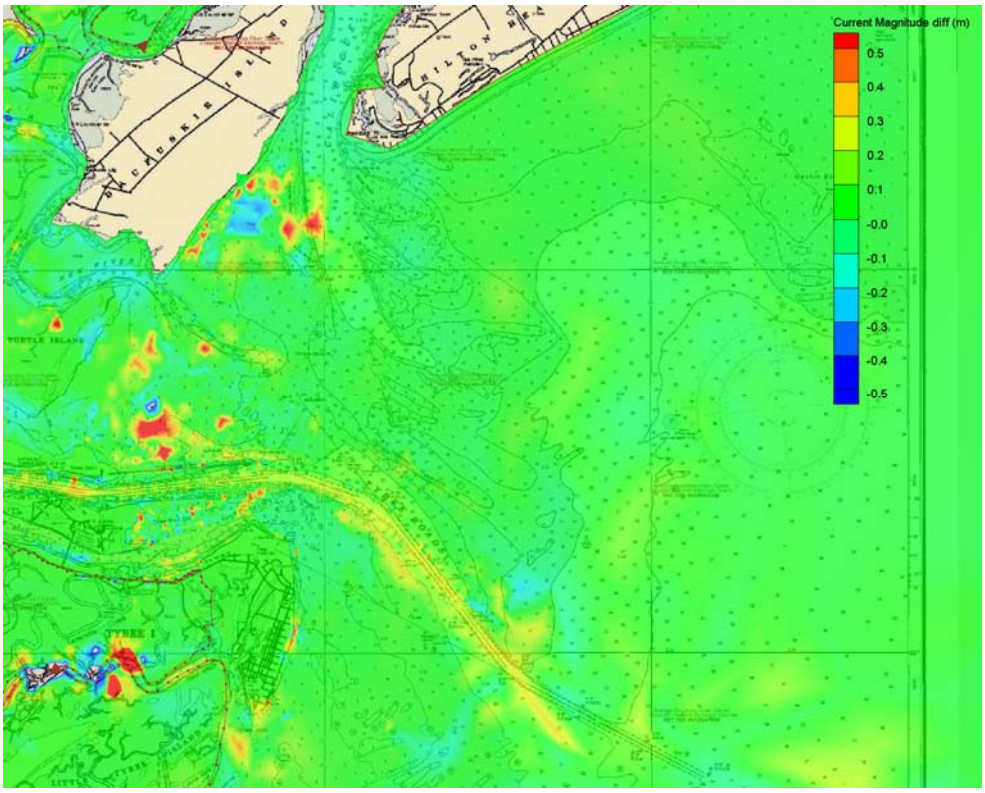

Figure 3-8. Difference in maximum current magnitudes for the re-tracked Hurricane Hugo (deepened channel minus existing bathymetry).

The inclusion of wave stresses in the ADCIRC simulations has a significant effect and is included in both the existing and deepened channel simulations. Figure 3-9 shows the increase in water surface elevation when wave stresses are included in the model forcing for the re-tracked Hurricane Hugo at the peak of the storm (existing condition). Water surface elevations increase by as much as 0.5 m at the Tybee Island shoreline and 0.2 to 0.3 m on the platform seaward of Tybee Island. Currents along the shoreline increase up to 1 m/sec (Figure 3-10). Comparing Figures 3-9 and 3-10, it is seen that the wave stresses manifest themselves more strongly in wave setup on the southern end of the island and longshore currents on the northern end at the peak of the storm. This is due to the curvature of the island at the northern end and the relatively more oblique wave angles forcing the current.

Figure 3-11 shows the residual currents for the re-tracked Hugo simulation. The residual currents are average currents calculated for each grid node for the entire simulation (a few points are excluded at the beginning and end of the simulation to match the phasing of the tide at the beginning and end of the simulation). The residual current patterns for all simulations are similar, although the patterns for the re-tracked Hugo are somewhat more chaotic because of the intensity of the event. The residual patterns show ebb dominance in the channels and generally flood dominance on the shoals. A divergence point in the residual currents is seen along the mid Tybee Island shoreline, with residual currents toward the north on the north end and toward the south on the south end. The southern trend is weaker in the other simulations. Figure 3-12 shows the difference in residual currents for the deepened channel (deepened – existing). The residual current are stronger in the channel (flowing offshore) and weaker on the shoals (including north Tybee) with the deepened channel. The maximum differences for this extreme event is approximately 0.1 m/sec

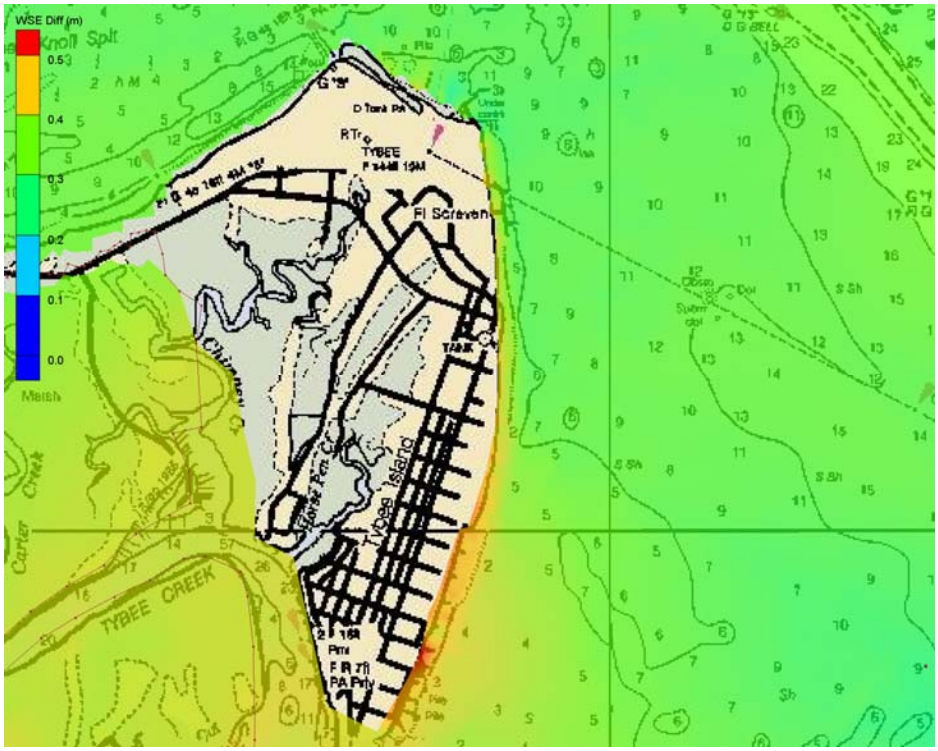

Figure 3-9. Difference in water surface elevation at the peak of the re-tracked Hurricane Hugo due to inclusion of wave stresses.

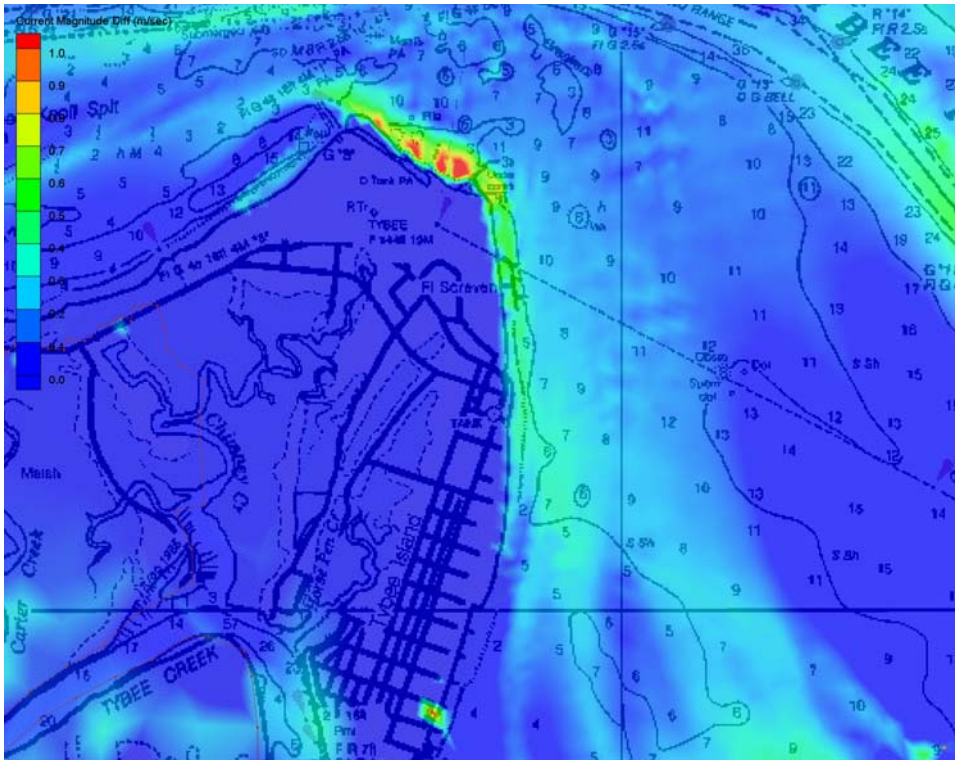

Figure 3-10. Difference in current magnitudes at the peak of the re-tracked Hurricane Hugo

due to inclusion of wave stresses.

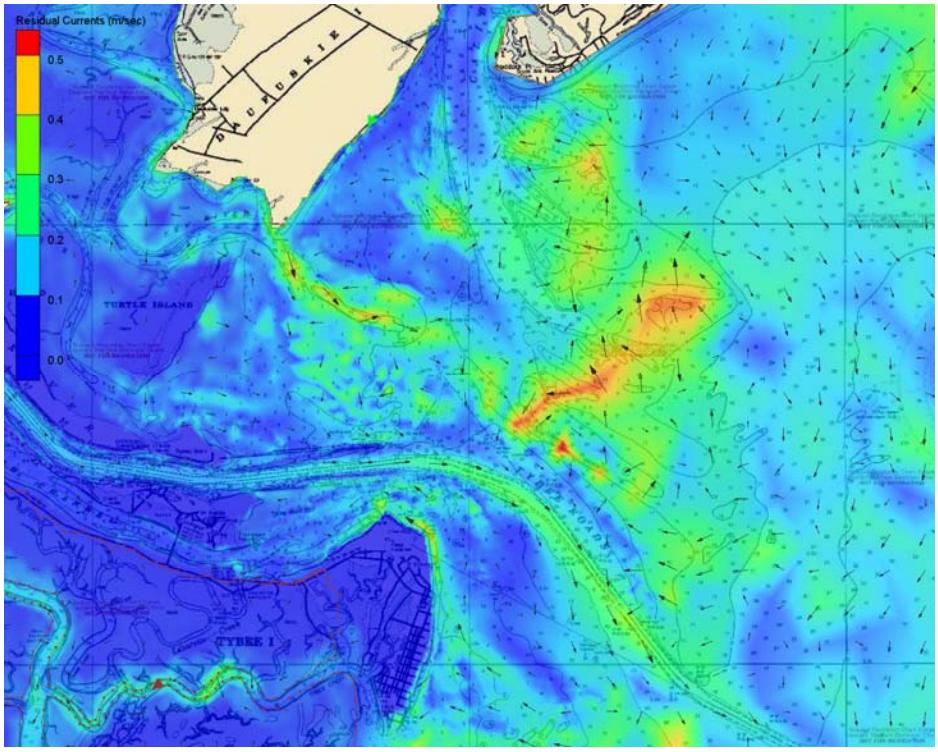

Figure 3-11. Residual currents for re-tracked Hurricane Hugo (existing condition).

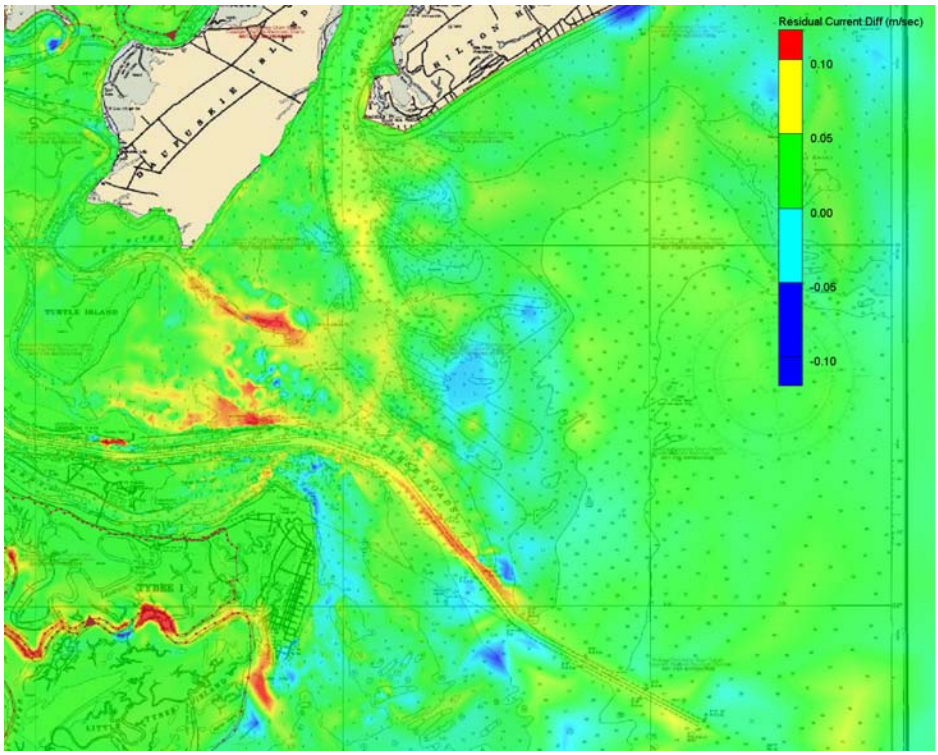

Figure 3-12. Difference in residual current magnitudes for re-tracked Hurricane Hugo (deepened channel minus existing bathymetry).

Figure 3-13 shows the difference in maximum water surface elevations for November 1979. The pattern of differences is more localized and variable than for the re-tracked Hurricane Hugo. The maximum water surface elevations are minimally lower at Tybee Island (0.01 m) and slightly higher at Turtle and Daufuskie Islands (0.012 m and 0.014 m, respectively). These magnitudes of differences are negligible. In areas of flooding and drying, larger local maximum differences are seen, on the order of 0.5 m. The differences in maximum depth-averaged current magnitude for November 1979 are shown in Figure 3-14. In the deepened channel, increases in maximum current magnitude are less than 0.08 m/sec. Maximum currents beside the channel are slightly decreased. Again, localized differences in current maxima occur in very shallow areas. Figure 3-15 shows the differences in residual current magnitude for November 1979. Although the maximum currents increased for the deepened channel, the residual currents tend to decrease slightly in the inner channel and increase slightly in the outer channel (generally less than +/-0.01 m/sec). Residual currents along northern Tybee Island are also slightly reduced.

Figures 3-16 and 3-17 show the maximum water surface elevation and current magnitude differences for January 1992. The maximum water surface elevations are generally 0.02 m lower on the inner shelf for the deepened channel, but 0.01 to 0.03 m higher in the inner channels and estuaries. Current magnitudes are a maximum of 0.09 m/sec larger in the channel. Figure 3-18 shows the differences in residual current magnitude for January 1992. The trends are similar to November 1979, with slight reductions in residual currents in the channel and north of Tybee.

Figures 3-19 and 3-20 show the maximum water surface elevation and current magnitude differences for July 1999. The maximum water surface elevations are generally 0.03 m higher at Turtle and Daufuskie Islands and lower by up to 0.02 m at southern Tybee Island for the deepened channel. Current magnitudes are a maximum of 0.07 m/sec larger in the channel. Figure 3-21 shows the differences in residual current magnitude for July 1999. The trends are similar to the previous simulations, with slight reductions in residual current in the channel and north of Tybee.

Figures 3-22 and 3-23 show the maximum water surface elevation and current magnitude differences for December 1999. The maximum water surface elevations are minimally lower at Tybee Island (0.01 m) and slightly higher at Turtle and Daufuskie Islands (0.007 m and 0.005 m, respectively). This pattern is similar to November 1979. Current magnitudes are a maximum of 0.06 m/sec larger in the channel. Figure 3-24 shows the differences in residual current magnitude for December 1999. The trends are similar to the previous simulations, with slight reductions in residual current in the channel and north of Tybee.

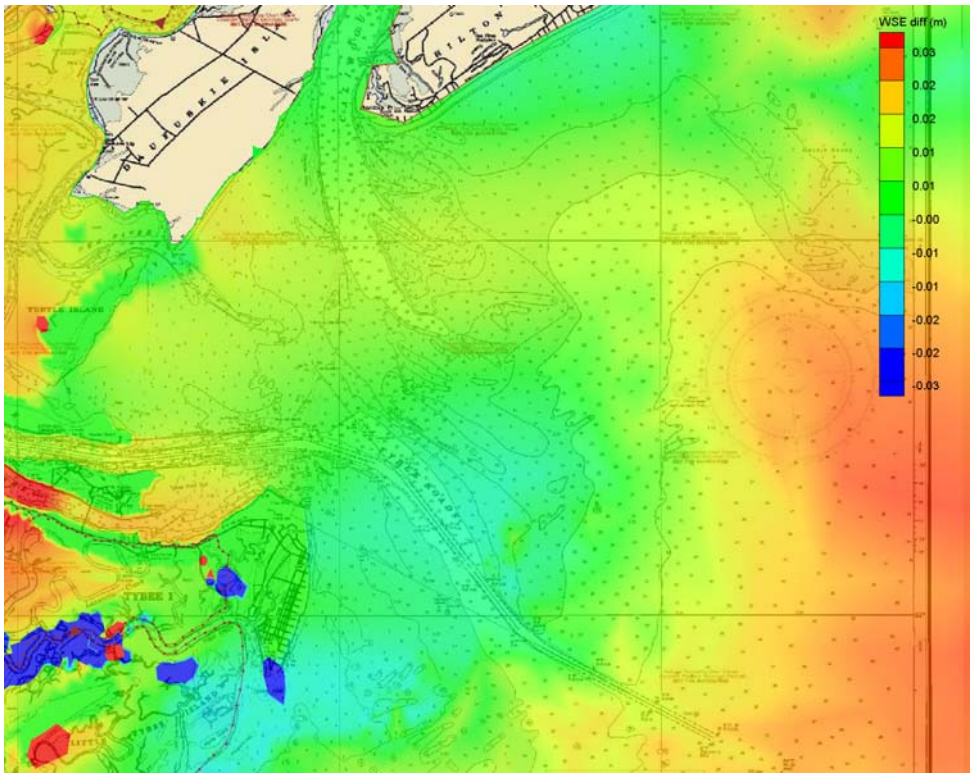

Figure 3-13. Difference in maximum water surface elevations for November 1979 (deepened channel minus existing bathymetry).

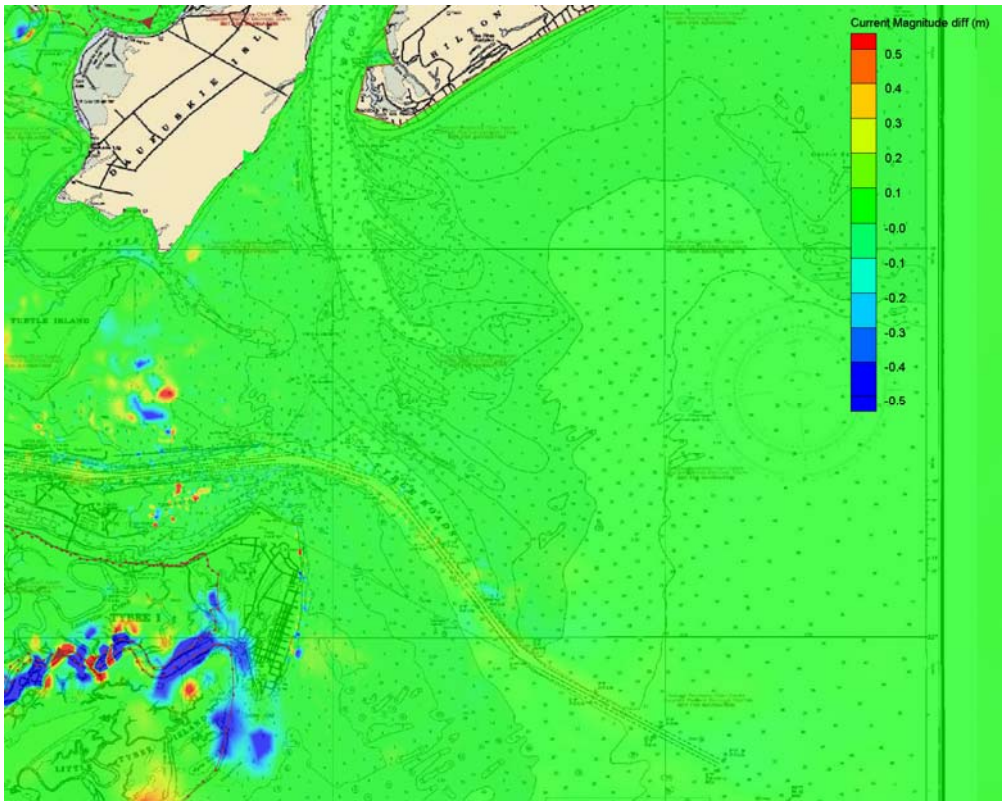

Figure 3-14. Difference in maximum current magnitudes for November 1979 (deepened channel minus existing bathymetry).

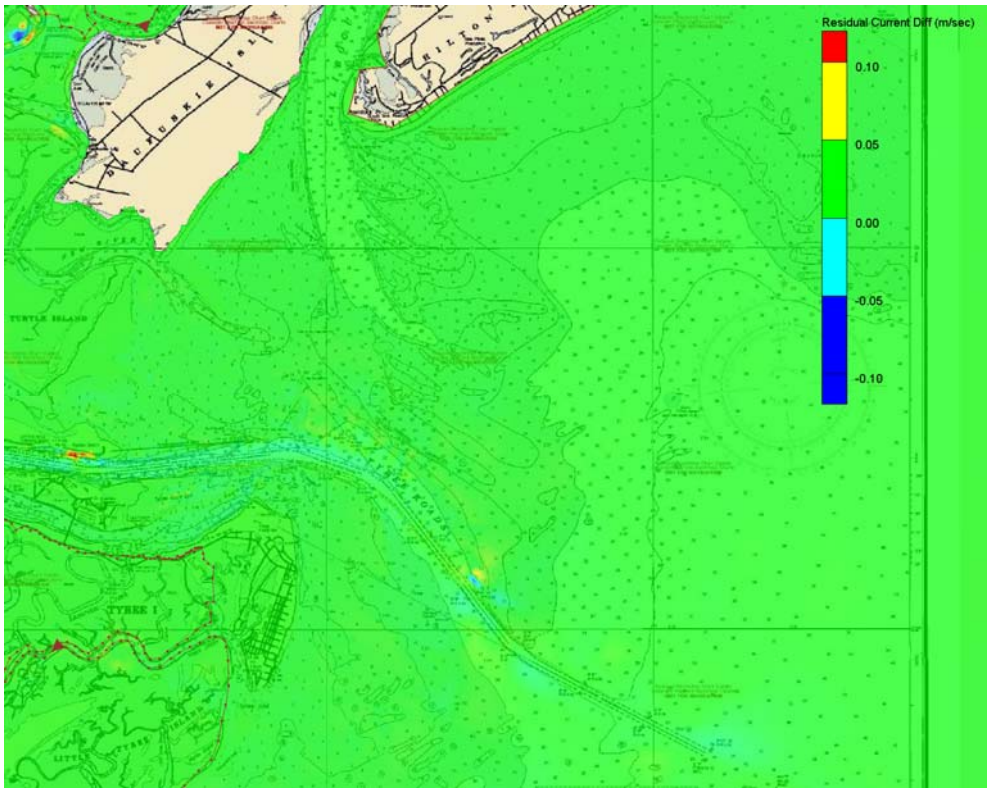

Figure 3-15. Difference in residual current magnitudes for November 1979 (deepened channel minus existing bathymetry)

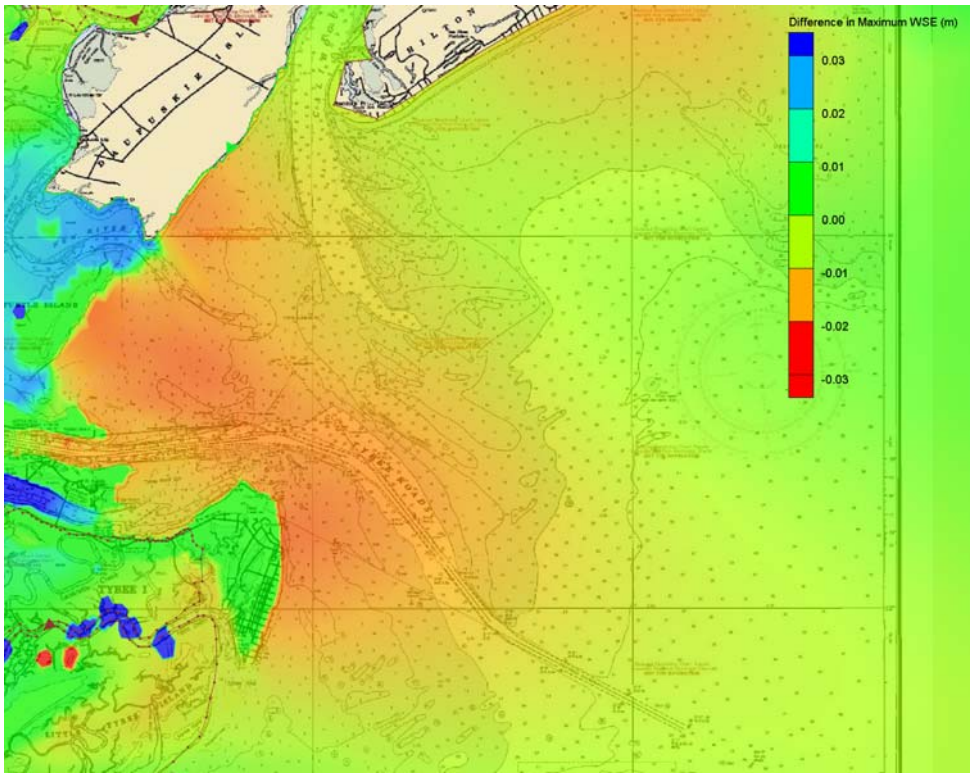

Figure 3-16. Difference in maximum water surface elevations for January 1992 (deepened channel minus existing bathymetry).

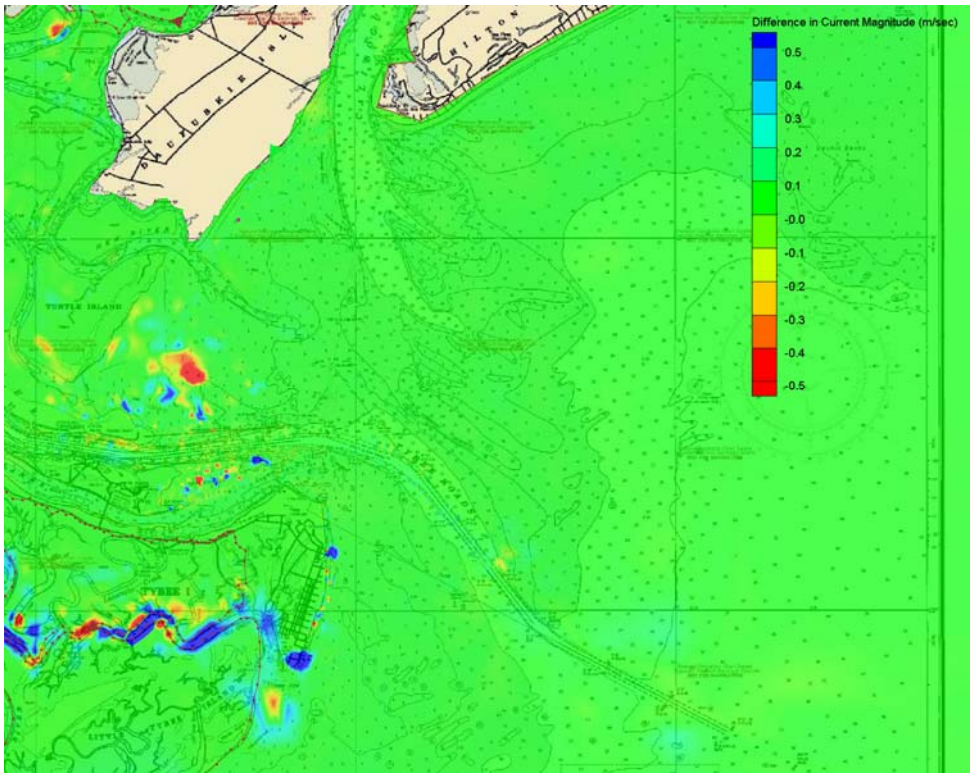

Figure 3-17. Difference in maximum current magnitudes for January 1992 (deepened channel minus existing bathymetry).

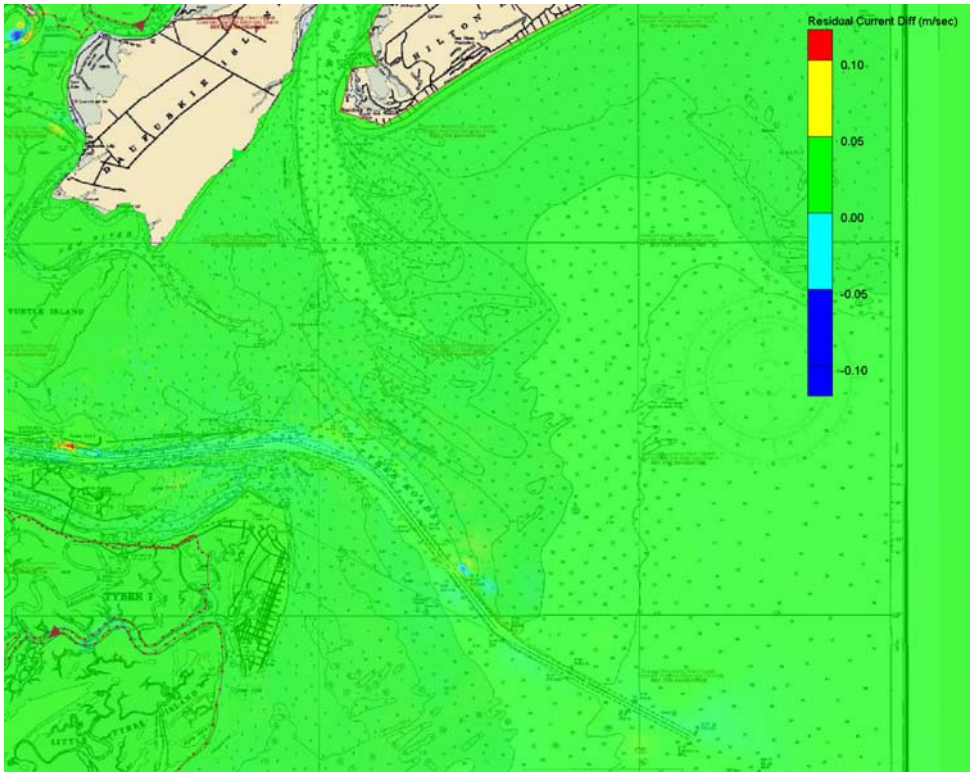

Figure 3-18. Difference in residual current magnitudes for January 1992 (deepened channel minus existing bathymetry).

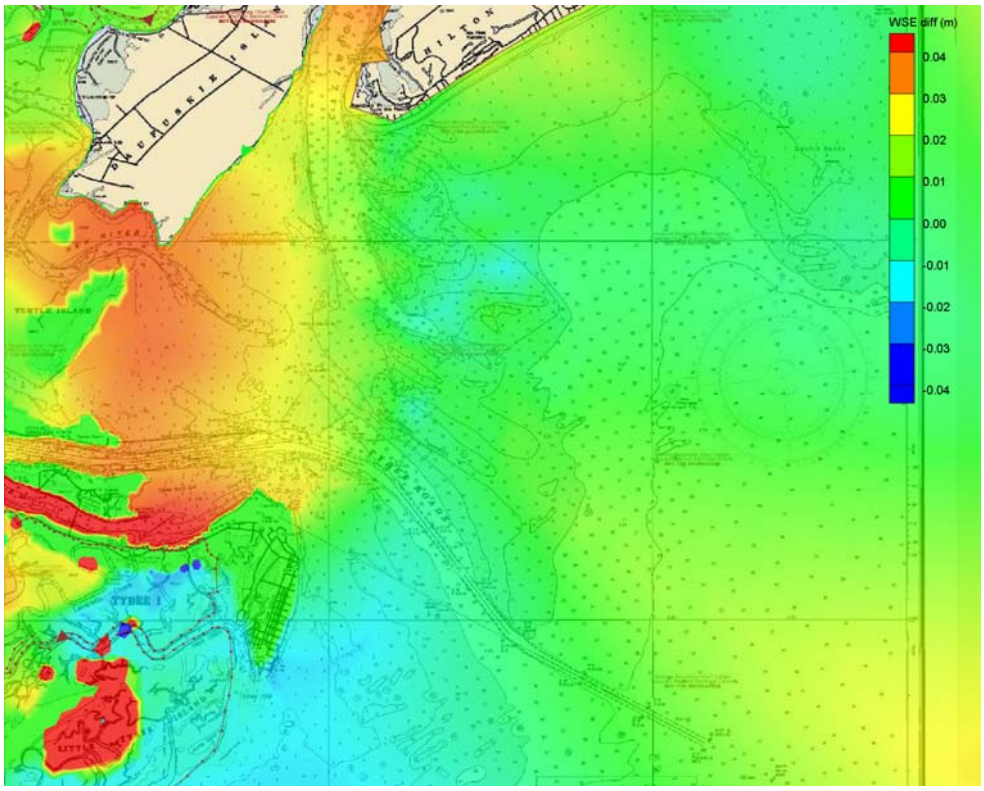

Figure 3-19. Difference in maximum water surface elevations for July 1999 (deepened channel minus existing bathymetry).

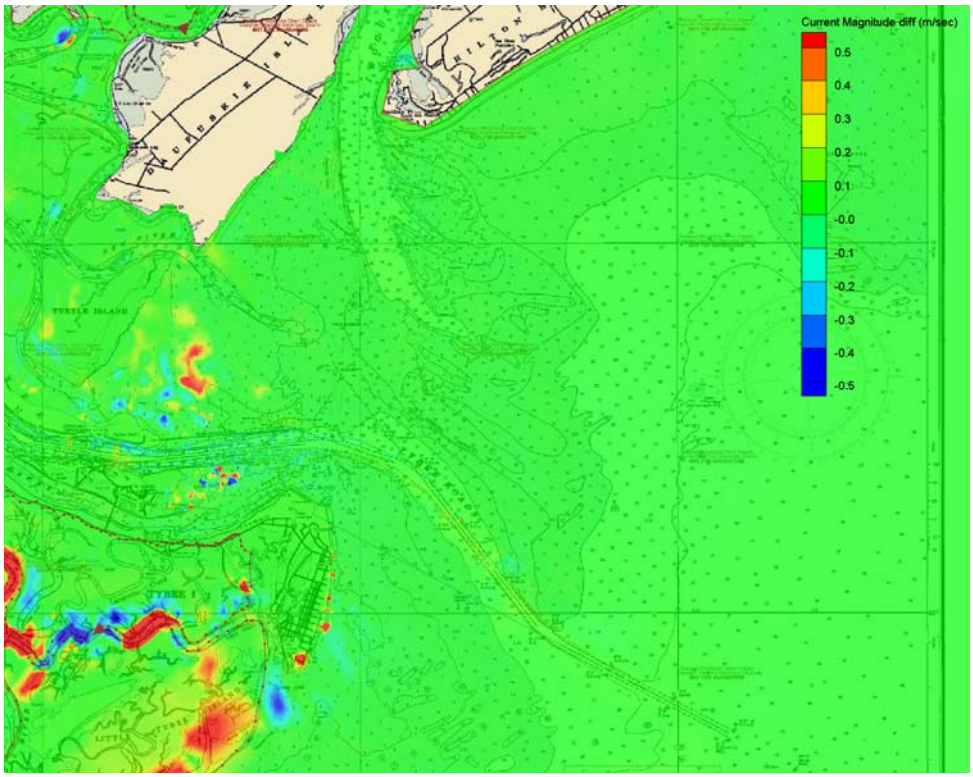

Figure 3-20. Difference in maximum current magnitudes for July 1999 (deepened channel minus existing bathymetry).

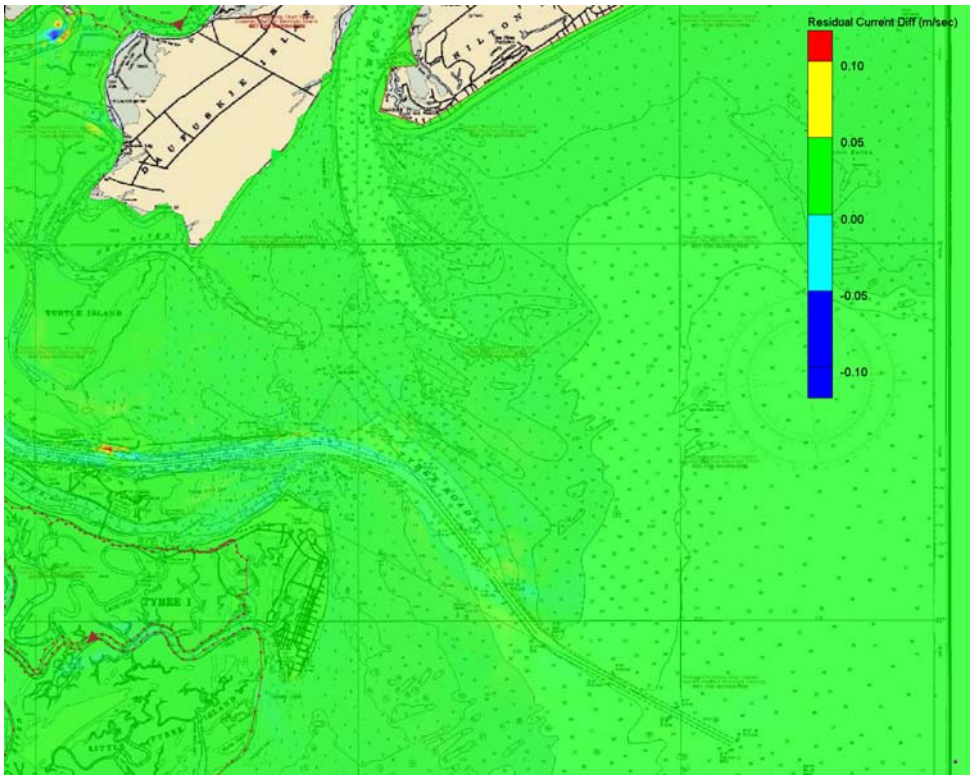

Figure 3-21. Difference in residual current magnitudes for July 1999 (dedeepened channel minus existing bathymetry).

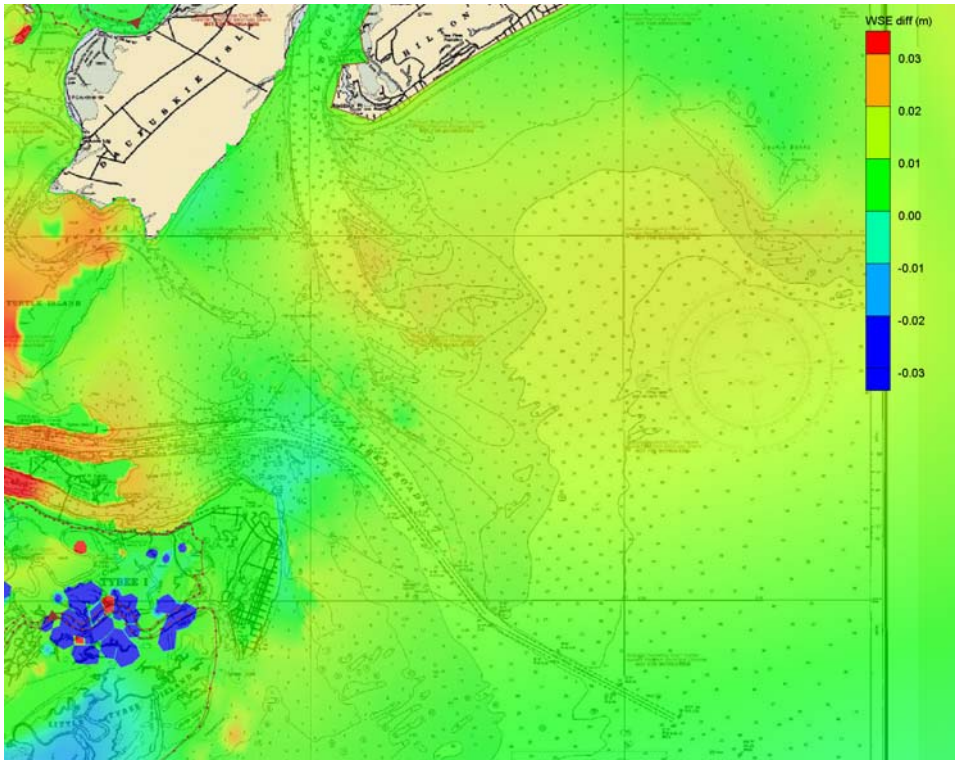

Figure 3-22. Difference in maximum water surface elevations for December 1999 (deepened channel minus existing bathymetry).

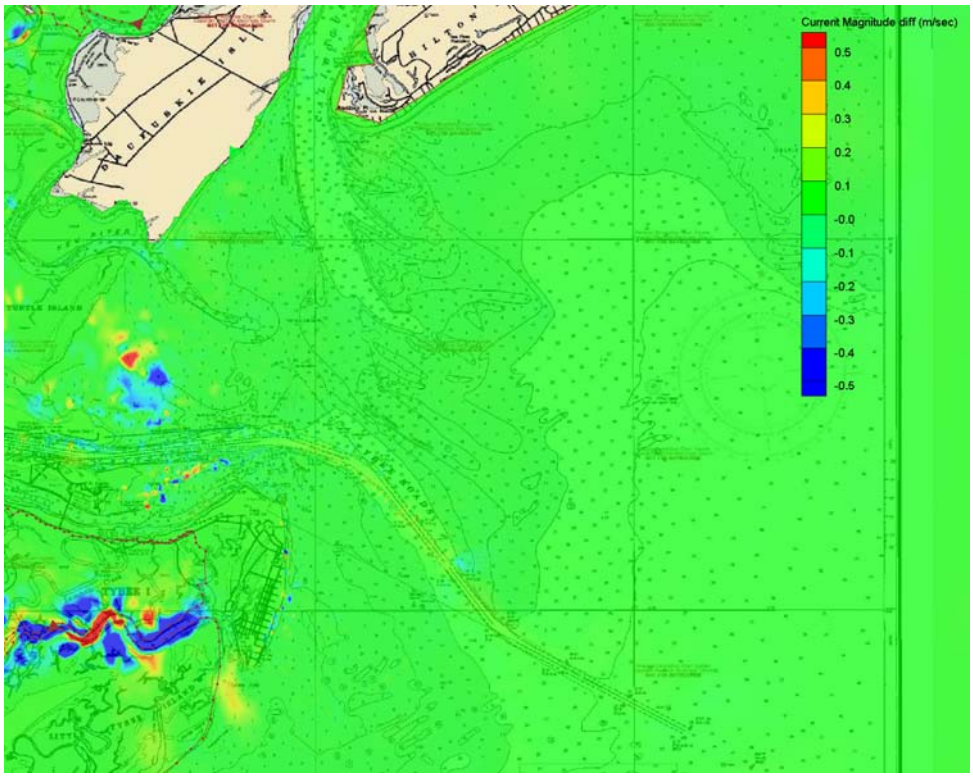

Figure 3-23. Difference in maximum current magnitudes for December 1999 (deepened channel minus existing bathymetry).

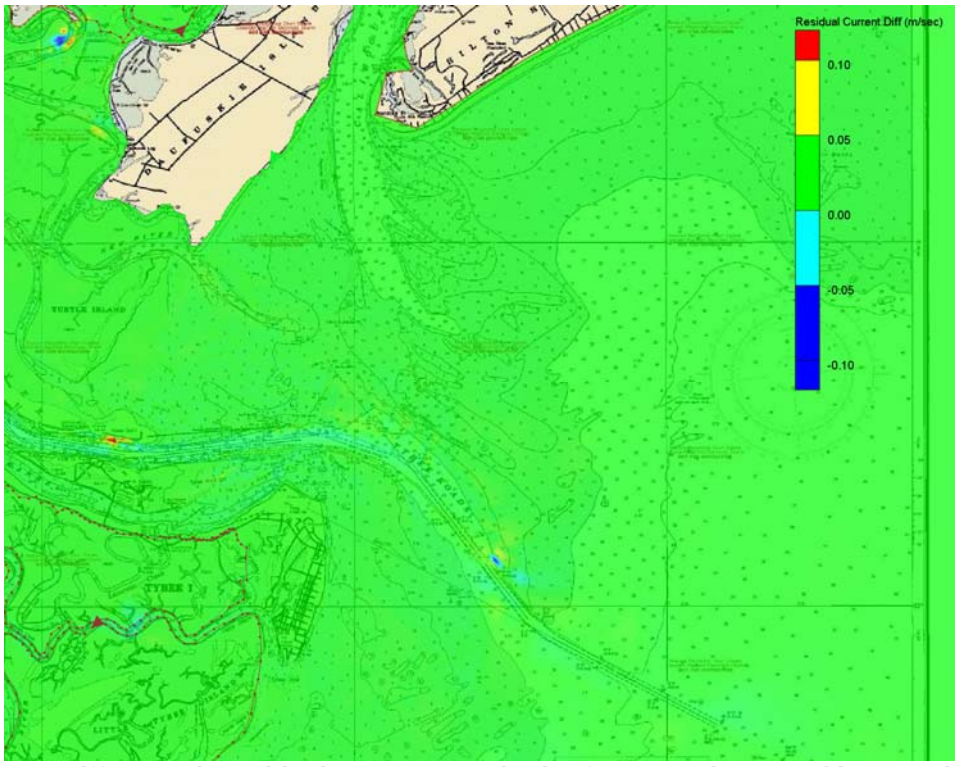

Figure 3-24. Difference in residual current magnitudes for December 1999 (deepened channel minus existing bathymetry).

Summary of Circulation Results

ADCIRC was applied for five time periods to cover a large range of conditions at Savannah. Forcing for ADIRC includes tides, wind, atmospheric pressure, river inflow, and wave stresses. ADCIRC was applied to provide water surface elevations to the wave model (Chapter 4) and tidal current and water depths to the sediment model (Chapter 5). The model results were also used to investigate the channel deepening impact on maximum water surface elevations and currents. In general, the channel deepening had a minimal influence on the maximum water surface elevation over a simulation (~ one month). Maximum differences were generally on the order of a few centimeters, but were as large at 0.2 m for the re-tracked hurricane Hugo. The maximum nearshore water surface elevations decreased for the deepened channel for Hugo because the peak water level near the shore arrived earlier, but with a slightly lower elevation. Hugo was a relatively fast-moving hurricane at landfall, so the reduced surge for the deepened channel will likely be minimal for a slow moving storm. Maximum current magnitudes generally increased in the deepened channel (up to 0.2 m/sec), but differences were generally very small elsewhere. The five time periods included large variations in forcing conditions and different patterns for small increases and decreases in surge, but differences between the existing and deepened channel maximum water surface elevations were insignificant (on the order of 0-3 cm). Maximum current magnitudes increased on the order of 0.1 m/sec, which again is insignificant. Residual currents generally decreased in the inner channel and along north Tybee and increased in the outer channel, but these differences were generally negligible (+/- 0.01 m/sec). The circulation model does give localized differences in maximum water level and current velocities in very shallow water and areas of flooding and drying, due to the nonlinearity of the processes and changes in phasing of flooding and drying, however, these effects are artifacts of the coarse resolution in those areas. The tidal creeks and marshes were not fully resolved in the model, but were designed to provide the proper inflow/outflow volumes.

4 Wave Modeling

Waves, together with tidal currents, drive sediment transport in the areas adjacent to the Savannah Federal navigation channel. Numerical model simulations of wave transformation were required to evaluate changes in the magnitude and spatial variation of wave parameters due to the deepened Savannah navigation channel. The wave results also serve as an input to estimates of sediment transport described in Chapter 5. The steady-state spectral wave model STWAVE (Smith, Sherlock, and Resio 2001) was applied for wave transformation modeling. STWAVE was forced with directional wave spectra based on typical and storm waves hindcast by the Wave Information Studies (WIS). The simulations include representative tide and surge water levels. This section describes the STWAVE wave transformation model, the model input, and model results.

STWAVE Model Description

The numerical model STWAVE was used to transform waves to the project sites. STWAVE numerically solves the steady-state conservation of spectral action balance along backward-traced wave rays:

$$(C_{ga})_x \frac{\partial}{\partial x}\frac{C_a C_{ga}\cos(\mu-\alpha)E(f,\alpha)}{\omega_r} + (C_{ga})_y \frac{\partial}{\partial y}\frac{C_a C_{ga}\cos(\mu-\alpha)E(f,\alpha)}{\omega_r} = \sum\frac{S}{\omega_r} \quad (4\text{-}1)$$

where

C_{ga} = absolute wave group celerity

x,y = spatial coordinates, subscripts indicate x and y components

C_a = absolute wave celerity

μ = current direction

α = propagation direction of spectral component

E = spectral energy density

f = frequency of spectral component

ω_r = relative angular frequency (frequency relative to the current)

S = energy source/sink terms

The source terms include wind input, nonlinear wave-wave interactions, dissipation within the wave field, and surf-zone breaking. The terms on the left-hand side of Equation 4-1 represent

wave propagation (refraction and shoaling), and the source terms on the right-hand side of the equation represent energy growth or decay in the spectrum.

The assumptions made in STWAVE are as follows:

a. Mild bottom slope and negligible wave reflection.

b. Steady waves, currents, and winds.

c. Linear refraction and shoaling.

d. Depth-uniform current.

The version of STWAVE applied here is a half-plane model, meaning that only waves propagating toward the coast are represented. Waves reflected from the coast or waves generated by winds blowing offshore are neglected. Wave breaking in the surf zone limits the maximum wave height based on the local water depth and wave steepness:

$$H_{mo_{\max}} = 0.1L \tanh kd \tag{4-2}$$

where

H_{mo} = zero-moment signficant wave height

L = wavelength

k = wave number

d = water depth

STWAVE is a finite-difference model and calculates wave spectra on a rectangular grid with square grid cells. The model outputs zero-moment wave height, peak wave period (T_p), and mean wave direction (α_m) at all grid points and two-dimensional spectra at selected grid points.

Wave Model Inputs

The inputs required to execute STWAVE are as follows:

a. Bathymetry grid (including shoreline position and grid size and resolution).

b. Incident frequency-direction wave spectrum on the offshore grid boundary.

c. Current field (optional).

d. Tide elevation, wind speed, and wind direction (optional).

Bathymetry grids. Two STWAVE Cartesian grids were generated for this study. The first grid represents the existing condition bathymetry, and the second grid represents the with-project bathymetry (deepened channel). The only differences between the existing condition and with-project STWAVE grids are the channel improvements. The STWAVE grids were created by combining the ADCIRC model mesh in and around the Federal navigation channel with a February 2005 bathymetric survey offshore of Tybee Island and topography and bathymetry previously used for the Savannah Harbor Entrance Channel: Nearshore Placement of Dredged Material study (Gailani et al. 2003). Significant improvements to the ADCIRC mesh were made to more accurately capture both the existing navigation channel conditions and the with-project channel geometry. These efforts produced a channel with smoothly sloping sides and proper

depths in the appropriate channel sections. The grid origin is x = 538104.6 m and y = 3548280.0 m in UTM NAD83 Zone 17, and the grid orientation is 140 deg (which is the orientation of the grid x-axis measured counter-clockwise from East). The grid domain is 21.7 km (cross shore, 434 cells) by 31.6 km (alongshore, 631 cells) with a resolution of 50 m. The grid extends seaward to approximately 12-15 m water depth. The bathymetry grids are shown in Figures 4-1 and 4-2.

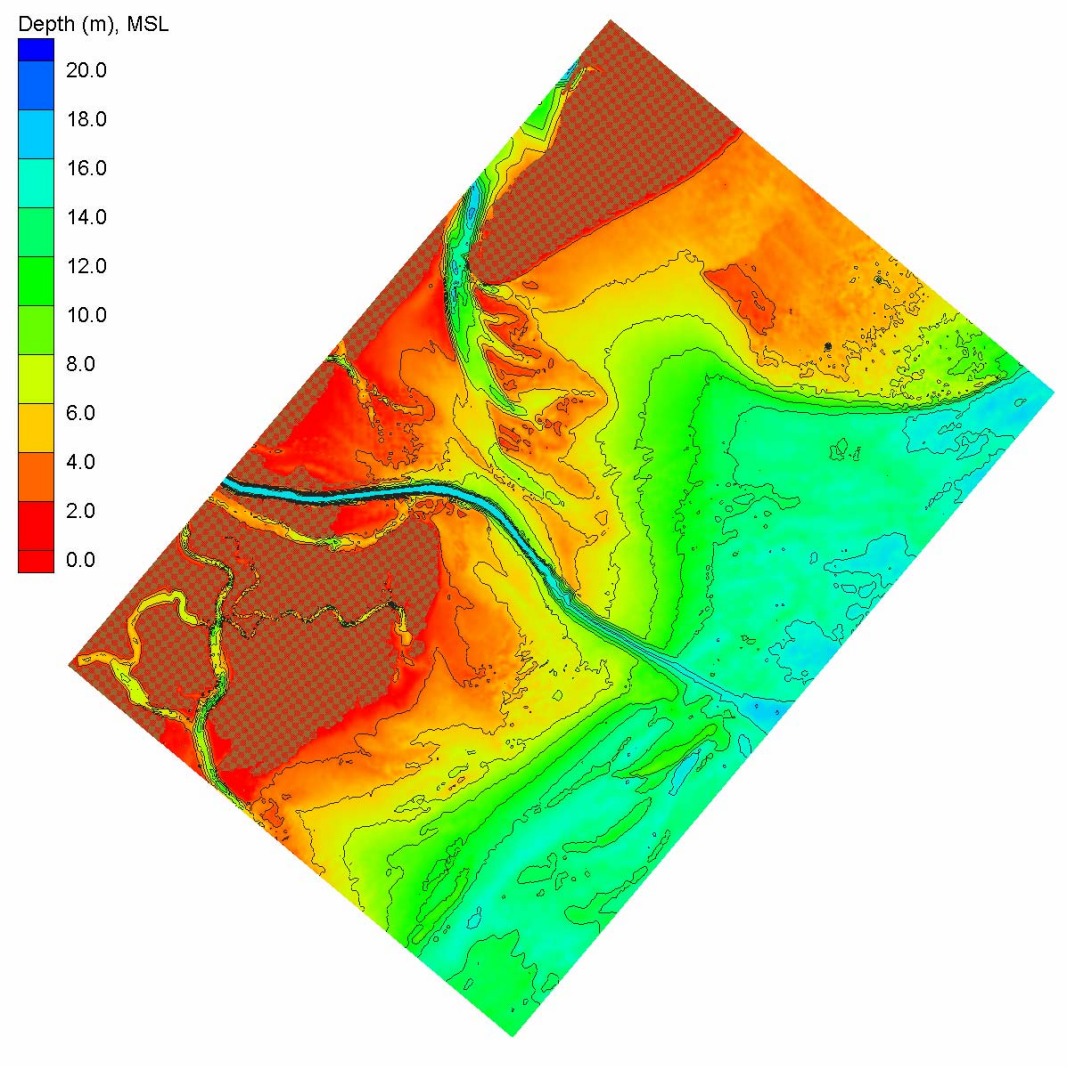

Figure 4-1. Existing condition grid (depths in meters, MSL). Land is shown in brown.

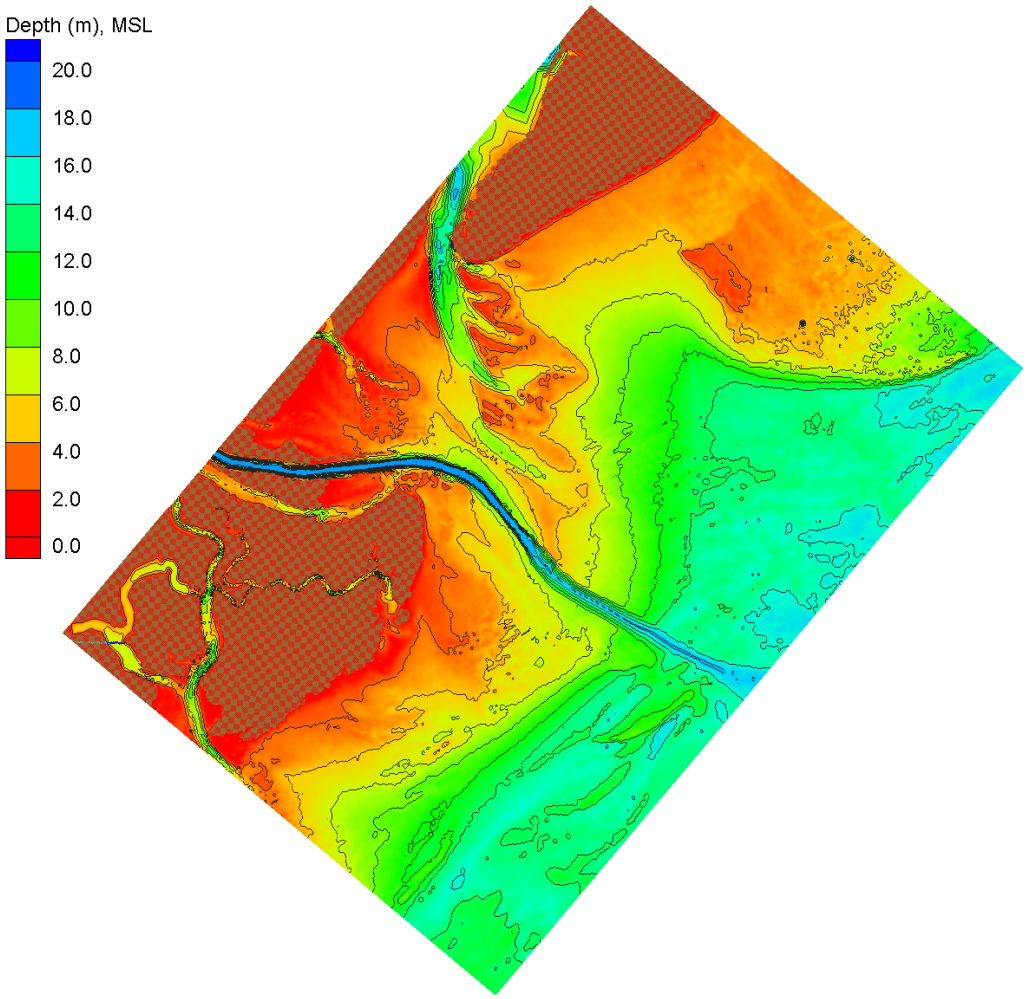

Figure 4-2. With-project grid (depths in meters, MSL). Land is shown in brown.

Input wave conditions. Five time periods were selected for wave simulation: a) December 1999 was simulated to represent the ADCIRC calibration period; b) a re-tracked Hurricane Hugo (tracked to hit near Savannah), 14-22 September 1989, was simulated to represent an extreme storm event; c) November 1979, which included a number of storms, was simulated to represent a stormy month; d) January 1992 was simulated to represent a typical winter month; and e) July 1999 was simulated to represent a typical summer month. The offshore wave information for all these simulations were hindcast by the Wave Information Studies (WIS) using the wave generation and propagation model WISWAVE (Hubertz 1992). For the January 1992, December 1999, and July 1999 simulations, hourly offshore wave conditions were taken from the latest WIS hindcast (1980-1999) at Station 368 (http://frf.usace.army.mil/cgi-bin/wis/atl/atl_main.html). WIS Station 368 is located at 32.0 deg North, 80.58 deg West in a water depth of approximately 15 m which is approximately on the offshore boundary of the STWAVE grids. The November 1979 time period is not included in the most recent WIS hindcast period, so it was necessary to use the 4-hourly data from the previous WIS study (Brooks and Brandon 1995) at Station 33 located at 32.0 deg North, 80.5 deg West in a water depth of approximately 13 m. Hurricane Hugo struck Charleston in September 1989 at a Category 4 storm. To evaluate the impact of an intense tropical storm, the Savannah Harbor nearshore placement of dredged material study

(Gailani et al. in prep.) simulated a hypothetical re-tracked Hurricane Hugo striking Savannah. The offshore waves for the re-tracked Hugo were generated using the WIS methodology. These same re-tracked Hugo offshore waves were used in this study. The re-tracked Hurricane Hugo wave information was available at 4-hour intervals. The simulation start and end times are summarized in Table 4-1.

Table4-1. Start and end times for STWAVE model simulations

Simulation	Start Date/Time (yyyymmddhh)	End Date/Time (yyyymmddhh)	Interval (hours)
Nov 79	1979110100	1979113021	3
Sep 89	1989091414	1989092209	3
Jan 92	1992010101	1992013100	1
Dec 99	1999120101	1999123100	1
Jul 99	1999070101	1999073100	1

Figures 4-3 to 4-7 show the time histories of offshore significant wave height, peak wave period, and mean wave direction for the five simulation time periods. Wave direction is reported in meteorological convention with waves from the north at 0 deg and waves from the east at 90 deg. The November 1979 and January 1992 simulations both have offshore wave heights exceeding 3 m and the re-tracked Hurricane Hugo has a maximum offshore wave height of 8 m (which is near depth-limited breaking at the offshore STWAVE grid boundary). Summary statistics of the offshore wave parameters are given in Table 4-2.

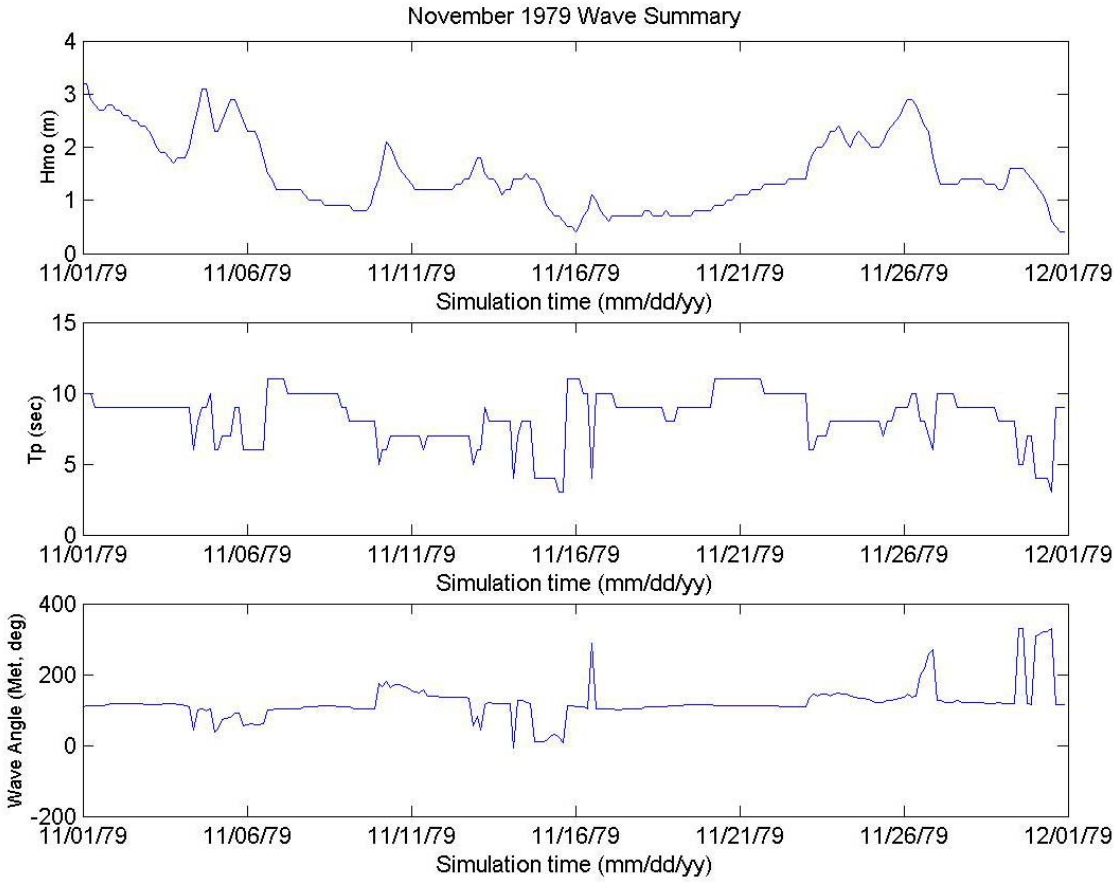

Figure 4-3. Offshore wave conditions for November 1979 at WIS Station 33.

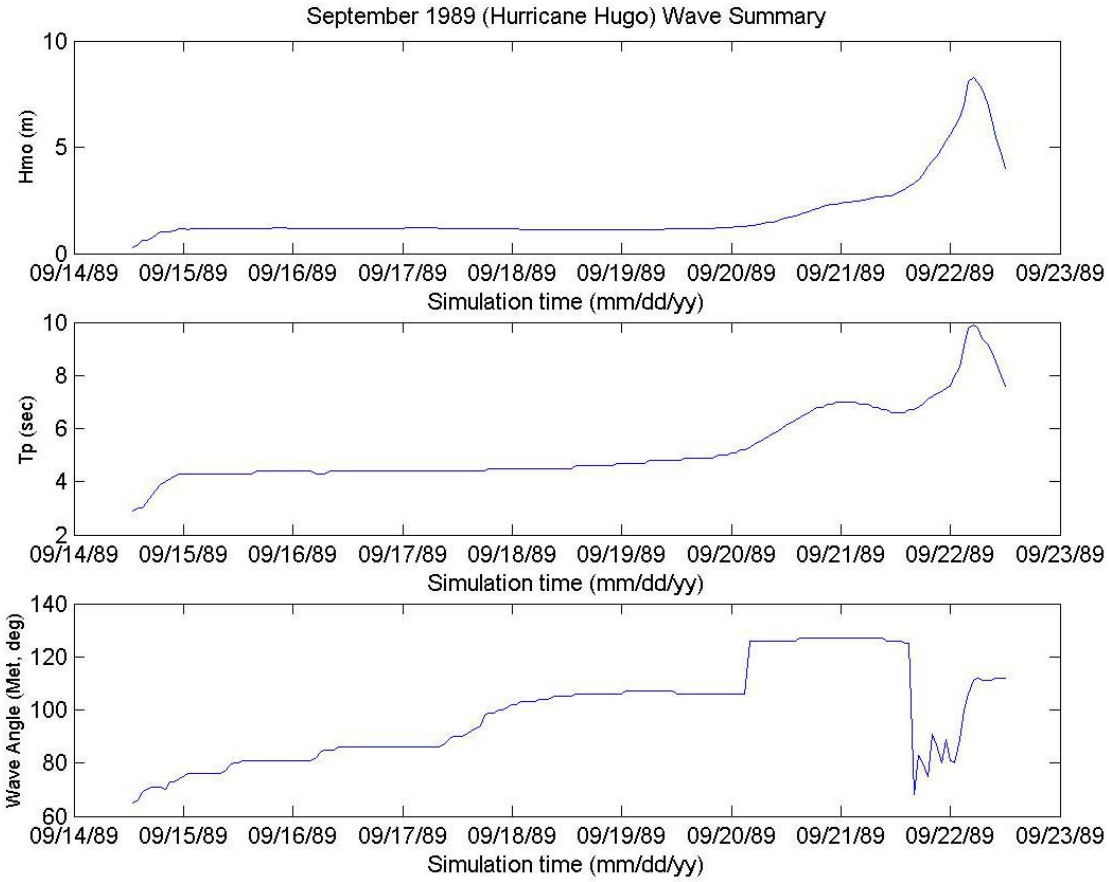

Figure 4-4. Offshore wave conditions for re-tracked Hurricane Hugo, September 1989.

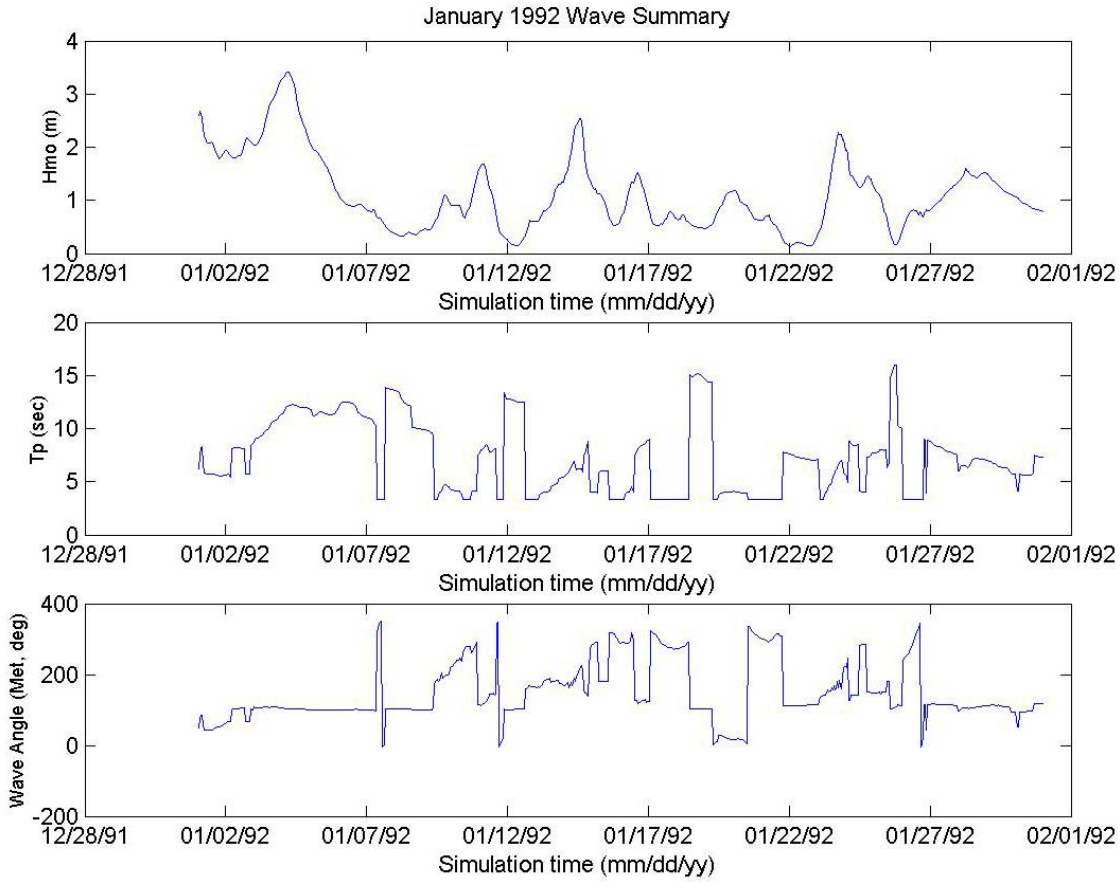

Figure 4-5. Offshore wave conditions for January 1992 at WIS Station 368.

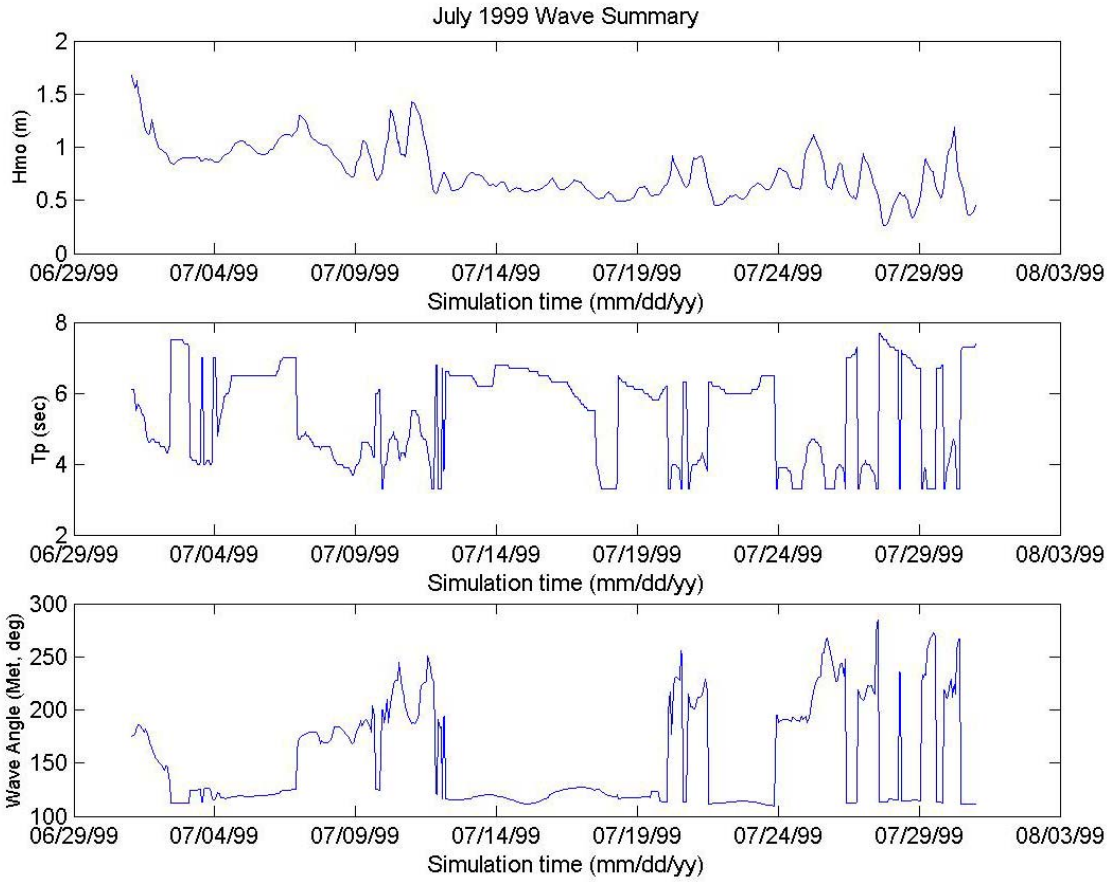

Figure 4-6. Offshore wave conditions for July 1999 at WIS Station 368.

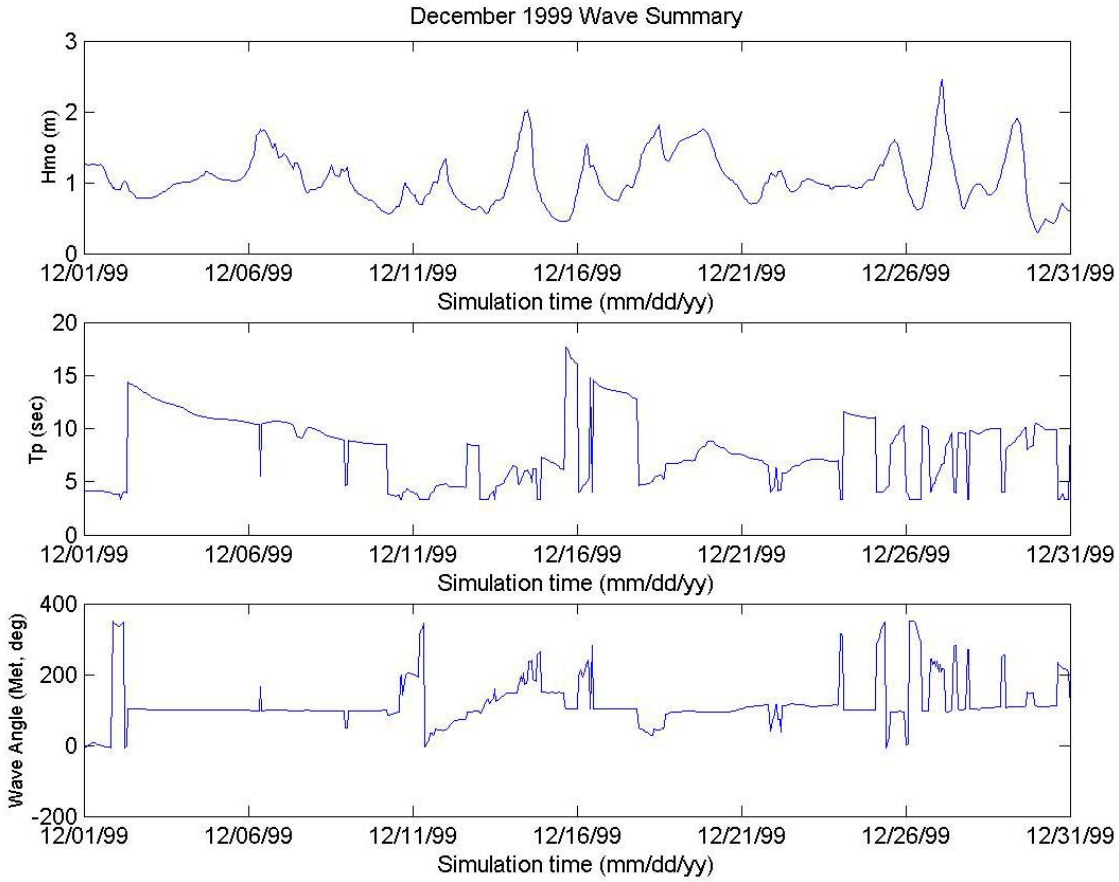

Figure 4-7. Offshore wave conditions for December 1999 at WIS Station 368.

Table 4-2. Statistical Summary of Offshore (WIS) Hindcast Wave Characteristics

Simulation	Max Wave Height (m)	Mean Wave Height (m)	Median Wave Height (m)	Min Wave Height (m)	Max Wave Period (sec)	Mean Wave Period (sec)	Median Wave Period (sec)	Min Wave Period (sec)
Nov 79	3.20	1.51	1.30	0.40	11.00	8.32	9.0	3.0
Sep 89	8.01	1.81	1.18	0.43	17.00	7.78	6.0	3.0
Jan 92	3.41	1.12	0.94	0.12	16.02	7.26	6.87	3.33
Dec 99	2.46	1.04	0.99	0.29	17.71	8.06	8.29	3.33
Jul 99	1.68	0.78	0.72	0.26	7.69	5.41	5.93	3.33

Input wave spectra are required to drive STWAVE on the offshore grid boundary. Parametric spectral shapes were used to generate the input spectra from the offshore wave parameters. The wave energy is distributed in frequency using the TMA spectral shape with a spectral peakedness parameter of 3.3 to 7 (Bouws et al. 1984) and in direction using a $\cos^{nn}(\alpha-\alpha_m)$ distribution, where α_m is the mean wave direction, with *nn* of 4 to 26. The input spectra for all cases except the re-tracked Hurricane Hugo have 30 frequencies, starting with 0.04 Hz and incrementing by 0.01 Hz. For the re-tracked Hurricane Hugo, 20 frequencies were used starting at 0.04167 Hz and incrementing exponentially to 0.333 Hz. The directional resolution for all simulations is 5 deg.

Water level. The water levels (combination of tide and storm surge) applied in STWAVE were determined by the ADCIRC model simulations (Chapter 3). The water levels were extracted from ADCIRC at the STWAVE boundary (WIS station location) and applied over the entire grid. The water level was updated with each new wave boundary condition (either every 1 or 3 hrs).

Winds and currents. Local wind wave generation within the STWAVE domain was not included in these simulations. A sensitivity analysis was performed to determine the importance of wave-current interaction (current-induced shoaling and refraction) within the model domain. The December 1999 time period was used for the sensitivity analysis. For this analysis, the input waves were generated as describe previous, water levels were taken from NOAA observations at Fort Pulaski, and currents were interpolated from the ADCIRC simulations. The conditions investigated included a range of wave heights (0.5 to 2.0 m), peak periods (4-14 sec), and wave directions. The majority of wave height differences (simulations with currents minus without currents) were in the range of +/- 0.01 to 0.05 m. The maximum increase in wave height was 0.40 m and the maximum decrease was 0.56 m. The maximum differences occurred locally in the channels were the currents were strongest. Based on this analysis and the result that current velocities changed minimally for the existing condition and with-project ADCIRC simulation, currents were not included in the STWAVE simulations.

A spectral wave model was selected for these simulations to realistically include the directional and frequency spread of wave energy in this open coastal setting (in contrast, monochromatic models generally have sharp gradients in wave parameters that are not seen in nature). These simulations include variations in water level (tide and surge), but neglect wave-current interaction because the impact is small and localized in the channel. Bottom friction was also neglected. The wave simulations were run for extended time periods (Table 4-1), which include a very wide range of incident conditions (wave heights, periods, directions, and water levels). STWAVE output is used to examine the impact of channel deepening on the waves, to provide radiation stress gradients to force wave-driven currents in the circulation model (Chapter 3), and to provide input to the sediment transport modeling (Chapter 5).

Wave Model Results

Some sample STWAVE results are shown is this section to illustrate the range of conditions simulated and the impact of the channel deepening. Figure 4-8 shows the wave height at the peak of the re-tracked Hugo simulation over the existing bathymetry. Offshore wave heights exceed 8 m at the grid boundary and the peak period is 14 sec. These are the most severe wave conditions simulated. The wave height decreased toward the shore due to depth-limited wave breaking. Wave heights along Tybee Island are in the range of 3-4 m. Figure 4-9 shows the differences in wave heights for the deepened channel minus the existing condition at the peak of the storm (22 September 0600 UTC). The wave heights in the outer channel are decreased by about 0.7 m and

increased on the edge of channel by up to 0.2 m. The decrease in the outer channel is due to decreased shoaling, and the increase on the edges of the channel is due to focusing as waves refract along the deeper channel. The Tybee Island area is shown in greater detailed at a magnified scale in Figure 4-10. Wave heights at the northern portion of Tybee are generally 0.05 to 0.1 m lower for the deepened channel and the wave heights on the southern portion of Tybee are unchanged. On the shallow shoal to the northeast of Tybee, the wave heights increase 0.03 to 0.05 m. These differences in wave height are small (maximum of 15 percent decrease in the channel and 5 percent decrease near the shore). Figures 4-10 and 4-11 show the maximum increases and decreases in wave height for each grid cell over the entire re-tracked Hugo simulations (9-22 September 1989). The maximum increases are generally along the edges of the outer channel; with a maximum increase is 0.25 m. The maximum decreases are generally within the outer channel; with a maximum decrease of 0.71 m. There are also small maximum decreases in wave height along the north Tybee shoreline. Figures 4-10 and 4-11 are plotted at the same scale for direct comparison. The mean differences at all points over the entire grid, calculated for the entire simulation are less than 0.01 m.

Although the highest rate of sediment transport occurs during storms, it is important to investigate a wide range of incident wave conditions. In addition to the retracked Hurricane Hugo, four months were simulated which include both winter and summer conditions with a wide range of incident wave height, period, and direction (Table 4-2, and Figures 4-3 to 4-7). Figures 4-12 through 4-19 show the maximum increases and decreases in wave height at each grid cell for each simulation period. All plots are provided on the same scale (maximum of 0.35 m, half the scale for the re-tracked Hugo plots), so they can be directly compared. The patterns of the maximums are generally very similar. The wave height increases are focused on the edges of the outer channel and generally larger north of the channel. The maximum increases ranged from 0.05 m (July 1999) to 0.25 m (re-tracked Hugo). The wave height decreases are largest in the outer channel and generally extend further south of the channel, including the nearshore area off of Tybee Island. The maximum decreases ranged from 0.10 m (July 1999) to 0.71 m (re-tracked Hugo). The nearshore maximum differences are small, in the range of 0.05 to 0.10 m. Mean differences in wave height at each grid cell over each simulation were less than 0.01 m.

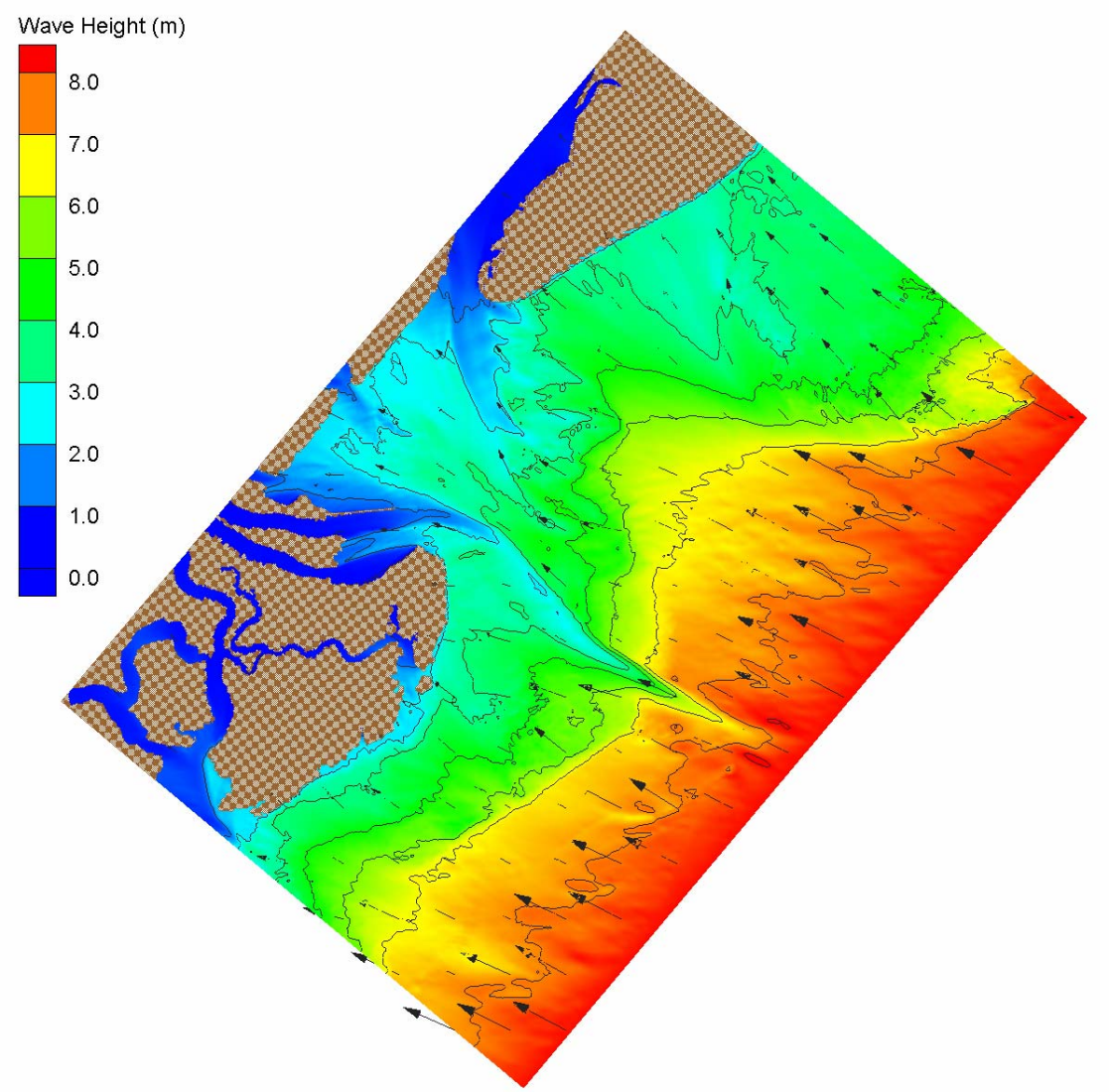

Figure 4-8. Wave Height for Existing Bathymetry at Peak of Hypothetical Retracked Hurricane Hugo, 22 September 1989.

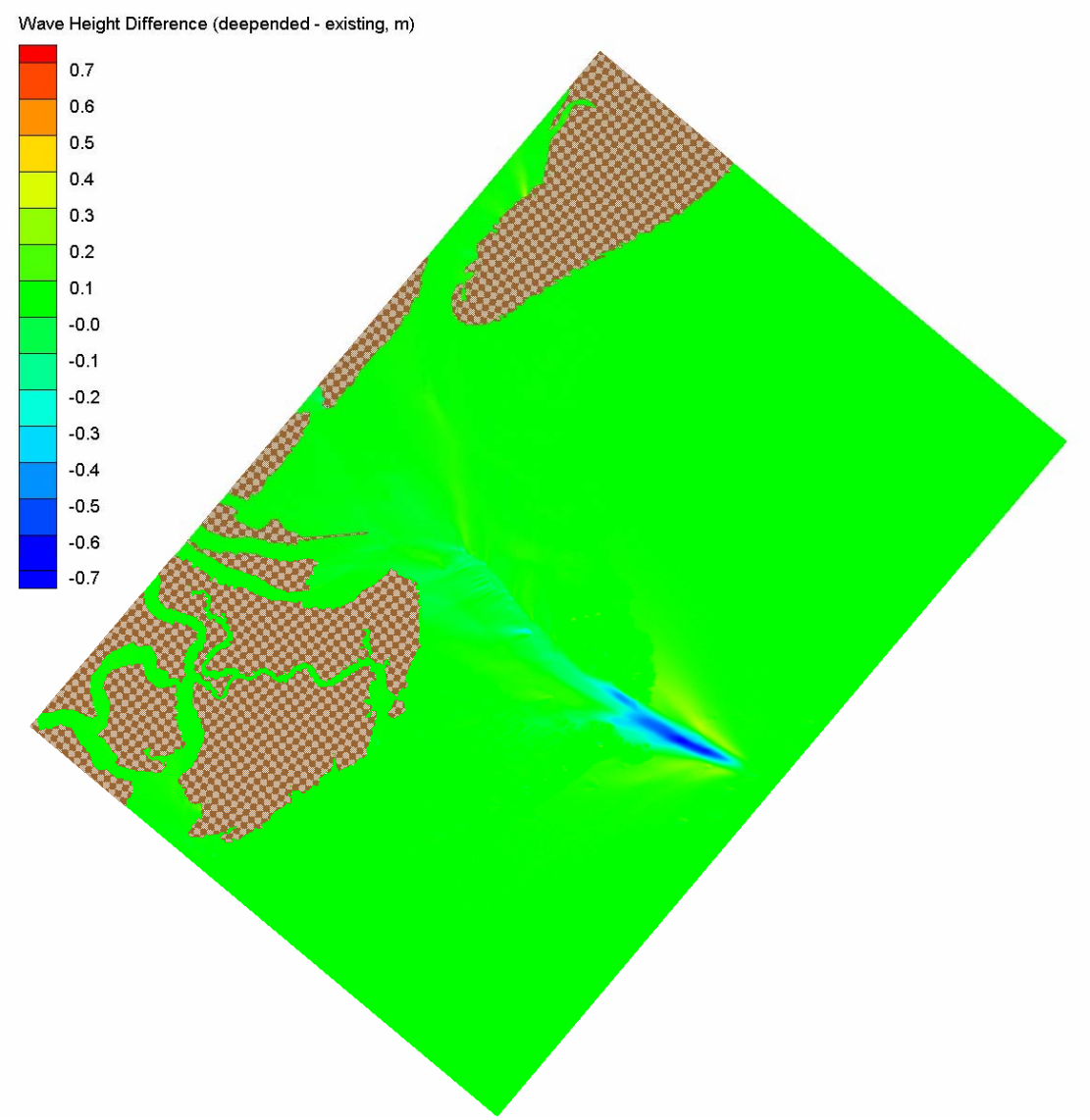

Figure 4-9. Wave Height Differences (Deepened – Existing Condition) at Peak of Hypothetical Retracked Hurricane Hugo, 22 September 1989.

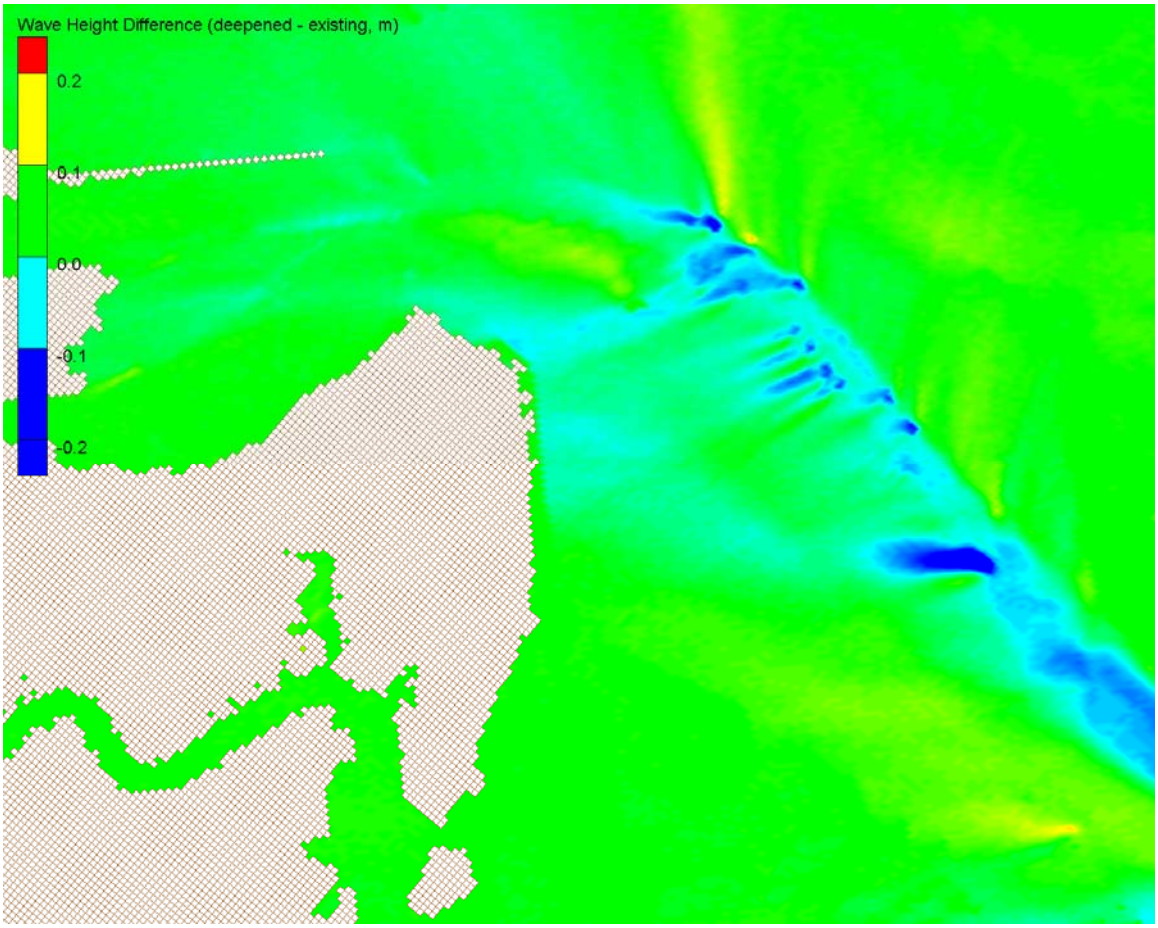

Figure 4-9. Wave Height Differences (Deepened – Existing Condition) at Tybee Island at Peak of Hypothetical Retracked Hurricane Hugo, 22 September 1989.

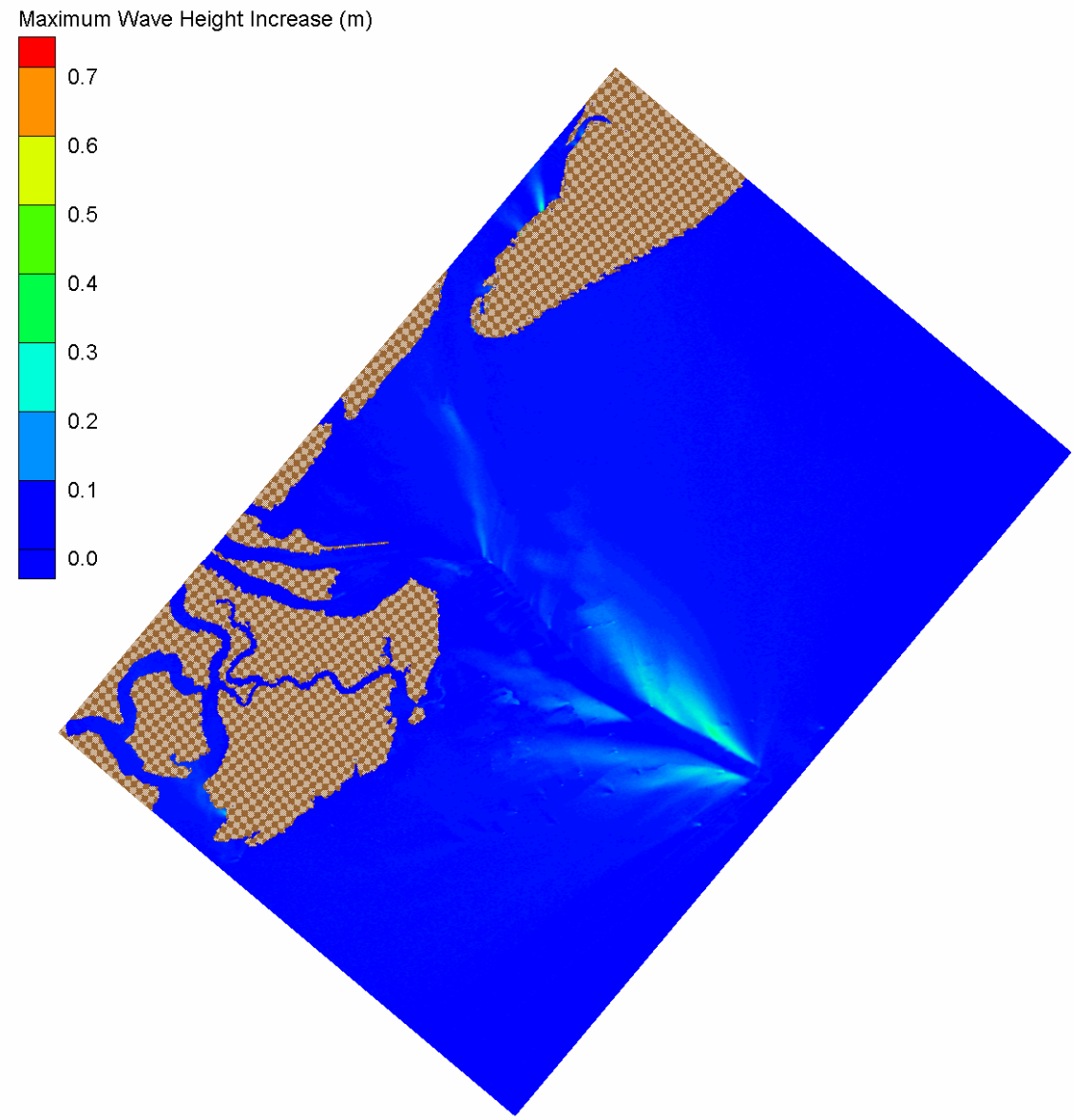

Figure 4-10. Maximum Wave Height Increases for Each Grid Cell for 9-22 September 1989 (Hypothetical Retracked Hurricane Hugo). Maximum Increase of 0.25 m.

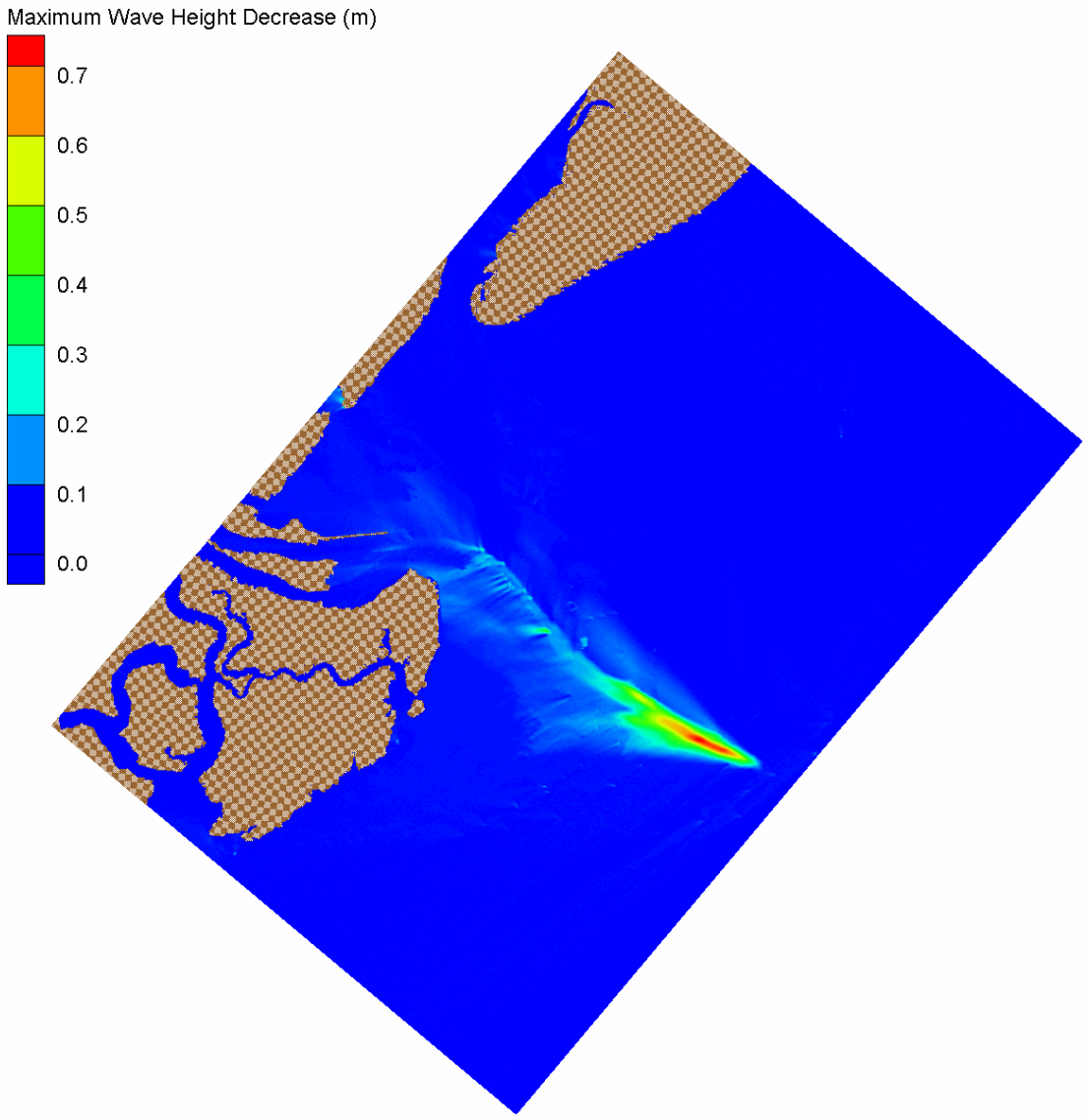

Figure 4-11. Maximum Wave Height Decreases for Each Grid Cell for 9-22 September 1989 (Hypothetical Retracked Hurricane Hugo). Maximum Decrease of 0.71 m.

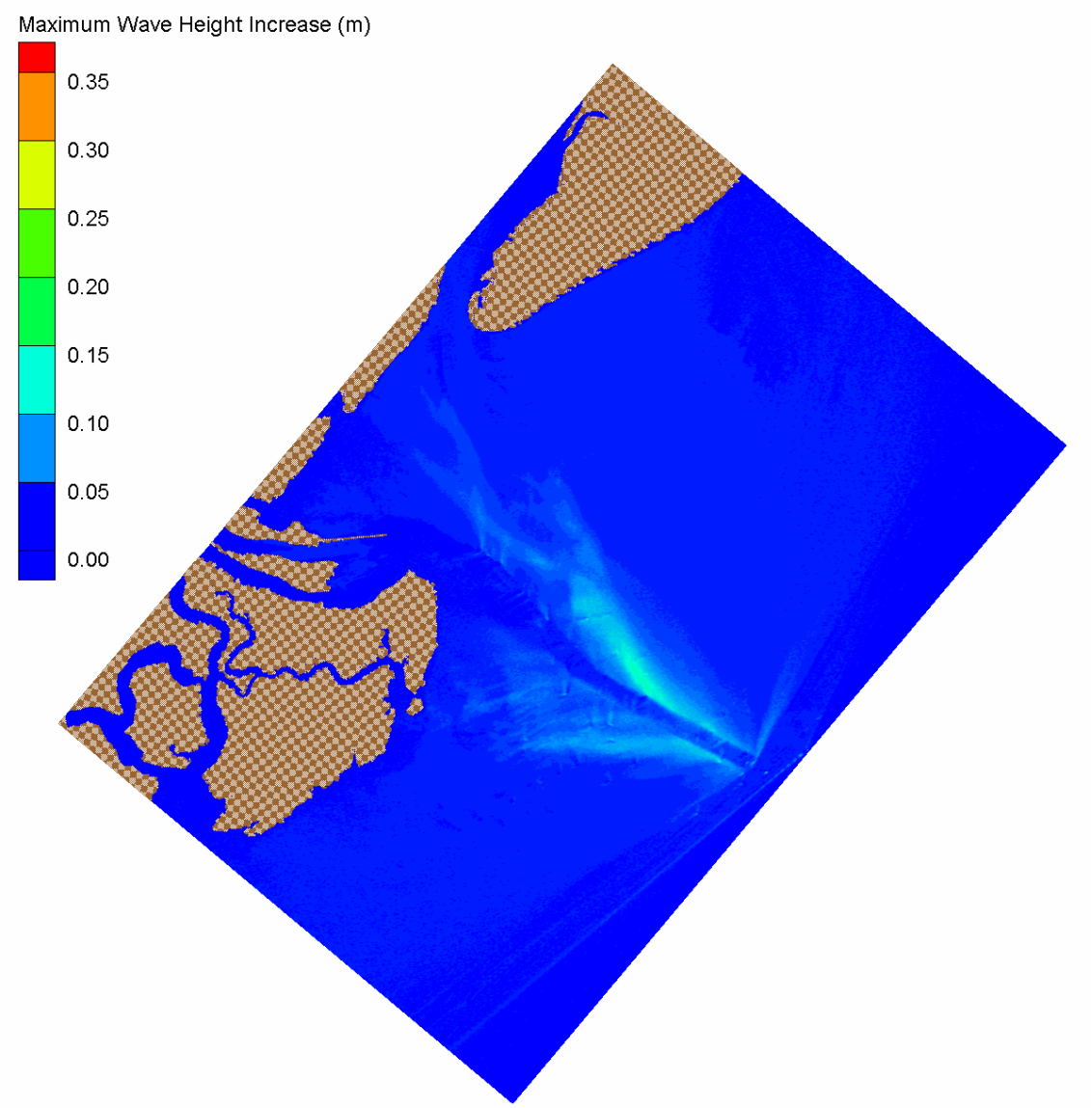

Figure 4-12. Maximum Wave Height Increases for Each Grid Cell for 1-30 November 1979. Maximum Increase of 0.12 m.

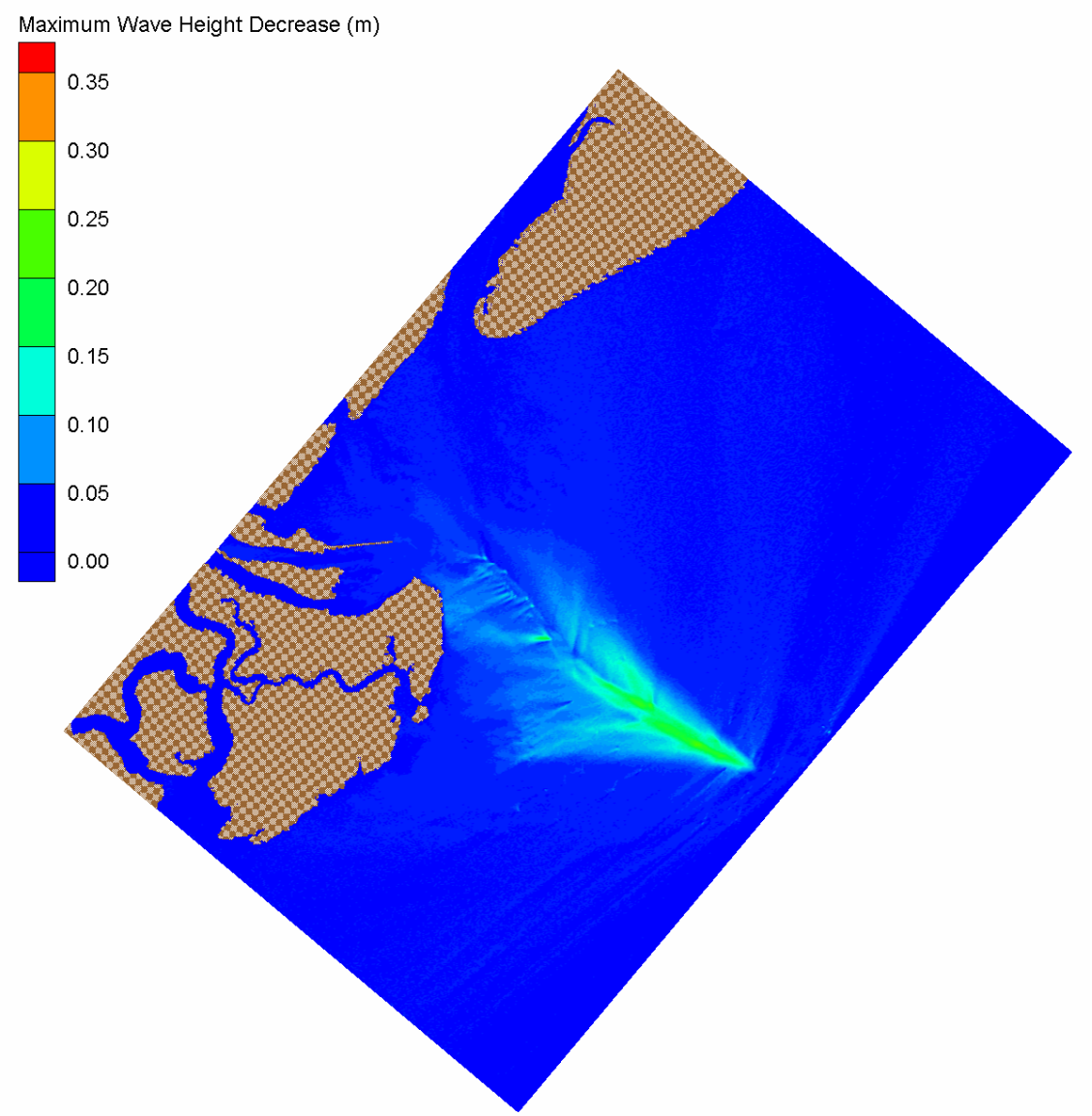

Figure 4-13. Maximum Wave Height Decreases for Each Grid Cell for 1-30 November 1979. Maximum decrease of 0.20 m.

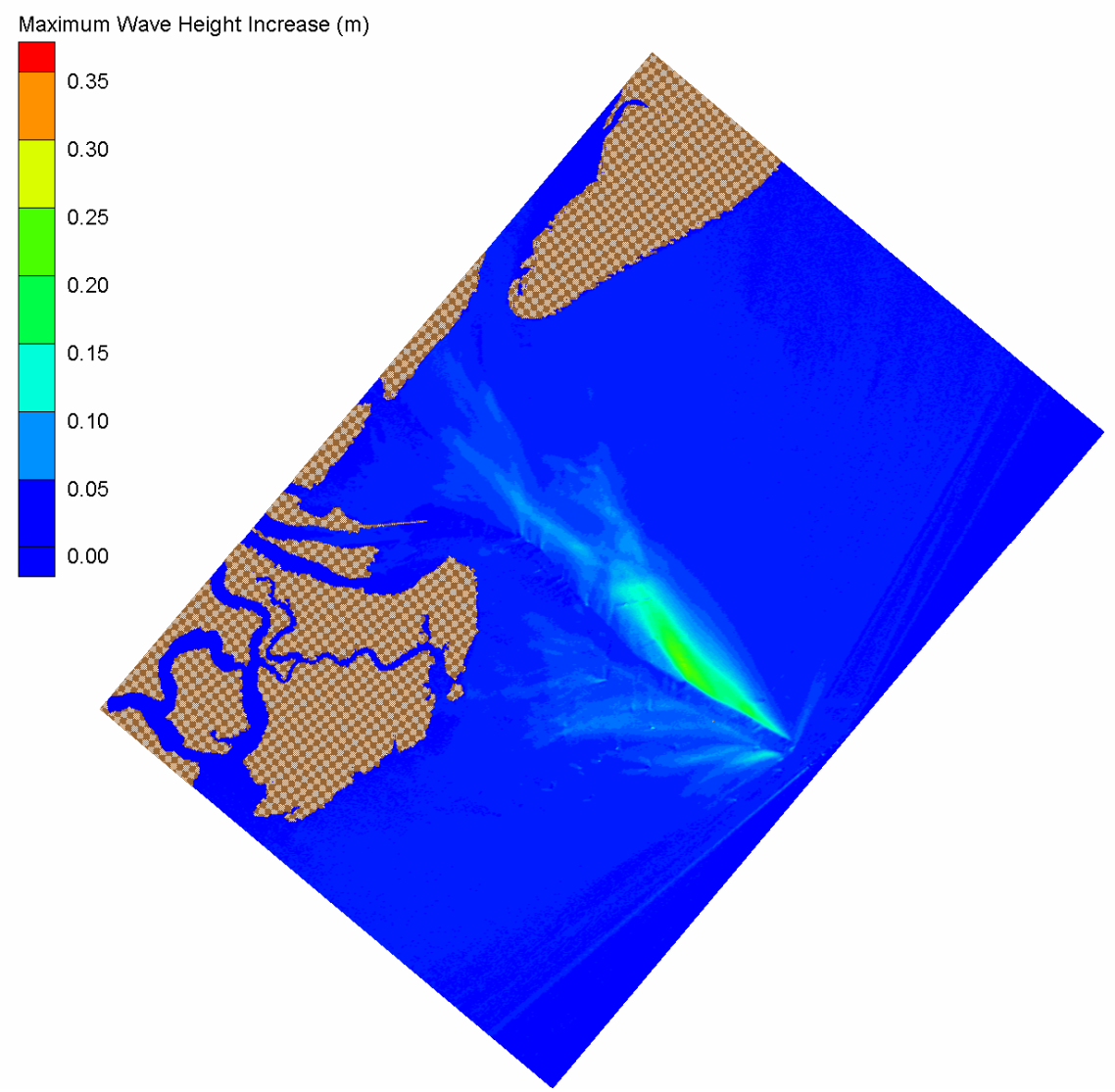

Figure 4-14. Maximum Wave Height Increases for Each Grid Cell for 1-31 January 1992. Maximum Increase of 0.21 m.

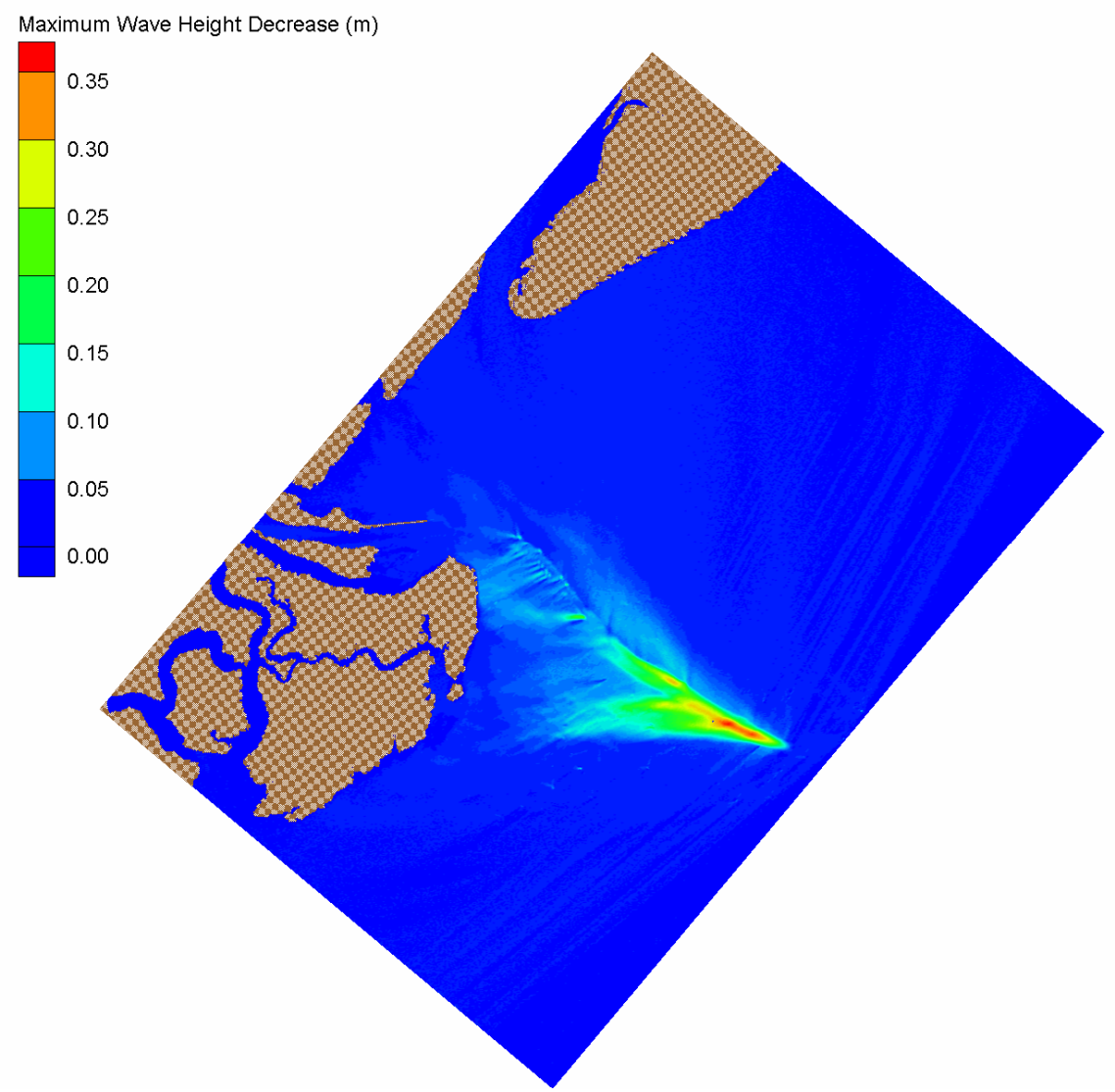

Figure 4-15. Maximum Wave Height Decreases for Each Grid Cell for 1-31 January 1992. Maximum Decrease of 0.35 m.

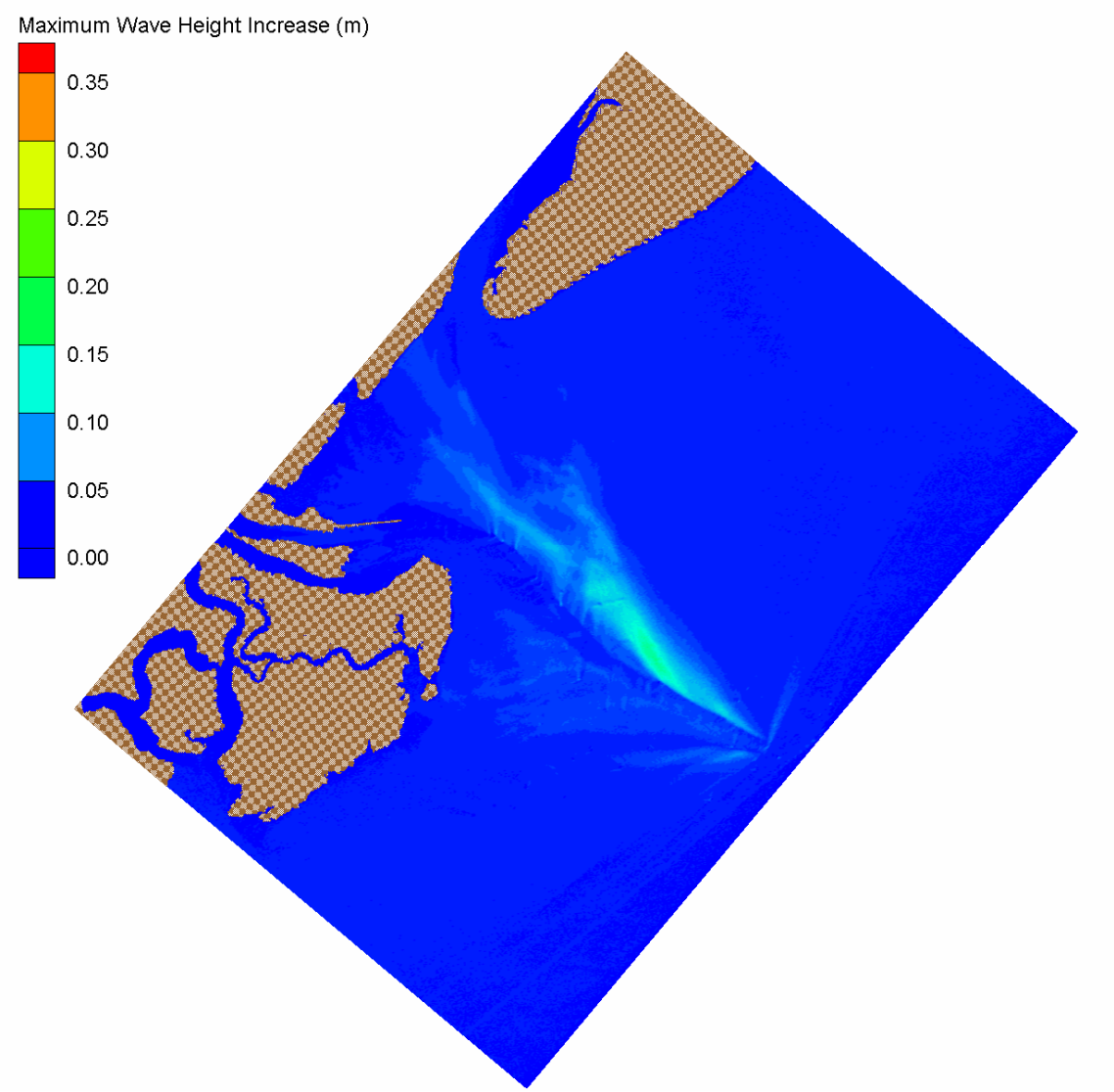

Figure 4-16. Maximum Wave Height Increases for Each Grid Cell for 1-31 December 1999. Maximum Increase of 0.13 m.

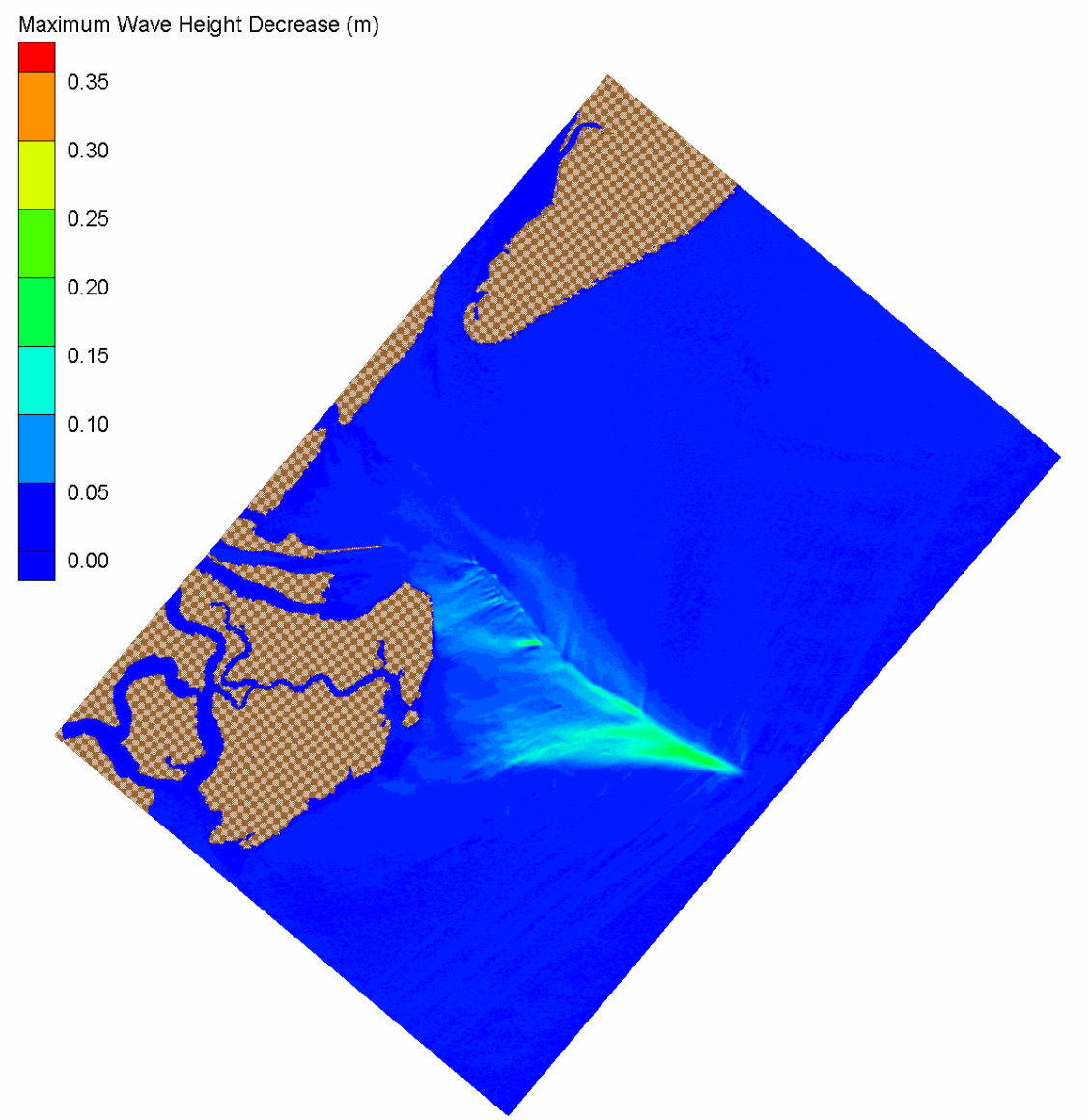

Figure 4-17. Maximum Wave Height Decreases for Each Grid Cell for 1-31 December 1999. Maximum Decrease of 0.17 m.

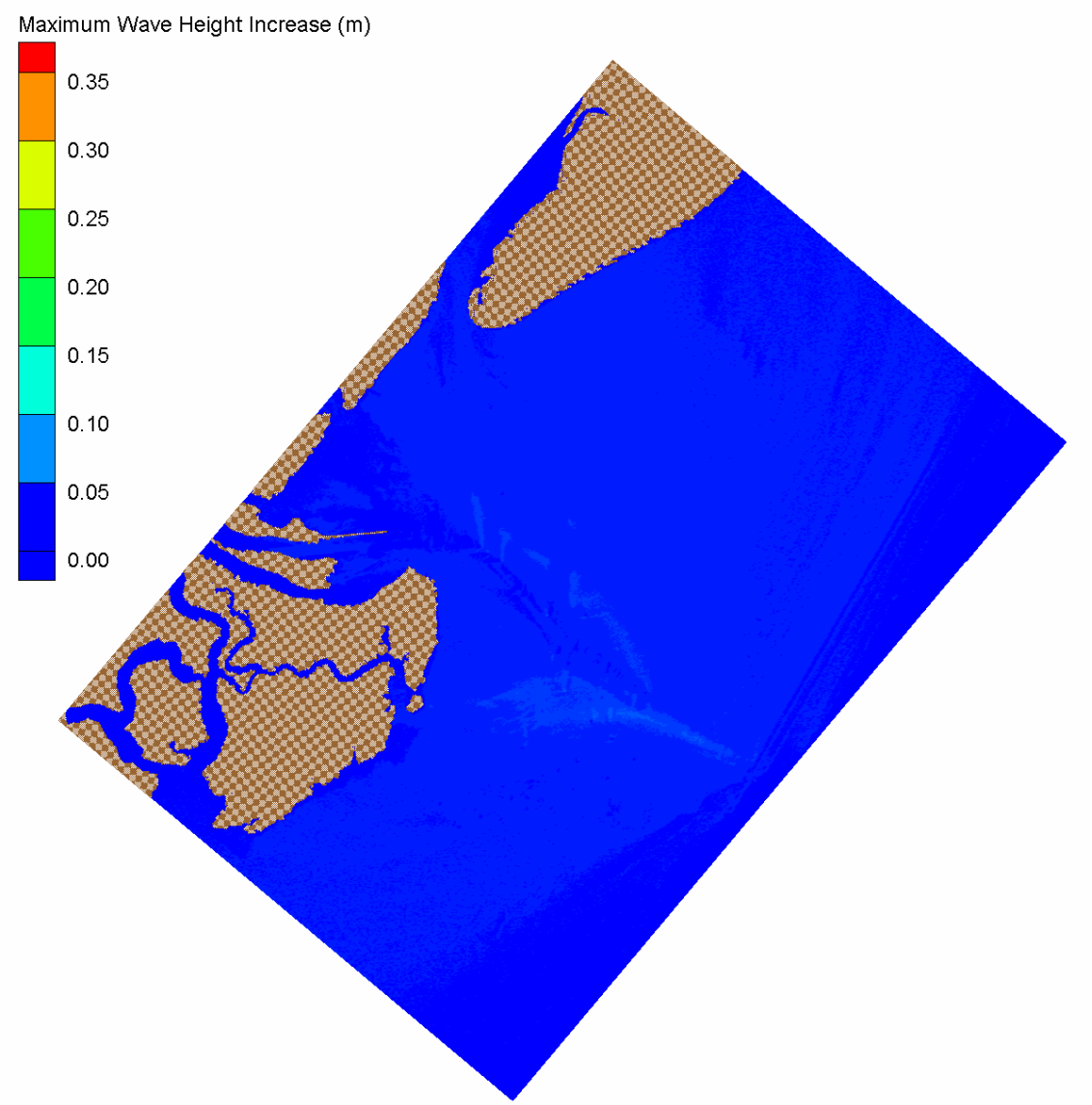

Figure 4-18. Maximum Wave Height Increases for Each Grid Cell for 1-31 July 1999. Maximum Increase of 0.05 m.

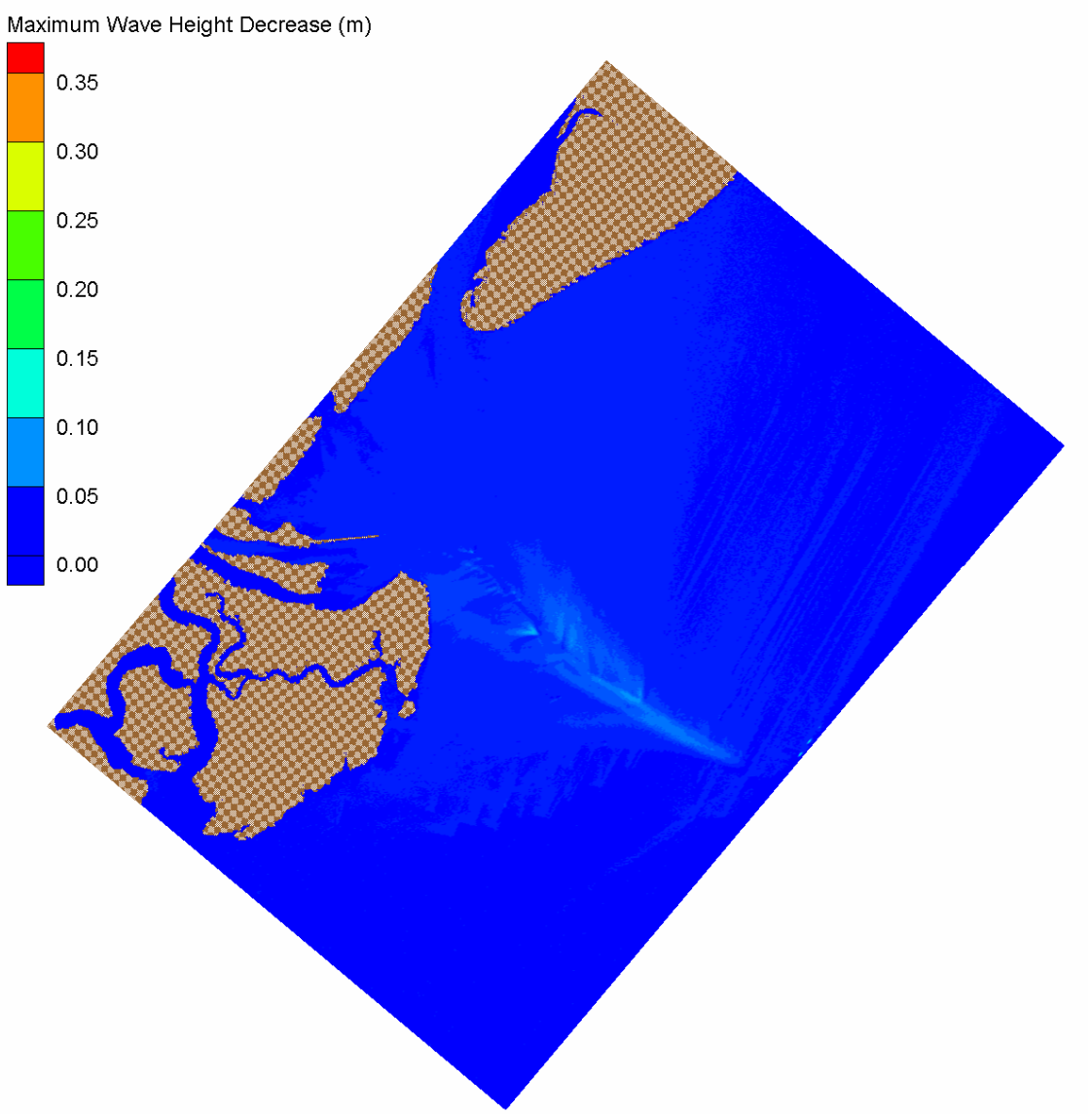

Figure 4-19. Maximum Wave Height Decreases for Each Grid Cell for 1-31 July 1999. Maximum Increase of 0.10 m.

Summary of Wave Results

Waves are one of the primary drivers of sediment transport. The impacts of deepening the Savannah navigation channel were investigated by applying the STWAVE wave model. Model simulations were made for the existing bathymetry and the deepened channel bathymetry for four historical time periods (November 1979, January 1992, December 1999, and July 1999) and a hypothetical extreme event (Hurricane Hugo re-tracked to strike Savannah). These simulations cover a wide range of incident wave height, period, and direction and water levels. The impact of the channel on waves was evaluated by comparing the wave height differences between the existing bathymetry and the deepened channel. The maximum wave height difference patterns are generally similar for all simulations. The maximum wave height increases are focused on the edges of the outer channel and are generally larger north of the channel. The maximum increases ranged from 0.05 m (July 1999) to 0.25 m (re-tracked Hugo). The wave height decreases are

largest in the outer channel and generally extend further south of the channel, including the nearshore area off of Tybee Island. The maximum decreases ranged from 0.10 m (July 1999) to 0.71 m (re-tracked Hugo). The nearshore maximum differences are small, in the range of 0.05 to 0.10 m. Mean differences in wave height at each grid cell over each simulation were less than 0.01 m. The main impact of the channel deepening is a decrease in wave height in the outer channel and an increase in wave height on the edges of the outer channel. On average, these differences are small (less than 15 percent of the wave height). In the Tybee nearshore region, the channel deepening impact is generally a small decrease in the maximum wave height (0.05 to 0.10 m).

5 Sediment Transport Modeling

This chapter describes modeling efforts to estimate sediment transport rates and the potential for changes in transport rates due to deepening the Savannah navigation channel. The simulations of sediment transport described in this chapter rely on the estimated environmental conditions at the site, specifically the ADCIRC circulation simulations (Chapter 3) and STWAVE wave simulations (Chapter 4). The first part of this section describes GTRAN (Jensen et al. 2002) simulations of sediment transport patterns over the entire nearshore. The second part analyzes the patterns of the existing conditions and deepened channel model runs for potential changes in sediment transport patterns.

Nearshore Sediment Transport Model

To estimate the transport in the nearshore, predictive techniques are applied with available knowledge of the environmental conditions and sediment properties. The sediment transport model GTRAN was supplied modeled currents, water levels, and waves to predict transport pathways in the study area. GTRAN is a point model, which estimates potential transport and does not solve continuity of mass, i.e., it is a gross transport and not net transport model. GTRAN includes effects of waves and current on transport of non-cohesive sediment. Tidal-, wind-, and wave-generated circulation and wave parameters are provided to GTRAN through the external simulations with ADCIRC and STWAVE. Sediment properties of the bed in the study area were determined from information available from: USACE, NOAA, the Skidaway Institute, and others. These data sources are discussed in more detail in the chapter on the sediment budget (Chapter 2). From input hydrodynamic, wave, and sediment bed conditions, GTRAN calculates sediment transport through a collection of sediment transport methods. A detailed description of the GTRAN sediment transport methods, including sediment transport equations, is provided in Appendix 5A.

To numerically estimate sediment transport, simplifying assumptions and representations of the natural processes must be developed. Making such approximations is standard practice in the field of numerical modeling and is not unique to sediment transport models. The following discussion of the approximations developed for estimating transport rates is limited to general descriptions of the approximations applied.

Wave-Generated Current and Transport.

ADCIRC simulations include currents driven by the tide, wind, waves, and river. Wave-generated currents (longshore currents and undertow) and asymmetry in the wave orbital motions are a significant or dominant factor in nearshore hydrodynamics at many sites and must be

considered in nearshore transport studies. This section will address the treatment of wave-induced hydrodynamics included in this study and the implications of neglecting certain components of the hydrodynamic forcing on model results.

Longshore Current. Longshore transport is defined as the quantity of nearshore sediment transport generated along the coast by the effects of breaking waves and the associated longshore currents. At Savannah, the shore parallel tidal and wind-driven currents augment this transport. The distinction between transport in the nearshore region and offshore (deep water) region is primarily in the transport processes of the two regions. In offshore transport, waves produce additional bottom shear stresses and increase turbulence that suspends sediment near the bottom. Surface waves contribute little to transport direction. Ocean circulation currents transport the suspended sediment (and sediment near the bed). In the most general terms, the waves act as a stirring mechanism, and the currents transport the sediment. In the case of nearshore transport, breaking waves also impart an increased shear stress and turbulence on the bottom sediments. In addition, breaking waves exert a stress that generates longshore currents and transport along with tidal and wind-driven currents. Depth-averaged wave-generated longshore currents are included in the ADCIRC simulation through forcing by gradients in radiation stresses calculated by STWAVE (see Chapters 3 and 4).

Undertow. In addition to longshore currents, waves generate an offshore-directed current or 'undertow' near the bottom to balance the shoreward mass flux that occurs above wave troughs. Undertow is a primary factor in offshore sediment transport in the surf zone during storms (Miller et al. 1999, Smith and Miller, in review). Undertow exists in the lower water column, influencing the sediment bed and is therefore a strong mechanism for offshore sediment transport during large wave events.

A simple estimation of undertow derived through mass balance was implemented in the GTRAN simulations. The undertow estimate (called stokes velocity), U_{Stokes} as described by Nielsen (1992) is:

$$U_{Stokes} = -\frac{gH^2}{8cD}$$

where: g = gravitational acceleration
H = wave height
c = wave celerity
D = water depth

Wave Asymmetry. Wave asymmetry is the imbalance of forward (onshore) and backward (offshore) components of the bottom orbital velocities resulting from the nonlinearity of surface waves in shallow water. Wave asymmetry becomes a mechanism for shoreward sediment transport primarily during milder wave conditions (when undertow is small). In deep water, waves have a sinusoidal form and generate equal backward and forward bottom velocities. As the waves approach shallow water, wave crests become short and steep, while the troughs become long and flat. Near the bottom, orbital velocities include short-bursts of strong, onshore velocity under the steep wave crest and weaker, longer duration offshore velocity under the trough. These onshore bursts generally move more sand than the longer-duration, lower-magnitude offshore velocities. The transport methods in GTRAN include the effect of wave asymmetry on transport.

Bed Sediment Characteristics

In addition to the ADCIRC and STWAVE model output previously discussed, GTRAN requires bed sediment information. Areas with similar sediment qualities must be defined spatially and characterized by a median grain size diameter and sorting parameter.

GTRAN model runs rely on historic sediment sample information compiled during the sediment budget analysis. The historic samples are concentrated within the navigation channel and immediately offshore of Tybee Island. Figure 5-1 provides the location of and mean grain size information for sediment samples taken by USACE, NOAA, the Skidaway Institute and others. Mean grain sizes are given in millimeters and in phi (ϕ) units. The phi unit can be related to the grain size using Equation 5-1 below.

$$\phi = -\log_2(d) \tag{5-1}$$

Conversely, the grain size (d) in millimeters can be determined from phi units using Equation 5-2.

$$2^{-\phi} = d \tag{5-2}$$

Another sediment quality required to generate a grain size distribution is the sediment sorting. The sorting of a sediment sample refers to the range of grain sizes present. A perfectly sorted sample contains sediment of a uniform diameter, while a poorly sorted sample containa widely varying sizes.

In order to incorporate the available data and best represent the sediment transport pathways in the study area, a spatially uniform mean grain size of 0.2 mm (2.25 phi) was selected to characterize the area's bed sediment. The sediment was also selected as moderately to poorly sorted, with a sorting parameter of 1.0. Figure 5-2 provides the grain size distribution generated from the selected sediment parameters.

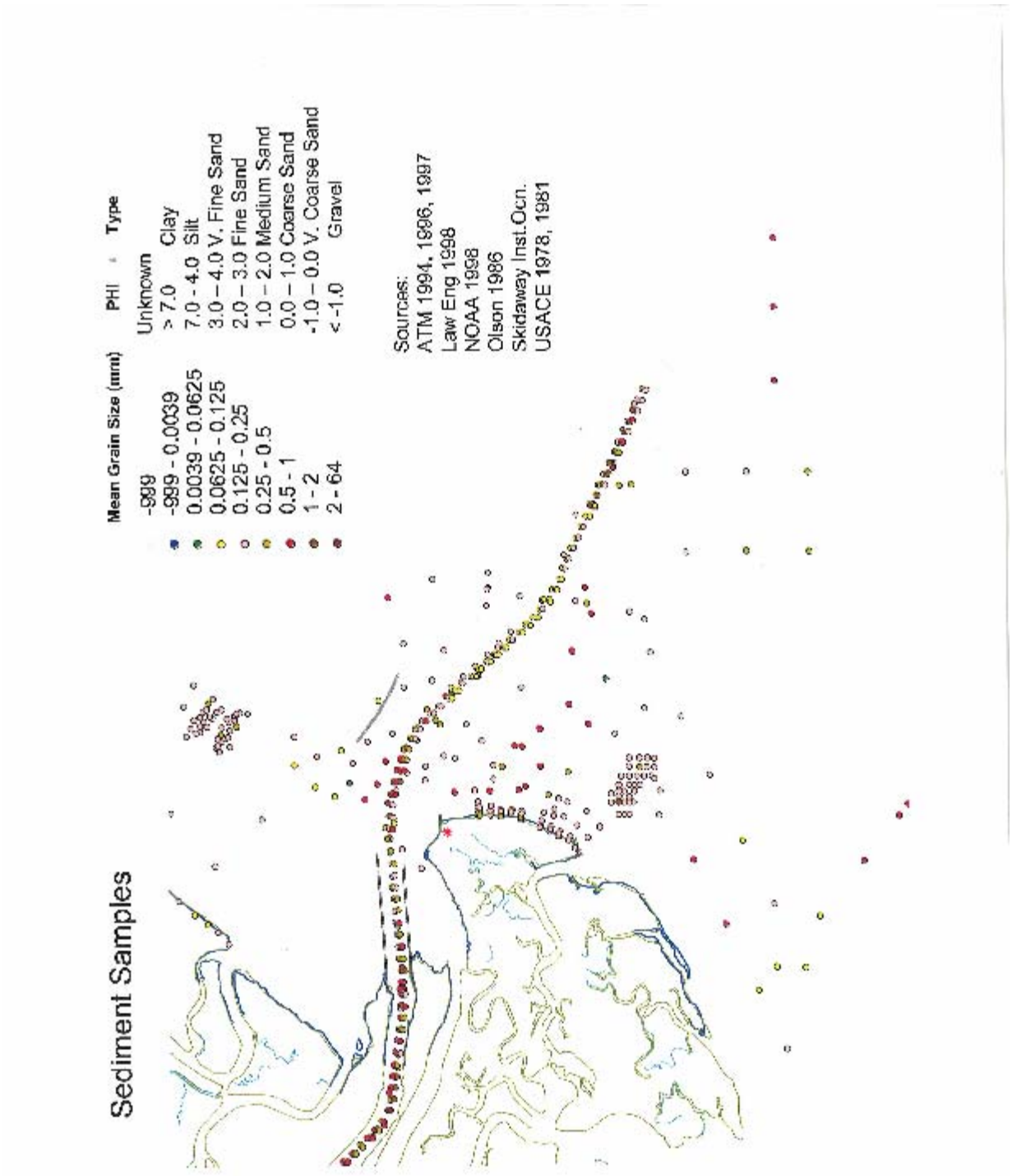

Figure 5-1. Locations and mean grain sizes of sediment samples taken within and around the federal navigation channel and Tybee Island.

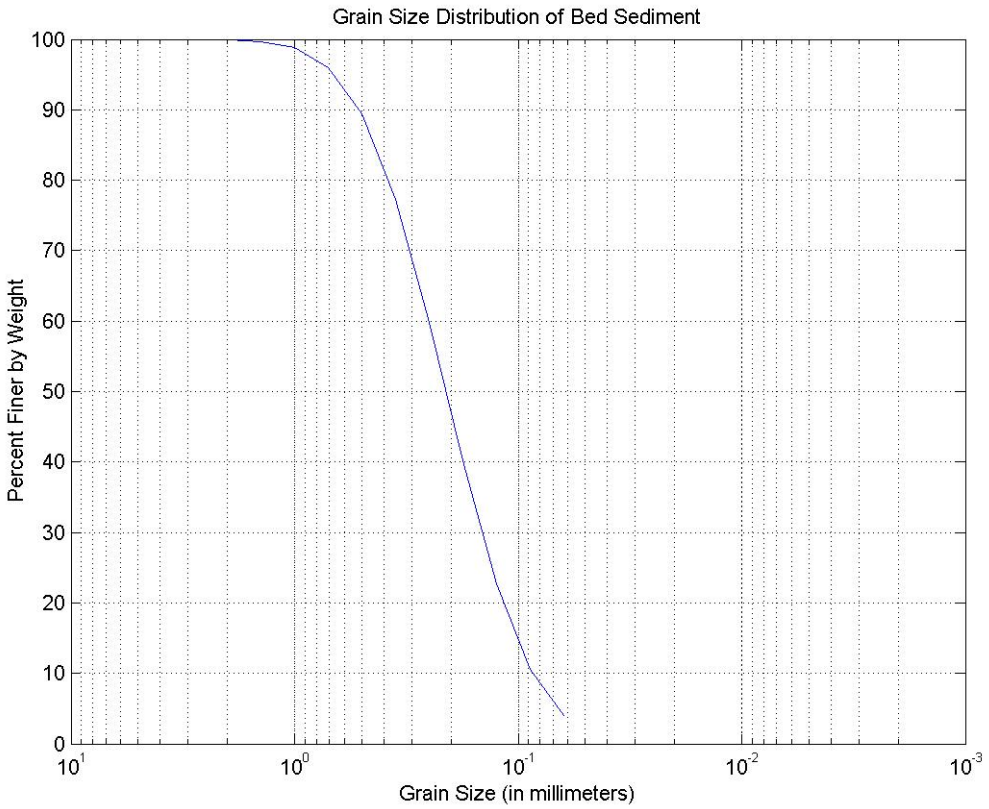

Figure 5-2. Grain size distribution of spatially uniform bed characteristics for GTRAN modeling.

Sediment Transport Patterns

Since GTRAN is a point model, the model requires that the locations where sediment transport is to be calculated be defined by X, Y, and Z coordinates. The computational domain of the model was defined by 239 calculation points selected within and adjacent to the channel and offshore of the surrounding islands to represent the variations in hydrodynamics (both waves and currents) with water depth. Figure 5-3 illustrates the calculation locations selected for the Savannah Harbor Expansion Project study.

Five distinct time periods were modeled in ADCIRC and STWAVE prior to the GTRAN modeling. Four of the time periods, November 1979, January 1992, July 1999, and December 1999 were month-long simulations, while September 1989 represented only the week surrounding a re-tracked Hurricane Hugo simulation. All of these time periods were modeled with the existing bathymetry and the deepened navigation channel and bathymetry. The cumulative transport plots (representing the integral of the point transport over the simulation period) should be cross referenced to the bathymetry change (Figure 2-21) for a more complete picture of the transport processes.

The cumulative sediment transport vectors and rose plots (directional distribution of transport) for these calculation points are presented in Appendices 5B and 5C, respectively. The reader should pay special attention to the vector scale for each simulation period. The scales vary between plots. The scale is based on the maximum cumulative sediment transport for each specific simulation. Therefore, the scale for the November 1979 simulation is different than the scale for the September 1989 simulation.

November 1979

Cumulative sediment transport (integral of point sediment fluxes over the month) in the existing condition November 1979 simulation is characterized by ebb dominated transport in and immediately adjacent to the federal navigation channel (Figures 5B-1). The largest cumulative sediment transport magnitude is approximately 380 m^3/m and is located offshore of New River at calculation point 25. Similar magnitudes are found at points 168 and 169 (375 and 350 m^3/m, respectively) in the Tybee Roads area of the channel. The area offshore of Turtle Island between New River and the federal channel is characterized by onshore directed cumulative transport in the north and offshore directed cumulative transport closer to the channel. The area immediately offshore of New River is ebb dominated and the magnitude of cumulative transport is larger than the surrounding areas. Offshore of Tybee Island, the southern areas demonstrate onshore cumulative transport and the northern areas show towards the North and Northwest. There is also a clockwise recirculation cell south and east of the finger shoal feature. Farther offshore near the Tybee Range portion of the federal navigation channel, transport within the channel remains ebb dominated, but areas to the north and south of the channel are characterized by onshore or channel-ward directed transport.

Cumulative sediment transport patterns in the November 1979 deepened channel simulation are very similar to the patterns exhibited during the existing conditions simulation. The largest cumulative sediment transport magnitude is 410 m^3/m and is located in the Tybee Roads area of the channel (calculation point number 168). Dominant transport directions in all areas of the model domain are consistent. In instances where cumulative transport differs from the existing conditions simulation, those differences are most often slight differences in the magnitude of cumulative transport. Figures 5B-1 through 5B-2 provide the cumulative sediment transport

vectors for the two November 1979 simulations and Figures 5C-1 through 5C-8 provide the sediment transport rose plots. Rose plots show the full distribution of transport over the simulation.

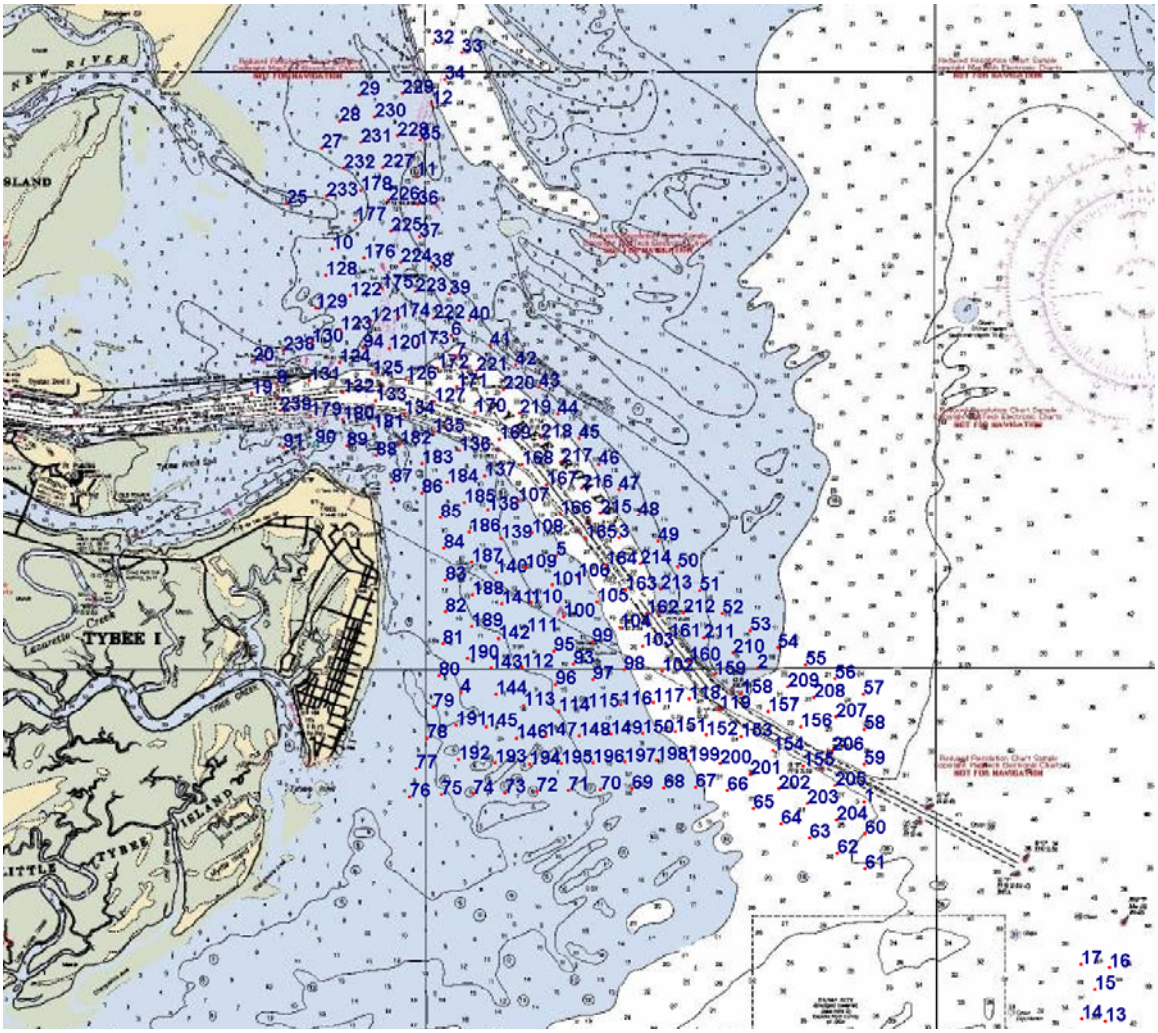

Figure 5-3. GTRAN calculation locations.

September 1989

Cumulative sediment transport in the existing conditions September 1989 simulation is similar to the November 1979 results. The cumulative transport is characterized by ebb dominated transport in and immediately adjacent to the federal navigation channel. The largest cumulative sediment transport magnitude is 300 m^3/m and is located in the channel between the Tybee Knoll and Jones Island Ranges at calculation point 132. Unlike the November 1979 simulation, transport offshore of the southern portion of Tybee Island is mostly westerly (onshore), while transport closer to Tybee Inlet is southwesterly. Farther offshore near the Tybee Range portion of the federal navigation channel, transport within the channel remains ebb dominated. However, transport in the area north of Tybee Range is flood or onshore directed and towards the channel. In addition, transport in the area south of Tybee Range is offshore and directed slightly south and away from the channel.

Cumulative sediment transport patterns in the September 1989 deepened channel simulation are very similar to the patterns exhibited during the existing conditions simulation. The largest cumulative sediment transport magnitude is 650 m^3/m and is located in the Tybee Roads area of the channel at calculation point number 168. Dominant transport directions in all areas of the model domain are consistent. Figures 5B-3 through 5B-4 provide the cumulative sediment transport vectors for the September 1989 simulations and Figures 5C-9 through 5C-16 provide the sediment transport rose plots.

January 1992

Cumulative sediment transport patterns during the existing conditions January 1992 simulation are very similar to the November 1979. The largest cumulative sediment transport magnitude is approximately 290 m^3/m and is located offshore of New River at calculation point 25.

Cumulative sediment transport patterns during the January 1992 deepened channel simulation are very similar to the patterns exhibited during the existing conditions simulation. The largest cumulative sediment transport magnitude is approximately 300 m^3/m and is located offshore of New River at calculation point 25. Dominant transport directions in all areas of the model domain are consistent. Where cumulative transport differs from the existing conditions simulation, those differences are generally slight differences in the magnitude of cumulative transport. Figures 5B-5 through 5B-6 provide the cumulative sediment transport vectors for the two January 1992 simulations and Figures 5C-17 through 5C-24 provide the sediment transport rose plots.

July 1999

Like the other simulations, cumulative sediment transport in the existing conditions July 1999 simulation is characterized by ebb dominated transport in and immediately adjacent to the federal navigation channel. The largest cumulative sediment transport magnitude is approximately 340 m^3/m and is located offshore of New River at calculation point 25. The magnitude of transport in the area offshore of Turtle Island between New River and the federal channel is less than most of the other simulation periods and there is little discernable pattern to the transport in this area. The area immediately offshore of New River is ebb dominated and the magnitude of cumulative transport is much larger than the surrounding areas. Offshore of Tybee Island, cumulative transport magnitudes are relatively small and uniformly northwesterly (onshore). Cumulative transport magnitudes continue to decrease farther offshore near the Tybee Range portion of the federal navigation channel, both within and adjacent to the channel. Transport within the channel remains ebb dominated. In general the cumulative sediment transport fluxes in all regions are less in the July simulation than the winter simulations, but the patterns are similar.

Cumulative sediment transport patterns in the July 1999 deepened channel simulation are very similar to the patterns exhibited during the existing conditions simulation. The largest cumulative sediment transport magnitude is approximately 350 m^3/m and is located offshore of New River at calculation point 25. Dominant transport directions in all areas of the model domain are consistent. In instances where cumulative transport differs from the existing conditions simulation, those differences are most often slight differences in the magnitude of cumulative transport. Figures 5B-7 through 5B-8 provide the cumulative sediment transport vectors for the two July 1999 simulations and Figures 5C-25 through 5C-32 provide the sediment transport rose plots.

December 1999

Cumulative sediment transport patterns during the existing conditions December 1999 simulation are similar to the winter months discussed above. The largest cumulative sediment transport magnitude is approximately 345 m^3/m and is located offshore of New River at calculation point 25.

Cumulative sediment transport patterns during the December 1999 deepened channel simulation are very similar to the patterns exhibited during the existing conditions simulation. The largest cumulative sediment transport magnitude is approximately 355 m^3/m and is located offshore of New River at calculation point 25. Dominant transport directions in all areas of the model domain are consistent. In instances where cumulative transport differs from the existing conditions simulation, those differences are most often slight differences in the magnitude of cumulative transport. Figures 5B-9 through 5B-10 provide the cumulative sediment transport vectors for the two December 1999 simulations and Figures 5C-33 through 5C-40 provide the sediment transport rose plots.

Changes to Sediment Transport Patterns

Changes in cumulative sediment transport due to deepening the channel were determined from the differences in cumulative sediment transport from the existing condition and deepened condition GTRAN model runs for each of the simulation periods. Differences were calculated by subtracting the existing conditions results from the deepened conditions results. Vector plots of changes to the cumulative sediment transport due to the deepening of the navigation channel for each of the simulations are presented in Appendix 5D. Again, the vector scales differ for each simulation period. With the exception of September 1989, the scale for the difference vectors are much smaller than the cumulative vectors in Appendix 5B.

The majority of the simulation periods show little difference in cumulative sediment transport outside of the federal navigation channel itself. The areas offshore of Tybee Island and Turtle Island show minor differences in cumulative transport, when any differences are present at all. Table 5-1 gives the average change in cumulative sediment transport magnitude (ΔQ, or deepened channel minus existing condition) for 10 regions. The regions are defined in Figure 5-4. The existing condition cumulative transport magnitude averaged over the region is also given for reference. The changes in cumulative transport magnitude are generally small ($< \pm 1$ m^3/m), except in the federal channel, where the cumulative transport magnitudes are large. September 1989 (re-tracked hurricane Hugo) is also an exception, with significant change in cumulative transport in most regions.

Figures 5-5 through 5-7 show the transport vectors for the Tybee Shelf area of the GTRAN computation domain for the December 1999 existing conditions, deepened conditions, and the vectors differences, respectively. The entire channel is ebb dominated in both the existing and deepened conditions results, but the difference vectors within the inner channel in Figure 5-8 point in the flood direction. These difference vectors indicate that the existing conditions magnitude is larger than the deepened condition magnitude. Most calculation points show very little change in transport angle between the existing and deepened conditions.

The changes in cumulative sediment transport vectors in Figure 5-7 are typical of the other changes during the other simulation periods. The exception is the re-tracked Hurricane Hugo (September 1989) simulation. The differences in cumulative sediment transport due to the

deepening during September 1989 are unique because larger magnitude changes are present adjacent to the channel and even extend offshore between the Tybee Roads and Tybee Range sections of the channel. The differences immediately on the Tybee Island shelf are minor except for the area between the southern jetty and the northern end of Tybee Island. All of the simulation periods and their associated changes in sediment transport are discussed in more detail below.

November 1979

Figure 5D-1 provides the changes in cumulative sediment transport vectors between the two November 1979 simulations. The ranges of differences in point magnitudes are -60 m^3/m to 50 m^3/m in the channel and -3 m^3/m to 6 m^3/m on the Tybee Island shelf. Cumulative transport magnitude decreased due to the deepening inside the channel from the jetties seaward to the beginning of the Tybee Roads area. The number of points exhibiting increases in cumulative sediment transport within the channel is balanced by those exhibiting decreases. The average magnitude differences over regions are given in Table 5-1. The deepening tends to decrease the ebb dominance in the inner channel (decrease is average cumulative transport magnitude of 16 m^3/m) and increase the ebb dominance in the Tybee Roads section of the channel (increase is cumulative transport magnitude of 3 m^3/m).

Table 5-1. Average Cumulative transport Rate Changes for Deepened Channel
(ΔQ = Deepened – Existing Sediment Flux, Q_{exist} = Sediment Flux for Existing Bathymetry)

Location	Nov 1979		Sep 1989		Jan 1992		Jul 1999		Dec 1999	
	ΔQ (m^3/m)	Q_{exist} (m^3/m)	ΔQ (m^3/m)	Q_{exist} (m^3/m)	ΔQ (m^3/m)	Q_{exist} (m^3/m)	ΔQ (m^3/m)	Q_{exist} (m^3/m)	ΔQ (m^3/m)	Q_{exist} (m^3/m)
Tybee Island Shelf	0.3	25.	0.2	14.	0.0	13.	0.1	7.0	0	8.8
North Tybee	-0.6	19.	7.4	18.	-0.7	12.	-1.0	17.	-0.5	13.
Tybee Knoll Bar Channel	-15.6	105	102.	203.	-9.7	52.	-11.7	54.	-10.1	69.
Tybee Roads	3.0	84.	93.	163.	0.8	34.	1.1	26.	2.0	42.
Tybee Range	0.7	16.	11.	49.	-0.2	10.	0	1.0	-0.2	3.9
North of Channel	-0.6	35.	16.	40.	-0.6	31.	0.2	5.2	0.2	20.
Turtle Island	0.1	23	16.	26.	0	10.	0.2	7.7	0.4	14.
New River	0.9	72.	76.	123.	0.9	48.	1.2	53.	1.5	58.
Daufuskie Island	0.2	8.	5.6	10.	0	4.2	0.1	5.2	0.1	6.7
Offshore	0.4	13.	41.0	138.	0.9	8.5	0	0.1	0.5	3.0

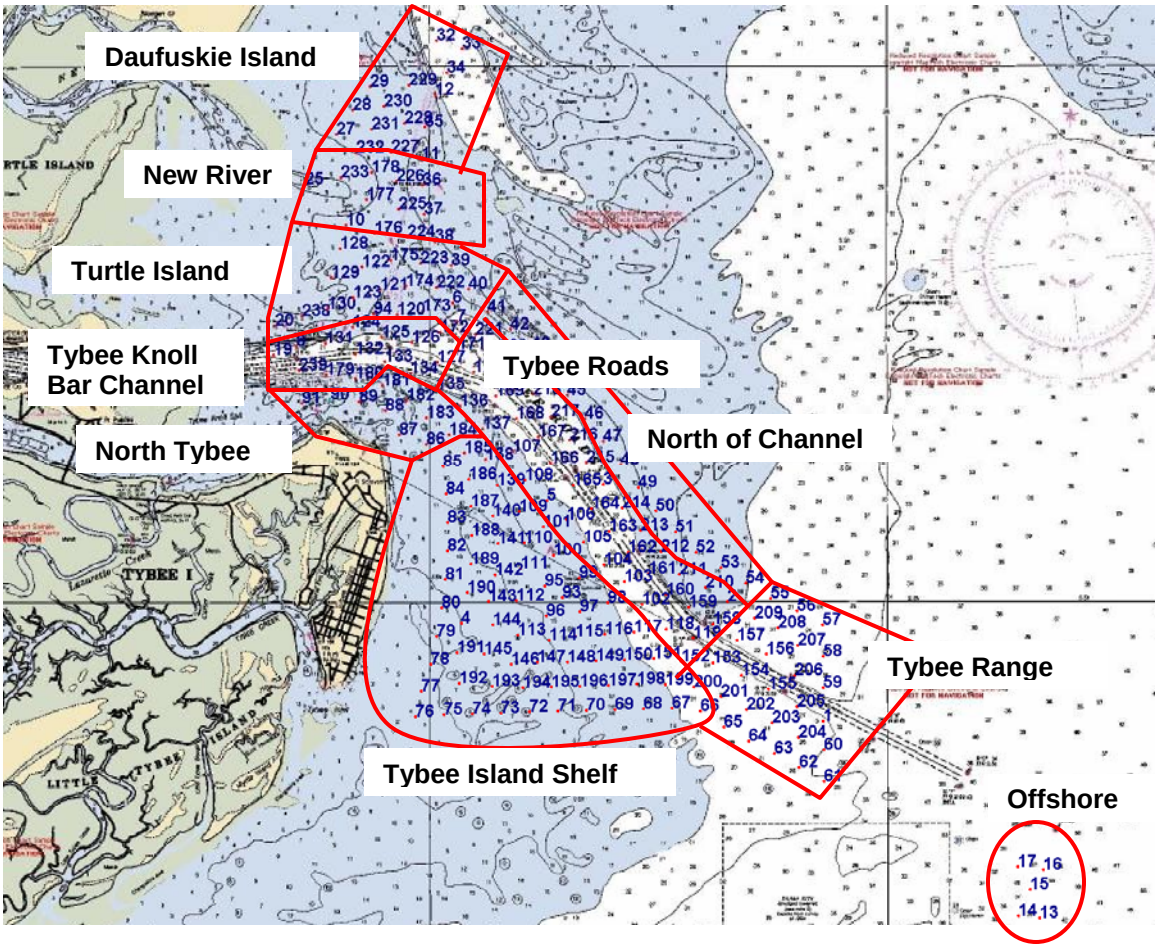

Figure 5-4. Summary of Regions Used in Table 5-1.

September 1989

Figure 5D-2 provides the changes in cumulative sediment transport vectors between the two September 1989 simulations. The ranges of differences in point magnitudes are -9 m^3/m to 390 m^3/m in the channel and -13 m^3/m to 10 m^3/m on the Tybee Island shelf. Unlike the other simulations, cumulative offshore transport increased throughout the channel due to the deepening. The average cumulative transport magnitude increases throughout the modeling for the deepened channel (Table 5-1). The largest increases are in the Tybee Knoll Bar and Tybee Roads sections of the channel (approximately 100 m^3/m).

January 1992

Figure 5D-3 provides the changes in cumulative sediment transport vectors between the January 1992 simulations. The ranges of differences in point magnitudes are -40 m^3/m to 22 m^3/m in the channel and -2 m^3/m to 1 m^3/m on the Tybee Island shelf. Cumulative transport magnitude decreased due to the deepening inside the channel from the jetties seaward to the beginning of the Tybee Roads area. The largest regional average difference in magnitudes is a decrease of 10 m^3/m in the inner channel (Table 5-1). The average differences by region are similar to November 1979.

July 1999

Figures 4D-4 provides the changes in cumulative sediment transport vectors between the two July 1999 simulations. The ranges of differences in point magnitudes are -53 m^3/m to 19 m^3/m in the channel and -0.4 m^3/m to 0.6 m^3/m on the Tybee Island shelf. Cumulative transport magnitude decreased due to the deepening inside the channel from the jetties seaward to the beginning of the Tybee Roads area. The largest regional average difference in magnitudes is a decrease of 12 m^3/m in the Tybee Knoll bar channel (Table 5-1). The average differences by region are similar to November 1979 and January 1992.

December 1999

Figure 5D-5 provides the changes in cumulative sediment transport vectors between the two December 1999 simulations. The ranges of difference in point magnitudes are -45 m^3/m to 31 m^3/m in the channel and -1.0 m^3/m to 1.1 m^3/m on the Tybee Island shelf. Cumulative transport magnitude decreased due to the deepening inside the channel from the jetties seaward to the beginning of the Tybee Roads area. The largest regional average difference in magnitudes is a decrease of 10 m^3/m in the Tybee Knoll bar channel (Table 5-1). The average differences by region are similar to November 1979, January 1992, and July 1999.

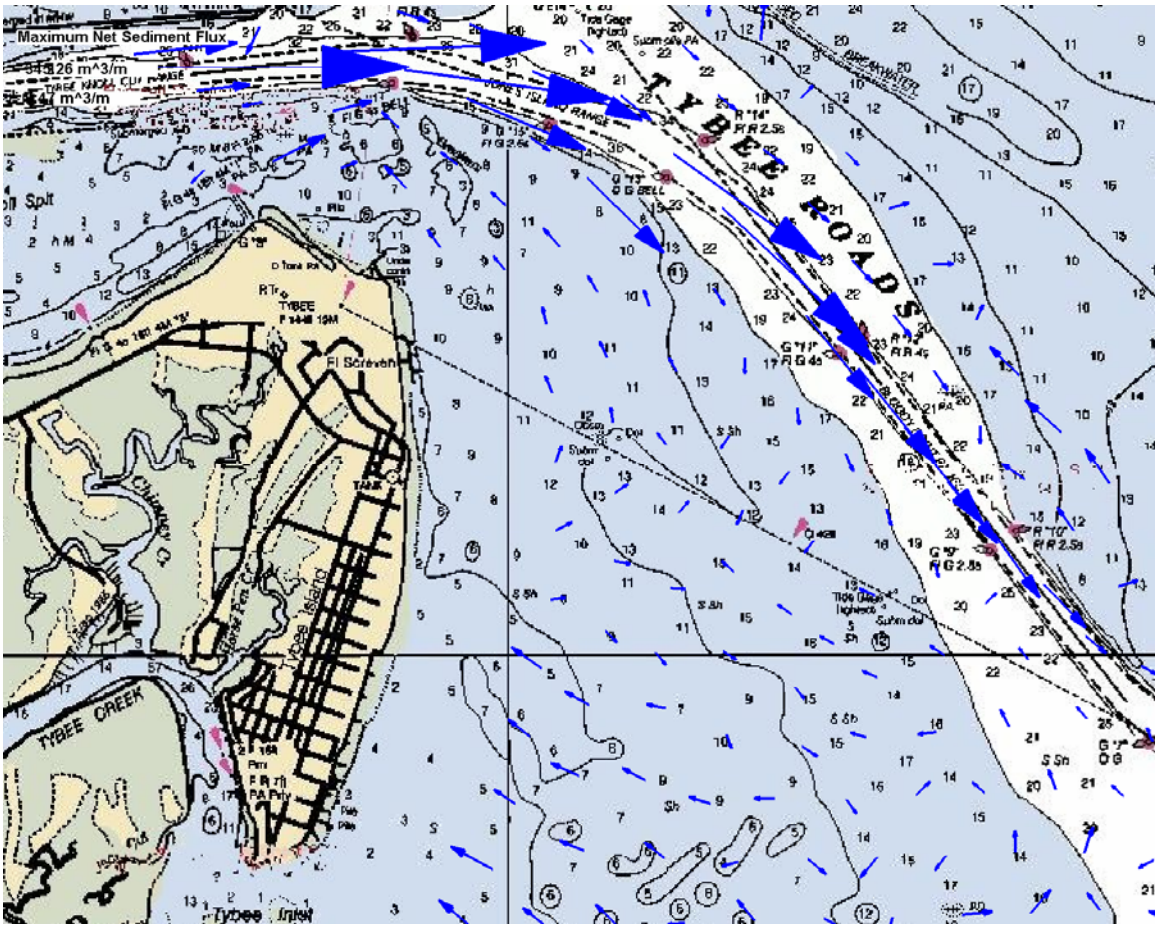

Figure 5-5. Cumulative sediment transport vectors for December 1999 existing conditions GTRAN simulation (Tybee Shelf).

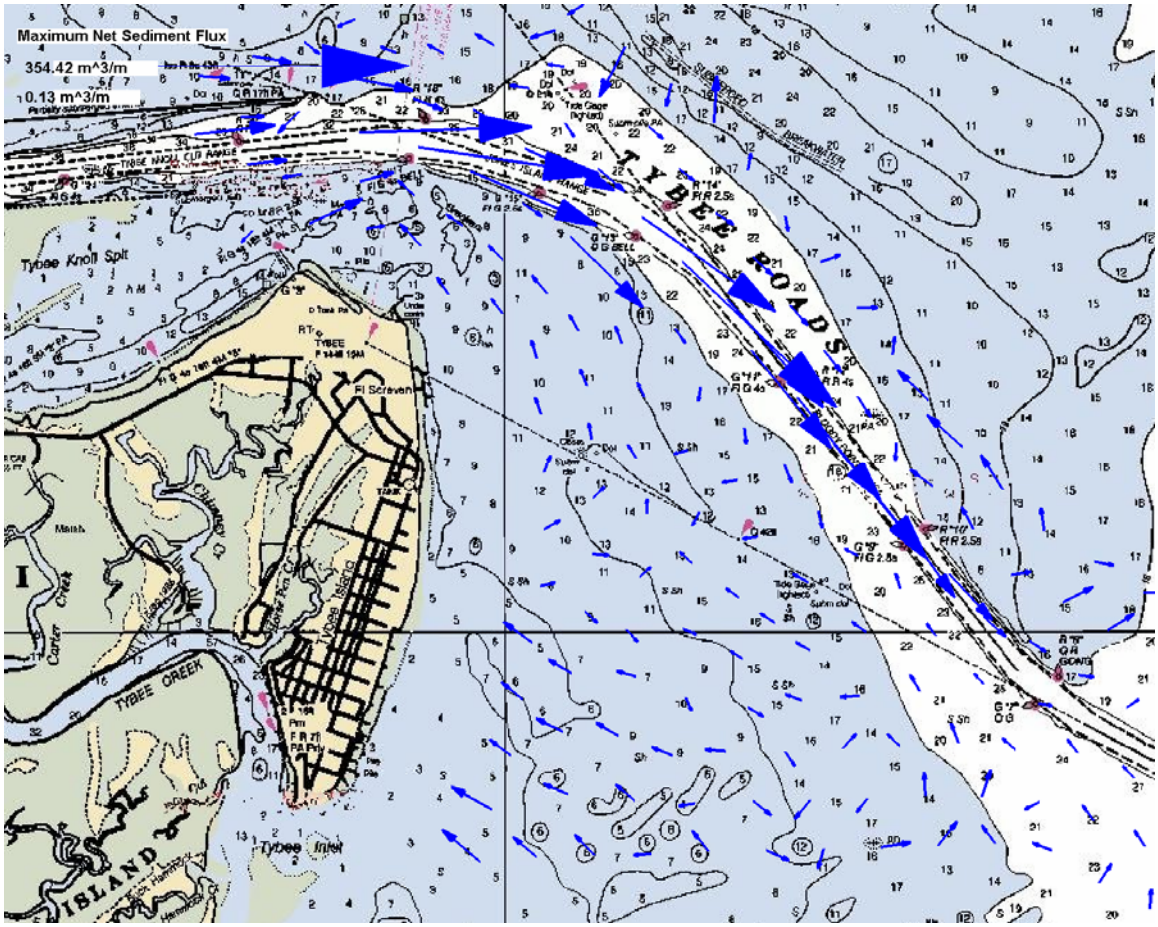

Figure 5-6. Cumulative sediment transport vectors for December 1999 deepened conditions GTRAN simulation (Tybee Shelf).

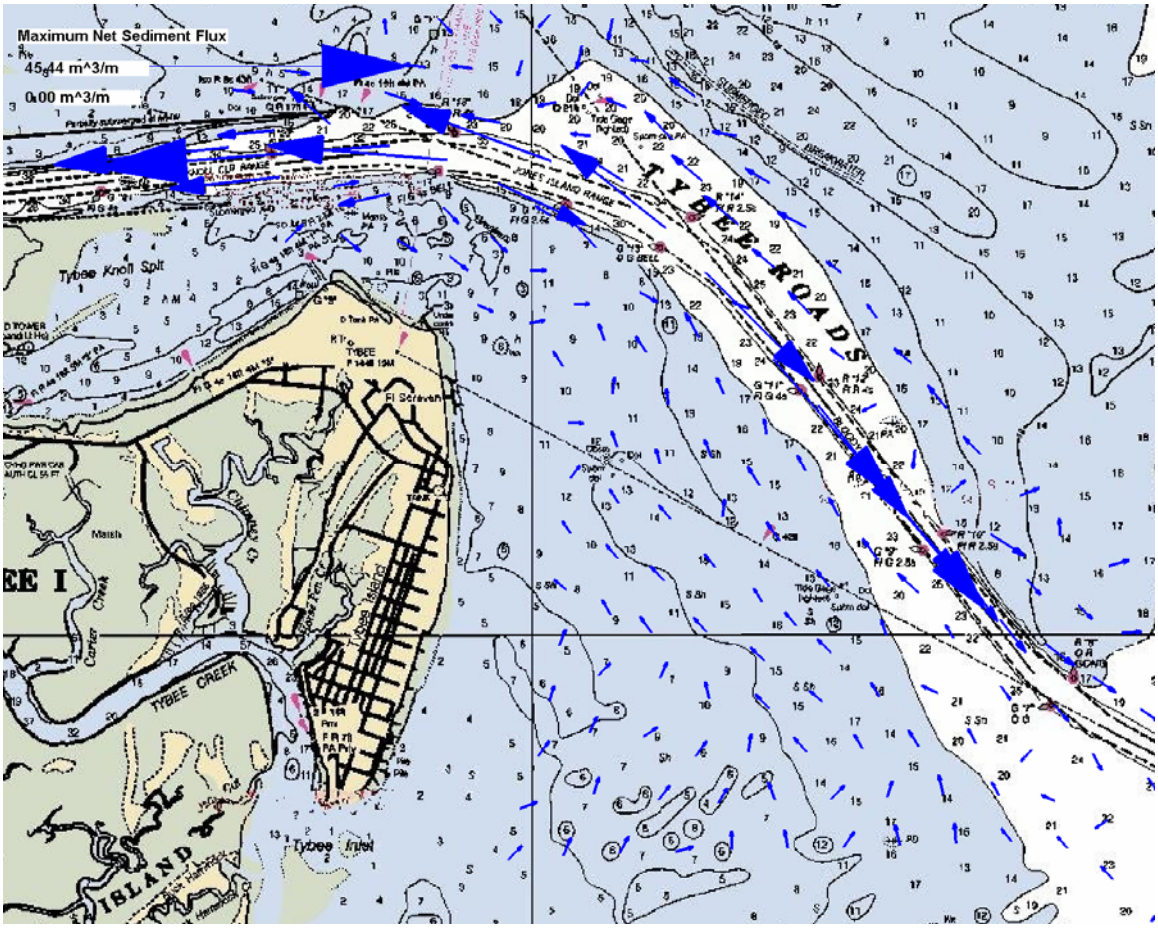

Figure 5-7. Change in cumulative sediment transport vectors for December 1999 GTRAN simulation (Tybee Shelf).

Sediment Transport Summary

With the exception of the re-tracked Hurricane Hugo (September 1989), changes in cumulative sediment transport due to deepening the federal channel show similar patterns and magnitudes across all GTRAN simulation periods. The November 1979, January 1992, July 1999, and December 1999 simulations show differences in average cumulative sediment transport magnitude inside the channel of between -16 to +3 m^3/m (point differences of -60 to +50 m^3/m) and differences in average cumulative sediment transport around Tybee Island of between -1.0 to +0.3 m^3/m (point differences of -3.2 to +5.9 m^3/m). The general trend is a decrease in ebb-directed cumulative sediment transport in the Tybee Knolls bar channel (10 to 16 m^3/m, 15-20 percent) and a slight increase in ebb-directed cumulative sediment transport in the Tybee Roads and Range sections of the channel (0-3 m^3/m, 0-5 percent). The other nearshore areas had small changes in the average cumulative transport: 0-1 percent increase in transport on the Tybee Island Shelf; 3-6 percent decrease on north of Tybee; 0-3 percent increase off Turtle Island, New River and Daufuskie Island; and 2 percent decrease to 4 percent increase north of the channel

The high intensity forcing (waves and currents) during the re-tracked Hurricane Hugo results in positive (increase) transport rates throughout the deepened channel. The increases in averaged cumulative sediment transport magnitude during September 1989 range from +11 to +102 m^3/m in the channel (point differences of -90 to +390 m^3/m). The increased transport is directed offshore in the channel. Increases in average cumulative sediment transport magnitude were seen in all regions, 0.3 m^3/m on the Tybee Island shelf, 5.5 m^3/m in north Tybee, 35 m^3/m north of the outer channel, 23 m^3/m off Turtle Island, 72 m^3/m at New River, and 8 m^3/m off of Daufuskie Island. The rates for the other simulation periods are averaged over one month simulation, and the re-tracked Hugo simulations are averaged only over 1 week, making any local differences (in space or time) more prominent. Hurricane Hugo is an extreme event, and the potential transport rates calculated with GTRAN do not account for evolution of the bathymetry through the storm or the response of waves and currents to the evolution of bathymetry (which would be significant in a hurricane).

These results support the hypothesis that the additional deepening will not have a major impact on the system, including north Tybee. The circulation and wave modeling indicated very small changes associated with the proposed deepening. GTRAN results for the existing condition and the deepened-channel condition indicate that the additional channel deepening will not change the general overall pattern of sediment transport in the region. The most noticeable changes were computed in the channel.

Appendix 5A. GTRAN Sediment Transport Methods

This section describes the sediment transport methods incorporated into the sediment transport model. These descriptions aim to provide a general overview of the predictive techniques.

Transport Methods

Algorithms that estimate sediment movement under specific wave and current conditions are referred to as transport methods. Presently there are no sediment transport methods that are universally applicable to all environments and sediment types. For instance, a transport method developed for cobbles and boulders in an alpine stream is not likely to correctly represent sediment transport in an estuary or open-coast application. To correctly and reliably estimate sediment transport, the transport method must represent the important transport processes within the region of application. A general description and overview will be given for each transport method applied.

Wikramanayake and Madsen. Under contract with the U.S. Army Corps of Engineers, Dredging Research Program (DRP), researchers at Massachusetts Institute of Technology developed non-cohesive sediment transport algorithms for combined wave-current environments. The algorithms include the effects of variation between current and wave directions. The methods are outlined in DRP reports (Madsen and Wikramanayake, 1991; Wikramanayake and Madsen, 1994a) and were specifically designed for nearshore transport in high-energy regions, although the initial validation and calibration were performed outside the surf zone. User input includes near-bottom orbital velocity, mean currents, bed slope, and grain size.

The method uses a time-invariant turbulent eddy viscosity model and a time-varying near-bottom concentration model to estimate suspended sediment transport fluxes. The method first calculates the bed roughness, using methods outlined by Wikramanayake and Madsen (1994b). Bed load and suspended sediment concentrations are then calculated using bottom shear stress. Estimates of vertical variation in suspended sediment concentration are based on a non-dimensional, time-varying, near-bottom reference concentration, $C_r(t)$. This concentration can be estimated as:

$$C_r(t) = \frac{C_b \gamma_o (|\Psi^*(t)| - \Psi_{cr})}{\Psi_{cr}} \qquad \text{(5A-1)}$$

where C_b is the volume fraction of sediment in the bed, γ_o is an empirical resuspension coefficient, $\Psi^*(t)$, the Shield's parameter based on instantaneous, skin-friction shear stress, and Ψ_{cr} , the critical Shield's parameter. Laboratory experiments have demonstrated that γ_o decreases with increasing Shield's parameter or wave skin friction shear stress. However, data were insufficient to develop empirical methods to relate the resuspension coefficient to Shield's parameter and constant values of γ_o are applied for rippled and flat beds, respectively. The Shield's parameters are defined by:

$$\Psi^*(t) = \frac{u^*(t)}{(s-1) g d_{50}} \qquad \text{(5A-2)}$$

$$\Psi_{cr} = \alpha_1 \tan(\phi) \tag{5A-3}$$

where $u^*(t)$ is the bed shear velocity, α_1 is a coefficient dependent on the local Reynolds number, s is the specific gravity of sediment, d_{50} is the median grain diameter, g is gravitational acceleration, and ϕ is the angle of repose of the sediment grains. The reference concentration is used to estimate vertically varying concentrations in the water column due to steady and oscillatory currents. The estimated suspended sediment concentration is coupled with the vertically varying velocities to estimate the total suspended sediment flux.

The Wikramanayake and Madsen model also includes a method for estimating the instantaneous bed-load flux based on the Meyer-Peter and Müller (1948) formula. This instantaneous bed-load flux, Q_b (cm^3/cm·s), is estimated by:

$$\vec{Q}_b(t) = \frac{d_{50}\sqrt{(s-1)gd_{50}}}{2\pi} \frac{8(|\Psi^*(t)| - \Psi_{cr})}{1 + \tan\beta_L \dfrac{\cos(\Phi_t - \Phi_{sw})}{\tan\Phi_f}} \frac{\vec{\tau}_b'(t)}{|\vec{\tau}_b'(t)|} \tag{5A-4}$$

where $\beta_L = h/6\delta$, h is the water depth, δ is the boundary layer length scale, Φ_t is the angle between the current and the wave direction, Φ_{sw} is the angle between the wave direction and bottom slope, and $\tau_b'(t)$ is the instantaneous skin friction shear stress.

Wikramanayake and Madsen (1994a) performed several tests to compare their results to field measurements in wave/current environments and found that the model accurately predicted the current-related and wave-related sediment fluxes and distributions in the water column. No verification was performed for the bed-load model estimates. Field verification of the transport method has been performed by CHL against data sets from the Columbia River mouth (Gailani et al. in preparation) and in the surf zone at the Field Research Facility, Duck, North Carolina, with favorable comparisons to field data. However, the Wikramanayake and Madsen transport method is unsuitable for conditions in which sediment suspension and/or wave-induced shear stresses are small, therefore other methods of approximating sediment transport were applied under bedload-dominated or current-dominated transport conditions.

Soulsby bedload transport method. Soulsby (1997) developed a formula for combined wave-current bedload by integrating the current-only bedload formula of Nielsen (1992) over a single sinusoidal wave cycle. The formula is expressed as follows:

$$\Phi_{x1} = 12\theta_m^{1/2}(\theta_m - \theta_{cr}) \tag{5A-5a}$$

$$\Phi_{x2} = 12(0.95 + 0.19\cos 2\phi)\theta_w^{1/2}\theta_m \tag{5A-5b}$$

$$\Phi_x = \text{maximum of } \Phi_{x1} \text{ and } \Phi_{x2} \tag{5A-5c}$$

$$q_{bx} = \Phi_x\left[g(s-1)d_{50}^3\right]^{1/2} \tag{5A-5d}$$

subject to $\Phi_x = 0$ if $\theta_{cr} \geq \theta_{max}$
where:

q_b = mean volumetric bedload transport rate per unit width
θ_m = mean Shield's parameter over a wave cycle
θ_w = amplitude of oscillatory component of θdue to waves
θ_{max} = maximum Shield's parameter from combined wave-current stresses
θ_{cr} = critical Shield's parameter for initiation of motion
ϕ = angle between current direction and direction of wave travel

Soulsby's combined wave-current bedload transport method was applied when sediment suspension was estimated to be near zero.

Van Rijn current-dominated transport method. The Van Rijn (1984) current-only total transport method was parameterized from Van Rijn's comprehensive theory of sediment transport in rivers. Although the method was developed for sediment transport in the riverine environment, the method may also be appropriately applied in the marine environment under conditions for which waves contribute little to the bottom shear stress. The simpler, parameterized formulae presented here approximate the full theory within ±25 percent and were developed for water depths between 1-20 m, velocities between 0.5 and 5 m/s, d50 between 0.1 and 2 mm, and for fresh water at 15 deg C. The resulting parameterized method estimates transport by the following simpler formulation:

$$q_t = q_b + q_s \tag{5A-6}$$

$$q_b = 0.005\overline{U}h\left\{\frac{\overline{U}-\overline{U}_{cr}}{\left[(s-1)gd_{50}\right]^{1/2}}\right\}^{2.4}\left(\frac{d_{50}}{h}\right)^{1.2} \tag{5A-7}$$

$$q_s = 0.012\overline{U}h\left\{\frac{\overline{U}-\overline{U}_{cr}}{\left[(s-1)gd_{50}\right]^{1/2}}\right\}^{2.4}\left(\frac{d_{50}}{h}\right)\left(D_*\right)^{-0.6} \tag{5A-8}$$

where,

$$\overline{U}_{cr} = 0.19(d_{50})^{0.1}\log_{10}\left(\frac{4h}{d_{90}}\right)\left\{0.1 \le d_{50} \le 0.5\,\text{mm}\right.$$

$$\overline{U}_{cr} = 8.50(d_{50})^{0.6}\log_{10}\left(\frac{4h}{d_{90}}\right)\left\{0.5 \le d_{50} \le 2.0\,\text{mm}\right.$$

$$D_* = \left[\frac{g(s-1)}{\nu^2}\right]^{1/3} d_{50}$$

q_b = bedload transport
q_s = suspended transport
$\overline{U}$ = depth-averaged current
h = water depth
d_{90} = sediment diameter for which 90 percent is finer by weight

Transport Model

Sediment transport processes along the length of the channel vary both spatially and temporally. A prime example of this variation is the difference between transport inside and outside of the surf zone. Waves and currents inside and outside the surf zone are responsible for transporting the sediment, but the transport mechanisms are different. Inside the surf zone, breaking waves increase turbulence and enhance sediment suspension while the wave-generated longshore currents transport the suspended sediment. Outside the surf zone, turbulence is much smaller, but the waves may suspend sediment over bedforms and the larger-scale, ocean circulation transports the sediment. Clearly, it would be difficult to represent the sediment transport in both of these regions with one transport method. The sediment transport model selects the appropriate transport method, develops the required input conditions, and tracks the spatial relationships, sediment characteristics, environmental conditions, and estimated sediment transport.

With the initial bed conditions specified, the model next distributes environmental forcing conditions from large-domain wave and circulation models to each of the computational points. The temporal resolution of the wave and current information is one-hour or three-hours as is the time step of the model. This resolution is adequate to define the temporal changes in wave and current conditions for representing sediment transport. With local wave and current conditions determined, the model proceeds to estimate the combined wave-current bottom shear stresses and to estimate the depth of the active sediment layer. The active sediment layer is defined as the depth of the sediment bed that is mobilized by sediment suspension and bed-load movement. Bottom shear stresses and non-cohesive sediment characteristics are further evaluated to determine the regime of sediment transport and the appropriate sediment transport method is selected to estimate the sediment transport rates. Jensen et al. (2002) give additional information regarding model development and application.

Appendix 5B. GTRAN Cumulative Sediment Transport Vectors

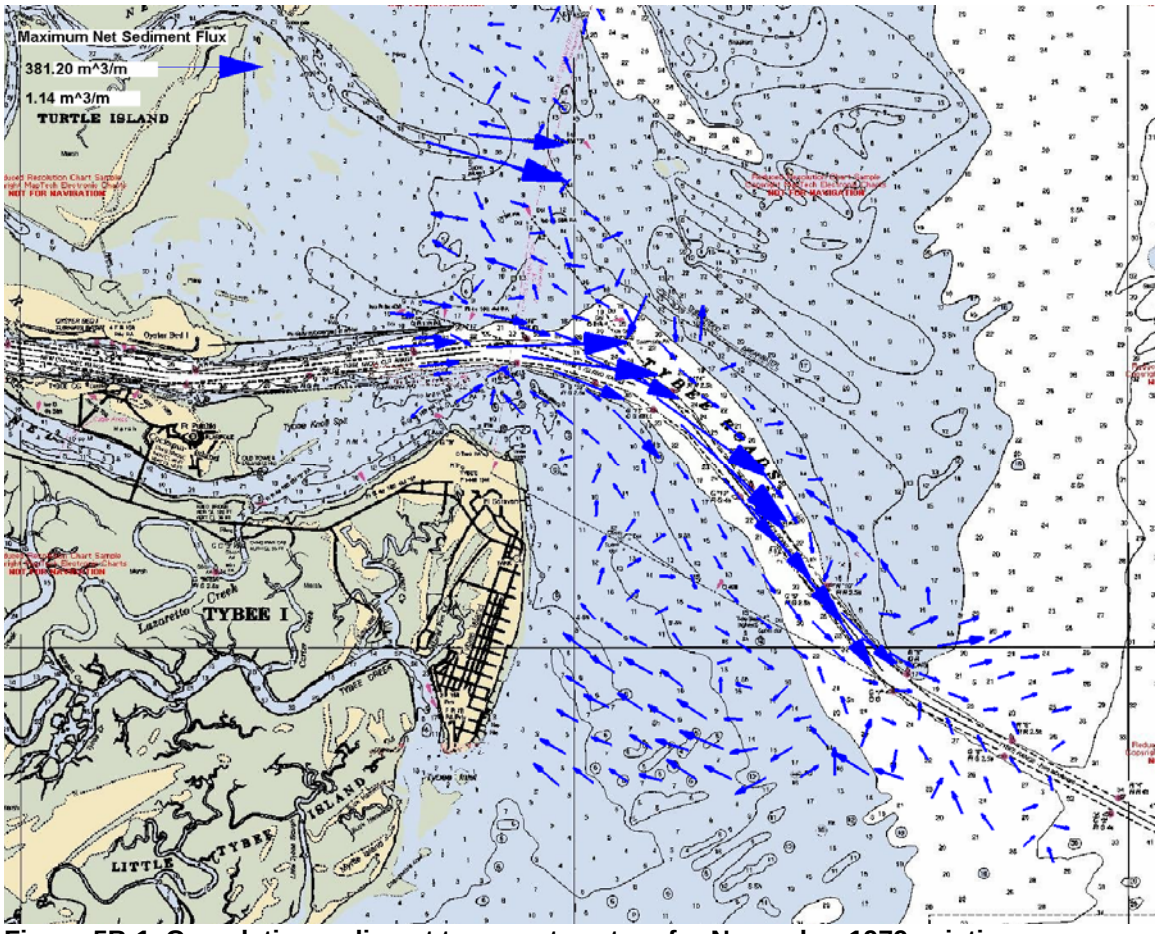

Figure 5B-1. Cumulative sediment transport vectors for November 1979 existing conditions GTRAN simulation.

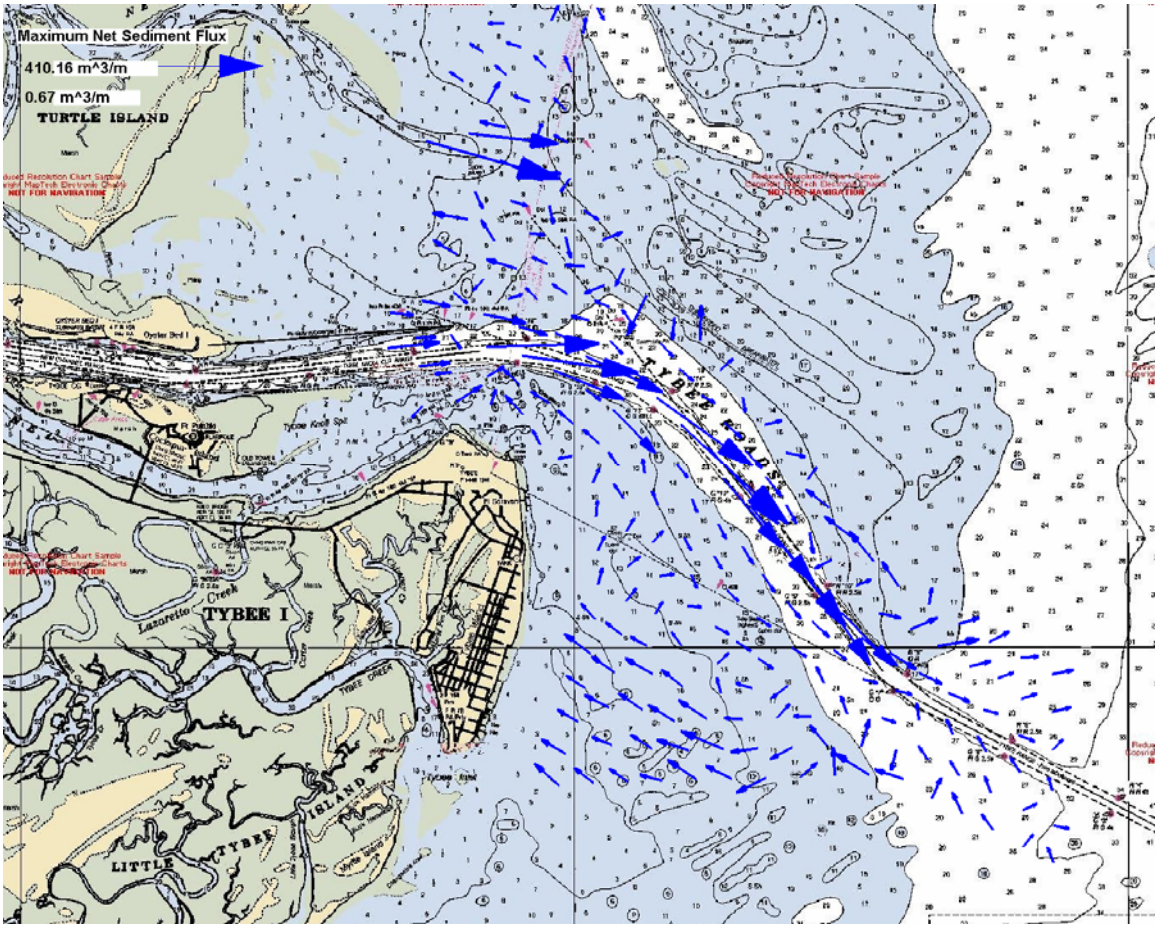

Figure 5B-2. Cumulative sediment transport vectors for November 1979 deepened conditions GTRAN simulation.

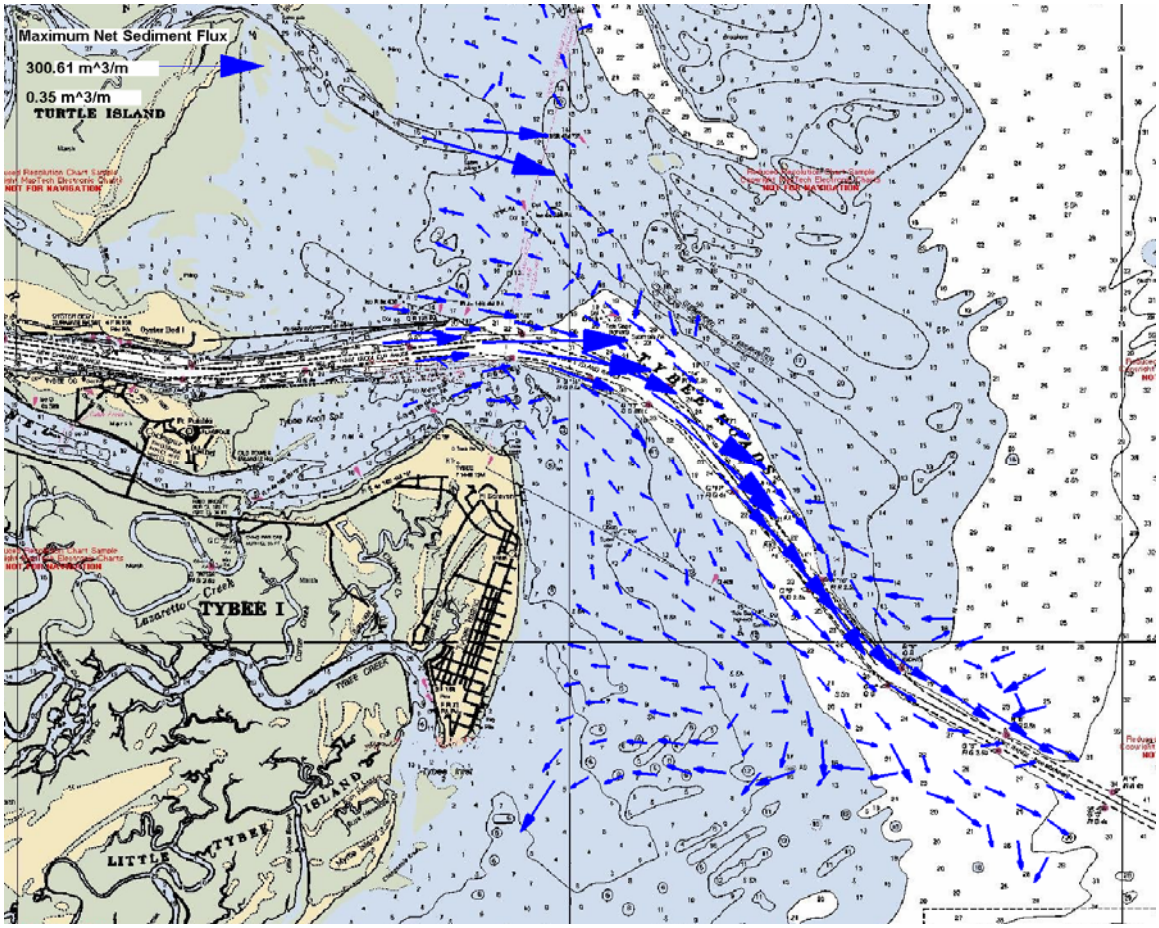

Figure 5B-3. Cumulative sediment transport vectors for September 1989 (Hugo) existing conditions GTRAN simulation.

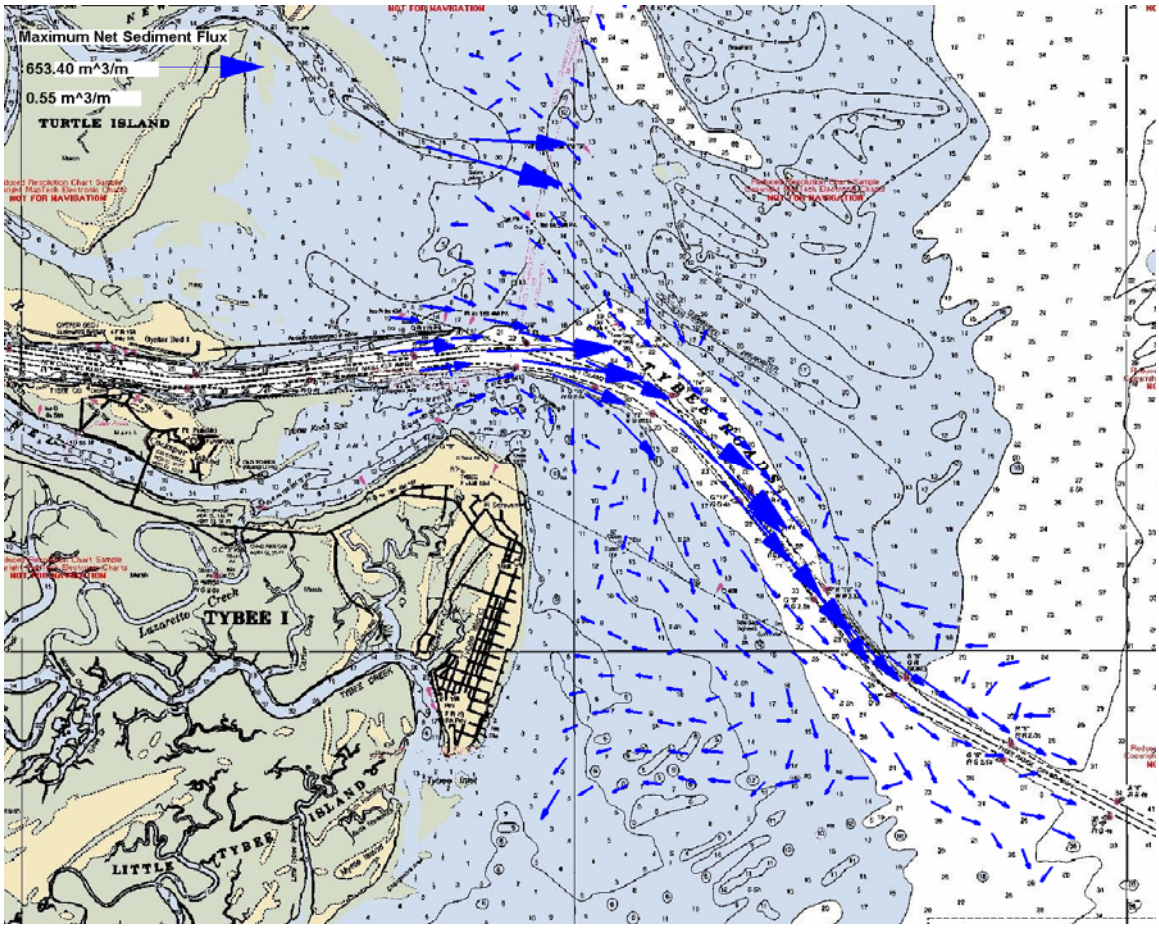

Figure 5B-4. Cumulative sediment transport vectors for September 1989 (Hugo) deepened conditions GTRAN simulation.

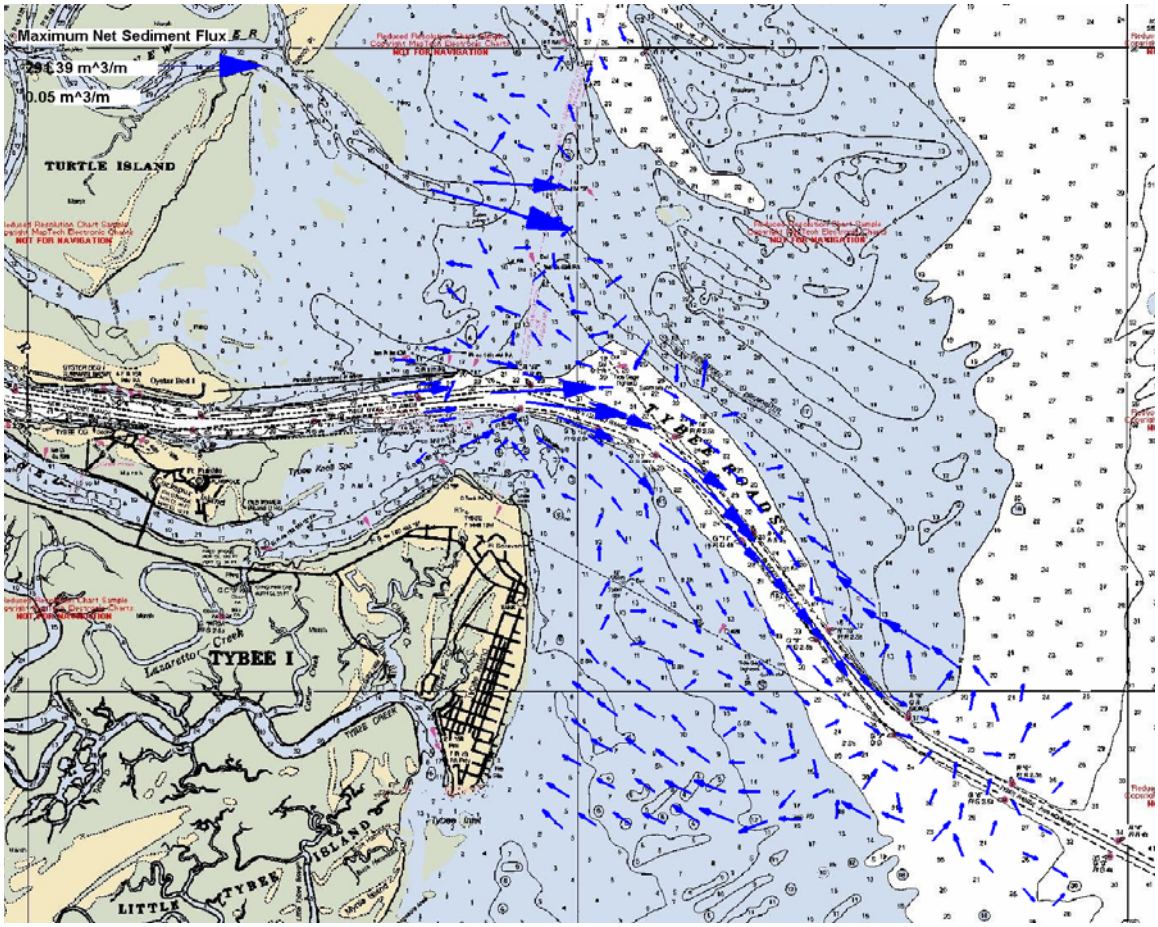

Figure 5B-5. Cumulative sediment transport vectors for January 1992 existing conditions GTRAN simulation.

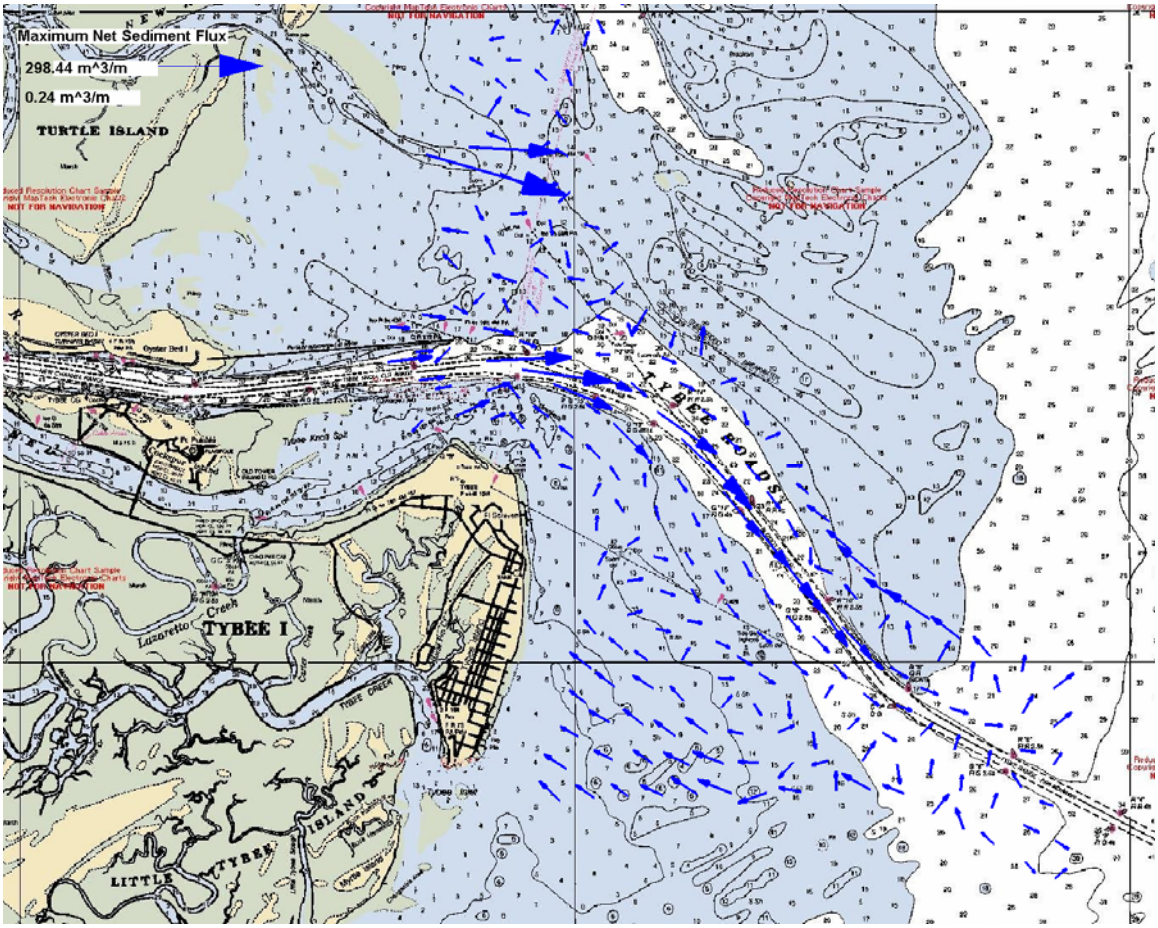

Figure 5B-6. Cumulative sediment transport vectors for January 1992 deepened conditions GTRAN simulation.

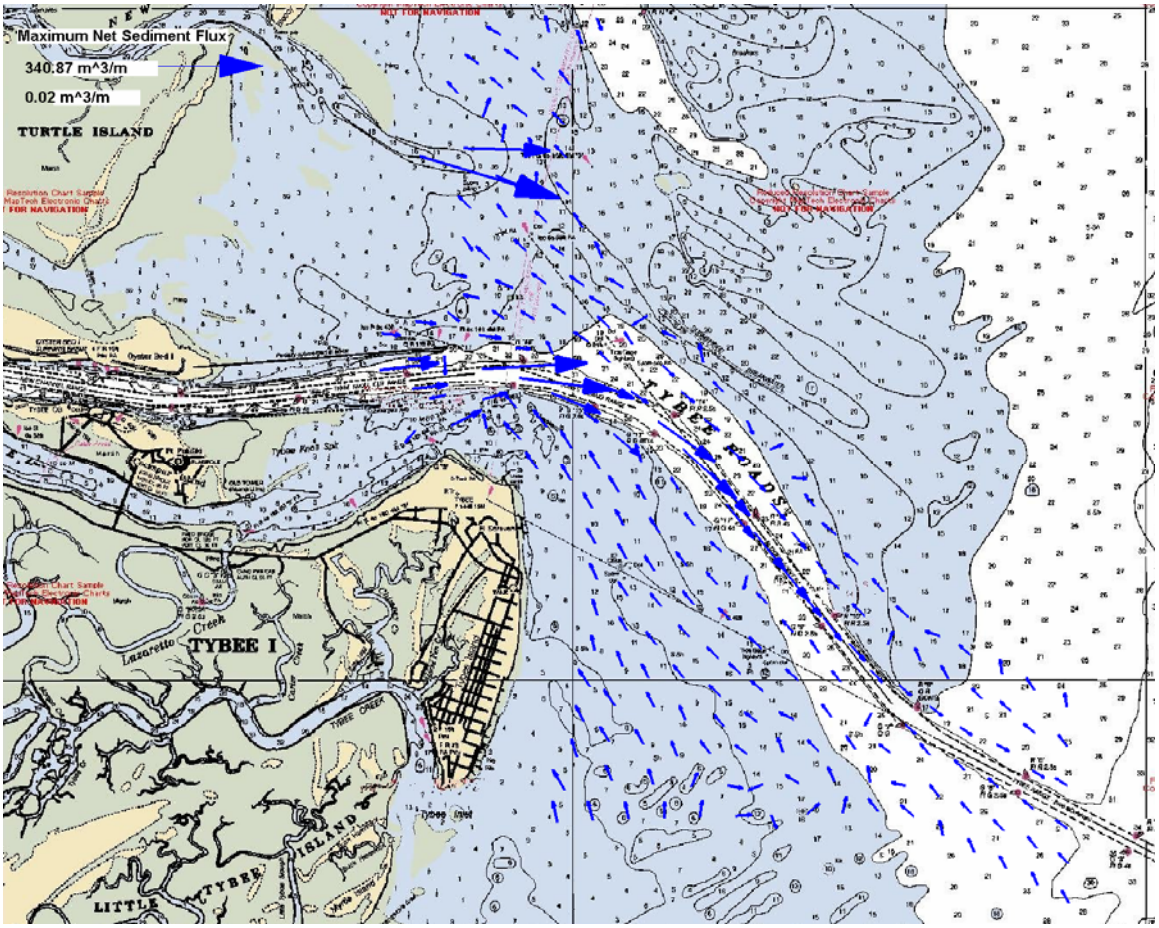

Figure 5B-7. Cumulative sediment transport vectors for July 1999 existing conditions GTRAN simulation.

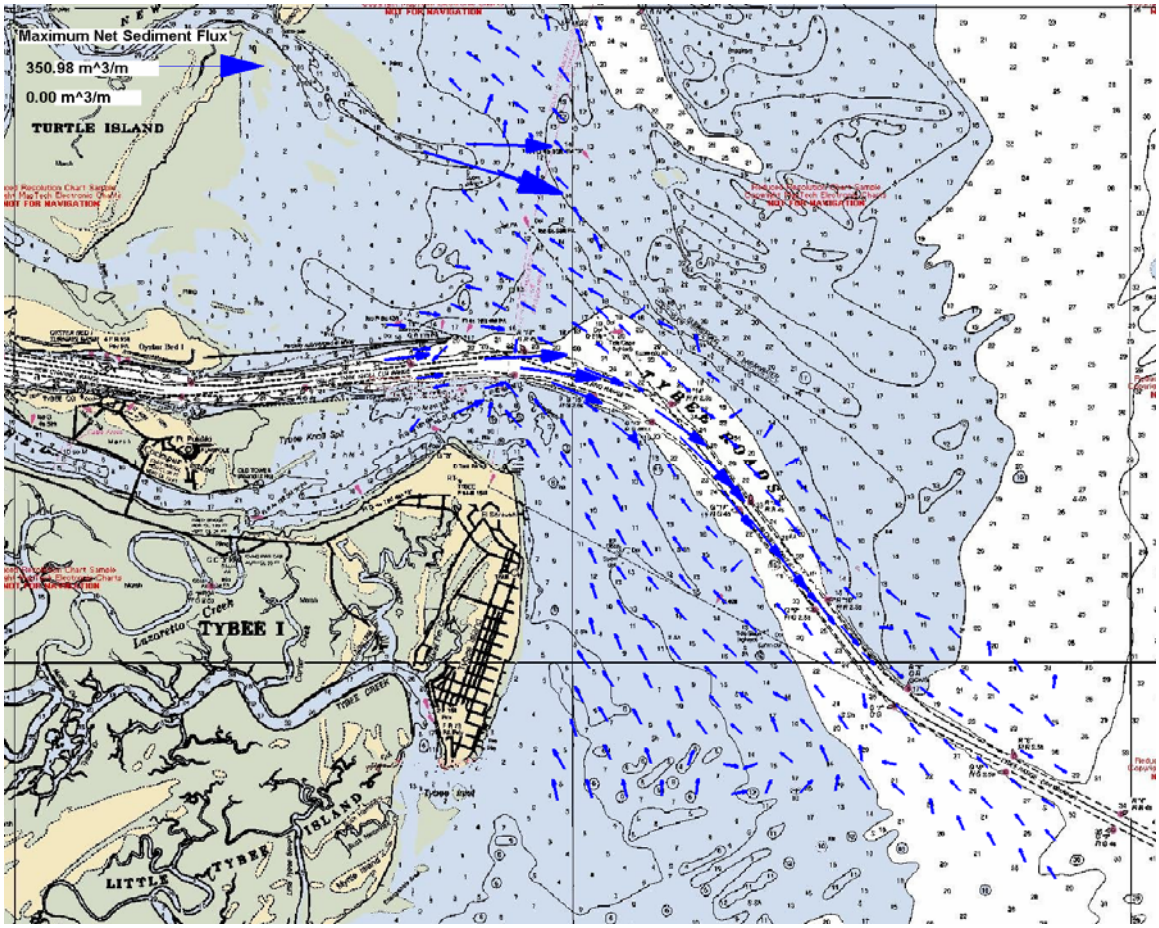

Figure 5B-8. Cumulative sediment transport vectors for July 1999 deepened conditions GTRAN simulation.

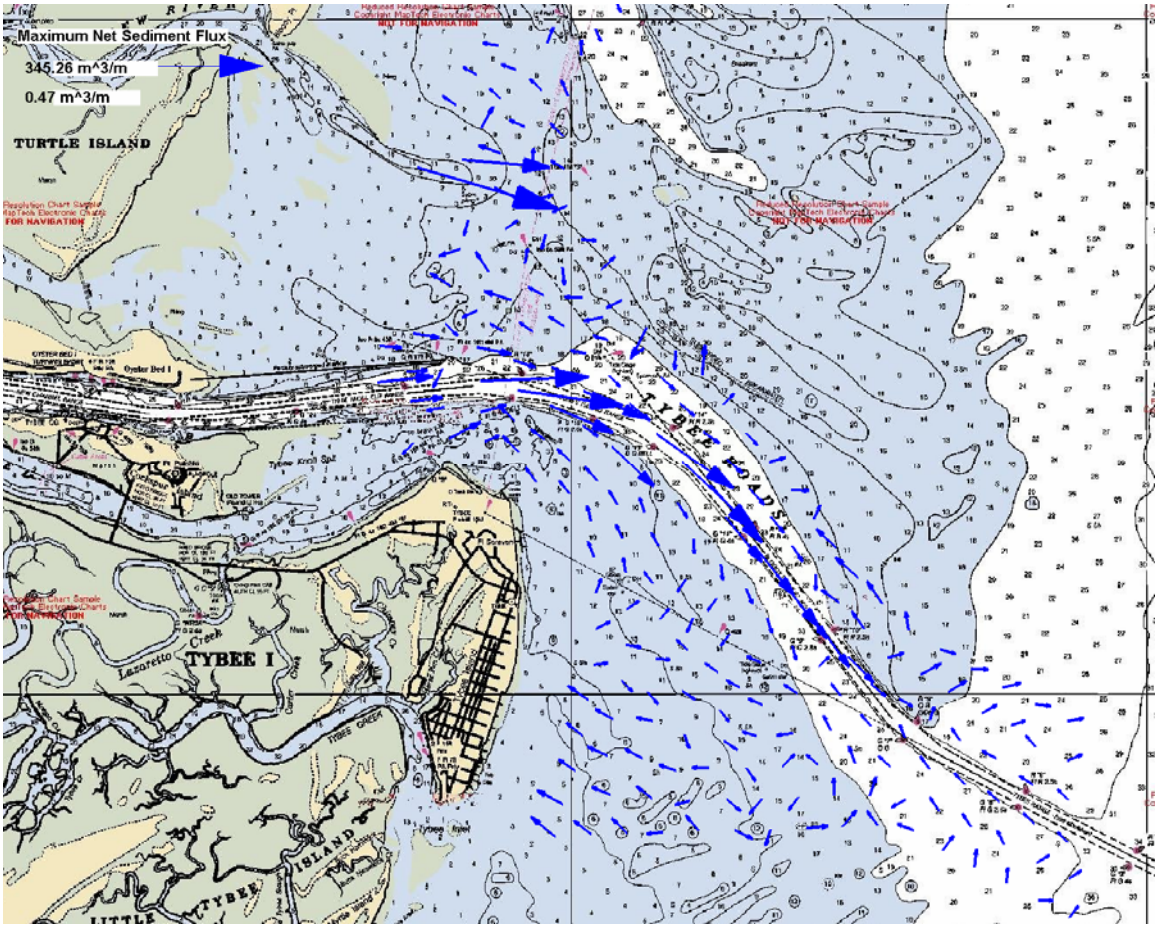

Figure 5B-9. Cumulative sediment transport vectors for December 1999 existing conditions GTRAN simulation.

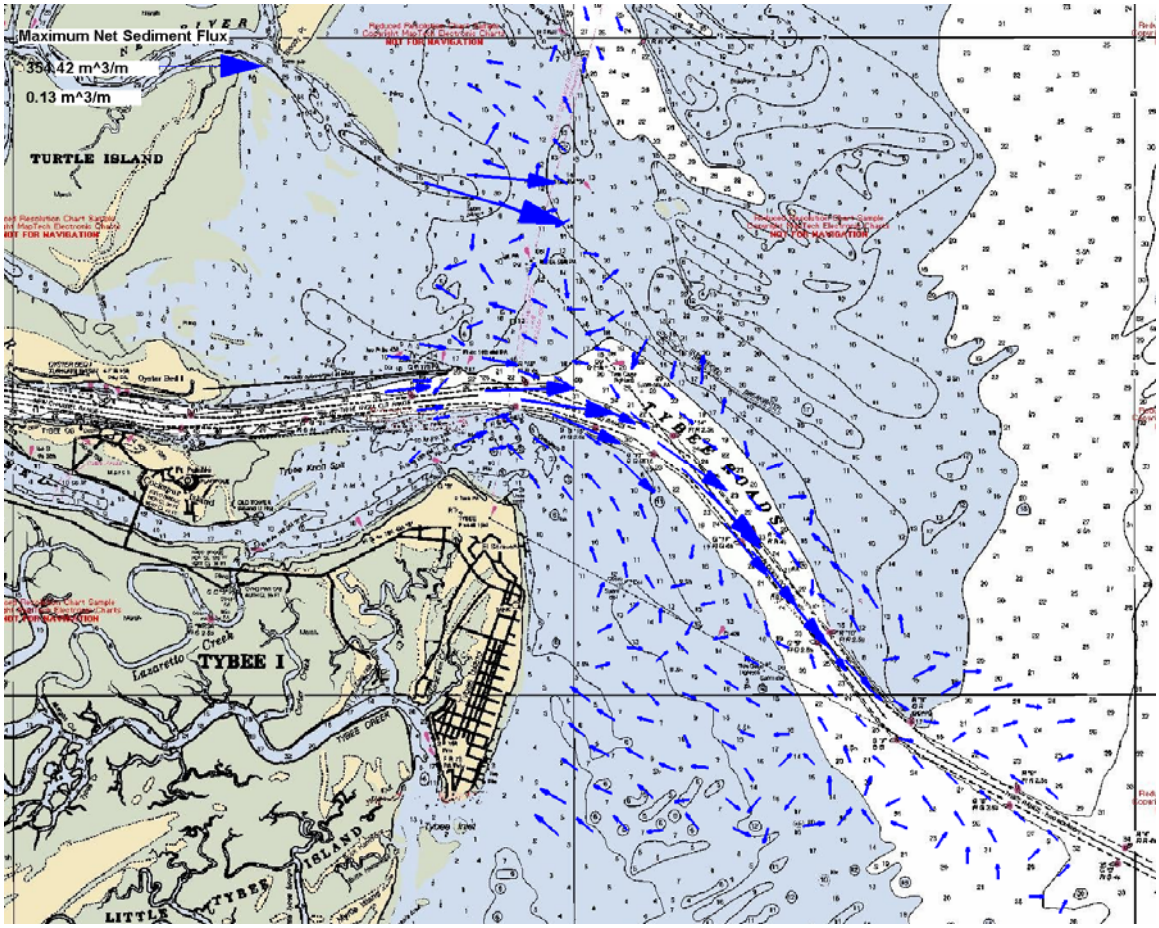

Figure 5B-10. Cumulative sediment transport vectors for December 1999 deepened conditions GTRAN simulation.

Appendix 5C. GTRAN Sediment Transport Rose Plots

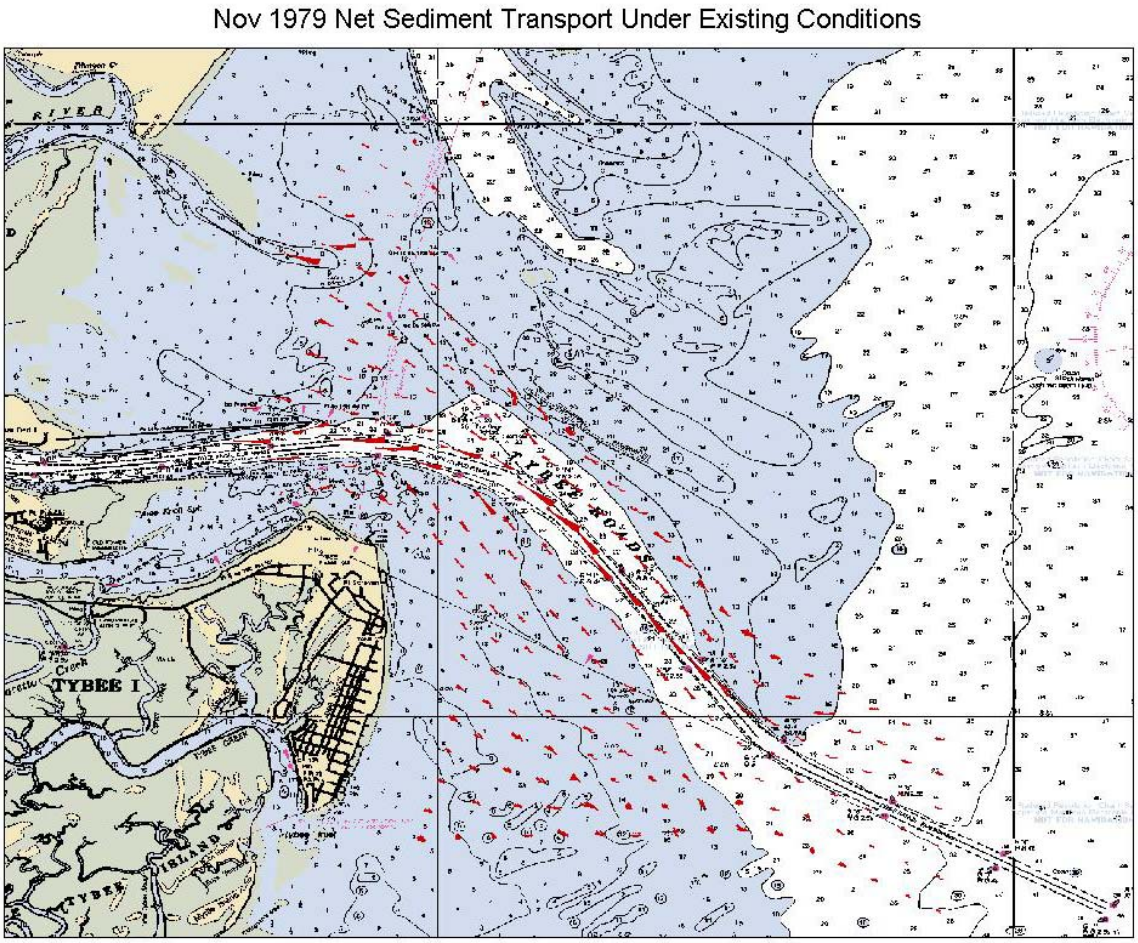

Figure 5C-1. Cumulative sediment transport rose plots for November 1979 existing conditions GTRAN simulation (full domain).

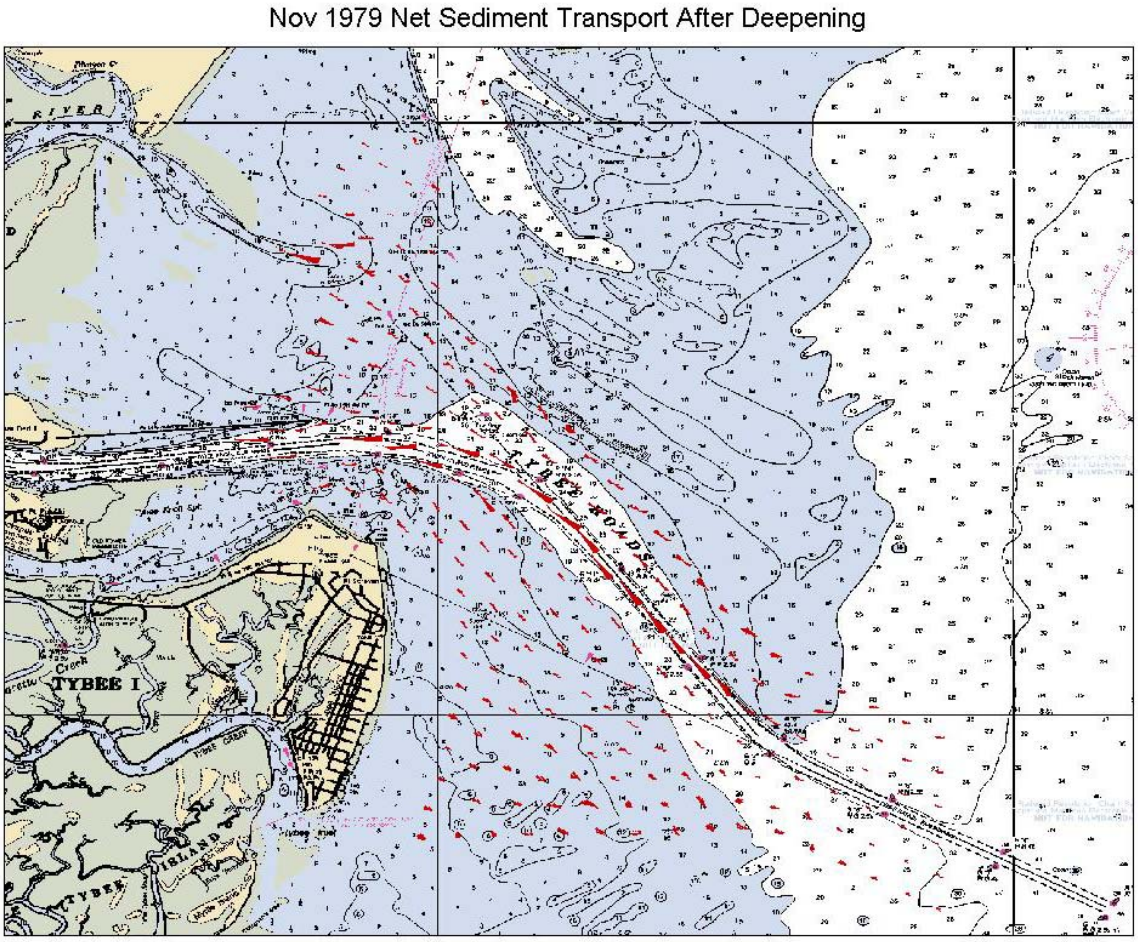

Figure 5C-2. Sediment transport rose plots for November 1979 deepened conditions GTRAN simulation (full domain).

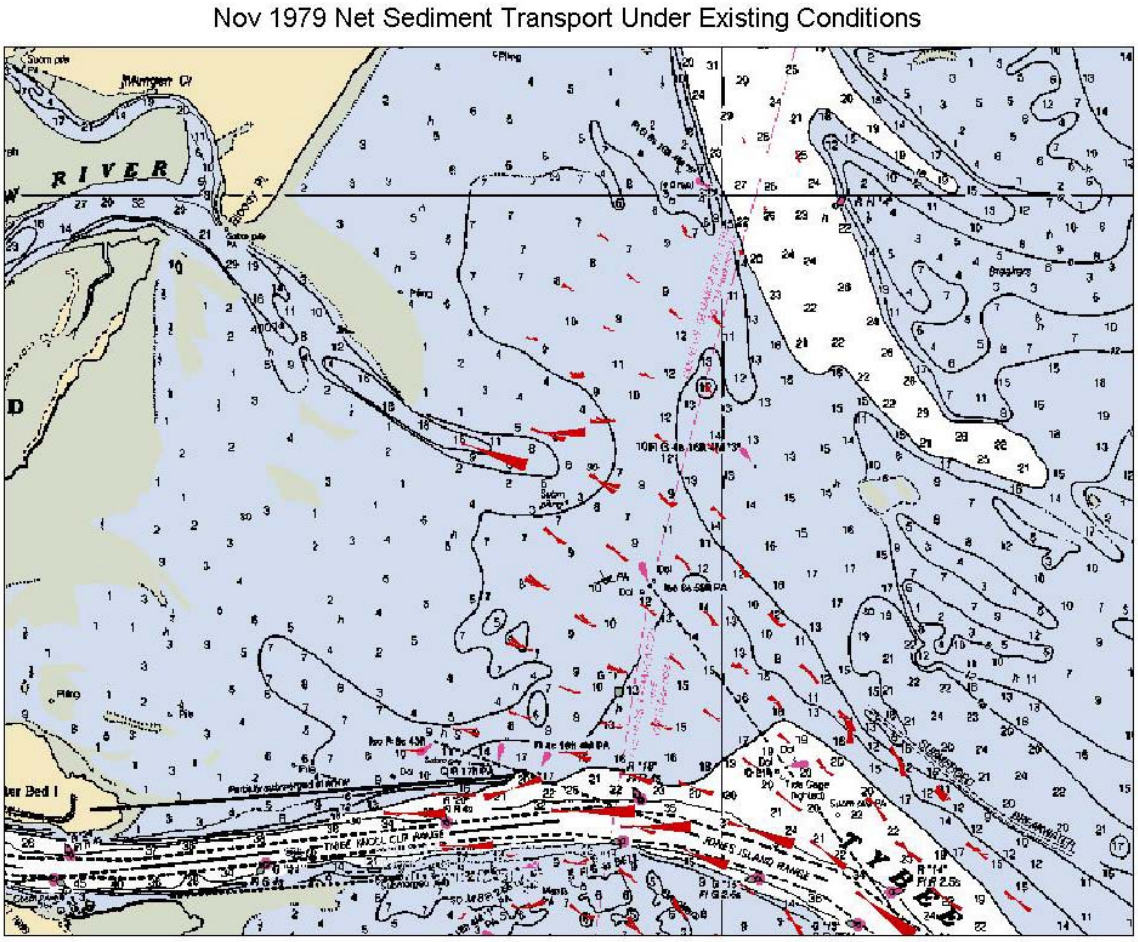

Figure 5C-3. Sediment transport rose plots for November 1979 existing conditions GTRAN simulation (northern domain).

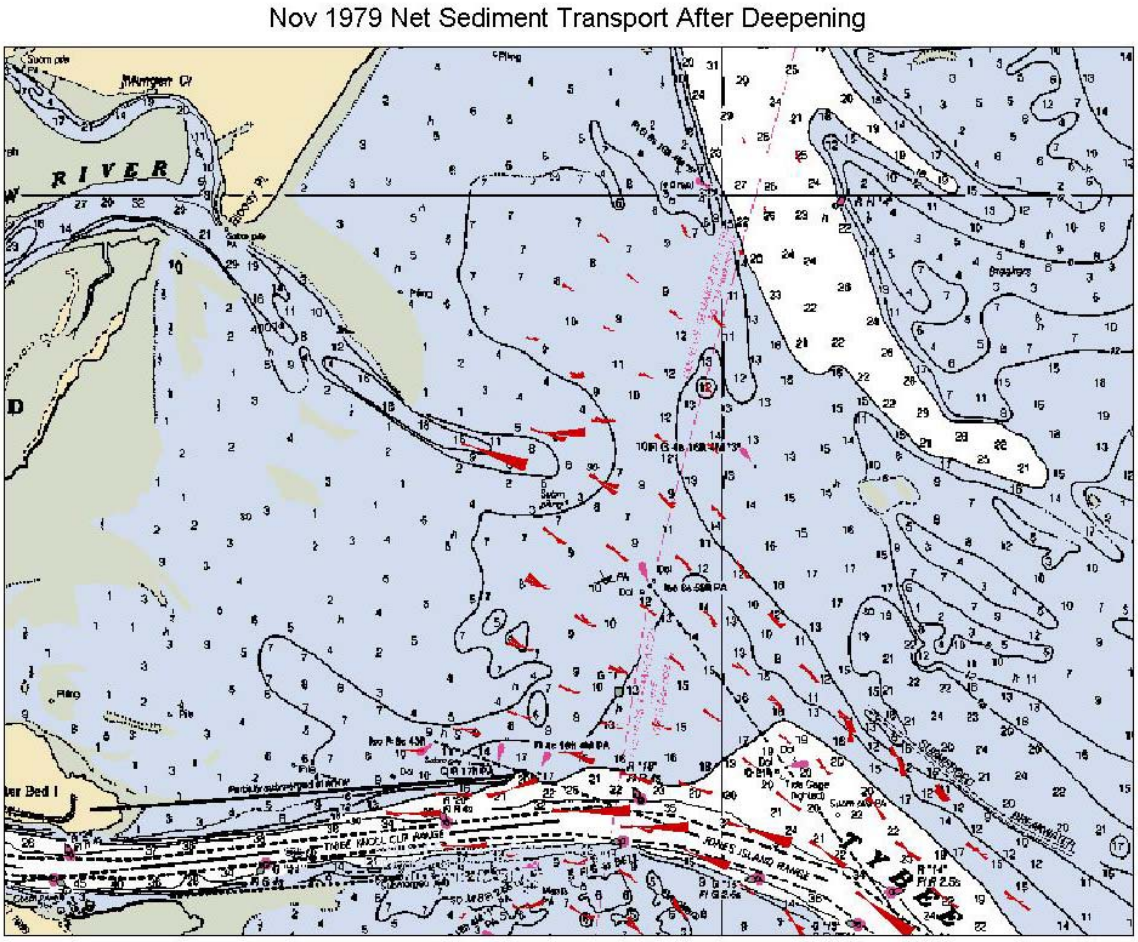

Figure 5C-4. Sediment transport rose plots for November 1979 deepened conditions GTRAN simulation (northern domain).

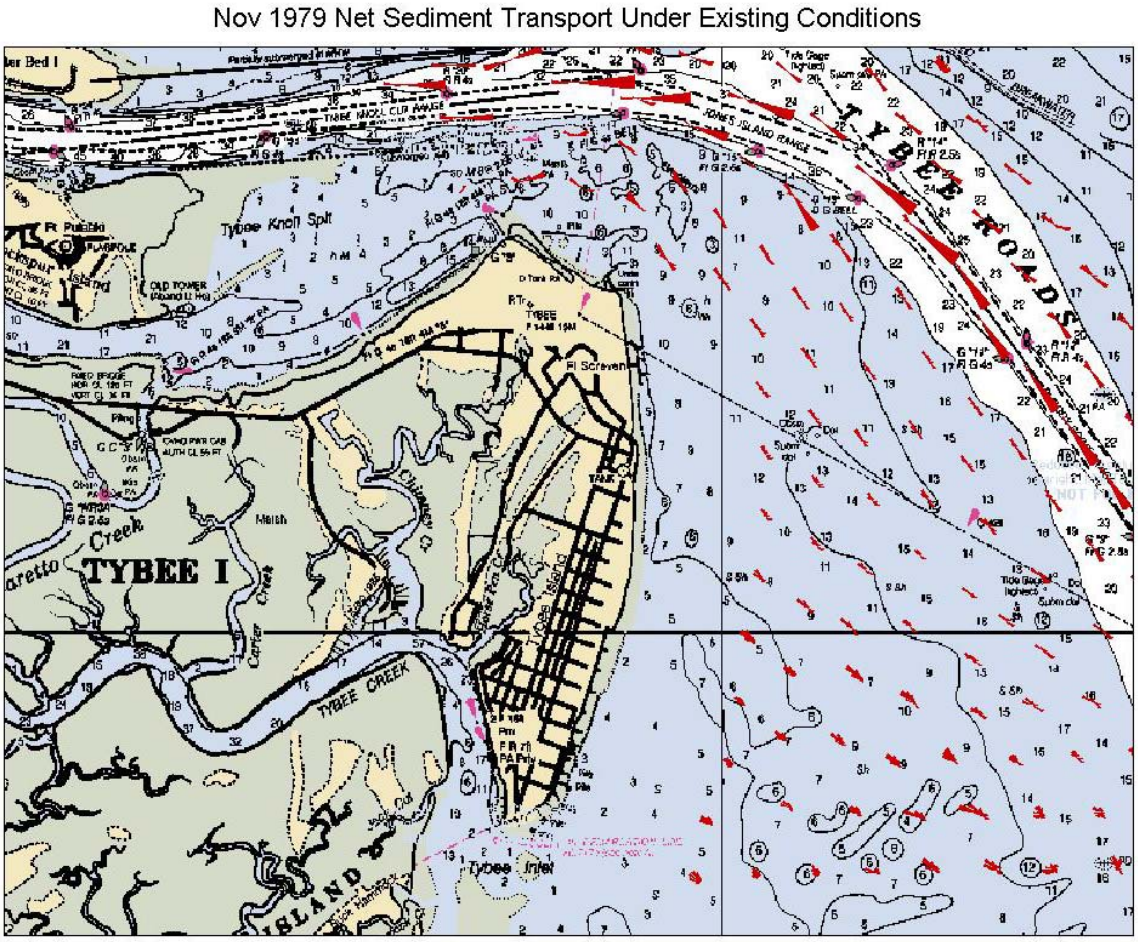

Figure 5C-5. Sediment transport rose plots for November 1979 existing conditions GTRAN simulation (southern domain).

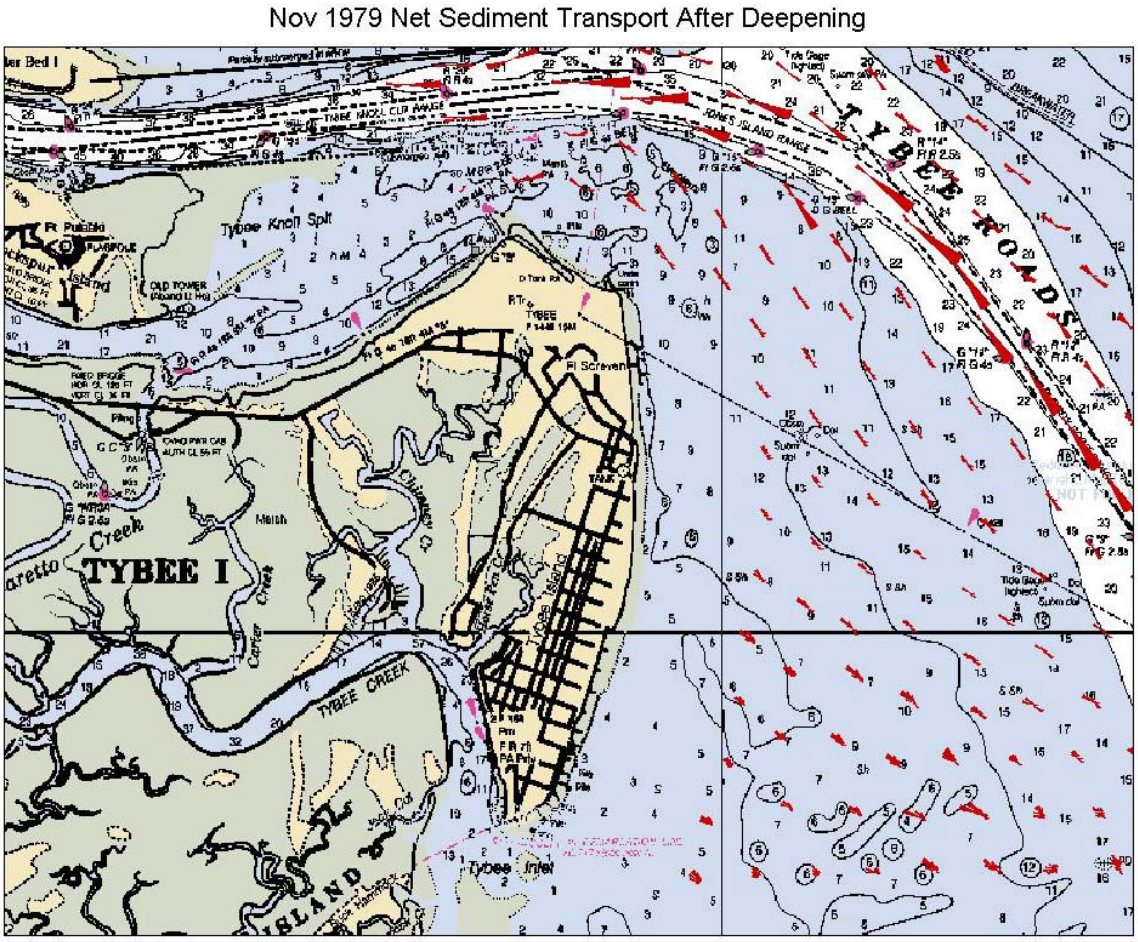

Figure 5C-6. Sediment transport rose plots for November 1979 deepened conditions GTRAN simulation (southern domain).

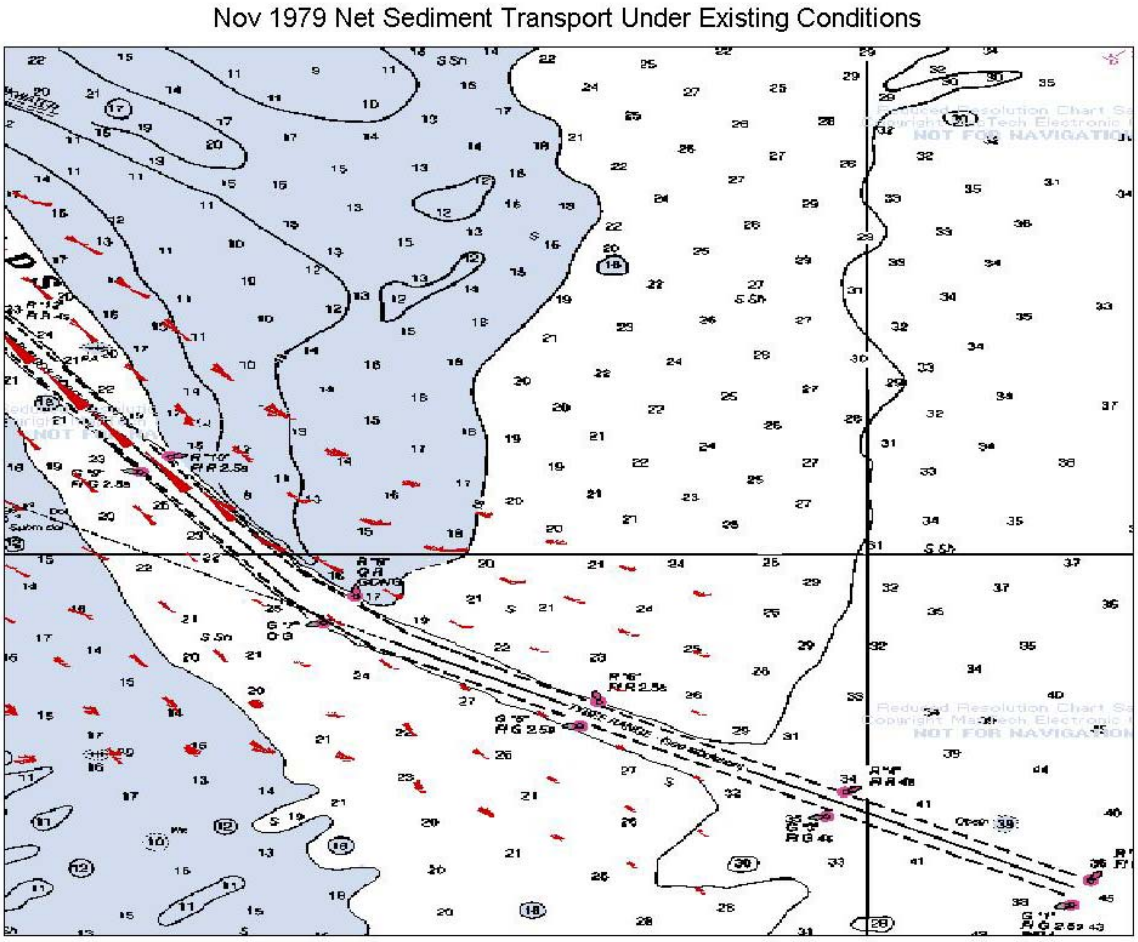

Figure 5C-7. Sediment transport rose plots for November 1979 existing conditions GTRAN simulation (southeastern domain).

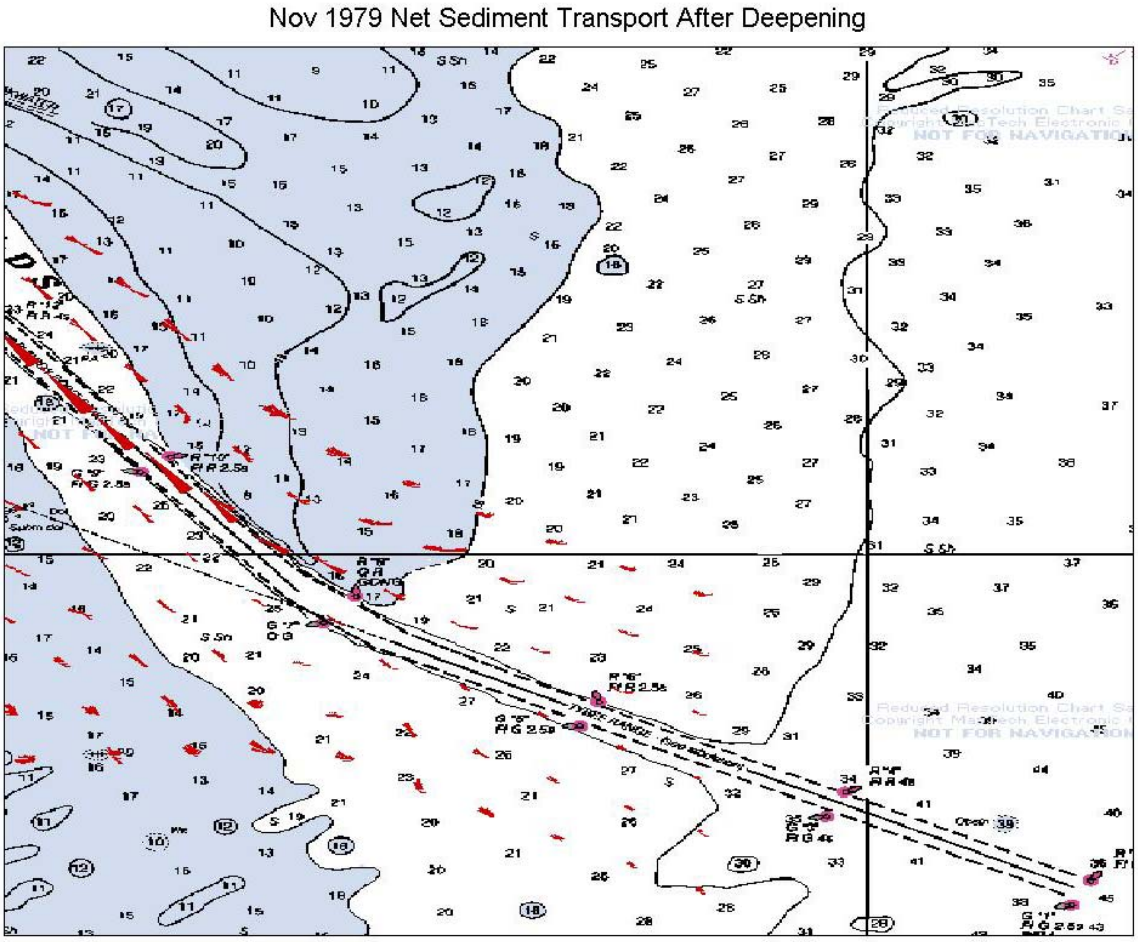

Figure 5C-8. Sediment transport rose plots for November 1979 deepened conditions GTRAN simulation (southeastern domain).

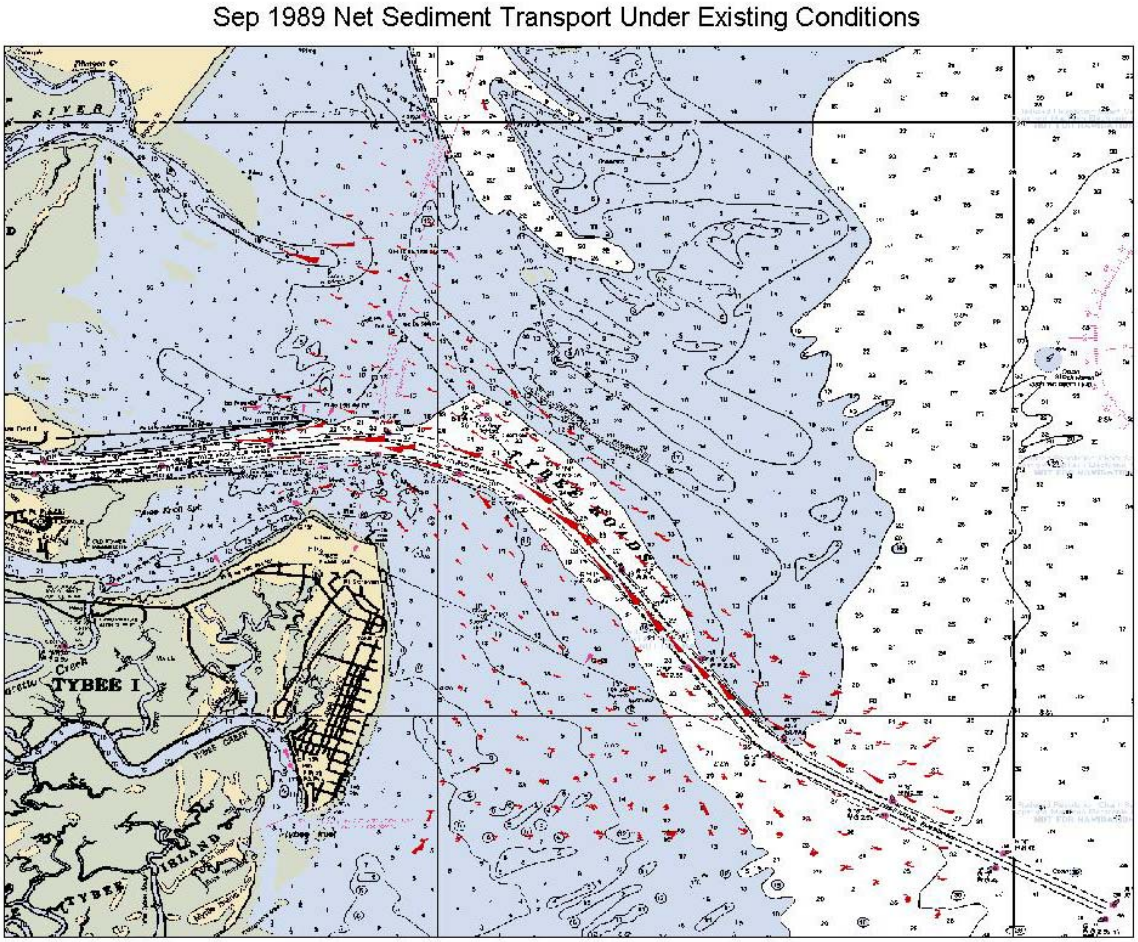

Figure 5C-9. Sediment transport rose plots for September 1989 (Hugo) existing conditions GTRAN simulation (full domain).

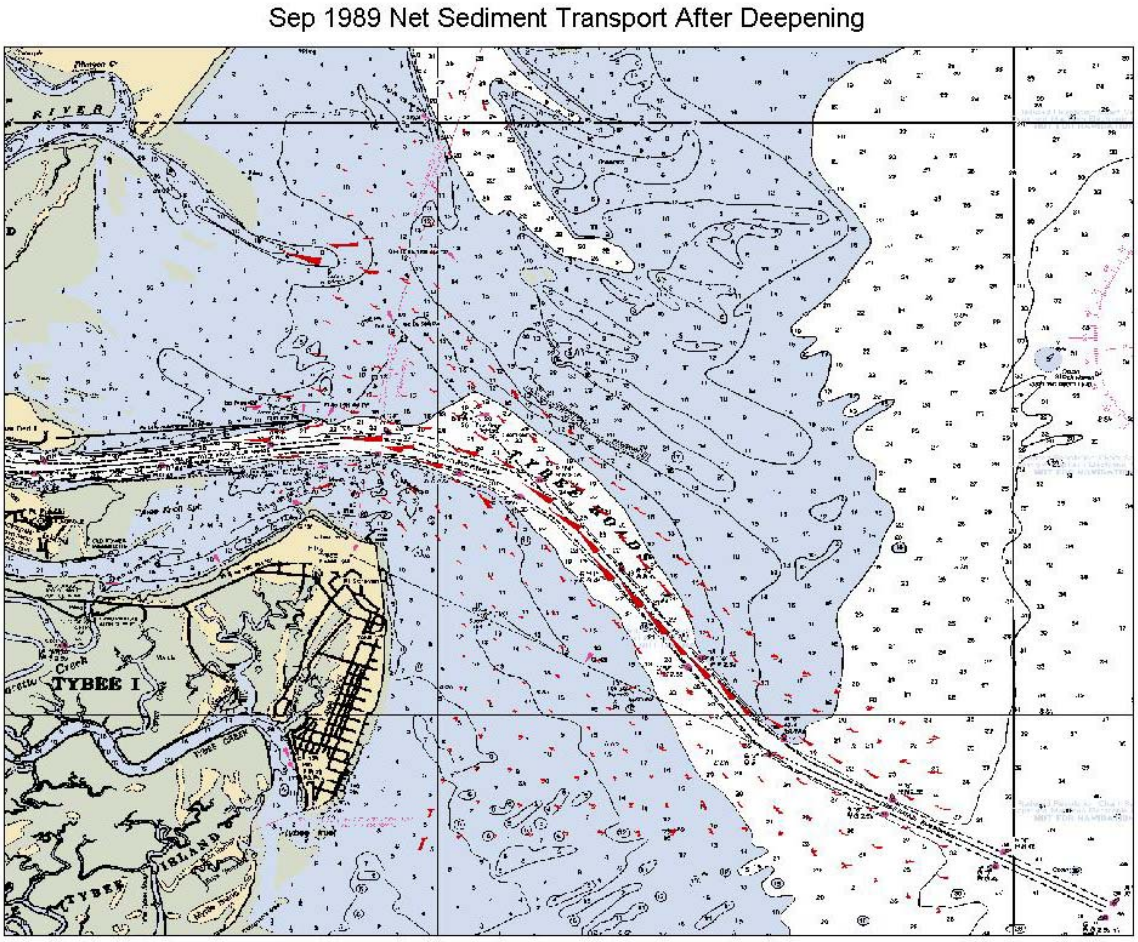

Figure 5C-10. Sediment transport rose plots for September 1989 (Hugo) deepened conditions GTRAN simulation (full domain).

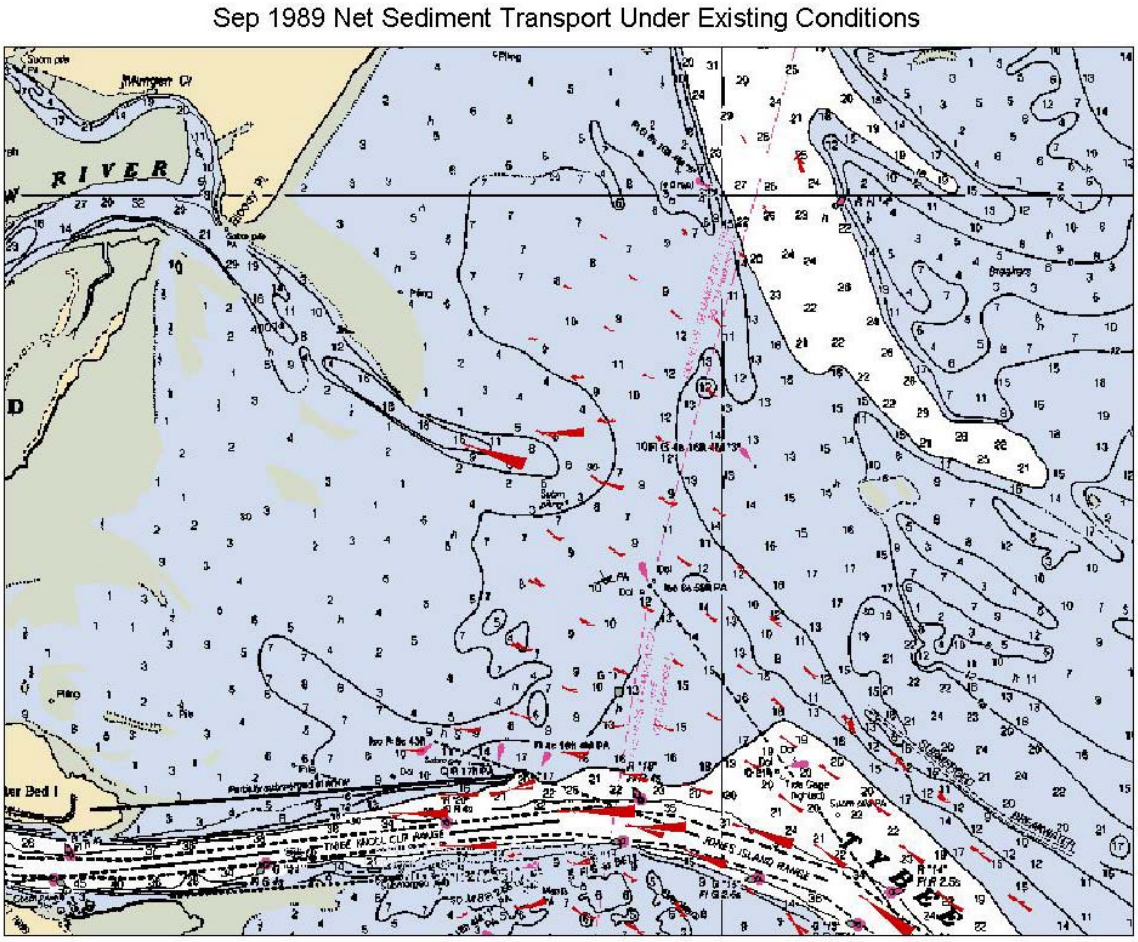

Figure 5C-11. Sediment transport rose plots for September 1989 (Hugo) existing conditions GTRAN simulation (northern domain).

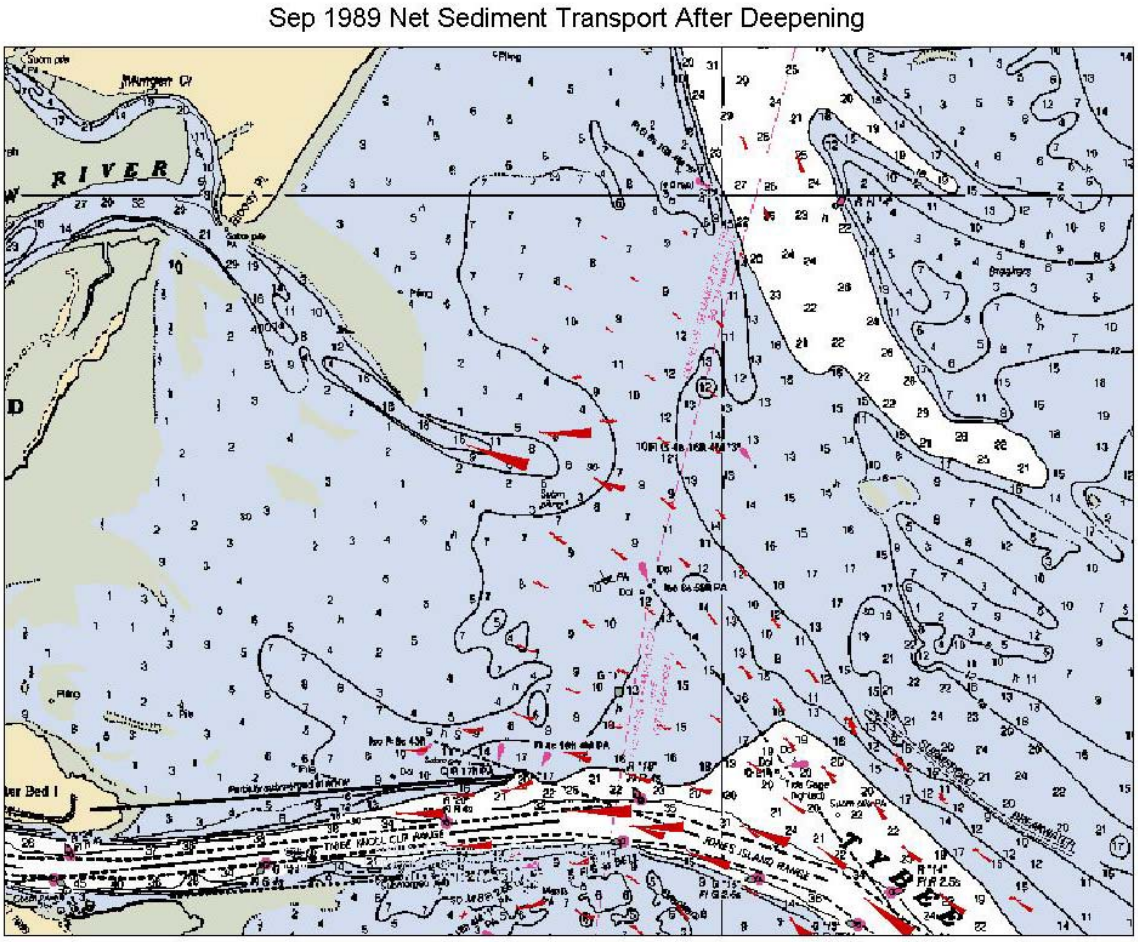

Figure 5C-12. Sediment transport rose plots for September 1989 (Hugo) deepened conditions GTRAN simulation (northern domain).

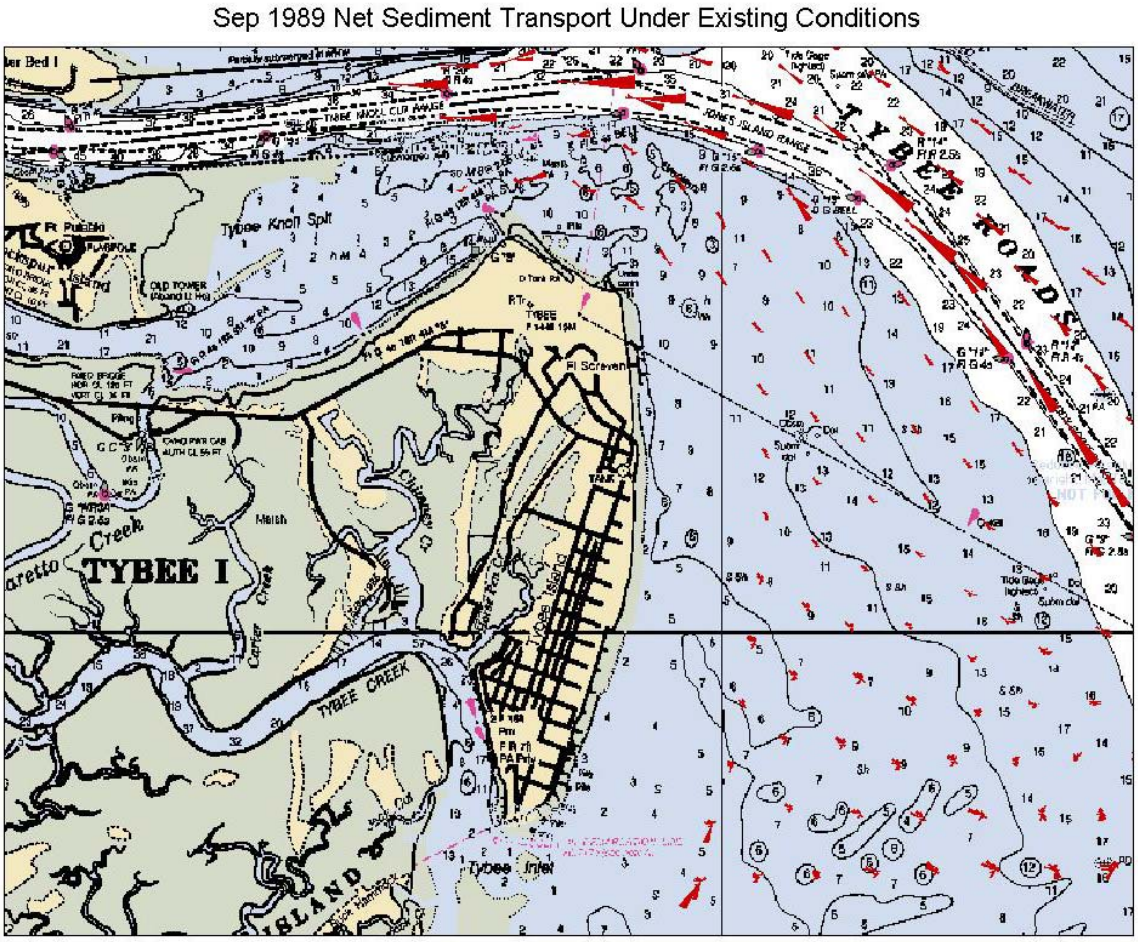

Figure 5C-13. Sediment transport rose plots for September 1989 (Hugo) existing conditions GTRAN simulation (southern domain).

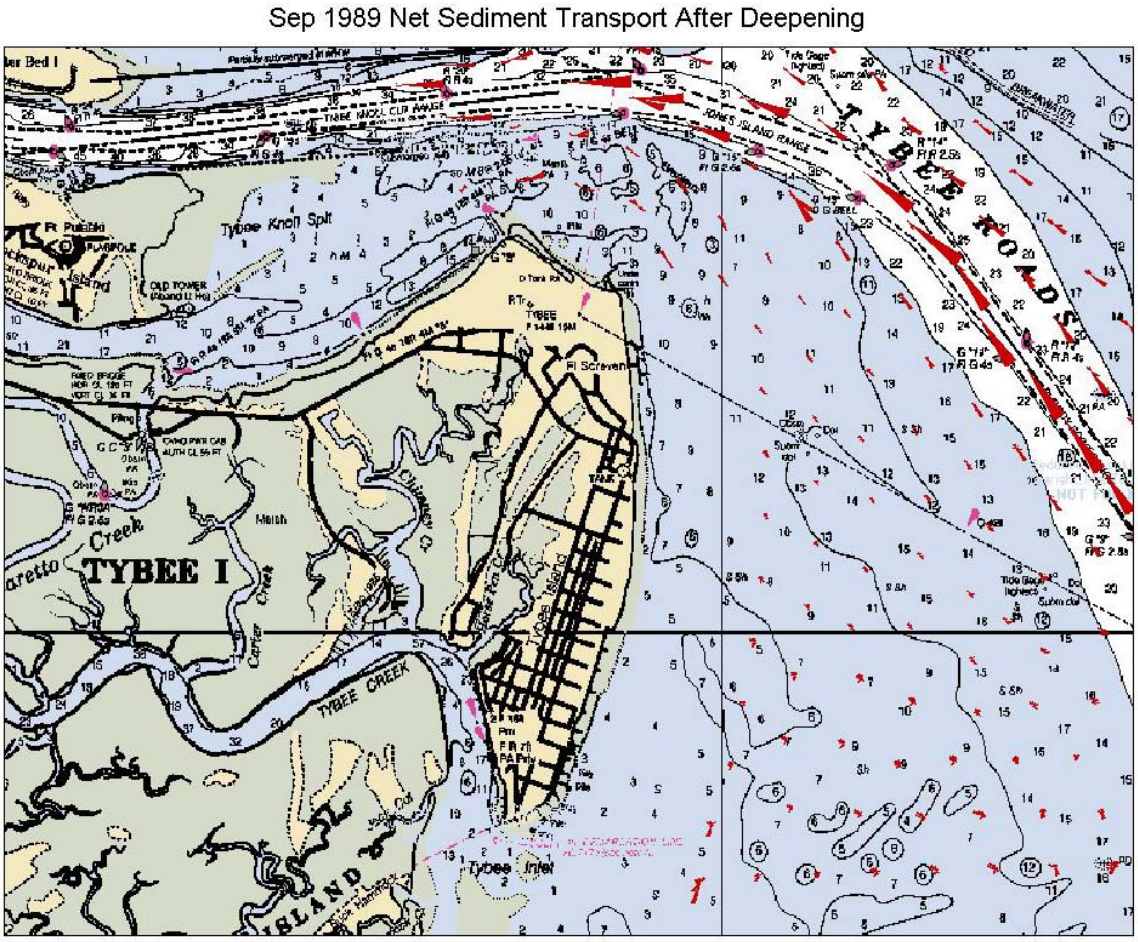

Figure 5C-14. Sediment transport rose plots for September 1989 (Hugo) deepened conditions GTRAN simulation (southern domain).

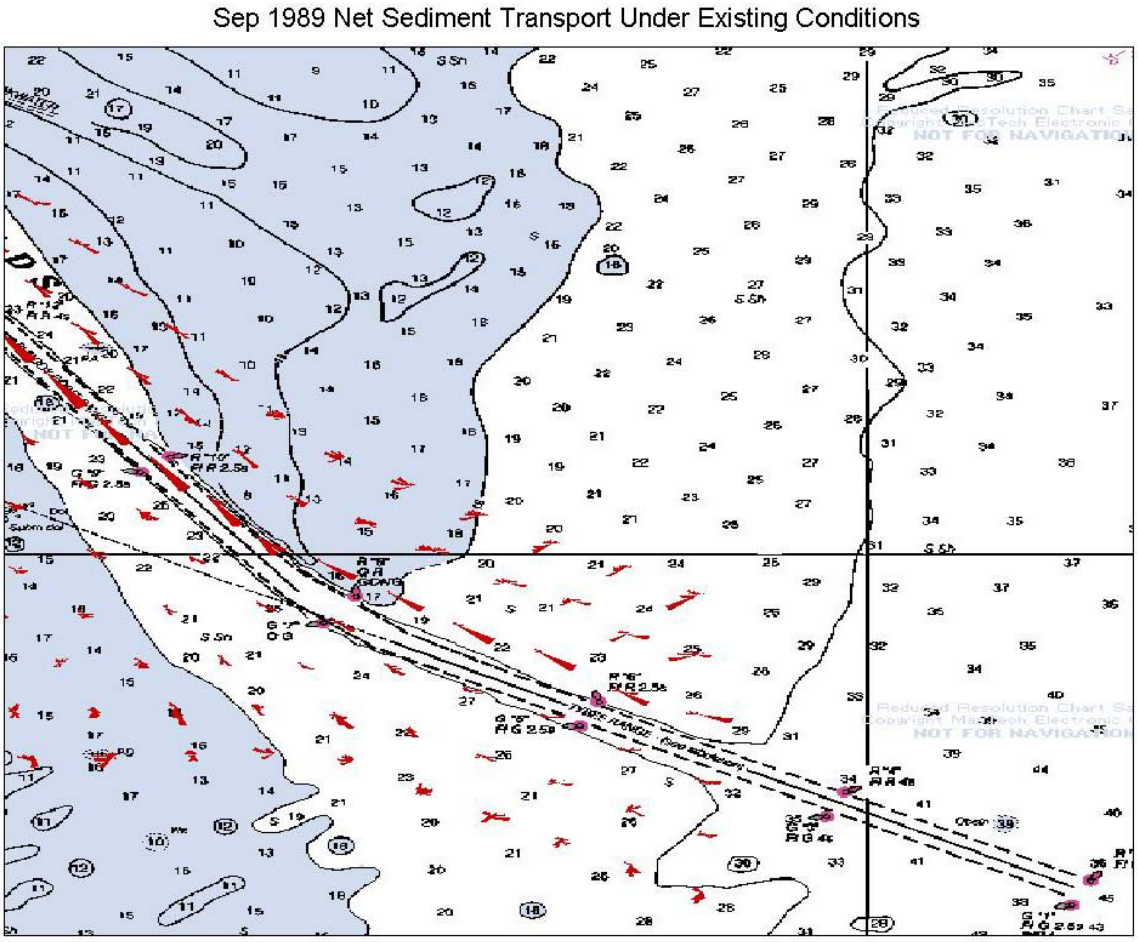

Figure 5C-15. Sediment transport rose plots for September 1989 (Hugo) existing conditions GTRAN simulation (southeastern domain).

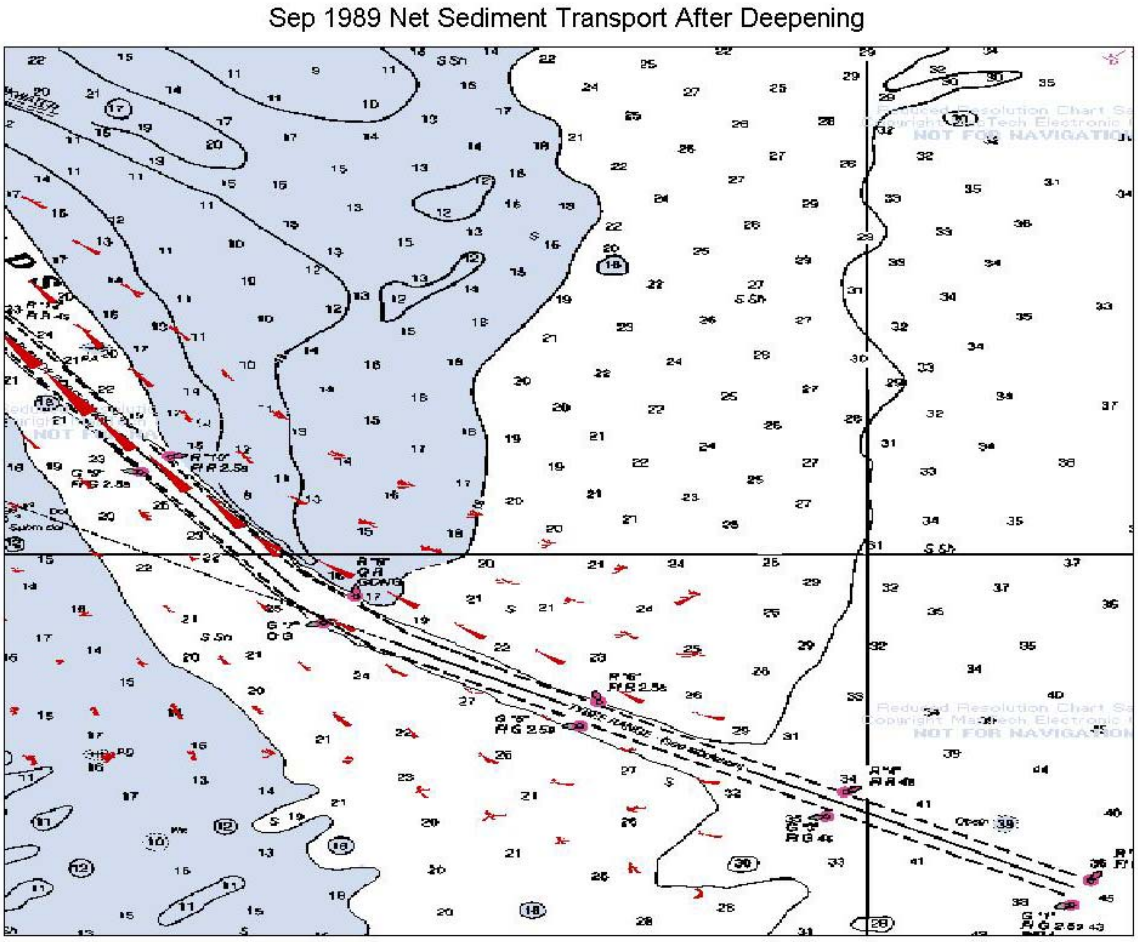

Figure 5C-16. Sediment transport rose plots for September 1989 (Hugo) deepened conditions GTRAN simulation (southeastern domain).

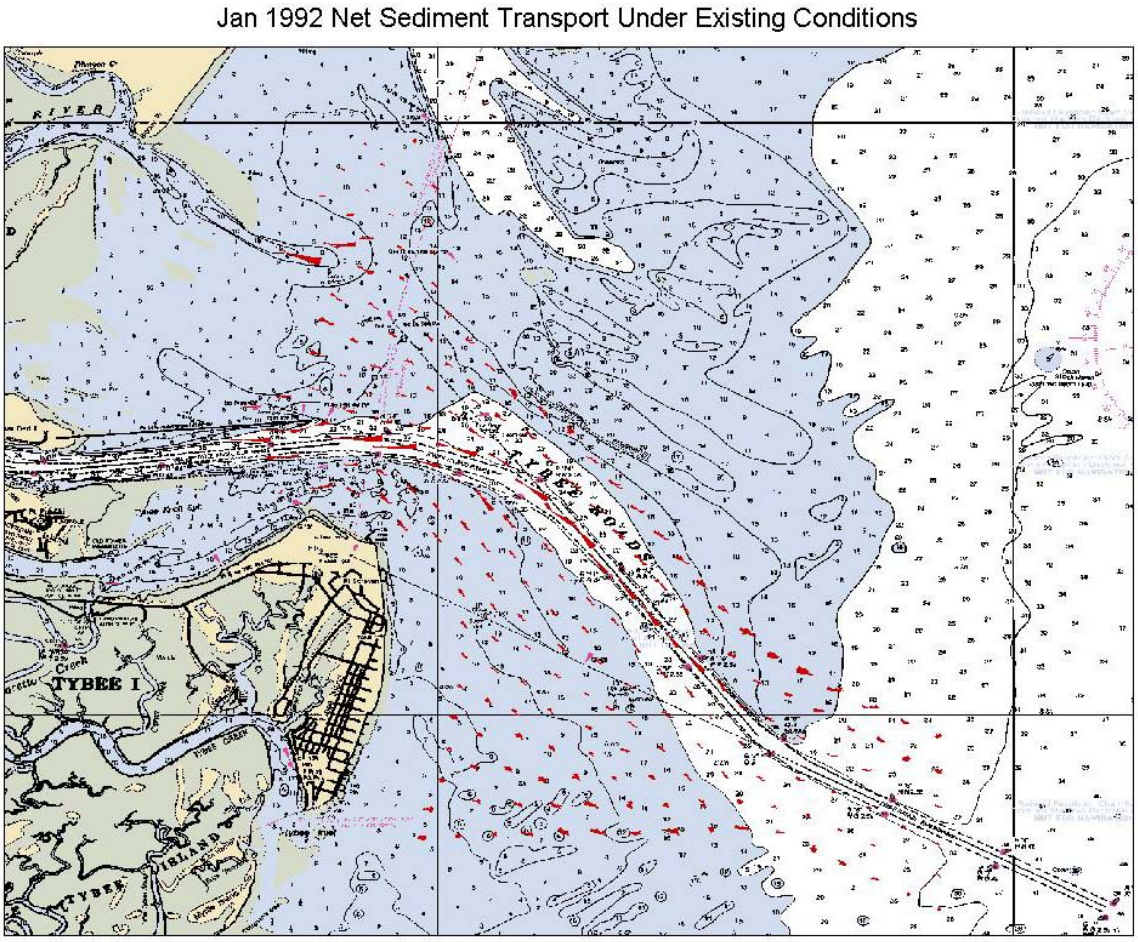

Figure 5C-17. Sediment transport rose plots for January 1992 existing conditions GTRAN simulation (full domain).

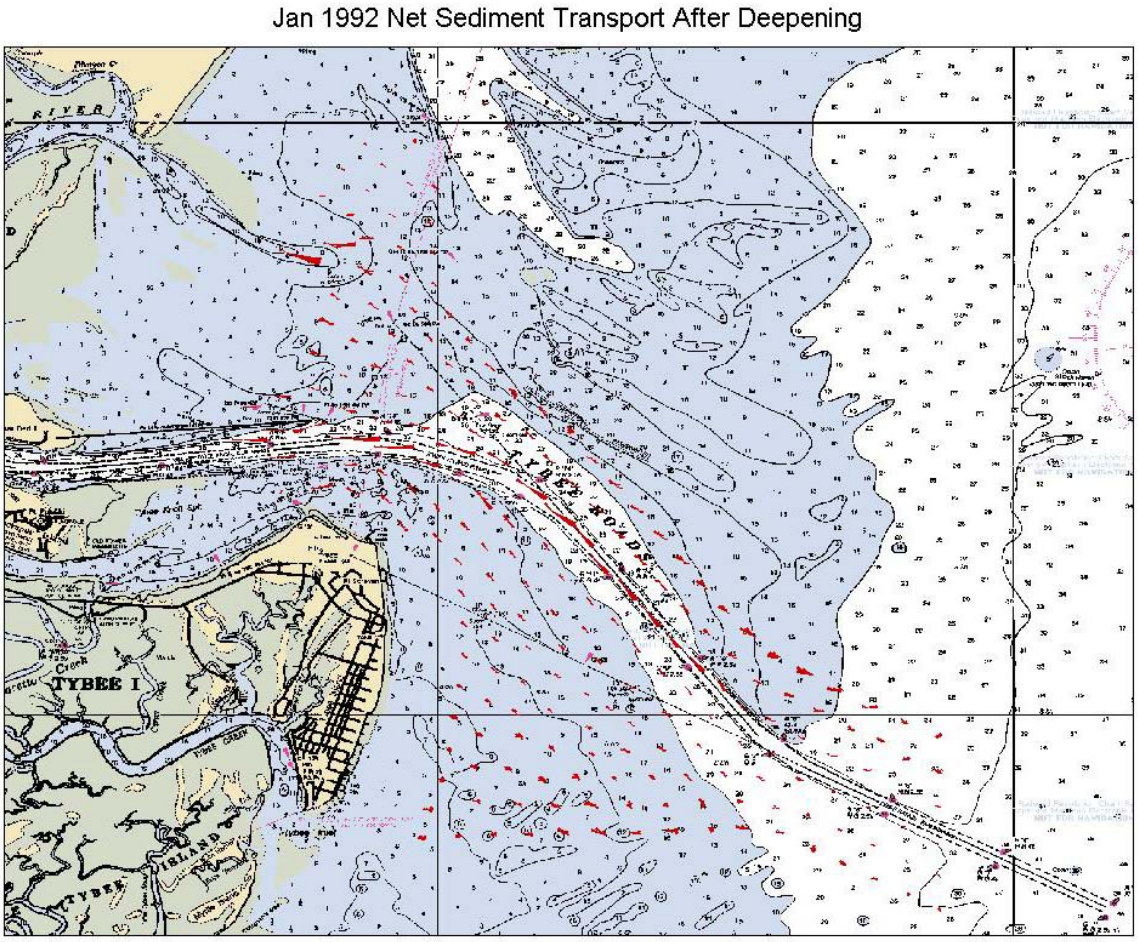

Figure 5C-18. Sediment transport rose plots for January 1992 deepened conditions GTRAN simulation (full domain).

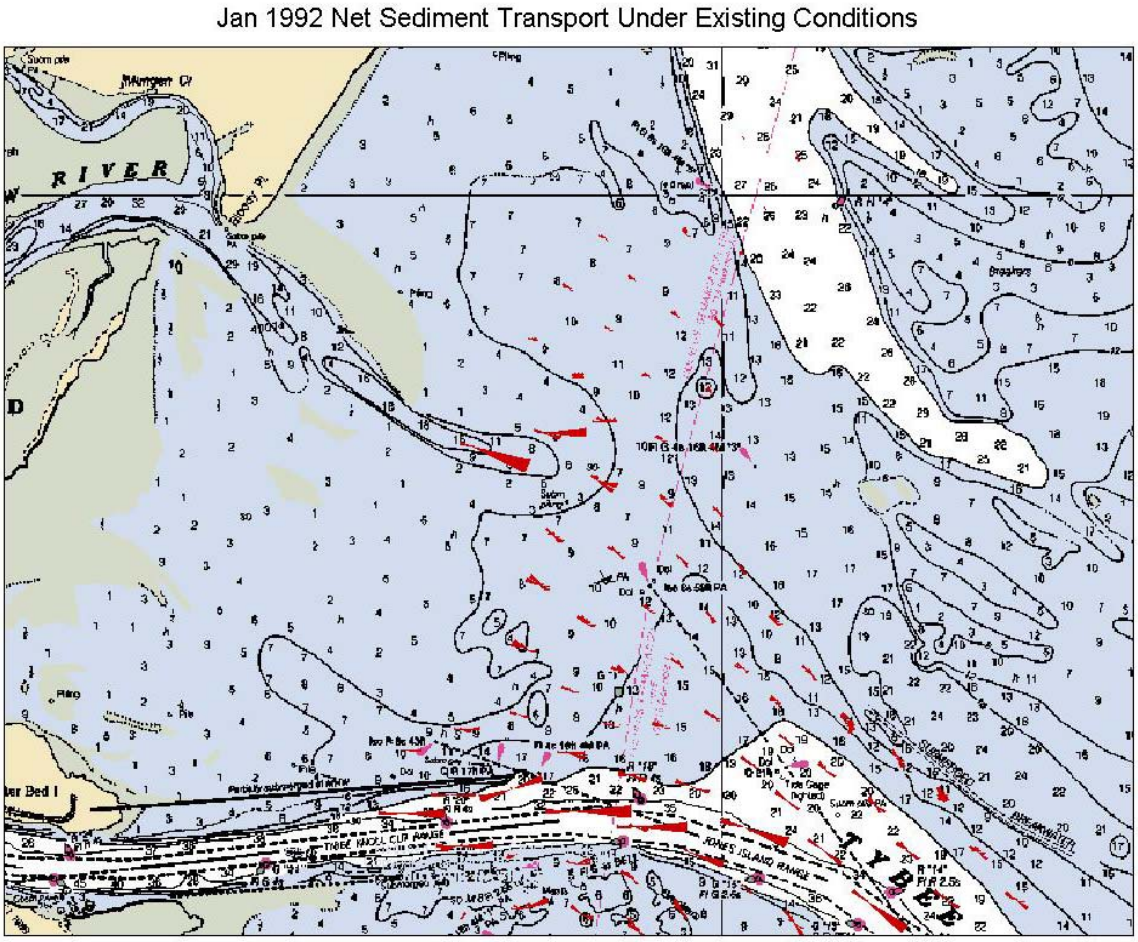

Figure 5C-19. Sediment transport rose plots for January 1992 existing conditions GTRAN simulation (northern domain).

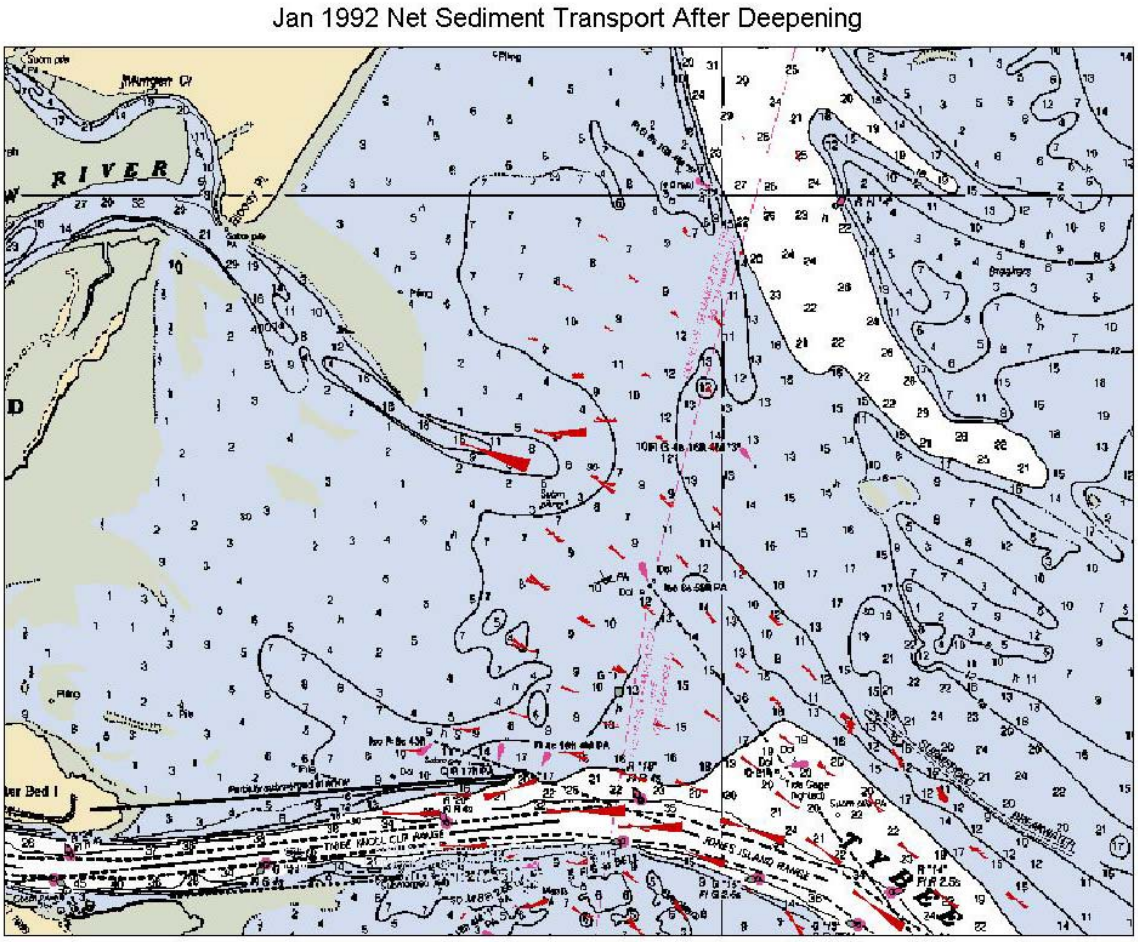

Figure 5C-20. Sediment transport rose plots for January 1992 deepened conditions GTRAN simulation (northern domain).

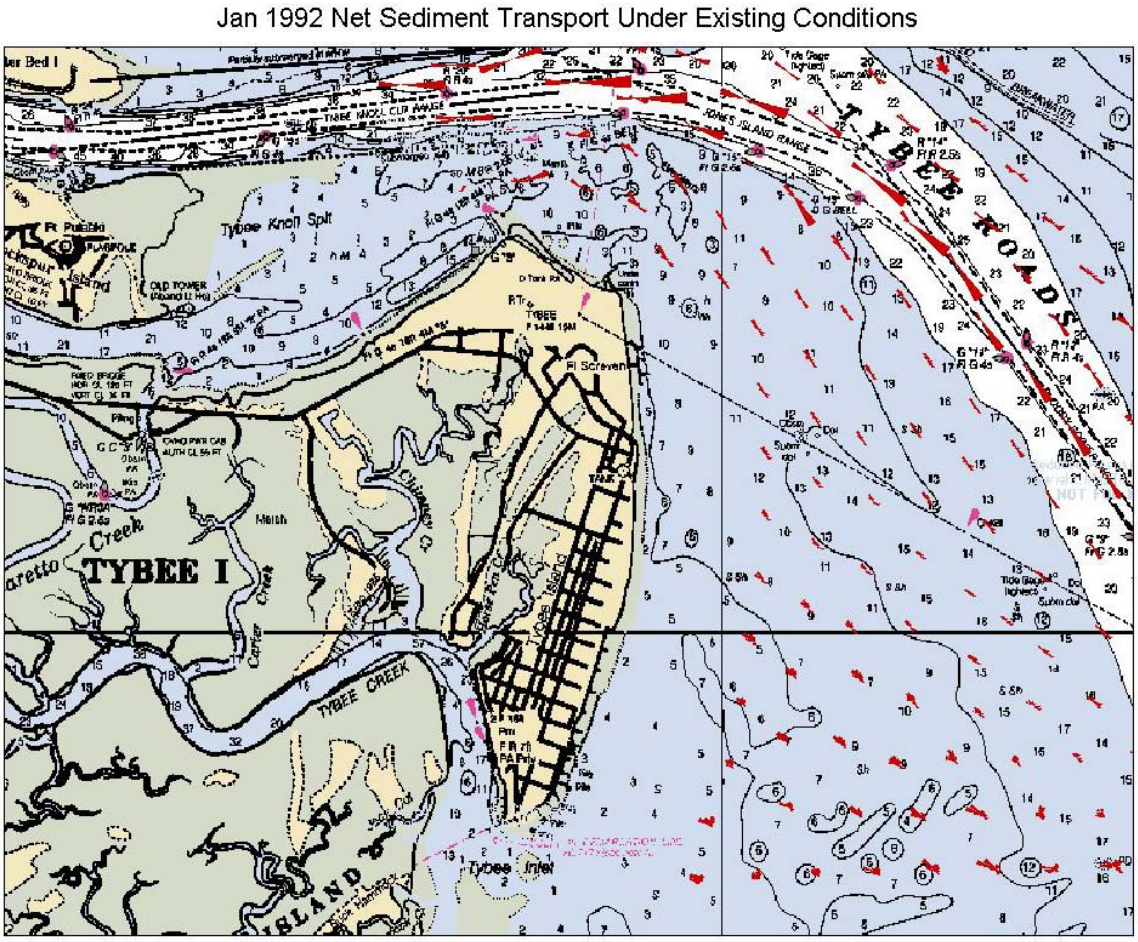

Figure 5C-21. Sediment transport rose plots for January 1992 existing conditions GTRAN simulation (southern domain).

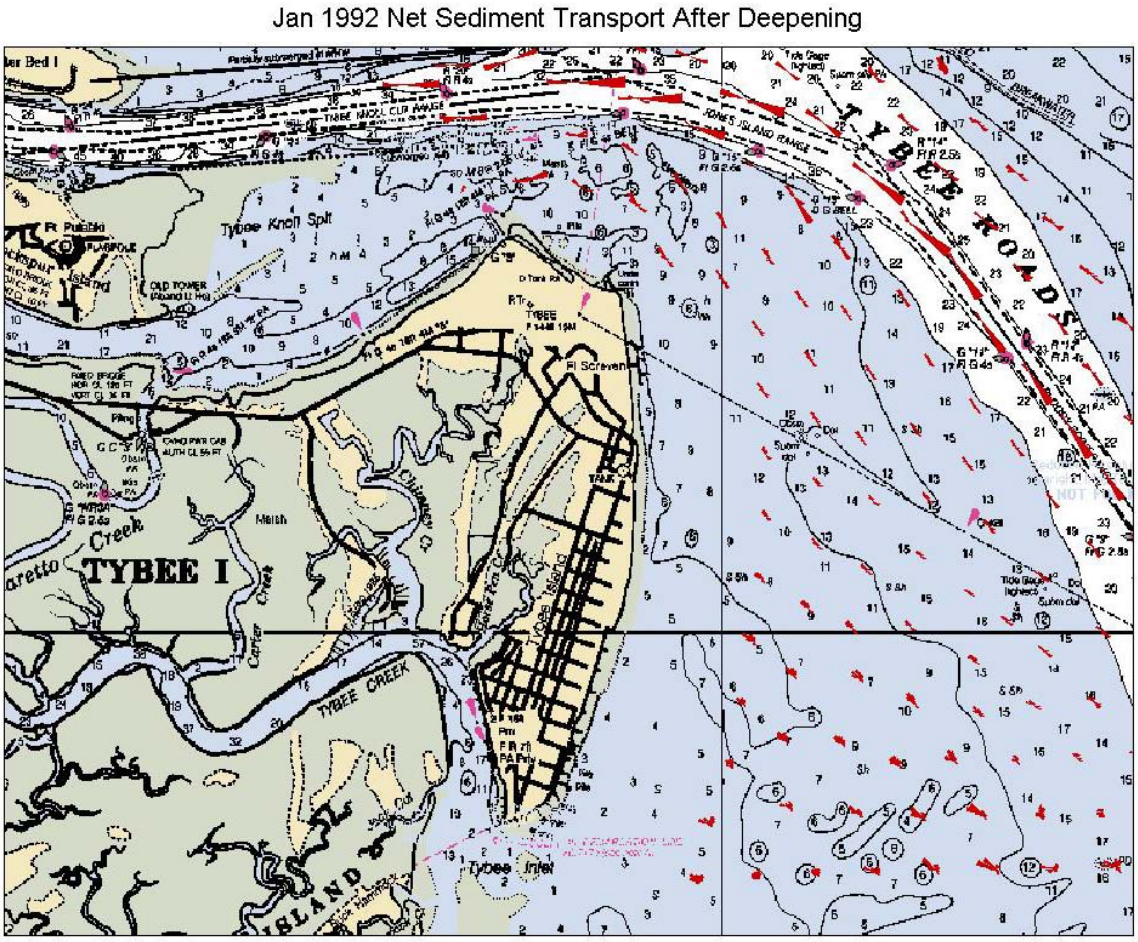

Figure 5C-22. Sediment transport rose plots for January 1992 deepened conditions GTRAN simulation (southern domain).

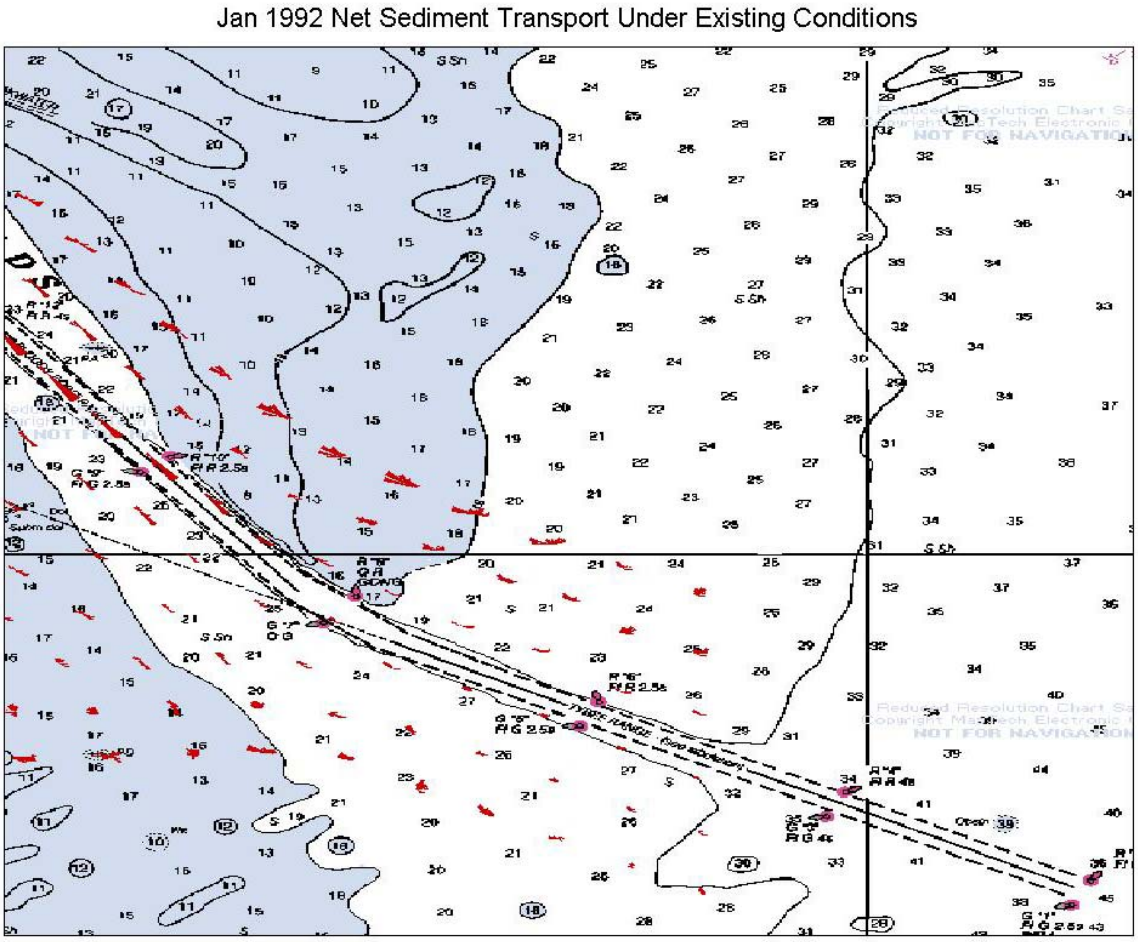

Figure 5C-23. Sediment transport rose plots for January 1992 existing conditions GTRAN simulation (southeastern domain).

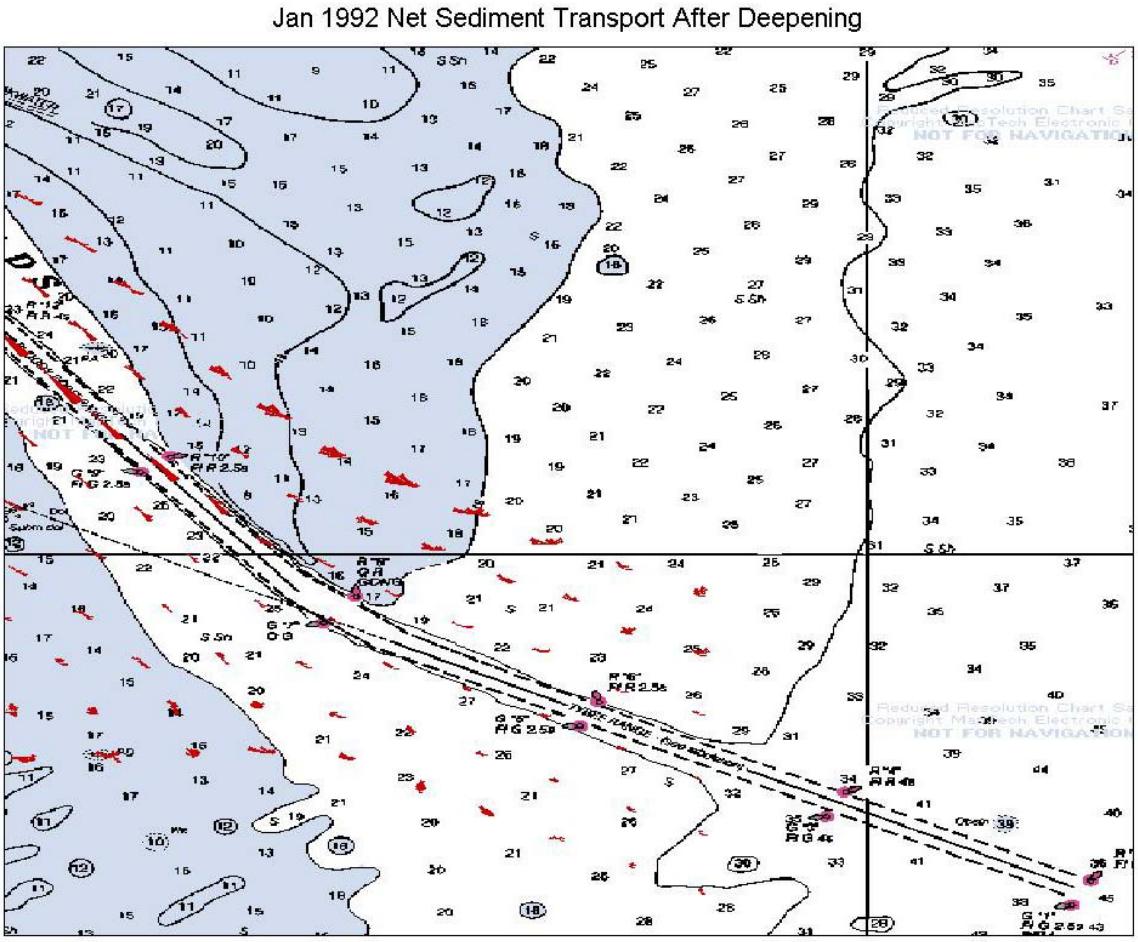

Figure 5C-24. Sediment transport rose plots for January 1992 deepened conditions GTRAN simulation (southeastern domain).

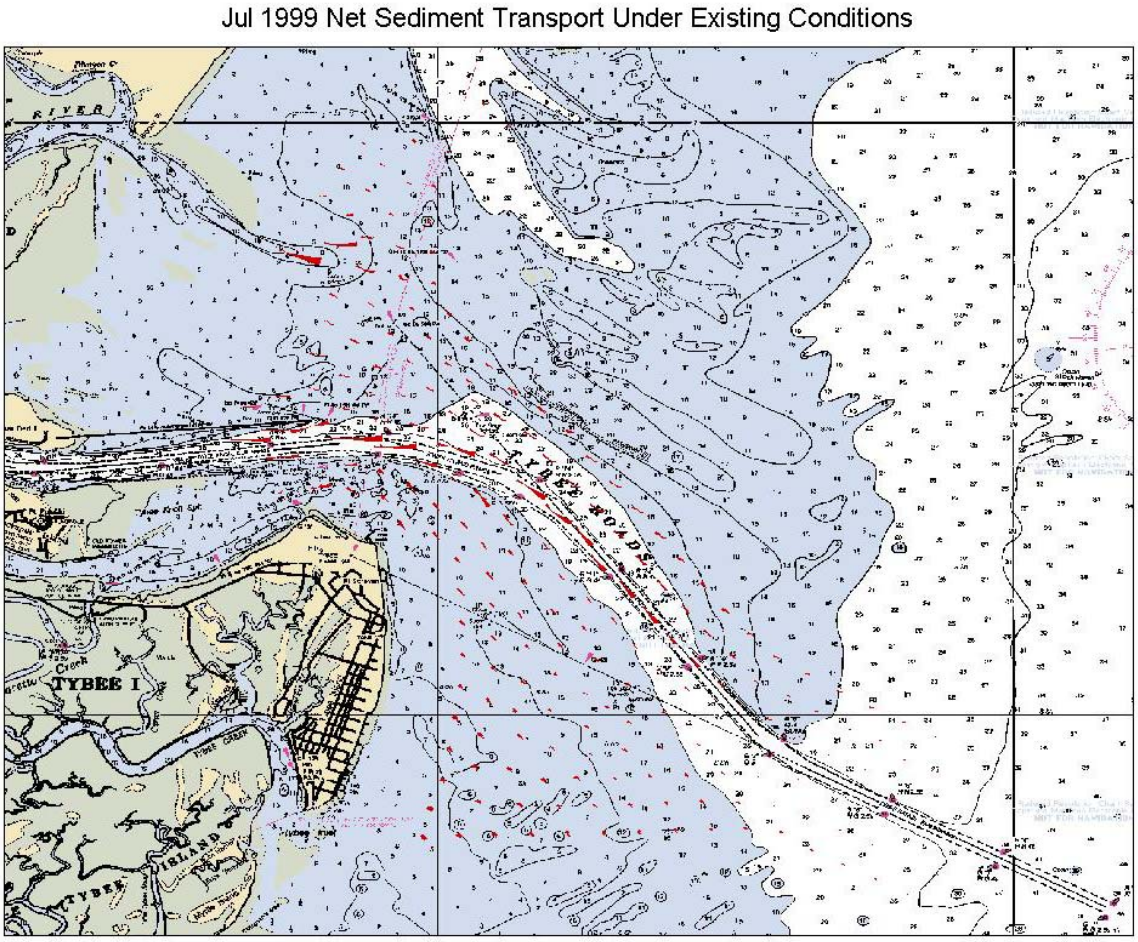

Figure 5C-25. Sediment transport rose plots for July 1999 existing conditions GTRAN simulation (full domain).

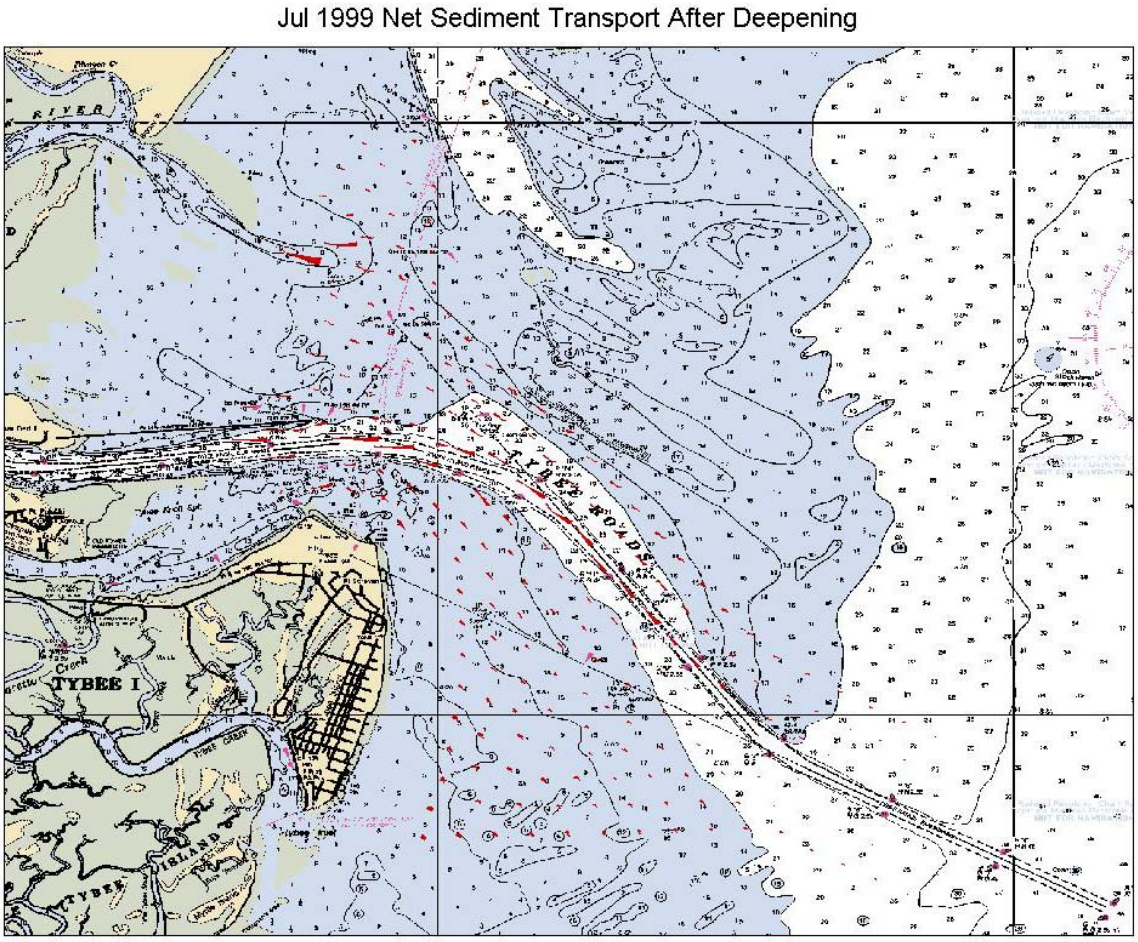

Figure 5C-26. Sediment transport rose plots for July 1999 deepened conditions GTRAN simulation (full domain).

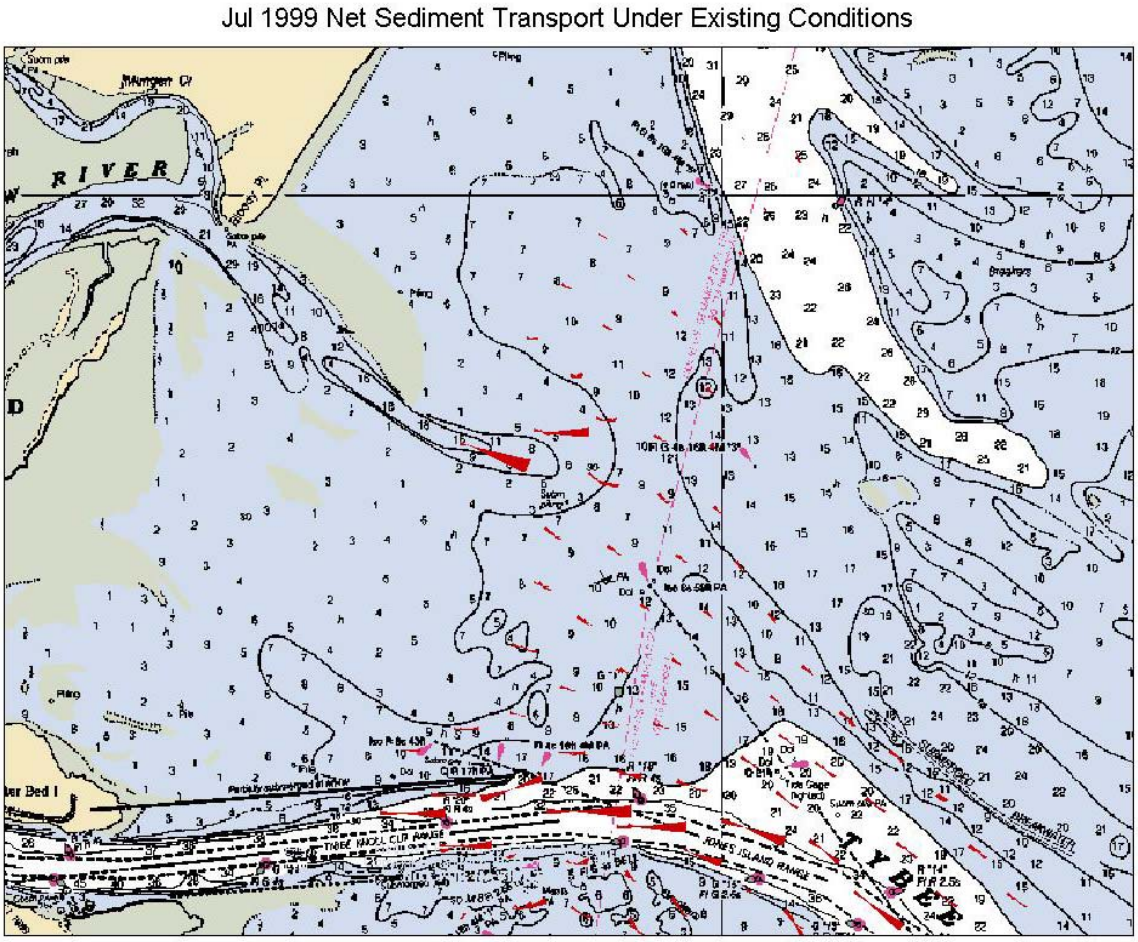

Figure 5C-27. Sediment transport rose plots for July 1999 existing conditions GTRAN simulation (northern domain).

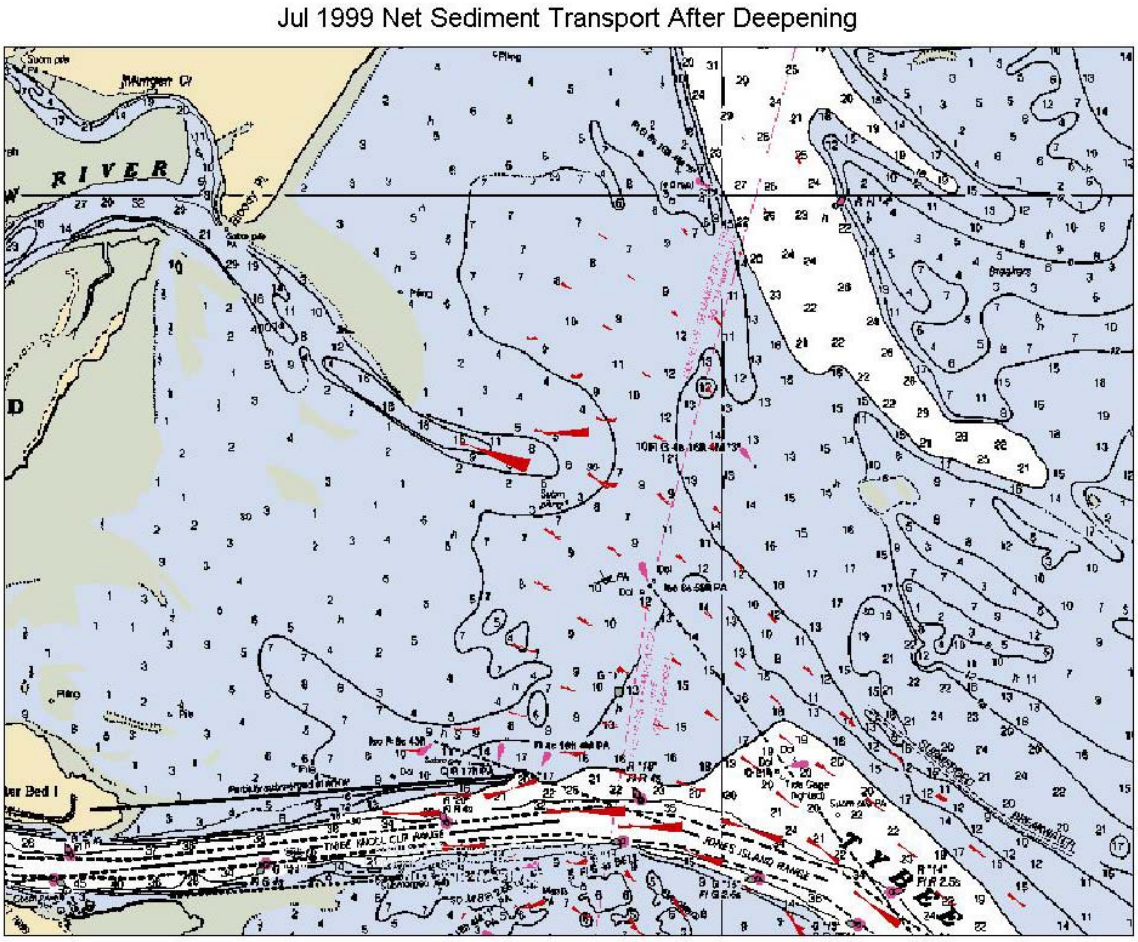

Figure 5C-28. Sediment transport rose plots for July 1999 deepened conditions GTRAN simulation (northern domain).

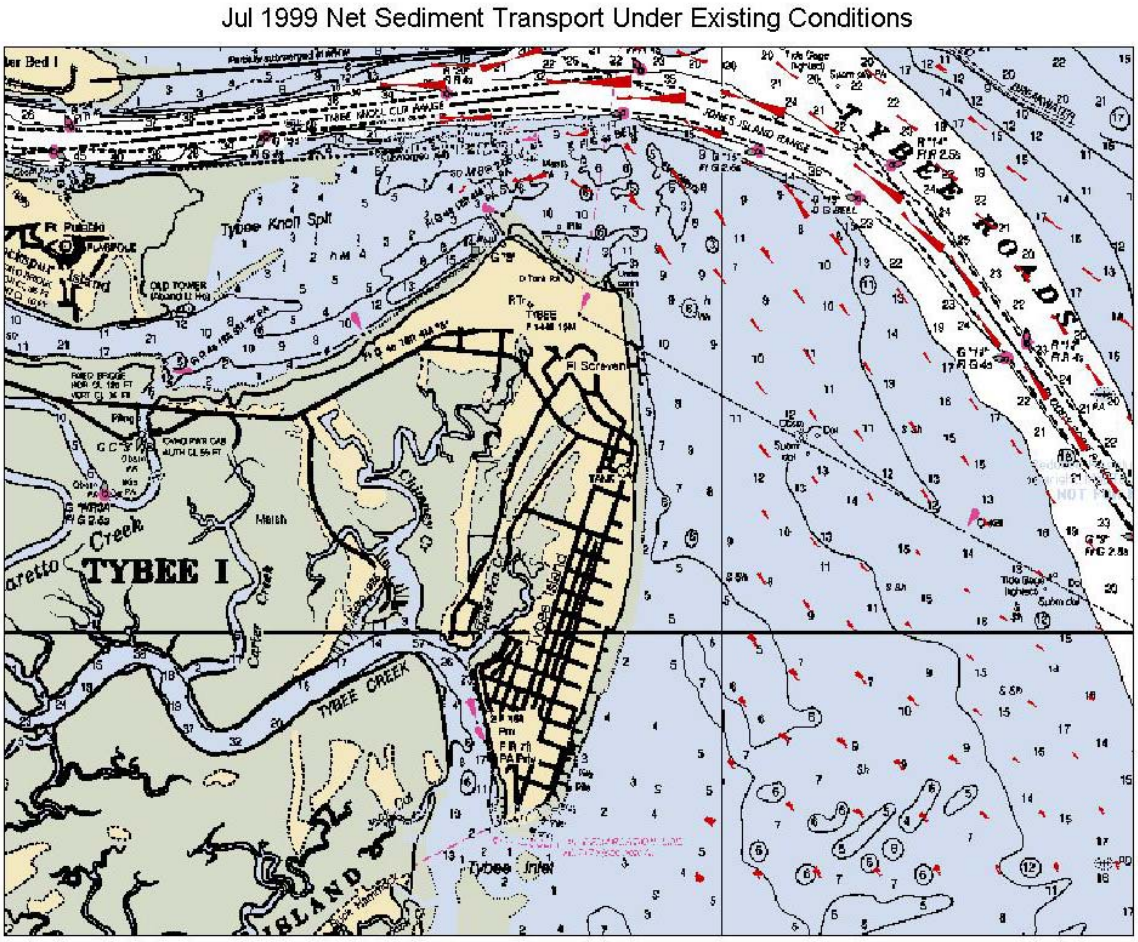

Figure 5C-29. Sediment transport rose plots for July 1999 existing conditions GTRAN simulation (southern domain).

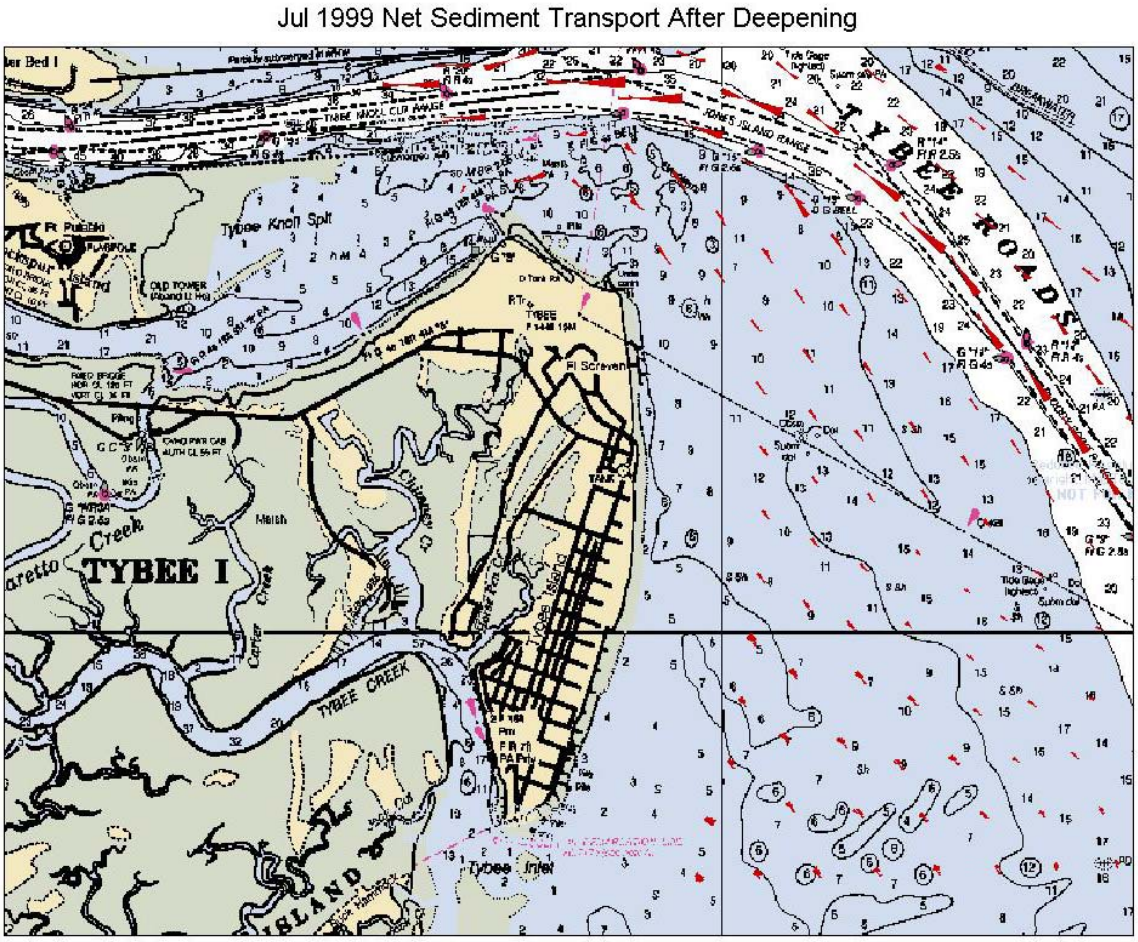

Figure 5C-30. Sediment transport rose plots for July 1999 deepened conditions GTRAN simulation (southern domain).

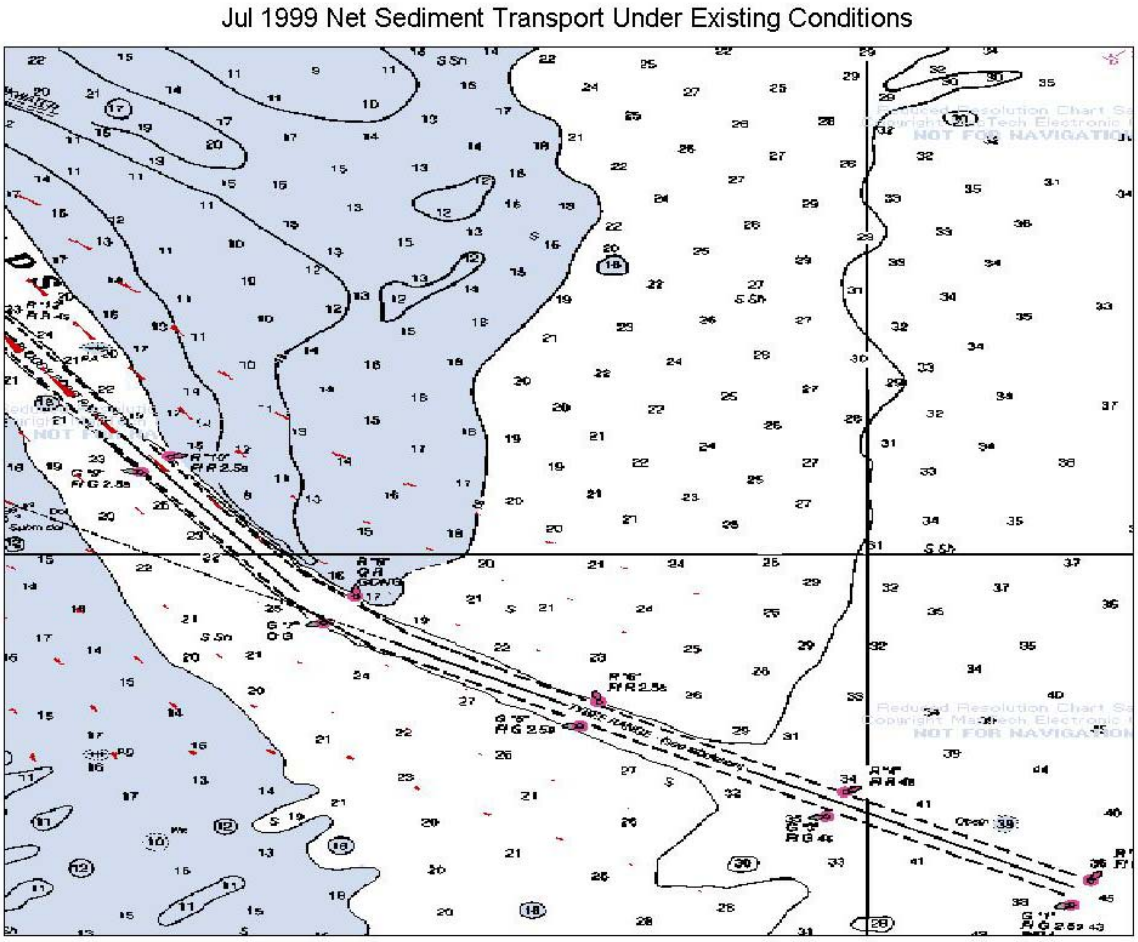

Figure 5C-31. Sediment transport rose plots for July 1999 existing conditions GTRAN simulation (southeastern domain).

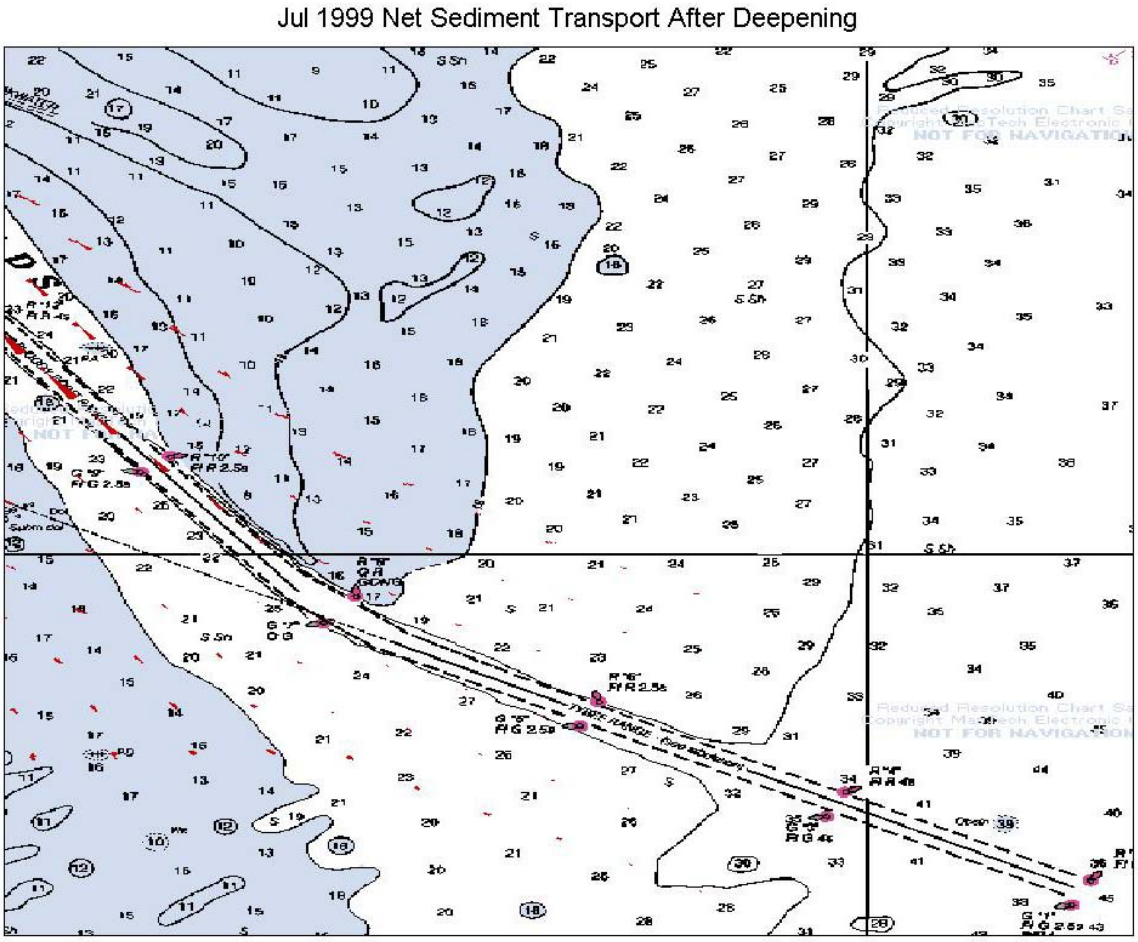

Figure 5C-32. Sediment transport rose plots for July 1999 deepened conditions GTRAN simulation (southeastern domain).

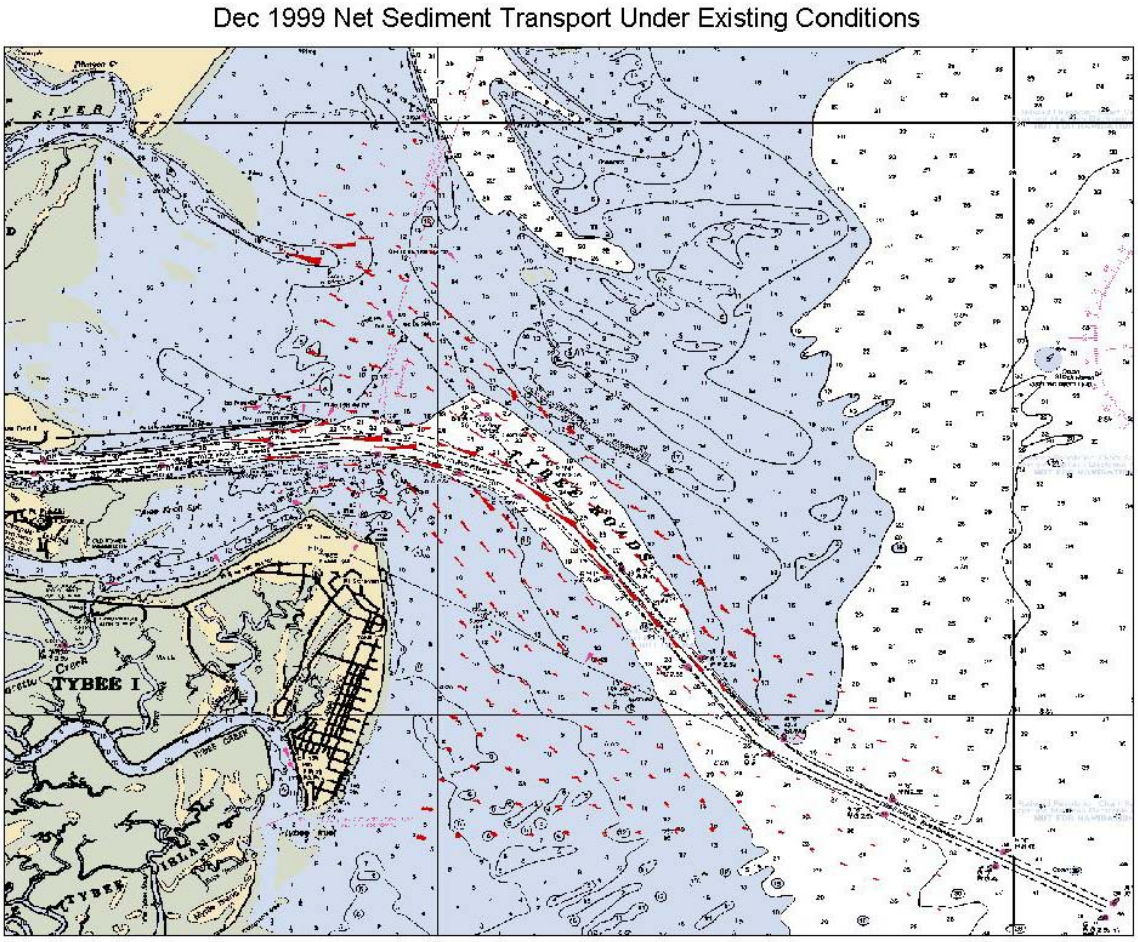

Figure 5C-33. Sediment transport rose plots for December 1999 existing conditions GTRAN simulation (full domain).

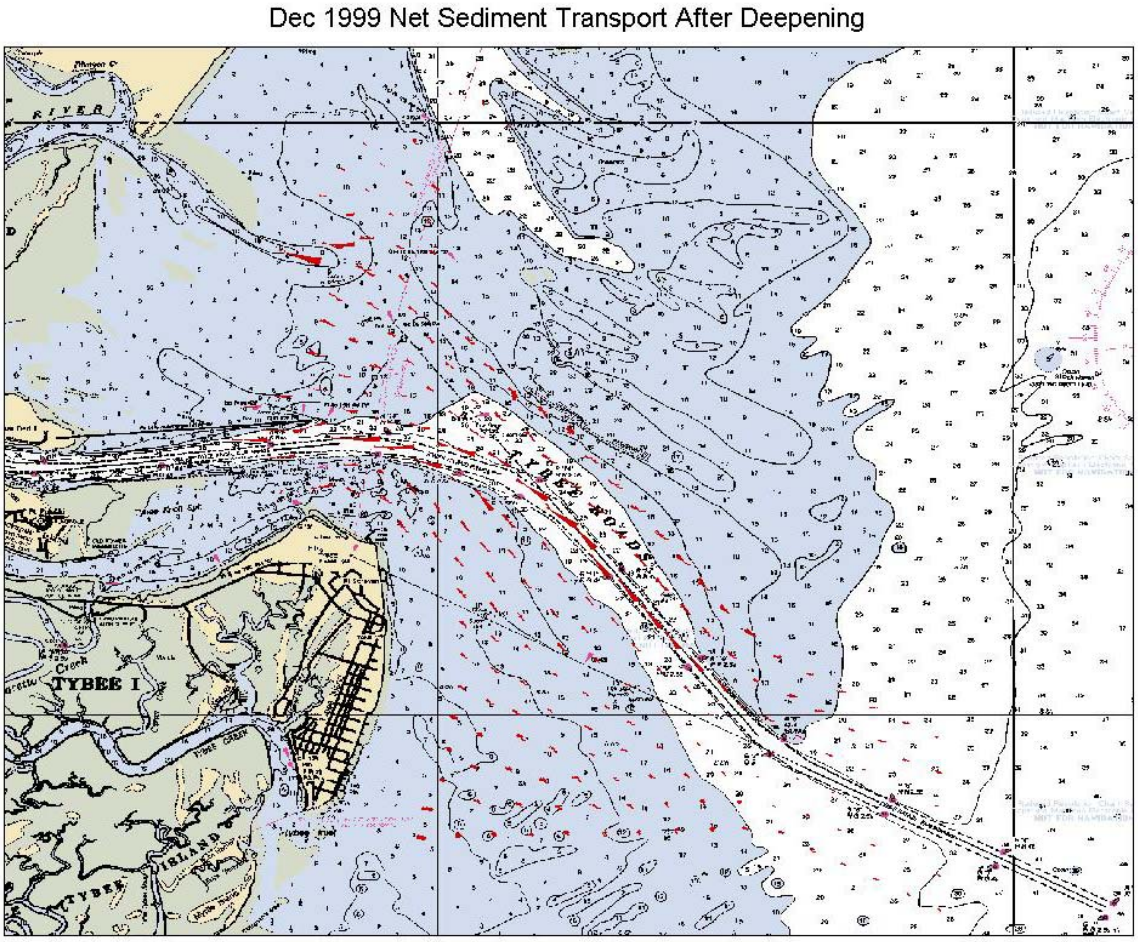

Figure 5C-34. Sediment transport rose plots for December 1999 deepened conditions GTRAN simulation (full domain).

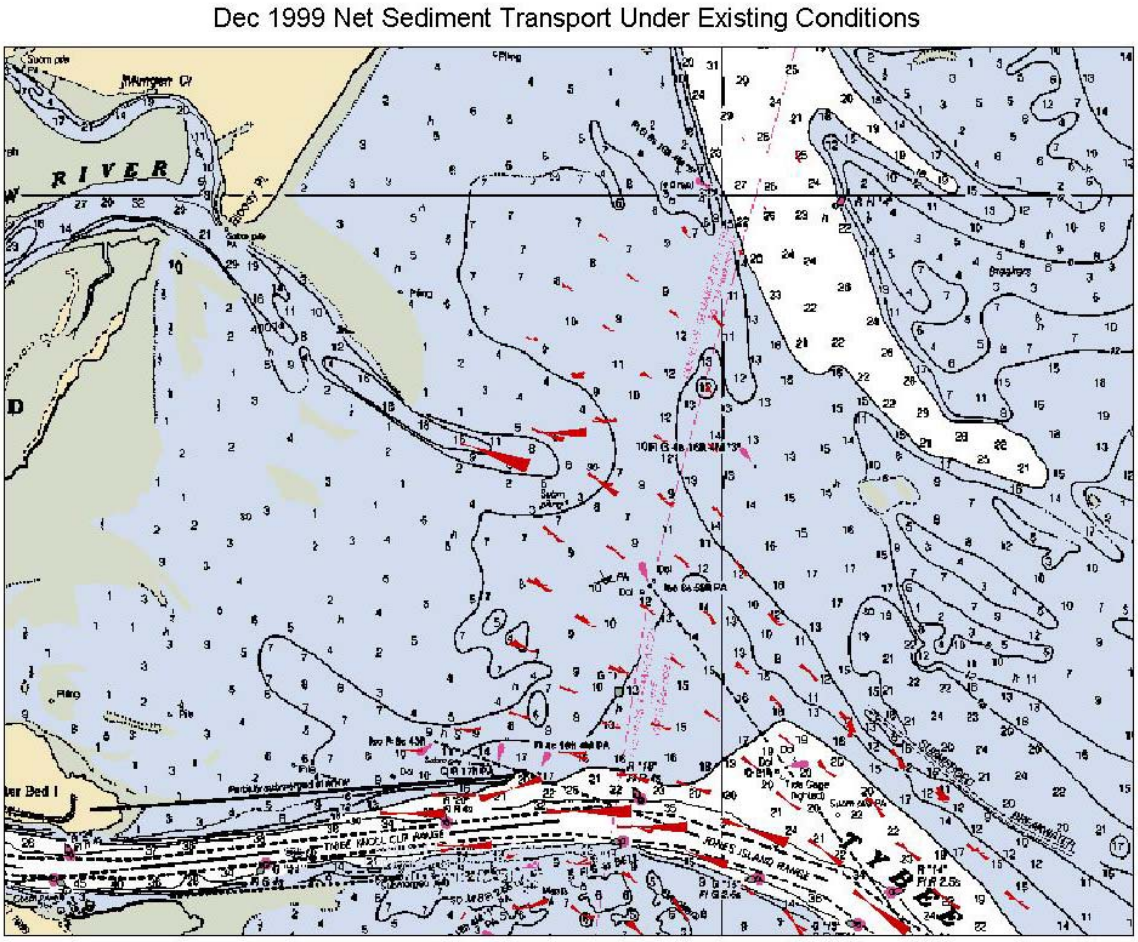

Figure 5C-35. Sediment transport rose plots for December 1999 existing conditions GTRAN simulation (northern domain).

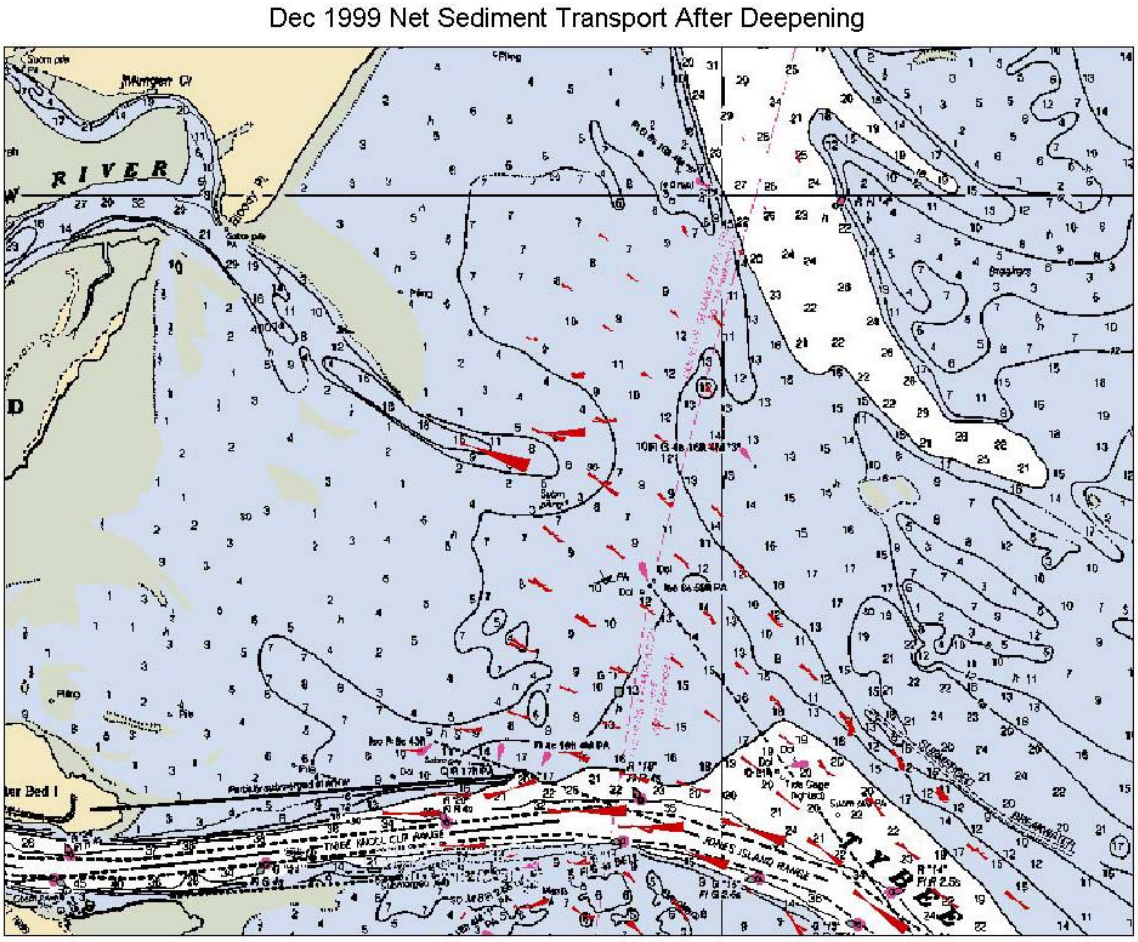

Figure 5C-36. Sediment transport rose plots for December 1999 deepened conditions GTRAN simulation (northern domain).

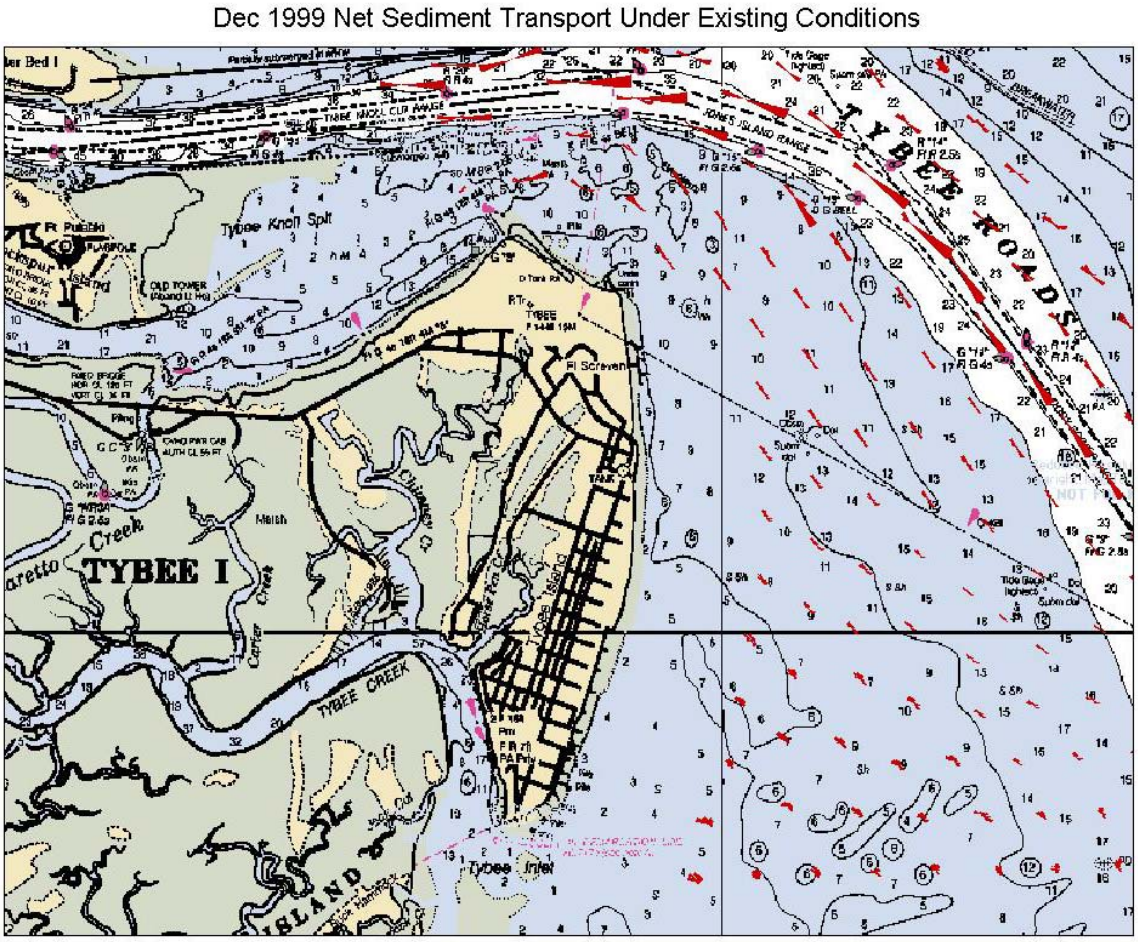

Figure 5C-37. Sediment transport rose plots for December 1999 existing conditions GTRAN simulation (southern domain).

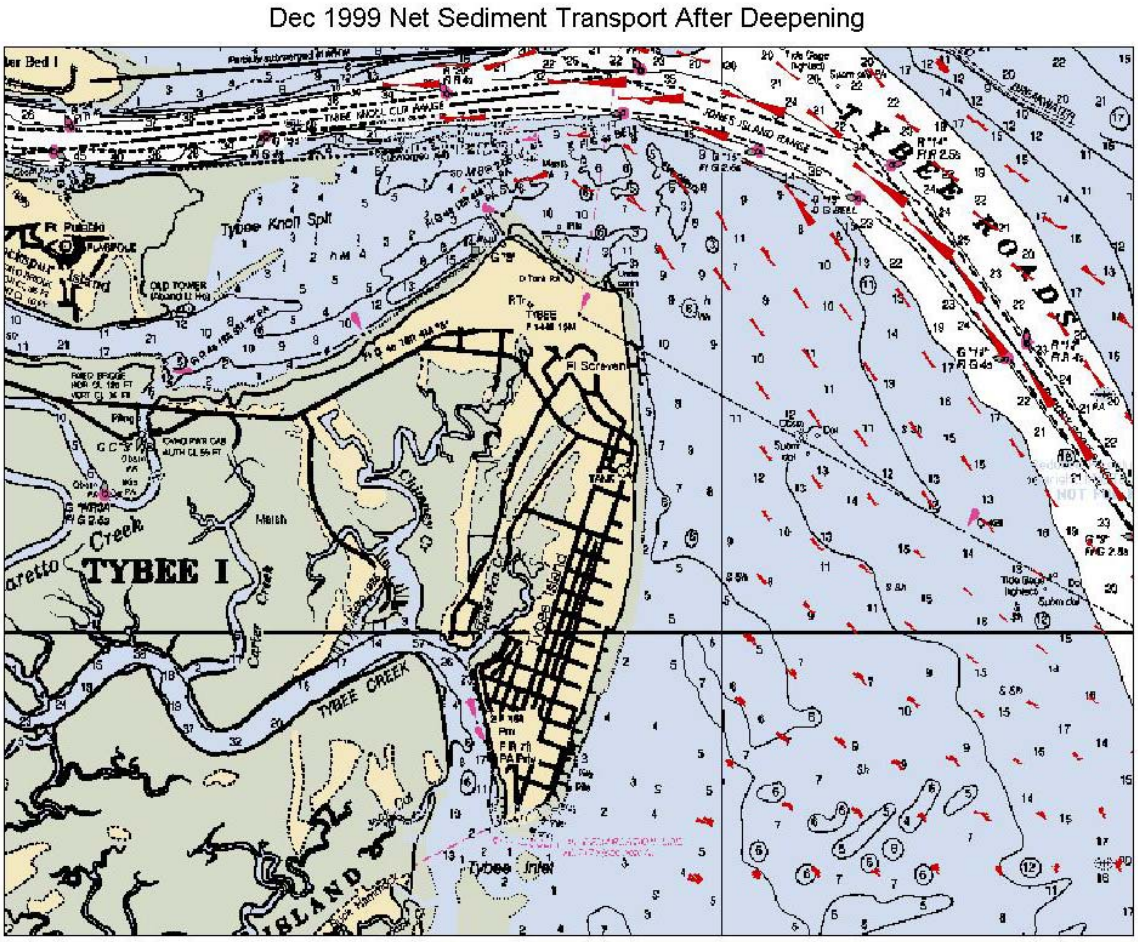

Figure 5C-38. Sediment transport rose plots for December 1999 deepened conditions GTRAN simulation (southern domain).

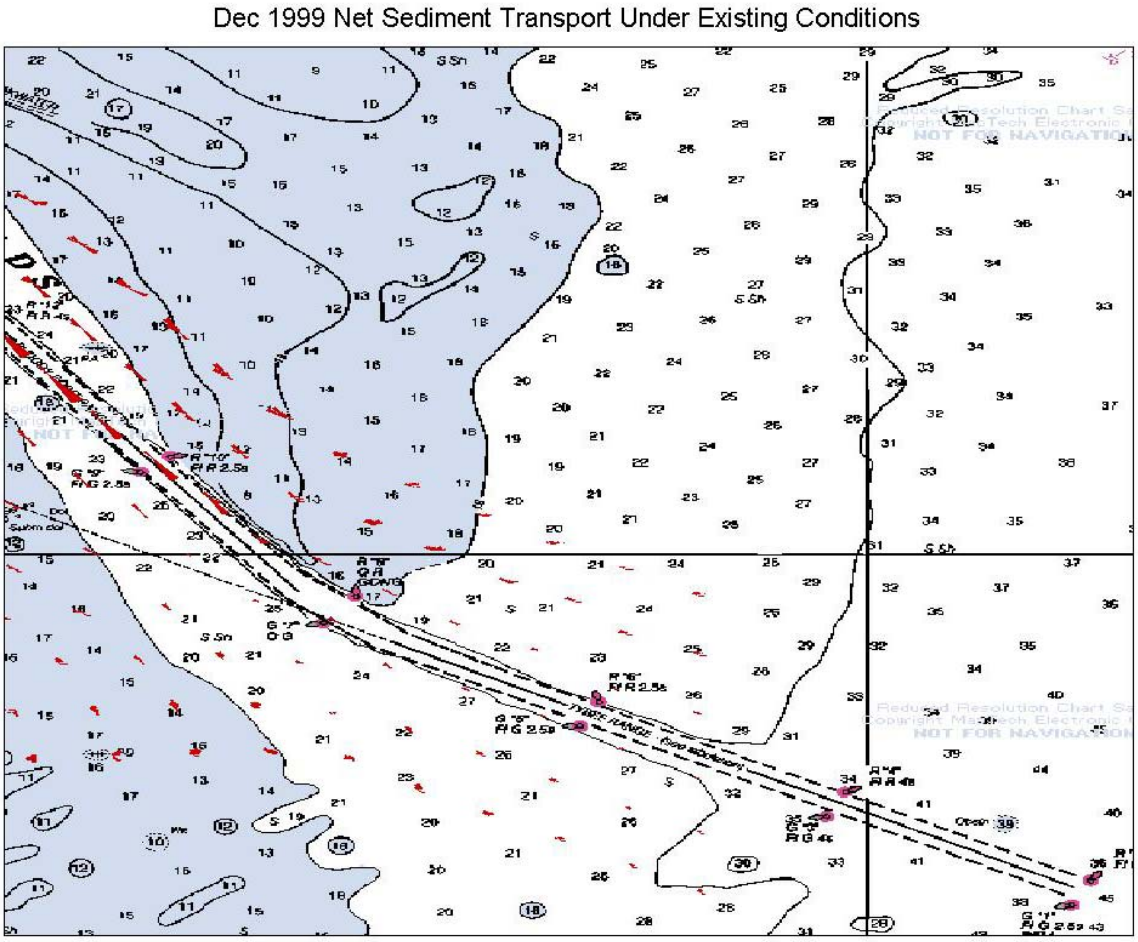

Figure 5C-39. Sediment transport rose plots for December 1999 existing conditions GTRAN simulation (southeastern domain).

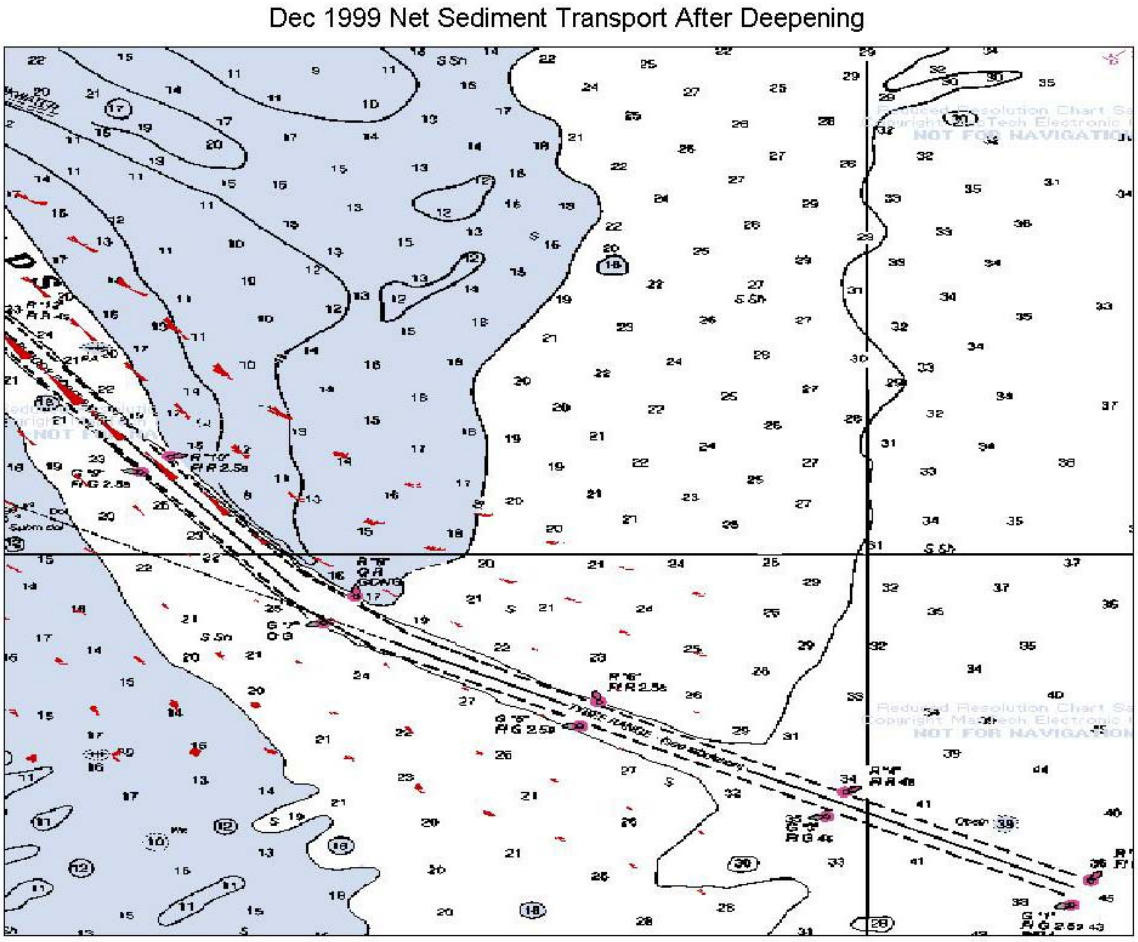

Figure 5C-40. Sediment transport rose plots for December 1999 deepened conditions GTRAN simulation (southeastern domain).

Appendix 5D. Change in Cumulative Sediment Transport Vectors from GTRAN Due to Deepening

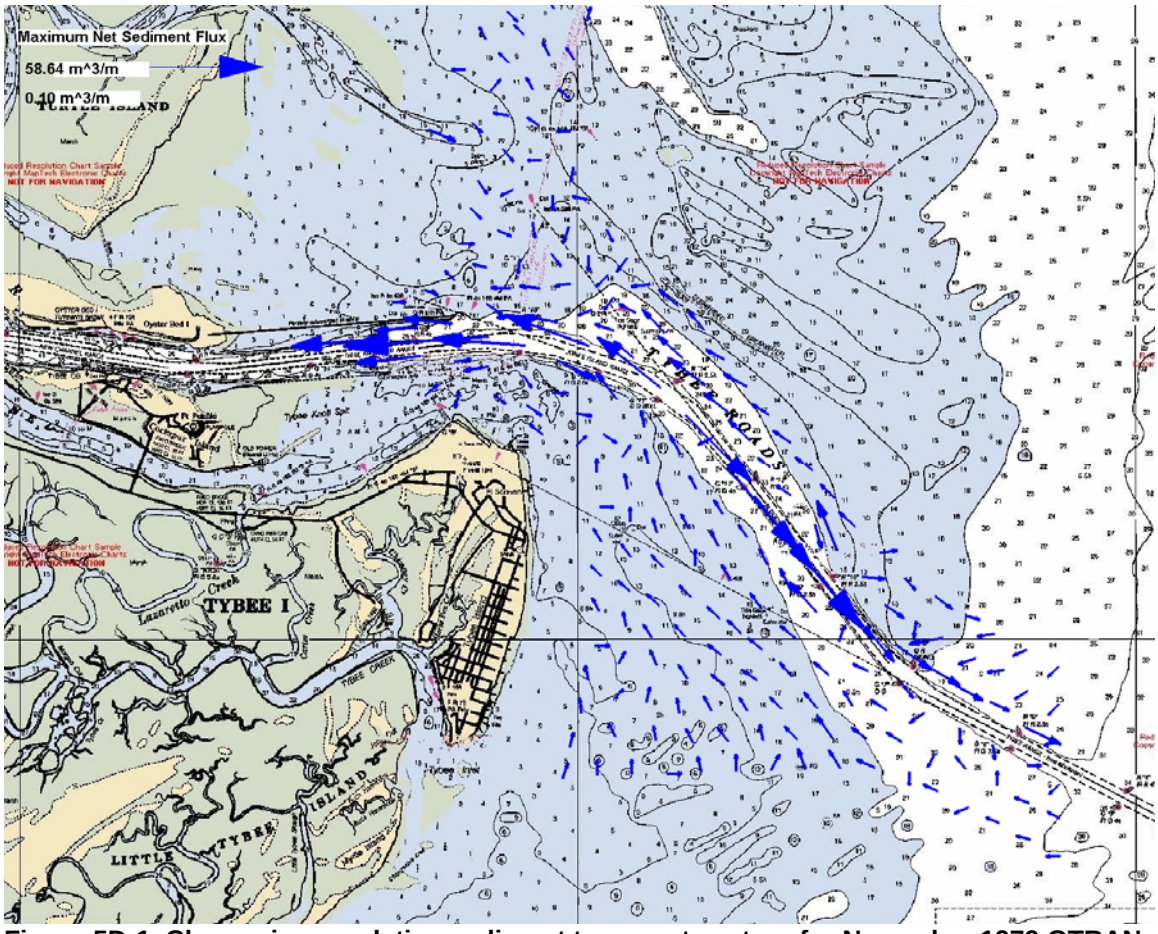

Figure 5D-1. Change in cumulative sediment transport vectors for November 1979 GTRAN simulation.

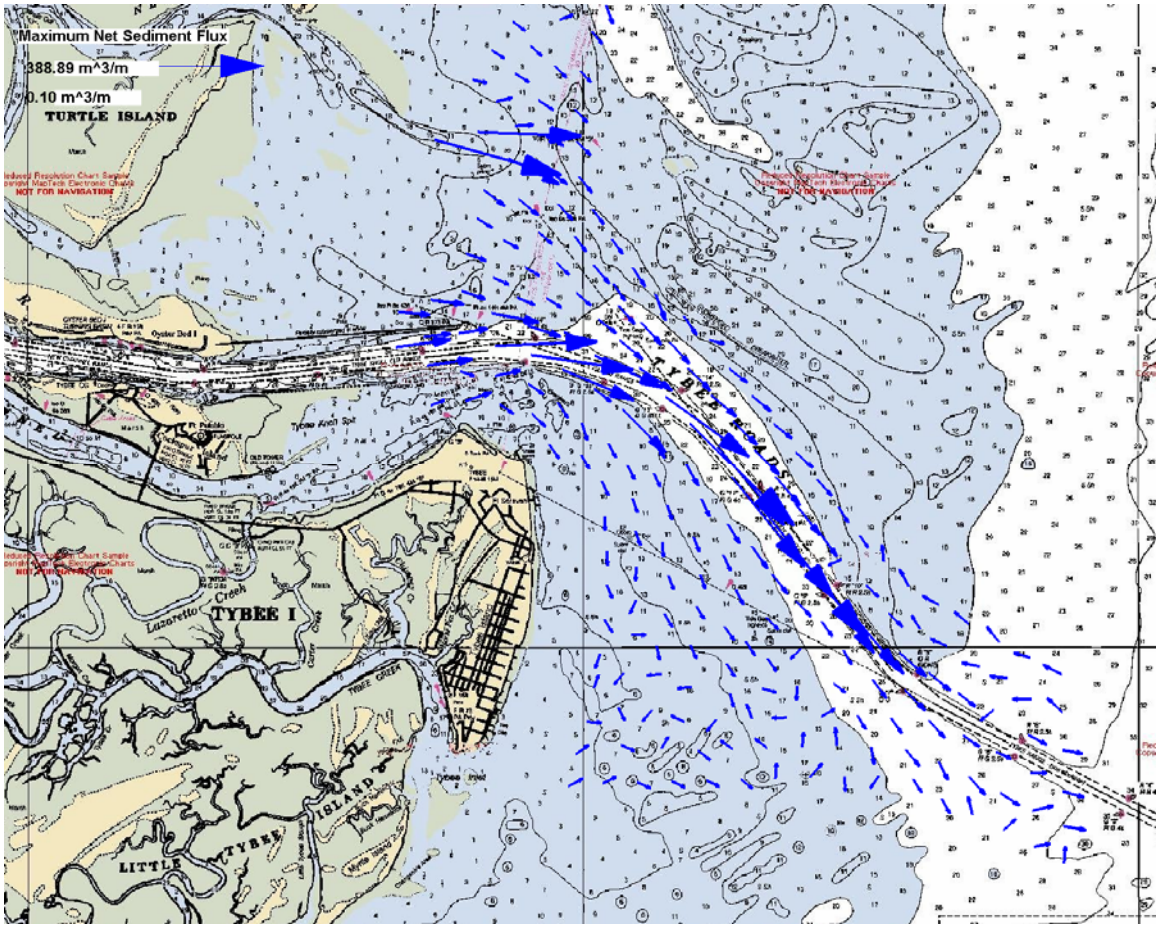

Figure 5D-2. Change in cumulative sediment transport vectors for September 1989 GTRAN simulation.

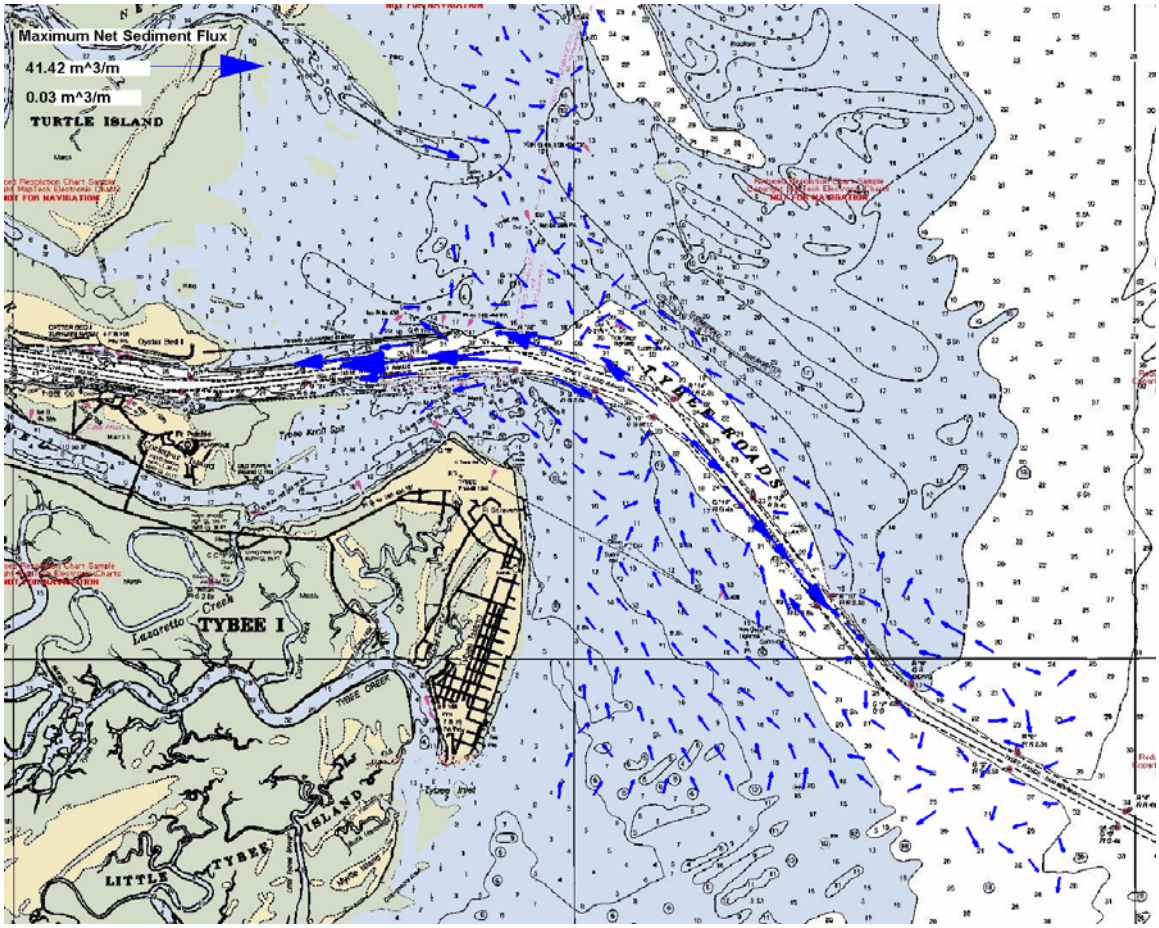

Figure 5D-3. Change in cumulative sediment transport vectors for January 1992 GTRAN simulation.

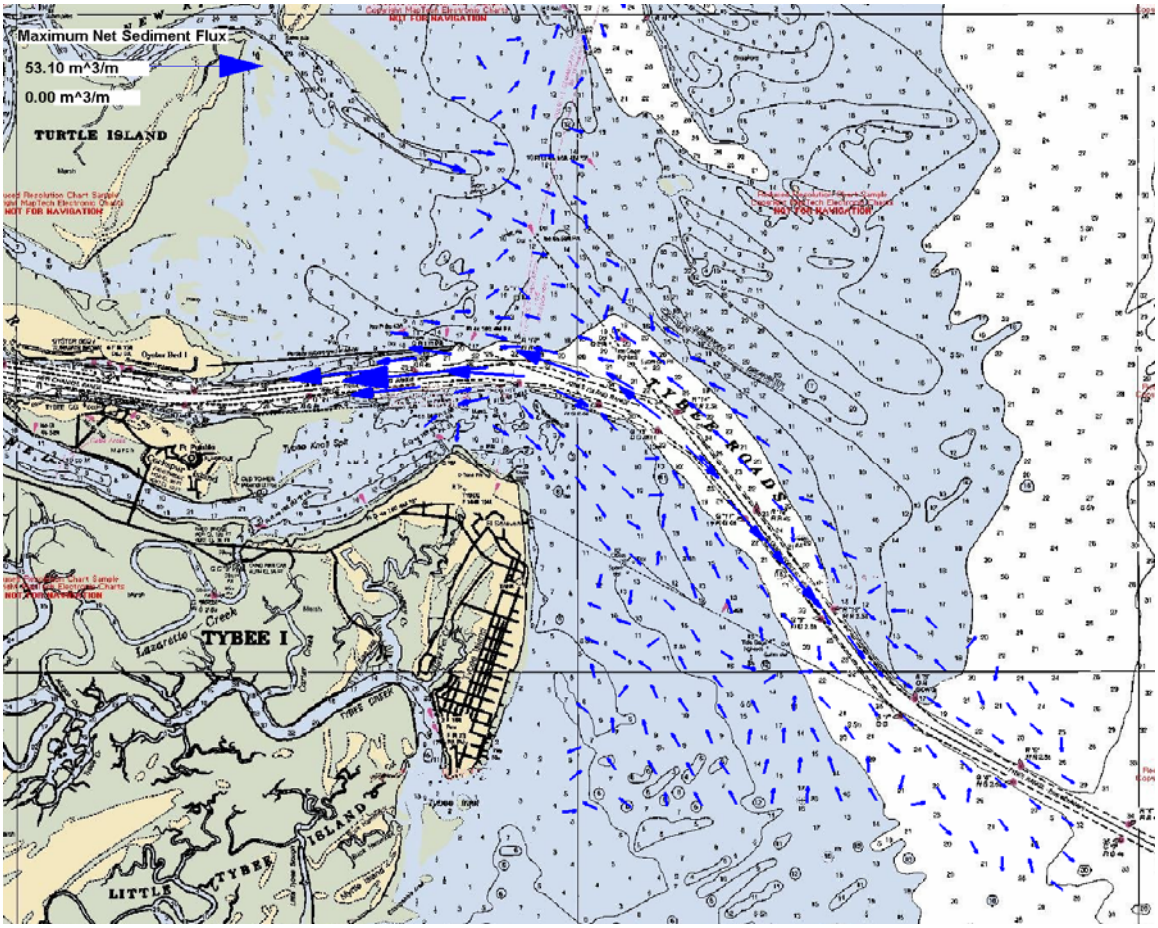

Figure 5D-4. Change in cumulative sediment transport vectors for July 1999 GTRAN simulation.

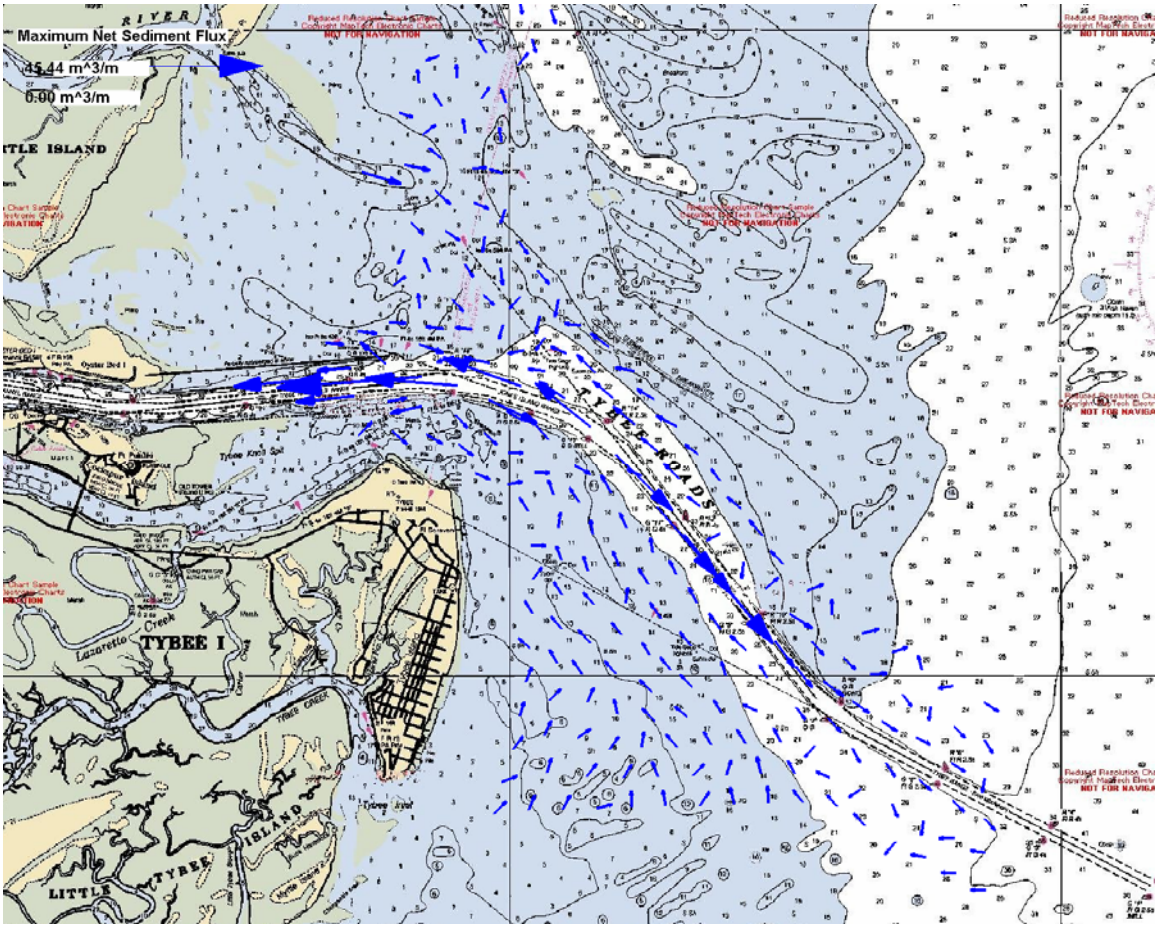

Figure 5D-5. Change in cumulative sediment transport vectors for December 1999 GTRAN simulation.

6 Summary and Conclusions

This study evaluated the impact of the proposed deepening of the Savannah Harbor navigation channel. A bathymetry and volume change analysis was conducted to provide the historical perspective of the Savannah nearshore evolution and to address review comments related to the ATM report. Numerical modeling of circulation, waves, and sediment transport was performed to compare pre- and post-deepening of the channel impacts on the coastal processes.

Deepening of the navigation channel, beginning in the 1870s, and subsequent construction of dual parallel jetties to stabilize the position of the navigation channel (1886-1897 time frame) are most likely the trigger for the changes in Tybee Island shoreline position that were observed between 1854/63 and 1900, and for the pattern of changes that has taken place since that time. There are no historical shoreline and bathymetric data available between 1854/63 and 1900 that would allow the details of that evolution, any variability in its rate of change during that time period, and a more direct linkage between navigation project construction and shoreline/morphology changes, to be examined or discerned further. However results of the historic shoreline analysis and volume change analysis, in addition to results from the circulation and GRTRAN sediment transport models, provide a consistent picture of circulation and sediment transport processes at work. We believe the following hypothesis to be the most likely explanation for evolution of the inlet since construction of the navigation project.

Deepening of the navigation channel and construction of the dual parallel jetties appear to have concentrated the ebb tidal flow into a narrower, more concentrated, stronger ebb tidal jet. The navigation project also has fixed the location of the channel, as intended, as has construction of the submerged breakwater. Fixing the location of the channel reinforces the morphological response that occurs in response to the ebb and tidal currents that enter and flow through the channel. Concentration of the flow by the project produces higher ebb currents within the jet. Prior to project construction, ebb velocities in this vicinity were probably weaker. Associated with enhanced ebb jet formation is increased gyre formation adjacent to the jet, i.e. on either side of the jet. This flow feature is observed at many structured inlets with high ebb currents. Enhanced gyre formation produces, at peak ebb within the channel, a return current on the flanks of the inlet that flows back toward the inlet entrance, in the same direction as that experienced during typical flood flow conditions. During the flood flow here, currents are directed toward the entrance throughout the ebb shoal region. Thus a situation is created where currents adjacent to the channel are directed toward the entrance (in the flood flow direction) a much larger percentage of the time. The duration of flood flow is greater than the duration of ebb flow along the flanks of the inlet. The north Tybee Island Shelf is the southern flank of the inlet. This change in predominance of flow direction adjacent to the ebb jet is expected to produce a corresponding change in the sediment transport patterns and morphology in these same regions, compared to conditions that existed prior to deepening and jetty construction. These changes to the circulation and sediment transport patterns, created by the navigation project, are thought to

explain the shoreline and morphologic changes that have occurred on Tybee Island, along with changes to sediment supply to the island from Barrett Shoals.

At present, the Tybee Island Shelf is in the flank of the jet, and is influenced by the return flow of the gyre. The GTRAN results show that the sediment transport regime in the channel and immediately adjacent to it are strongly ebb directed. The strong transport computed for the channel is consistent with the ebb dominance of this inlet system as evidenced by its massive ebb tidal delta. GTRAN results also show that a short distance away from the channel sediment net sediment transport is directed toward the entrance, both north and south of the channel, albeit with much smaller transport rates than those computed in the channel. The GTRAN results also indicate that on the Tybee Island Shelf to the east of northern Tybee Island, sediment transport is directed toward the northwest in a net sense. This direction of transport suggests that the sediment from this region moves toward the North Tybee Shoal. The accumulation of sediment in the North Tybee Shoal (and associated migration of the South Channel to the north which has likely happened in response to the sediment accumulation there), and deflation of the Tybee Island Shelf are consistent with the results of the GTRAN model. It is likely that the sediment transport regime in this region has been altered compared to the regime that existed prior to construction of the navigation project, in response to changes in the circulation patterns and local dominance of ebb/flood flow. Additional simulations of the wave, circulation, and GTRAN models for an inlet configuration representing the pre-construction condition could shed additional light on the working hypothesis for the shoreline and beach evolution observed on north Tybee.

The GTRAN results reflect conditions in deeper water where waves tend to agitate and suspend sediment and currents tend to move the sediment, not the shallow surf zone region along the Tybee Island shoreline. The very shallow nearshore region is much more wave dominated than the offshore region for which GTRAN was applied. Shoreline change modeling to examine this inner surf zone region was not part of the scope of this effort, but the minor changes in the nearshore wave results indicate that the deepening will have little impact on the shoreline. The historical shoreline change analysis showed the presence of a nodal zone around 2nd Street, north of which sand appears to be transported to the north by wave action, and south of which sand appears to be transported to the south. The hot-spot is in the region of the nodal zone, a divergent zone in which sediment tends to leave the region in both directions, in a net sense. The erosion within this nodal zone along north Tybee, is likely to be caused both by the ebb tidal deflation that occurs offshore as well as the gradients in alongshore transport created by the wave-dominated transport in the very nearshore zone.

Another possible factor in the evolution of the north half of Tybee Island is the unusually frequent and severe tropical storm activity during the period from 1879 to 1899. This increase in storm activity could have exacerbated the situation created by initial project construction and produced unusually high rates of sediment transport and morphology change. However, it seems unlikely that a single extreme event, or sequence of hurricane/tropical storm events in the region alone are capable of stimulating the shoreline and offshore morphology changes that have occurred on Tybee Island and in the Tybee Island Shelf. The GTRAN sediment modeling results indicate that the sediment transport regime during a single episodic event, like Hugo (which was re-tracked to have a much larger impact on the area than it actually had), is similar to the pattern seen for non-hurricane conditions, but is greater in magnitude in some locations (not all) than any of the months of normal winter storm activity that were examined. But where the magnitude was greater, the increase is only a factor of 1 to 5 greater. For this magnitude of difference, and in light of the infrequence and short duration of episodic events, the more typical month-to-month forcing in response to an increasingly deeper channel and tighter ebb tidal jet appears to be a more likely trigger for the shoreline and beach evolution that has taken place.

GTRAN results show that the net sediment movement on the southern half of the Tybee Island Shelf is toward the west, i.e. toward the island. This computed result is consistent with the relative health of the southern half of Tybee Island, compared to the northern half. Historic shoreline changes showed the southern half of the island to be accretionary for a significant time following construction of the project. Observations from other inlets suggest that as the ebb delta grows the down drift attachment bar migrates to the south. The attachment bar is the location on the ebb delta where sand moving around the ebb delta, from updrift to downdrift in a net sense, feeds the nearshore zone of the downdrift beach. This process may also be occurring at Tybee Island, and at present the feeding appears to be occurring at the southern half of the island. Some of the sediment eroded from the bulge in shoreline (present in 1854/1863, but not in 1900) appears to have moved south and accreted on the southern half of the island following project construction. The shoreline position of south Tybee prior to beach fill placement was well seaward of its position prior to construction of the navigation project. The current navigation channel appears to be a nearly complete sink for any sediment moving from north to south along the shelf (suggested by pre- and post-dredging surveys and the consistency of dredging volumes following deepenings). Placement of dredged material back into the nearshore zone of Tybee Island would be a means for restoring this supply of sand to the Tybee beach system.

The circulation and wave modeling indicate very small changes associated with the proposed deepening. The GTRAN results provide insight about what this deepening will do in terms of sediment transport regime, which is expected to be similar to that of past deepenings. GTRAN results for the existing condition and the with-deepened-channel condition indicate that the additional channel deepening will not change the general overall pattern of sediment transport in the region. The most noticeable changes were computed in the channel.

Transport in the Tybee Knoll Bar Channel reach showed decreases in magnitude for all four of the typical months of simulation, but conditions remain strongly ebb-dominant. The magnitude of change was greatest here (15-20 percent), compared to changes throughout the rest of the system (changes elsewhere were generally quite small, several percent). Some small increases to shoaling rates in this sector of the channel might be expected in light of these decreases, but gradients in transport (which dictate accumulation rates) do not appear to be altered very much. For the extreme hurricane event (expected to be a very rare event), conditions remain ebb dominant and transport rates increase (factor of 2 greater) rather than decrease as they do for the other four months.

Transport in the Tybee Roads Channel reach consistently shows increases for each of the typical months, but only very slight increases, a few percent. No significant changes in sedimentation are expected in this reach of the navigation channel. Transport rates increase in this portion of the channel for the re-tracked Hugo event (about a factor of 2 greater), as they do for all sections of the main channel. Transport remains strongly ebb dominant in this reach.

In the Tybee Range Channel reach, the outer limits of the navigation channel, changes in transport rate are also very small. The deepening increases rates for one month, shows zero change for one, and shows slight decreases for two of the months. All increases or decreases are small (a few percent). For re-tracked Hugo, the deepening only increases transport by about 20%, compared to a factor of 2 in the other channel reaches. This section of channel remains ebb-dominant. These changes do not suggest any significant changes in channel shoaling and they suggest that the channel region will remain strongly ebb-dominant in terms of sediment transport direction.

Average transport within the Tybee Island Shelf region consistently shows slight increases or no change for each of the four typical months, and an increase for the extreme event. No decreases were computed. Patterns appear unchanged and the net direction of movement appears

to remain to the northwest. Slight increases suggest a tendency for sediment to be transported from the shelf region to the northwest at a higher rate. This would be consistent with the hypothesized model for how sand has been moving to the northwest in response to initial project construction and subsequent deepening. This proposed deepening seems to produce a result consistent with that hypothesis. However, the magnitudes of change are quite small, in the range from 0 to 2 percent for all months and even for the extreme hurricane event. Zero change was computed for two of the four months. Computations show that channel deepening will have negligible effect on the Tybee Island Shelf.

For North Tybee Shoal region, computations show a consistent decrease in transport rate for all four months, about 5 percent or less; however, for the extreme hurricane event transport rates are increased by about 40%. These changes suggest that sediment being transported into the north Tybee shoal region will have less tendency to leave the region, but this is more dictated by changes to the transport gradients. Such a trend would be consistent with historic accumulation of sediment in these shoals.

References

Anders, F.J., Reed, D.W., and Meisbeurger, E.P., 1990. Shoreline Movements, Report 2, Tybee Island, Georgia to Cape Fear, North Carolina, 1851-1983. Technical Report CERC-83-1, U.S. Army Engineer Waterways Experiment Station, Vicksburg, MS.

Applied Technology and Management, Inc. 2001, Draft Savannah Harbor Beach Erosion Study: Savannah Harbor Expansion Project. Prepared for the Georgia Port Authority. Charleston, SC.

Bouws, E., Gunther, H., Rosenthal, W., and Vincent, C. L. 1985. Similarity of the wind wave spectrum in finite depth waves; 1. Spectral form. *Journal of Geophysical Research*, 90(C1), 975-986.

Brooks, R. M., and Brandon, W. A. 1995. Hindcast Wave Information for the U.S. Atlantic Coast: Update 1976-1993 with Hurricanes. WIS Report 33, U.S. Army Engineer Waterway Experiment Station Vicksburg, MS.

Byrnes, M. R., Baker, J. L., and Li, F. 2002. Quantifying Potential Measurement Errors and Uncertainties Associated with Bathymetric Change Analysis. ERDC/CHL CHETN-IV-50, U.S. Army Engineer Research and Development Center, Vicksburg, MS.

Gailani, J.Z., Smith, S.J., and Kraus, N.C. In preparation. Monitoring dredged material disposal at the mouth of the Columbia River, Washington/Oregon, USA. US Army Engineer Research and Development Center. Vicksburg, MS.

Gailani, J.Z., Smith, S.J., Raad, L., and Ebersole, B.A. In prep. Savannah Harbor Entrance Channel: Nearshore Placement of Dredged Material. Technical Report ERDC/CHL TR-03-X. US Army Engineer Research and Development Center, Vicksburg, MS.

Gibbs, A. E., and Gelfenbaum, G. 1999. Bathymetric change off the Washington-Oregon Coast. Proceedings, Coastal Sediments'99, ASCE, 1627-1642.

Hubertz, J. M. 1992. User's Guide to the Wave Information Studies (WIS) Wave Model, Version 2.0. WIS Report 27, U.S. Army Engineer Waterway Experiment Station Vicksburg, MS.

Jensen, R., Scheffner, N., Smith, S.J., Webb, D., and Ebersole, B.A. 2002. Engineering studies in support of Delong Mountain Terminal project. Technical Report ERDC/CHL TR-02-26. US Army Engineer Research and Development Center, Vicksburg, MS.

Komen, G. L, Cavaleri, L., Donelan, M., Hasselmann, K., Hasselmann, S., Janssen, P. A. E. M. 1994. *Dynamics and Modelling of Ocean Waves.* Cambridge University Press, 522 pp.

Kraus, N. C., and Rosati, J. D. 1998. Estimation of Uncertainty in Coastal-Sediment Budgets at Inlets. Coastal Engineering Technical Note IV-16, US Army Engineer Research and Development Center, Vicksburg, MS.

Luettich, R. A., Jr., and Westerink, J. J. 2005. A (Parallel) Advanced Circulation Model for Oceanic, Coastal, and Estuarine Waters. On-Line User's Guide. http://www.marine.unc.edu/C_CATS/adcirc/document/ADCIRC_title_page.html

Luettich, R. A., Jr., and Westerink, J. J. 2004. Formulation and Numerical Implementation of the 2D/3D ADCIRC Finite Element Model Version 44.XX, Theory Report and Formulation, http://www.marine.unc.edu/C_CATS/adcirc/adcirc_theory_2004_12_08.pdf

Luettich, R. A., Westerink, J. J., and Scheffner, N. W. 1992. ADCIRC: An advanced three-dimensional circulation model for shelves, coasts, and estuaries, Report 1: Theory and methodology of ADCIRC-2DDI and ADCIRC-3DL, Technical Report DRP-92-6, US Army Engineer Waterways Experiment Station, Vicksburg, MS.

Madsen, O.S., and Wikramanayake, P.N. 1991. Simple models for turbulent wave-current bottom boundary layer flow. Contract Report DRP-91-1, US Army Engineer Waterway Experiment Station, Vicksburg, MS.

McNeil, J., Taylor, C., and Lick, W. 1996. Measurements of erosion of undisturbed bottom sediments with depth. *Journal of Hydraulic Engineering*, ASCE, 122(6): 316-324.

Meyer-Peter, E. and Müller, R. 1948. Formulas for bed-load transport. Second International Association of Hydraulic Engineering and Research (IAHR) Congress, Stockholm, Sweden. IAHR, Delft, Netherlands.

Miller, T.L., Morton, R.A. and Sallenger, A.H., 2005. The National Assessment of Shoreline Change: A GIS Compilation of Vector Shorelines and Associated Shoreline Change Data for the U.S. Southeast Atlantic Coast, USGS Open File Report 2005-1326, United States Geological Survey, St. Petersburg, FL.

Miller, H.C., Smith, S.J., Hamilton, D.G., and Resio, D.T. 1999. Cross-shore transport processes during onshore bar migration. Proceedings of Coastal Sediments '99, ASCE, 1065-1080.

Mills, J. 2006 personal communication. NOAA Office of Coastal Survey.

Oertel, G.F., Fowler, J.E., and Pope, J., 1985. History of Erosion and Erosion Control Efforts at Tybee Island, Georgia. Miscellaneous Paper CERC-85-1, U.S. Army Engineer Waterways Experiment Station, Vicksburg, MS.

Nielsen, P. 1992. *Coastal Bottom Boundary Layers and Sediment Transport*. World Scientific Publishing, Singapore, Advanced Series on Ocean Engineering, vol. 4.

Reid, J.M., Reid, J.A., Jenkins, C.J., Hastings, M.E., Williams, S.J., and Poppe, L.J. 2005. usSEABED: Atlantic coast offshore surficial sediment data release: U.S. Geological Survey Data Series 118, version 1.0. Online at http://pubs.usgs.gov/ds/2005/118/

Sargent, F.E. 1988. Case Histories of Corps Breakwater and Jetty Structures, Report 2 South Atlantic Division. WES TR-REMR-C0-3, US Army Corps of Engineers Waterways Experiment Station, Vicksburg, MS.

Smith, J. M., Sherlock, A. R. and Resio, D. T. 2001. STWAVE: Steady-State spectral Wave Model User's manual for STWAVE, Version 3.0. ERDC/CHL SR-01-1, US Army Corps of Engineers Engineer Research and Development Center, Vicksburg, MS. http://chl.wes.army.mil/research/wave/wavesprg/numeric/wtransformation/downld/erdc-chl-sr-01-11.pdf

Soulsby, R.L., 1997. *Dynamics of marine sands*. Thomas Telford, London. 249 pp.
Van Rijn, L. C. 1984. Sediment transport: Part i: bed load transport; Part ii: suspended load transport; Part iii: bed forms and alluvial roughness. *Journal of Hydraulic Engineering* 110(10): 1431-1456; 110(11): 1613-1641, 110(12): 1733-1754.

Valverde, H.R., Trembanis, A.C. and Pilkey, O.H., 1999, Summary of Beach Nourishment Episodes on the U.S. East Coast Barrier Islands, *Journal of coastal Research*, V15, No4, 1100-1118.

Wikramanayake, P.N., and Madsen, O.S. 1994a. Calculation of suspended sediment transport by combined wave-current flows. Contract Report DRP-94-7, US Army Engineer Waterway Experiment Station, Vicksburg, MS.

Wikramanayake, P.N., and Madsen, O.S. 1994b. Calculation of movable bed friction factors. Contract Report DRP-94-5, US Army Engineer Waterway Experiment Station, Vicksburg, MS.